DÉPARTEMENT DE PHYSIQUE
DE L'ÉCOLE NORMALE SUPÉRIEURE
LABORATOIRE KASTLER BROSSEL

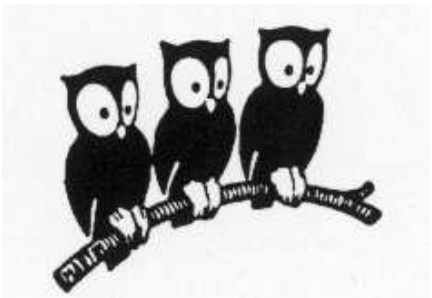

HABILITATION À DIRIGER LES RECHERCHES
DE L'UNIVERSITÉ PARIS VI

présentée par

Yvan CASTIN

sur le sujet :

ÉTUDES THÉORIQUES DES ATOMES FROIDS : DU REFROIDISSEMENT LASER AUX CONDENSATS DE BOSE-EINSTEIN

soutenue le 1er juillet 2005 devant le jury composé de :

M. Claude Cohen-Tannoudji	Président
M. Gora Shlyapnikov	Rapporteur
M. Sandro Stringari	Rapporteur
M. Philippe Chomaz	Rapporteur
M. Chris Westbrook	
M. Roland Combescot	
M. Jean Dalibard	

Table des matières

Chapitre 1

Vue d'ensemble et points forts

Mon activité de recherche au Laboratoire Kastler Brossel a commencé en 1988 et se décompose en deux périodes.

De 1988 à 1995, j'ai travaillé essentiellement sur le refroidissement d'atomes par laser. En 1988, le groupe de W. Phillips avait découvert que le refroidissement laser conduisait à des températures beaucoup plus basses que celles prévues par la théorie du refroidissement Doppler, et de "nouveaux" mécanismes de refroidissement, dits à gradients de polarisation, comme l'effet Sisyphe, avaient été identifiés, en particulier par Jean Dalibard et Claude Cohen-Tannoudji. Mon travail était de calculer les nouvelles "températures" minimales correspondant à ces mécanismes. L'approche théorique existante, dite semi-classique, qui traitait classiquement le mouvement des atomes, ne permettait pas de faire ce calcul. J'ai alors développé de nouvelles méthodes permettant de résoudre les équations traitant quantiquement le mouvement atomique : (i) la méthode des bandes et (ii) la méthode des fonctions d'onde Monte-Carlo. Ceci m'a permis de répondre complètement à la question et de retrouver les résultats expérimentaux à 3D. Par ailleurs, dans un registre différent, j'ai proposé une expérience ayant conduit à la première observation des oscillations de Bloch.

À partir de juillet 1995, à la suite de l'observation de la condensation de Bose-Einstein d'atomes de rubidium, par Eric Cornell et Carl Wieman, je suis passé à l'étude théorique des gaz quantiques, en couplage fort avec les expériences menées au Laboratoire par les groupes de Jean Dalibard et Christophe Salomon. Mes travaux ont porté essentiellement sur les bosons jusqu'en 2002, date à laquelle les premiers gaz de fermions en interaction forte ont été stabilisés. Depuis cette date, les fermions prennent dans mes travaux une importance croissante.

Voici les principaux résultats que j'ai obtenus sur les gaz quantiques.

- l'approfondissement du concept de phase d'un champ atomique : la description microscopique de l'apparition de franges d'interférences entre deux condensats de phase relative initialement non définie, au fur et à mesure que l'on détecte les particules ; la dynamique de cette phase lorsqu'elle est initialement bien définie, dynamique constituée de brouillages et de résurgences quantiques successives.
- la découverte des mécanismes de nucléation de tourbillons quantiques et de cristallisation de ces tourbillons en un réseau, dans les expériences sur les gaz quantiques en rotation.
- la découverte de solutions analytiques donnant l'évolution d'un condensat avec interactions de champ moyen dans un potentiel harmonique dépendant du temps (solutions dites du changement d'échelle) ; ceci ayant permis l'interprétation des mesures par temps de vol effectuées dans toutes les expériences ; généralisation de cette solution à une solution exacte de l'équation de Schrödinger à N corps pour le

gaz quantique unitaire.
- le développement de nouveaux outils théoriques ou le perfectionnement d'outils existants : développement d'une approche de Bogoliubov pour les condensats plus précise que l'approche existante et respectant la symétrie $U(1)$ du problème ; extension de la méthode de Bogoliubov au cas des quasi-condensats donc applicable aux systèmes à 1D et 2D ; développement de nouvelles méthodes de Monte-Carlo quantique, ayant permis le premier calcul exact de la distribution de probabilité du nombre d'atomes dans le condensat, à une température quelconque (y compris au voisinage de la température critique).
- la découverte d'un moyen expérimental pour produire et détecter les premiers solitons d'onde de matière.
- très récemment, l'idée de transformer adiabatiquement un condensat moléculaire en un gaz de Fermi attractif ultrafroid, pour chercher à observer la transition BCS dans le régime d'interaction faible.

Soulignons que tout ceci est bien sûr le résultat d'un travail de groupe, groupe que je dirige scientifiquement depuis 1995 et constitué en moyenne d'un étudiant en thèse (que je codirige) et de un à trois visiteurs post-doctoraux, avec la visite occasionnelle de chercheurs confirmés comme G. Shlyapnikov. J'ai aussi bénéficié de séjours de courte durée à l'étranger, d'une durée de 6 semaines dans le groupe de W. Phillips et d'une durée de deux fois 6 semaines chez Anthony Leggett (dans le cadre d'une collaboration CNRS-University of Illinois).

Chapitre 2

Les travaux sur le refroidissement laser

Les numéros entre crochets font référence à la liste de mes publications, disponible en fin de document.

2.1 Les limites du refroidissement Doppler

Cette étude a été effectuée en collaboration avec un visiteur allemand, Harmut Wallis.

Le refroidissement Doppler est le schéma de refroidissement laser originel, tel qu'il fut proposé en 1975 par Hänsch et Schawlow. Son analyse complètement quantique n'avait cependant jamais été effectuée : la littérature s'était restreinte au cas limite d'une raie large (taux d'émission spontanée Γ bien supérieur à la fréquence de recul $\hbar k^2/2m$ d'un atome), qui est étudiable par une approximation semi-classique et prédit une énergie cinétique minimale proportionnelle à $\hbar\Gamma$. Que se passe-t-il donc dans la limite inverse d'une raie étroite, c'est-à-dire dans la limite où $\Gamma \to 0$ à fréquence de recul fixée ? La température limite tend-elle vers zéro ? Un article de Wineland et Dehmelt donnait une réponse, affirmative, à partir de l'hypothèse cependant non réaliste expérimentalement d'un gaz à l'équilibre thermodynamique strict.

Nous avons découvert, remarquablement, qu'il existe un modèle exactement soluble de refroidissement Doppler à une dimension, pour lequel nous avons obtenu une expression analytique de tous les moments de la distribution en impulsion. Le verdict est que l'énergie cinétique minimale tend vers 0.53 fois l'énergie de recul, dans la limite $\Gamma \to 0$ [1].

2.2 Le refroidissement laser 1D dans un champ lumineux $\sigma_+ - \sigma_-$.

Cette étude a été effectuée en collaboration avec un visiteur danois, Klaus Mølmer.

Le refroidissement à 1D d'un atome avec une dégénérescence Zeeman dans l'état fondamental par un champ laser superposition de deux ondes contre-propageantes de polarisations σ_+ et σ_- conduit à des énergies cinétiques inférieures à la limite Doppler, mais ne repose pas sur l'effet Sisyphe. Dans la limite semi-classique, le mécanisme de friction avait été identifié par Claude Cohen-Tannoudji et Jean Dalibard. Il restait à étudier le coefficient de diffusion pour obtenir la "température" à partir de la relation d'Einstein, ce que nous avons fait [2]. Nous avons effectué également une résolution numérique de l'équation

pilote entièrement quantique, qui a confirmé la validité de l'approche semi-classique dans un certain domaine de paramètres.

Nous avons découvert, que dans certaines conditions, le coefficient de diffusion dans la configuration $\sigma_+ - \sigma_-$ est anormalement grand, parce que des corrélations existent entre les impulsions des photons laser successifs absorbés par un atome : ainsi, sur une transition d'un moment cinétique J vers un moment cinétique $J+1$, un atome au repos dans l'état interne $m = J$ absorbe les photons σ_+ avec un taux $(J+1)(2J+1)$ fois plus élevé que les photons σ_-, dans le rapport des coefficients de Clebsch-Gordan au carré.

Par la suite, nous avons réalisé que le coefficient de diffusion était rarement étudié dans la littérature car il manquait un formalisme permettant de le calculer simplement. Nous avons développé ce formalisme en collaboration avec l'Université d'Århus au Danemark [5].

2.3 Description quantique du refroidissement Sisyphe à l'aide d'états de Bloch

Le refroidissement d'un atome de moment cinétique interne non nul dans un champ laser présentant un gradient de polarisation conduit à des énergies cinétiques moyennes sub-Doppler, à cause de mécanismes dont le plus important est l'effet Sisyphe : l'atome monte des collines de potentiel créées par les déplacements lumineux induits par le laser ; au sommet de la colline, un processus de pompage optique change l'état interne de l'atome, qui se trouve dès lors au fond d'une vallée de potentiel ; l'atome passe ainsi 'son temps' à monter des collines de potentiel, ce qui réduit son énergie cinétique.

L'analyse de ce mécanisme de refroidissement par la méthode semi-classique prédit une énergie cinétique proportionnelle à la profondeur de modulation des déplacements lumineux, c'est-à-dire proportionnelle à l'intensité laser et inversement proportionnelle au désaccord en fréquence entre atome et champ. Suffit-il donc de faire tendre l'intensité lumineuse vers zéro (c'est-à-dire d'éteindre le laser...) pour avoir une énergie cinétique arbitrairement basse ? La réponse est certes non, mais que vaut vraiment l'optimum du refroidissement ?

Pour répondre précisément à cette question, il faut résoudre l'équation pilote sur la matrice densité atomique en traitant quantiquement le mouvement du centre de masse atomique, ce qui est une tâche formidable. Dans le régime où les atomes ont le temps d'osciller plusieurs fois au fond des puits créés par les déplacements lumineux avant de subir un processus de pompage optique, nous avons heureusement pu trouver un moyen de simplifier considérablement ce traitement quantique.

Nous considérons d'abord le mouvement quantique purement hamiltonien d'un atome dans le potentiel périodique créé par les déplacements lumineux. On peut utiliser alors le théorème de Bloch, comme pour les électrons dans un cristal. Le spectre d'énergie à 1D est composé d'une alternance de bandes d'énergies permises, séparées par des intervalles d'énergies interdites (gap). Les bandes de plus basse énergie sont extrêmement étroites et correspondent essentiellement à des niveaux vibrationnels des atomes au fond de chaque micro-puits du réseau optique, couplés par un effet tunnel d'amplitude très faible. Les bandes de haute énergie correspondent à un mouvement quasi-libre des atomes au dessus des puits de potentiel lumineux.

Nous considérons ensuite la partie dissipative de l'équation pilote dans la base des états propres du hamiltonien. Dans le régime considéré, le taux de pompage optique est faible devant les fréquences typiques du mouvement hamiltonien : c'est le régime dit 'séculaire',

dans lequel la partie dissipative a le seul effet de coupler les populations de la matrice densité aux populations. On a ainsi réduit, de façon justifiée, l'équation pilote entièrement quantique à des équations de taux.

Ceci nous a permis de trouver l'optimum du refroidissement dans le cas d'un modèle simple à 1D [3], et de comprendre aussi en détail la dynamique quantique du mouvement atomique dans le refroidissement Sisyphe. Cette méthode originale, dite 'des bandes', a également suscité une série d'expériences de spectroscopie de type pompe-sonde (dans le groupe de Gilbert Grynberg au Laboratoire Kastler Brossel) ou de fluorescence (dans le groupe de William Phillips au NIST) permettant de révéler la quantification du mouvement des atomes dans une mélasse optique.

2.4 Application de la méthode des bandes à 2D et découverte d'une signature de l'effet tunnel

Cette étude a été effectuée en collaboration avec une visiteuse danoise, Kirstine Berg-Sørensen.

Nous avons appliqué la méthode des bandes précédemment décrite au refroidissement Sisyphe d'un atome dans un réseau optique à 2D. On entend ici par réseau optique une configuration de refroidissement d'atomes par laser qui accumule les atomes au voisinage des points du réseau périodique où le champ laser est polarisé circulairement.

Dans le régime quantique séculaire, nous avons montré que la dynamique du refroidissement est sensible au passage des atomes par effet tunnel d'un puits de potentiel lumineux à un autre, sur une distance donc d'une fraction de μm [7]. Cet effet tunnel se manifeste par des résonances (pics étroits) sur la population de la bande d'énergie fondamentale, et donc aussi sur l'énergie cinétique moyenne, en fonction de l'intensité ou du désaccord en fréquence du champ laser. On peut ainsi détecter un effet purement quantique sur un état stationnaire issu d'une dynamique dissipative, celle du refroidissement laser ! Les conditions d'observation de ce phénomène ont été précisées par une résolution numérique de l'équation exacte sur la matrice densité atomique [9]. À ce jour, ce phénomène n'a à notre connaissance pas encore été observé.

2.5 La méthode des fonctions d'onde Monte-Carlo

En collaboration avec Jean Dalibard et Klaus Mølmer, j'ai développé une méthode de résolution des équations pilote sur l'opérateur densité d'un système applicable à une classe générale de systèmes quantiques dissipatifs [4,6,13] : ceux dont l'équation pilote est de la forme de Lindblad. Cette classe est effectivement générale car Lindblad a démontré le caractère nécessaire de la forme portant son nom, sous des hypothèses raisonnables comme le maintien de la positivité de l'opérateur densité à tout temps.

La méthode consiste à approximer la matrice densité $\rho(t)$ par n fonctions d'onde stochastiques $|\psi_i(t)\rangle$, dont l'évolution est telle que le mélange statistique des $|\psi_i(t)\rangle$ converge vers $\rho(t)$ lorsque n tend vers l'infini. L'évolution de chaque fonction d'onde est une succession d'évolutions déterministes hamiltoniennes (avec un Hamiltonien non hermitien), interrompues par des sauts quantiques aléatoires. A n fini, on peut ainsi calculer la moyenne d'une observable atomique avec une incertitude statistique en $1/\sqrt{n}$.

L'intérêt pratique de la méthode est qu'une fonction d'onde n'a que N composantes, quand ρ en a N^2. Ceci nous a permis de résoudre numériquement les équations quantiques du refroidissement laser à 3D, voir plus bas. Mais elle a été utilisée par de nombreux autres

chercheurs, pour l'étude du refroidissement laser mais aussi de l'évolution dissipative de champs quantiques en cavité, etc.

De plus, la méthode apporte souvent un éclairage physique très utile sur l'évolution quantique du système : il est très facile de se représenter l'émission spontanée d'un photon par un atome en terme de saut quantique, plutôt que par une série d'équations sur la matrice densité, de même qu'en physique classique, la représentation du mouvement brownien en termes de forces de Langevin est plus intuitive que l'équation de Fokker-Planck. Par exemple, cet éclairage physique a été exploité avec profit par C. Cohen-Tannoudji, P. Bouchaud, F. Bardou et A. Aspect pour l'analyse du refroidissement VSCPT.

Cette méthode rejoint par ailleurs certains aspects fondamentaux de la mécanique quantique, comme la théorie de la mesure, et nous a permis de faire la connaissance de théoriciens comme Perceval et Gisin, qui avaient développé un formalisme similaire avec une motivation totalement différente.

2.6 Application des fonctions d'onde Monte-Carlo : refroidissement laser à trois dimensions.

En collaboration avec Klaus Mølmer, de l'Université d'Aarhus, j'ai effectué une étude du refroidissement laser à trois dimensions, par une résolution numérique des équations quantiques exactes.

Ces équations quantiques exactes portent sur la matrice densité atomique $\rho(t)$. Elles ne peuvent pas être résolues numériquement sous cette forme à trois dimensions, car la taille de $\rho(t)$ excède de plusieurs ordres de grandeur la taille des mémoires des ordinateurs usuels et le temps de calcul est rédhibitoire (même encore en 2005 !).

Nous avons donc utilisé la méthode des fonctions d'onde Monte-Carlo (en fait, c'était dans ce but que nous avions développé la méthode). Dans le cas du refroidissement à 3D qui nous intéresse, cette méthode fait gagner un facteur 10^4 sur la taille mémoire et le temps de calcul, par rapport à l'approche habituelle en termes de matrice densité ($N \simeq 10^5$). Les calculs restent lourds cependant, et ont utilisé largement les Cray C94 et C98 de l'IDRIS (projet 940155), ainsi qu'un ordinateur MasPar (massivement parallèle) de la NASA.

Les configurations considérées dans le calcul numérique de la référence [11] sont les mélasses optiques qui ont fait l'objet dans le monde (en particulier au Laboratoire) d'études expérimentales précises. Le calcul numérique est en parfait accord avec les expériences, et donne accès à des quantités non encore mesurées, comme la distribution spatiale des atomes à l'échelle de la longueur d'onde optique. L'apparition de lignes de fuite sur la distribution en impulsion des atomes au voisinage du seuil du refroidissement, prédite analytiquement [9], est confirmée par ces calculs à 3D [11].

J'ai également étudié, à l'aide de ces calculs, des configurations dites réseaux gris, qui ont l'avantage de fortement réduire le taux de fluorescence des atomes refroidis donc *a priori* les forces de pression de radiation qui limitent la densité atomique. Les résultats numériques sont en bon accord avec les mesures effectuées au Laboratoire sur ces configurations [15] ; ils ont l'avantage de prédire le taux de fluorescence des atomes, difficilement mesurable à mieux qu'un facteur 2 expérimentalement.

Ces calculs ont constitué le point final de toute une problématique de recherche, en montrant que la théorie pouvait rendre compte complètement des résultats expérimentaux sur les mélasses optiques.

2.7 Etude du piège magnéto-optique

Le piège magnéto-optique est une configuration très utilisée expérimentalement dans le monde, et très étudiée au Laboratoire ; elle réalise simultanément un refroidissement et un confinement des atomes en superposant un gradient de champ magnétique statique au champ laser de refroidissement.

Mon objectif était d'étudier ce type de piège dans le régime idéal où les effets collectifs entre atomes (collisions, réabsorption de photons de fluorescence) sont négligeables. J'ai commencé par montrer que la modélisation du piège à une dimension donne des résultats en désaccord avec les expériences [8].

La résolution numérique multidimensionnelle du problème est impraticable car la périodicité spatiale qui rendait possible les calculs précédents est détruite par le champ magnétique inhomogène. J'ai donc développé un formalisme prenant en compte perturbativement l'effet d'un potentiel extérieur lentement variable sur le refroidissement. Le résultat est une équation de transport classique (de type Schmoluchowsky) sur la distribution spatiale des atomes à grande échelle (i.e. grande devant la longueur d'onde optique λ et devant la longueur de cohérence spatiale des atomes). Les coefficients de l'équation de transport sont obtenus par la résolution quantique de problèmes périodiques spatialement.

Pour caractériser le fonctionnement du piège magnéto-optique (temps de relaxation et état stationnaire), il me suffit ainsi de connaître le coefficient de diffusion spatiale et la vitesse moyenne des atomes refroidis en présence d'un champ magnétique uniforme (vitesse de dérive magnétique). Ces quantités sont par ailleurs intéressantes en elles-mêmes.

Le coefficient de diffusion spatiale et la vitesse de dérive magnétique que j'ai ainsi obtenus dans un modèle à 2D sont en accord avec les mesures expérimentales à 3D. Par contre, les prédictions sur la taille du nuage atomique dans le piège magnéto-optique sont inférieures aux valeurs mesurées, probablement à cause des forces radiatives entre les atomes. Nous n'avons pas poursuivi plus avant ces études, l'observation en 1995 de la condensation de Bose-Einstein nous ayant convaincu de changer de thématique.

2.8 Etude des oscillations de Bloch

Lorsqu'on soumet un conducteur parfait à un champ électrique uniforme, on obtient non pas un courant continu, mais un courant alternatif. Ce phénomène quantique est connu en physique des solides sous le nom d'oscillations de Bloch ; son observation est rendue difficile par les défauts du réseau, qui introduit de la dissipation, et par les interactions électroniques.

Christophe Salomon et moi-même avons réalisé que des atomes ultra-froids placés dans une onde lumineuse stationnaire très désaccordée (en accélération uniforme par rapport au référentiel du laboratoire) constituaient un système très pur (non dissipatif) pour étudier ce phénomène.

Ma contribution à ce travail a été de déterminer théoriquement une procédure expérimentale permettant de voir ces oscillations, ce qui inclut le problème de la préparation de l'état initial (les atomes doivent se trouver dans une bande d'énergie bien déterminée, avec un vecteur de Bloch également bien déterminé). Et de vérifier que les mesures étaient en accord avec mes prédictions théoriques [14,18].

L'observation de ce phénomène, qui n'avait à l'époque pas été vu clairement en physique de la matière condensée, a connu un certain retentissement. Par ailleurs, les oscillations de Bloch d'ondes de matière peuvent avoir aussi une utilité pratique, celle d'accélérer les atomes de façon parfaitement contrôlée, en augmentant leur impulsion d'un multiple

connu de l'impulsion d'un photon [19], ce qui est utilisé actuellement dans une expérience de mesure de haute précision de h/m dans le groupe de François Biraben au Laboratoire Kastler Brossel.

2.9 Optique atomique dans des potentiels périodiques

En collaboration avec Claude Cohen-Tannoudji et Jean Dalibard, j'ai dirigé le travail de thèse de Pippa Storey, qui portait sur le développement de méthodes semi-classiques pour des problèmes d'optique atomique périodiques (temporellement ou spatialement).

Notre objet d'étude était plus particulièrement le modulateur électro-optique pour des ondes de matière, qui a été démontré expérimentalement au Laboratoire.

Ce modulateur repose sur le principe suivant. Lorsqu'on envoie un paquet d'ondes atomiques d'énergie bien définie E_i sur un puits de potentiel dont l'amplitude est modulée à la fréquence angulaire ω, le paquet d'ondes émergeant est une superposition cohérente de composantes d'énergie $E_f = E_i + n\hbar\omega$, où n est entier. Les différentes composantes, se propageant à des vitesses différentes en vol libre, finissent par se séparer spatialement. Les quantités à déterminer sont les poids des différentes composantes.

L'approche semi-classique utilisée habituellement en optique atomique pour étudier ce genre de systèmes est de type réseau de phase mince. Elle traite perturbativement l'effet de la partie modulée en temps du potentiel. Nous avons développé une approche semi-classique s'affranchissant de cette approximation. Le problème était rendu non trivial par l'apparition de caustiques (points de focalisation des trajectoires classiques) dans le potentiel, qui mettent en échec l'approche WKB la plus simple, et par le fait que ces caustiques, qui se répètent périodiquement en temps, peuvent être proches les unes des autres, ce qui rend insuffisantes les approximations semi-classiques uniformes habituelles, qui étendent l'approche WKB au voisinage d'une caustique ou d'un petit nombre de caustiques.

Nous qualifions notre approche d'uniforme périodique, car elle régularise l'approche WKB simultanément au voisinage d'un nombre infini de caustiques, séparées les unes des autres d'une période du potentiel. Les résultats obtenus sont en excellent accord avec la résolution numérique directe de l'équation de Schrödinger.

2.10 Diffusion de la lumière par un condensat

En collaboration avec Jean Dalibard et Olivier Morice (dont c'était le sujet de thèse) j'ai mené une réflexion théorique sur les effets de statistique quantique dans la diffusion de la lumière par un gaz d'atomes bosoniques ultra-froids, en prévision de résultats expérimentaux à venir.

L'idée était de caractériser la dégénérescence de l'échantillon atomique à l'aide d'un faisceau sonde lumineux très peu intense. L'effet de la lumière sur le mouvement des atomes est alors négligeable pendant le temps d'établissement d'un régime forcé pour les dipôles atomiques, et les moyennes à un temps des observables de la lumière diffusée par les N atomes (amplitude, intensité) dépendent seulement de la distribution spatiale à N corps $\rho(\vec{r}_1, \ldots, \vec{r}_N)$. Dans un développement systématique en puissances de la densité atomique, on fait apparaître successivement la densité à un corps (obtenue par trace de $\rho(\vec{r}_1, \ldots, \vec{r}_N)$ sur $N-1$ atomes), à deux corps (trace sur $N-2$ atomes), etc. Nous avons ainsi déterminé rigoureusement la dépendance de l'indice de réfraction du gaz en termes de la distribution de paire des atomes, sensible à la statistique quantique [10].

En collaboration avec Ralph Dum (en séjour post-doctoral au Laboratoire), j'ai développé une approche numérique permettant de déterminer toutes les moyennes à un temps du champ lumineux diffusé, quelle que soit la densité atomique, pour des échantillons à petit nombre d'atomes. En particulier, l'échantillonnage de la distribution atomique à N corps est obtenue par la méthode Monte-Carlo quantique dans sa forme la plus simple, celle du gaz parfait.

Le calcul de l'indice s'est révélé utile, non pas parce que le changement d'indice pouvait révéler l'apparition d'un condensat, mais parce qu'il était important de connaître la valeur de l'indice pour interpréter les images des gaz condensés obtenues par la suite.

2.11 Equations pilote non linéaires et fonctions d'onde stochastiques

Les années 1990 ont vu l'apparition dans la littérature d'équations pilote non linéaires décrivant de façon approchée la dynamique dissipative des atomes (émission spontanée) en présence d'effets collectifs (interactions entre les atomes, effets de statistique quantique). Ces équations sont présentées par leurs auteurs (cf. les travaux de P. Meystre, de W. Zhang et D. Walls) comme les fondements de l'optique atomique non linéaire. En particulier, un comportement de type soliton a été prédit pour la propagation d'un condensat de Bose-Einstein dans un champ lumineux. J'ai développé une réflexion sur ces problèmes avec Klaus Mølmer.

Dans un premier temps, nous avons effectué un travail de clarification, montrant comment retrouver ces équations pilote non linéaires de facon élémentaire, à partir des équations de Maxwell-Bloch [12], ce qui permet une présentation unifiée de l'optique non linéaire et l'optique atomique non linéaire, et identifie clairement l'origine physique de l'effet soliton (déphasage et atténuation du champ à la traversée du nuage atomique). Notre présentation prédit aussi les limites de validité des équations pilote non linéaires en question (par exemple, les équations de Maxwell-Bloch ne prennent en compte que la partie cohérente du champ rayonné par les atomes).

Dans un deuxième temps, nous avons étendu l'outil des fonctions d'onde stochastiques, qui a fait preuve de son efficacité dans le cas linéaire, à une classe générale d'équations pilote non linéaires (incluant celles de l'optique atomique non linéaire). Cette extension a posé des problèmes assez techniques de convergence de la simulation vers le résultat exact (les fonctions d'onde stochastiques étant maintenant rendues statistiquement corrélées par les termes non linéaires). Nous avons appliqué cette nouvelle technique au refroidissement laser de bosons piégés (qui a permis de justifier certains aspects du modèle de "laser à atomes" de la section suivante) [16].

Ce domaine de recherche, progressivement délaissé depuis 1995 au profit de la non linéarité contenue dans l'équation de Gross-Pitaevskii et due aux interactions entre atomes dans l'état fondamental, semble connaître ces dernières années une certaine reprise.

2.12 Peut-on obtenir la condensation de Bose-Einstein par refroidissement laser ?

Un enjeu important du refroidissement d'atomes par laser était la préparation d'échantillons atomiques dans lesquels les effets de dégénérescence quantique, liés à la statistique bosonique ou fermionique, ne sont pas négligeables. Au Laboratoire Kastler Brossel, cet

enjeu a motivé le développement de techniques de refroidissement sous l'énergie de recul (températures très inférieures au μK) et de pièges non dissipatifs.

Avec Jean Dalibard et Maxim Olshanii, j'ai développé un modèle simple prenant en compte les effets de statistique quantique sur le refroidissement. Dans le cas des bosons, la dynamique ressemble alors à celle d'un laser : l'émission stimulée d'atomes dans le mode du piège de durée de vie la plus longue augmente l'efficacité du refroidissement et peut conduire à la formation d'un condensat de Bose-Einstein hors d'équilibre thermodynamique, une sorte de "laser à atomes" [68].

Comme le laser ordinaire, ce système présente une condition de seuil, dont nous avons montré qu'elle est difficile à satisfaire dans les conditions expérimentales habituelles, à cause de la réabsorption des photons de fluorescence chargés d'évacuer l'énergie du système, qui se produit avec une section efficace σ importante, indépendante de la fréquence du laser et de l'ordre de λ^2, où λ est la longueur d'onde optique [68].

J'ai confirmé cette prédiction sur la valeur de σ (paradoxale lorsque la lumière laser est loin de résonance) par l'analyse des résultats expérimentaux obtenus au Laboratoire sur les "réseaux gris", qui montrent en effet [15] l'existence d'un terme de chauffage dépendant du nombre d'atomes dans le gaz.

Nous avons étudié quelques scénarii permettent de réduire la valeur de σ. En collaboration avec Ignacio Cirac (à l'époque à Innsbruck) et Maciej Lewenstein, nous avons montré en particulier qu'il est possible de jouer sur le taux de pompage optique (l'un des paramètres du refroidissement laser) pour réduire la réabsorption des photons de fluorescence. Lorsque le taux de pompage devient plus faible que les fréquences d'oscillation des atomes dans le piège, l'on doit pouvoir atteindre le seuil de condensation avec une probabilité de réabsorption très petite [24]. Cette prédiction a reçu une confirmation expérimentale partielle par un groupe japonais, qui s'est approché très près de la condensation de Bose-Einstein par refroidissement laser d'un gaz sur une raie étroite.

L'obtention d'un condensat par refroidissement par évaporation a mis en veilleuse cette ligne de recherche.

Chapitre 3

Les travaux sur les condensats de Bose-Einstein

Les numéros entre crochets font référence à la liste de mes publications, fournie en fin de document.

3.1 La cohérence de phase : aspects fondamentaux, aspects pratiques

3.1.1 Effet Josephson : couplage cohérent entre deux condensats

L'obtention expérimentale au JILA de deux condensats d'états internes différents mais dans un même piège magnétique a rendu à nouveau pertinente l'étude de l'effet d'un couplage entre deux condensats. Cette situation est analogue à celle rencontrée en physique de la matière condensée, cf. l'apparition d'un courant alternatif par couplage tunnel entre deux superfluides (effet Josephson). L'avantage des systèmes atomiques est la connaissance expérimentale parfaite de tous les paramètres, l'existence d'une théorie entièrement microscopique, et la possibilité d'étudier le couplage dans le cas résonnant (les deux condensats avant couplage ont le même potentiel chimique).

En collaboration avec Maxim Olshanii, Ralph Dum et Isabelle Bouchoule, j'ai obtenu une solution analytique à l'équation de Gross-Pitaevskii pour l'évolution de deux condensats en couplage faible résonnant. Ceci détermine l'amplitude et la période des oscillations du nombre de particules dans chacun des condensats. Dans le cas de deux condensats séparés par une barrière, nous avons également déterminé par une approche semi-classique la valeur du couplage tunnel compte tenu des interactions entre les particules.

Toutes ces prédictions sont en accord avec la résolution numérique d'un modèle à une dimension. Ce travail a fait l'objet de présentation d'affiches, mais pas de publication.

3.1.2 Phase atomique et approche de Bogoliubov : au-delà de la brisure de symétrie $U(1)$

Le concept de brisure de symétrie $U(1)$ pour un condensat de Bose-Einstein (existence d'une valeur moyenne non nulle de l'opérateur champ atomique) est considéré comme fondamental en physique de la matière condensée : on associe ainsi à un condensat de Bose-Einstein un champ atomique classique mettant immédiatement en évidence ses propriétés de cohérence, et qui est l'analogue du champ électromagnétique classique utilisé

en optique dans la description d'un faisceau laser. De plus, une symétrie brisée donne automatiquement naissance à un mode de Goldstone, dont l'existence fournit en général une information précieuse sur la dynamique du système. Pour les condensats, le mode de Goldstone conduit à la prédiction d'une durée de cohérence finie de la phase atomique pour un système de taille finie [22,23].

Cependant, la brisure de symétrie $U(1)$ est introduite de force dans le formalisme. Cette introduction de force est-elle nécessaire pour compléter un formalisme insuffisant, ou le formalisme quantique habituel permet-il de faire l'économie d'un choix arbitraire d'une phase pour le condensat ?

Pour répondre à cette question, nous avons étudié en détail l'expérience de pensée consistant à faire interférer deux condensats n'ayant initialement aucune relation de phase bien définie entre eux [20]. Dans le point de vue quantique habituel, l'état initial du système est décrit par un état de Fock à N particules dans le condensat 1 et à N particules dans le condensat 2. Dans le point de vue brisure de symétrie, l'état initial du système est décrit pour une réalisation expérimentale donnée par un état cohérent d'amplitude $N^{1/2}\exp(i\theta_1)$ dans le mode du condensat 1 et d'amplitude $N^{1/2}\exp(i\theta_2)$ dans le mode du condensat 2, les phases θ_1 et θ_2 variant de façon aléatoire d'une réalisation expérimentale à l'autre. A l'aide de la théorie de la mesure en continu, nous avons prouvé que les descriptions avec et sans brisure de symétrie sont équivalentes à la limite d'un grand nombre de particules N, c'est-à-dire qu'elles prédisent toutes deux un phénomène d'interférence entre les deux condensats si l'on les fait se recouvrir spatialement. Cette prédiction a été confirmée par la suite lors d'une expérience du groupe de Wolfgang Ketterle au MIT.

De plus, le phénomène de brouillage de phase de deux condensats ayant cette fois une phase initiale relative bien définie, phénomène que l'on obtient dans le point de vue à symétrie brisée comme une conséquence de l'existence d'un mode de Goldstone, se produit également dans le point de vue habituel sans brisure de symétrie et y obtient une interprétation physique claire [20,22,23].

Un autre argument est avancé parfois pour justifier la nécessité d'une brisure de symétrie $U(1)$. Il s'agit de la méthode de Bogoliubov qui, dans sa formulation originelle, remplace l'opérateur champ dans le mode du condensat par un nombre complexe. Nous avons montré que la méthode de Bogoliubov peut être construite de façon parfaitement rigoureuse sans brisure de symétrie $U(1)$ [23], en utilisant de façon systématique comme petit paramètre la fraction d'atomes non condensés ; la formulation que nous avons obtenue apporte une justification sérieuse à l'équation de Gross-Pitaevskii, et permet de calculer la première correction à l'équation de Gross-Pitaevskii sur la fonction d'onde du condensat (même dans le cas dépendant du temps) ; dans la description de la partie non condensée du gaz, elle est en fait plus précise que la formulation habituelle dans le régime où les quanta d'oscillation des atomes dans le piège ne sont pas négligeables devant l'énergie d'interaction par particule ; elle a l'avantage de supprimer la divergence linéaire en temps des fluctuations de phase due au mode de Goldstone dans la théorie à symétrie brisée. Ce travail, pourtant assez formel et de lecture difficile, connaît un certain succès et a été remarqué en particulier par Anthony Leggett et Lev Pitaevskii.

En conclusion, la brisure de symétrie $U(1)$ est donc un outil commode mais non indispensable pour décrire les condensats.

3.1.3 Dynamique de phase d'un mélange de deux condensats

Des expériences effectuées au JILA ont préparé deux condensats avec une phase relative bien déterminée, puis ont mesuré la durée de vie de cette cohérence de phase. Les deux

condensats du JILA correspondaient à deux états atomiques internes différents. Ils étaient piégés dans le même potentiel et interagissaient fortement entre eux ; ceci rendait inapplicables les prédictions de temps de cohérence de phase disponibles dans la littérature, car elles étaient établies pour des condensats spatialement séparés.

Nous avons donc étendu les études théoriques de dynamique de phase au cas de deux condensats en interaction mutuelle [31].

Dans le cas où la constante de couplage décrivant les interactions entre atomes de condensats différents est inférieure aux constantes de couplage décrivant les interactions entre atomes d'un même condensat, il existe une solution particulière stable des équations du mouvement correspondant à une pulsation en phase des deux condensats. Cette solution est une généralisation à deux condensats de la solution dite du changement d'échelle pour un condensat (voir plus loin). Elle permet d'obtenir des prédictions analytiques simples sur la cohérence de phase du mélange. On trouve que le temps de cohérence de phase peut être considérablement allongé par rapport au cas de condensats séparés lorsque les constantes de couplage ont des valeurs proches les unes des autres [31].

Dans le cas du JILA, la valeur de la constante de couplage mutuelle se trouve entre les constantes de couplage internes à chaque condensat. La solution analytique précédente n'étant pas applicable, nous avons effectué une étude numérique. Le temps de cohérence maximal prédit excède le temps mesuré de plus d'un ordre de grandeur. Ce désaccord avec l'expérience peut être ramené à un facteur trois seulement si l'on inclut les fluctuations du nombre de particules d'une réalisation de l'expérience à l'autre [31].

3.1.4 Les résurgences de phase entre deux condensats sont-elles observables ?

Comme nous l'avons vu, une propriété importante des condensats (en particulier pour leurs applications en optique atomique) est celle de leur cohérence de phase. Nous avons prédit avec Jean Dalibard que les interactions entre atomes conduisent à un brouillage de la phase relative de deux condensats, suivi aux temps longs d'une résurgence sur la phase atomique [20].

Alors que le brouillage est un phénomène essentiellement classique du point de vue du champ atomique, la résurgence est une caractéristique quantique du champ, qu'il serait très joli d'observer, mais qui est très sensible à la décohérence.

Nous avons étudié l'effet d'un mécanisme de décohérence intrinsèque, qui subsiste même en cas de couplage très faible des condensats à leur environnement, l'effet des pertes d'atomes du condensat par collisions inélastiques à deux corps ou trois corps [25]. Nous avons montré que l'amplitude de la résurgence de phase est supprimée exponentiellement, en $\exp[-n]$, où n est le nombre total moyen de collisions inélastiques survenues dans le gaz jusqu'à l'instant de la résurgence.

L'observation expérimentale doit être possible, en particulier depuis l'avènement des micro-puces à atomes, dans un système à petit nombre d'atomes (quelques centaines) dans un très bon vide, avec deux condensats assez symétriques en nombre d'atomes et mode spatial. Dans le cas limite de deux ou trois atomes par mode, pour des atomes piégés aux nœuds d'un réseau optique, les résurgences prévues ont effectivement été observées dans le groupe de T. Hänsch et I. Bloch.

3.1.5 Vers une source cohérente et continue d'ondes de matière

Comme plusieurs groupes l'ont montré, il est possible d'obtenir une source cohérente d'ondes de matière en provoquant, à l'aide d'un champ électromagnétique, une fuite cohérente d'atomes en dehors d'un condensat piégé. Une telle source est cependant pulsée, puisqu'elle se tarit lorsque tous les atomes du condensat ont été extraits du piège. Son flux moyen est limité par le temps de préparation d'un condensat (de l'ordre de la seconde) et par le nombre d'atomes condensés (de l'ordre d'un million).

Il serait intéressant, en particulier pour des applications d'optique atomique, de disposer d'une source cohérente continue d'ondes de matière, avec un flux le plus élevé possible. Le schéma que nous avons proposé consiste à injecter continûment des atomes d'une mélasse en mouvement dans un guide magnétique, et à effectuer du refroidissement par évaporation dans le guide magnétique [32].

Par résolution de l'équation de Boltzmann pour un gaz classique, nous avons déterminé la longueur du guide requise pour atteindre le régime quantique dégénéré. Pour des valeurs *a priori* réalistes de température, densité et vitesse d'entraînement du nuage atomique injecté dans le guide, les longueurs requises sont de quelques mètres [32].

Nous avons ensuite cherché à prédire les propriétés de cohérence du jet en régime quantique dégénéré, sous l'hypothèse que le gaz a atteint l'équilibre thermodynamique dans un référentiel en mouvement à la vitesse moyenne du jet.

Dans le modèle du gaz parfait, nous trouvons que le gaz subit une condensation de Bose-Einstein transverse, c'est à dire qu'une fraction importante des particules du gaz se trouve dans l'état fondamental du mouvement harmonique transverse à l'axe du guide magnétique [32]. En termes d'opticien, le jet atomique peut devenir quasi-monomode transverse. Le long de l'axe du guide, la longueur de cohérence du gaz est proportionnelle au produit de la longueur d'onde thermique au carré et de la densité linéique d'atomes dans le condensat transverse. A température fixée, elle est donc bien plus grande que la longueur de cohérence d'un gaz classique, qui n'est autre que la longueur d'onde thermique.

En revanche, le gaz parfait est sujet à d'importantes fluctuations de densité le long de l'axe du guide, dues au phénomène de groupement bosonique bien connu pour les sources lumineuses thermiques (voir l'expérience de Hanbury-Brown et Twiss). Nous avons donc pris en compte, dans un second article [33], l'effet des interactions entre les atomes, à l'aide d'un modèle de gaz unidimensionnel. Lorsque les interactions sont assez répulsives, il devient énergétiquement défavorable d'introduire des inhomogénéités dans la distribution spatiale des atomes : les fluctuations de densité du jet sont fortement réduites. Les fluctuations de phase du champ atomique, et donc la longueur de cohérence du jet, sont par contre peu affectées par les interactions.

Une expérience de "laser à atomes" en cours au Laboratoire, sous la direction de Jean Dalibard et David Guéry-Odelin.

3.2 Dynamique non linéaire et équation de Gross-Pitaevskii dépendant du temps

3.2.1 Dynamique non linéaire d'un condensat piégé : solution par changement d'échelle

En présence des interactions, le mode $|\phi\rangle$ dans lequel les atomes se condensent peut être déterminé à température nulle par l'équation de Gross-Pitaevskii (équation de Schrödinger

non linéaire) qui prend en compte, au niveau de l'approximation de champ moyen, l'effet des interactions entre les atomes du condensat.

La plupart des résultats expérimentaux sur les condensats depuis 1995 ont utilisé la technique du temps de vol pour prendre des images : le piège contenant le condensat est coupé brutalement, et la densité du nuage atomique est mesurée après une durée ajustable d'expansion libre. Préalablement à la coupure du piège, le condensat peut être porté, par modulation des fréquences du piège, dans un état collectivement excité dépendant du temps $|\phi(t)\rangle$.

En cherchant à analyser ces expériences, ce qui nécessite la prise en compte des interactions atomiques, je suis parvenu, en collaboration avec Ralph Dum, à obtenir une solution approchée analytique de cette équation à l'aide de changements d'échelle et de jauge qui absorbent l'essentiel de la dépendance temporelle de $|\phi(t)\rangle$ [17]. Cette solution est en fait exacte dans la limite dite de Thomas-Fermi, où l'énergie d'interaction par atome condensé est beaucoup plus grande que le quantum d'oscillation d'un atome dans son piège.

Cette solution nous donne d'abord la forme du nuage en expansion après ouverture du piège ; nous avons ainsi pu faire un ajustement des temps de vol effectués au MIT et déterminer la longueur de diffusion a du sodium, paramètre crucial de la théorie caractérisant le potentiel d'interaction atomique. Le résultat est en excellent accord avec des mesures directes de a effectuées indépendamment (i.e. en l'absence de condensat) [17].

Notre solution analytique permet également de prédire, sans paramètre ajustable, la fréquence et l'amplitude des oscillations du condensat observées au MIT. Il y a très bon accord avec les mesures [17].

Depuis la publication de ce travail, ces transformations d'échelle reçoivent une application très large dans les laboratoires étudiant les condensats de Bose-Einstein. C'est que la plupart des condensats dans le monde sont dans le régime de Thomas-Fermi et sont piégés dans des potentiels harmoniques !

Nous avons découvert une application intéressante des transformations d'échelle, l'étude de la dynamique d'un système quantique macroscopique porté dans un état très excité, loin de l'équilibre thermodynamique. Les condensats, parce qu'ils sont très faiblement couplés à leur environnement, constituent la réalisation expérimentale idéale d'un tel problème !

Nous avons caractérisé la première étape de cette dynamique à basse température, dans le cas de condensats piégés excités par modulation temporelle des constantes de raideur du piège harmonique [21], technique expérimentalement bien maîtrisée. L'outil théorique utilisé est celui de la transformation de Bogoliubov sans brisure spontanée de symétrie $U(1)$ [23].

Le premier régime consiste en le cas d'excitations de faible énergie, la vitesse du condensat excité ne dépassant pas la vitesse du son. Ce régime correspond à un point de quasi-intégrabilité de l'équation de Gross-Pitaevskii ; l'évolution du condensat est une succession régulière de dilatations et compressions, prédites par la transformation d'échelle, avec un temps d'amortissement relativement long prédit par la théorie de Bogoliubov.

Le second régime est atteint au-delà d'un seuil d'énergie d'excitation. L'évolution du condensat devient instable ; nous avons déterminé analytiquement les premiers modes instables et leur exposant de Lyapunov, à l'aide de la transformation d'échelle. La fonction d'onde du condensat peut devenir chaotique, avec un amortissement rapide des compressions-dilatations par transfert d'énergie vers ces modes instables. Cette étude présente un autre intérêt qui nous a été indiqué plus tard, son lien formel avec certains modèles cosmologiques d'univers en expansion !

3.2.2 Dynamique chaotique d'un mélange de deux condensats

La dynamique d'un mélange de condensats ayant des états atomiques de spin différents est plus riche que celle d'un condensat seul, à cause de l'existence de modes de démixion en différentes composantes spatiales.

Une telle dynamique de démixion a été observée au JILA (Boulder). Les deux condensats, se recouvrant spatialement initialement, se séparent en effectuant des oscillations relatives rapidement amorties. L'origine de cet amortissement, qui préservait la cohérence de phase entre les deux condensats (comme l'ont montré les expériences d'interférence du JILA), était inexpliquée.

Nous avons attaqué le problème en résolvant numériquement l'équation de Gross-Pitaevskii pour les deux condensats couplés. Nous avons trouvé que la fonction d'onde des condensats apparaît comme la superposition d'une composante lisse spatialement et évoluant lentement, et d'une composante très bruitée, quasi stochastique, caractérisée par un spectre en fréquence large et quasi-continu [26].

Au moins une partie de l'amortissement des oscillations observé au JILA est due au transfert d'énergie de la composante lisse vers la composante stochastique des fonctions d'onde. La composante lisse assure la préservation des propriétés de cohérence de phase des deux condensats.

3.2.3 Approximation de champ classique pour un gaz de Bose dégénéré

Il est maintenant bien établi qu'à basse température, l'équation de Gross-Pitaevskii (ou équation de Schrödinger non linéaire) donne une description correcte de la fonction d'onde $\phi(\vec{r})$ du condensat dans l'état stationnaire, l'essentiel des effets de température non nulle étant pris en compte par un ajustement du nombre de particules N_0 dans le condensat. Dans le cas dépendant du temps, par exemple lorsque le condensat est excité par une variation du potentiel de piégeage, l'accord avec les résultats expérimentaux est cependant peu satisfaisant, car une fraction même petite d'atomes non condensés, toujours présente dans l'expérience, induit un amortissement des oscillations du condensat non prédit par l'équation de Gross-Pitaevskii.

Nous avons travaillé sur la possibilité de remédier à cette insuffisance en ajoutant à la fonction d'onde macroscopique $N_0^{1/2}\phi(\vec{r})$ initiale du condensat un champ classique représentant les atomes non condensés, et en faisant évoluer le champ total résultant avec l'équation de Gross-Pitaevskii. La non linéarité de l'équation couple alors le condensat à la partie non condensée, induisant un amortissement.

En pratique [39], nous utilisons le formalisme de la représentation de Wigner de l'opérateur densité, bien connu en optique quantique, et qui introduit une quasi-distribution de probabilité $W(\{\psi\})$, fonctionnelle du champ classique $\psi(\vec{r})$. Pour un potentiel d'interaction binaire entre les atomes, les équations du mouvement quantiques pour l'opérateur densité donnent naissance à une équation d'évolution pour $W(\{\psi\}, t)$ avec des dérivées fonctionnelles première et troisième de W par rapport au champ ψ. L'idée intuitive précédemment exposée revient à négliger les termes de dérivée troisième dans l'équation sur W, ce qui devrait être correct dans le cas fortement dégénéré (ψ est 'grand' donc les dérivées d'ordre successif par rapport à ψ sont de plus en plus petites). L'équation obtenue correspond à l'évolution du champ ψ suivant l'équation de Gross-Pitaevskii, et constitue physiquement l'approximation de champ classique au problème de champ quantique initial. Cette méthode approchée, que l'appelle 'Wigner tronqué', pose deux problèmes, le

problème pratique de sa mise en œuvre et le problème fondamental de ses conditions de validité.

La mise en œuvre suppose que l'on soit capable de tirer au sort des champs ψ échantillonnant la distribution de Wigner de l'équilibre thermodynamique initial. Nous avons mis sur pied une procédure Monte-Carlo répondant à ce besoin dans le cadre de l'approximation de Bogoliubov (basse température, interaction faible) [34]. Une retombée de cette formulation est que l'on peut maintenant utiliser la théorie de Bogoliubov sans avoir à diagonaliser numériquement l'opérateur de Bogoliubov, ce qui est un avantage crucial pour les systèmes tridimensionnels sans invariance par rotation.

Qu'en est-il des conditions de validité ? Nous avons d'abord montré que la méthode de 'Wigner tronqué' reproduit correctement les prédictions de la théorie de Bogoliubov dépendant du temps que nous avions développée en 1997, théorie valable cependant seulement aux temps courts. Que se passe-t-il aux temps longs ? Nous avons testé la méthode de 'Wigner tronqué' sur le modèle bien connu de l'amortissement de Beliaev-Landau pour un condensat dans une boîte cubique. Nous avons alors découvert que les prédictions de 'Wigner tronqué' dépendent de l'énergie maximale $\epsilon_{\max}$ des modes du champ inclus dans la simulation, et surestiment le taux d'amortissement lorsque $\epsilon_{\max}$ est trop grand. Cette dépendance en l'énergie de coupure vient du fait que la distribution de Wigner initiale, représentant l'état **quantique** du champ à la température T, n'est pas stationnaire pour l'évolution de champ **classique** donnée par Gross-Pitaevskii : l'équation de Schrödinger non linéaire est ergodique dans une boîte à trois dimensions, si bien que la distribution de ψ se 'thermalise' vers une distribution de champ classique avec une température T_{class}. Comme les fluctuations quantiques du champ sont prises en compte dans le point de vue de Wigner par ajout de bruit classique, on démontre que $T_{\text{class}} > T$ et que T_{class} est une fonction croissante de l'énergie de coupure $\epsilon_{\max}$. Ceci explique l'excès d'amortissement constaté. En pratique, il faut donc se limiter à $\epsilon_{\max}$ de l'ordre de quelques $k_B T$ au plus. Comme on ne peut pas faire tendre $\epsilon_{\max}$ vers zéro sans introduire d'effets de troncature, l'utilisation de Wigner tronqué est limitée aux suffisamment hautes températures [44].

3.3 Les tourbillons quantiques

3.3.1 Condensats stationnaires avec vortex dans des pièges tournants

Une manière de montrer le caractère superfluide des condensats atomiques est de produire des courants de matière permanents, par exemple en étudiant la durée de vie d'un vortex dans un condensat.

La production et l'étude de tourbillons quantiques dans un condensat atomique est une expérience toujours en cours au Laboratoire, sous la direction de Jean Dalibard, mais qui, à l'époque de ce travail, n'avait pas encore abouti. Il était connu à l'époque que les vortex ne sont pas thermodynamiquement stables dans un piège harmonique statique ; en d'autres termes, les vortex ne sont pas des minima locaux d'énergie du système.

Nous avons étudié la possibilité de stabiliser les vortex dans des pièges anisotropes en rotation. Nous avons développé une méthode numérique permettant de chercher des minima locaux de l'énergie ayant un nombre *a priori* quelconque de vortex [29].

Nous avons ensuite développé à deux dimensions une approche variationnelle simple permettant de retrouver avec grande précision les résultats numériques [29]. Dans cette approche variationnelle, un ensemble de k vortex apparaît formellement comme un gaz de k particules fictives dans un potentiel extérieur W et interagissant par un potentiel V

(ici répulsif, car les vortex sont de même charge), la position des particules fictives étant celle des cœurs des vortex.

Lorsque la fréquence de rotation du piège est trop faible, le potentiel W est anti-piégeant, et les cœurs des vortex sont expulsés en dehors du condensat. Lorsque le piège tourne assez vite, W devient piégeant, et l'on obtient des configurations stables à un, puis deux, trois, etc vortex, les cœurs des vortex s'arrangeant sur des cercles concentriques pour minimiser leur énergie de répulsion.

Nous avons également étudié quelques méthodes permettant la mise en évidence expérimentale des vortex [29]. Ces méthodes ont été mises en œuvre au Laboratoire : agrandissement du diamètre des cœurs des vortex par expansion balistique permettant leur observation directe sous forme de trous dans la densité du gaz, et détection de vortex par réalisation d'interférences d'ondes de matière.

3.3.2 Nucléation de vortex dans un condensat de Bose-Einstein en rotation

La réponse d'un superfluide à une mise en rotation est très différente de celle d'un fluide classique : le superfluide ne peut pas développer le champ de vitesse $\vec{v}(\vec{r}) = \vec{\Omega} \wedge \vec{r}$ de la rotation solide à la vitesse angulaire Ω, car son champ de vitesse, dérivant d'un gradient, doit être irrotationnel. Le superfluide peut cependant réagir en formant des tourbillons quantiques, ou vortex, qui sont des lignes de singularité rotationnelles du champ de vitesse.

Ce phénomène de formation de vortex par mise en rotation, observé dans les condensats atomiques gazeux (cf. les expériences dans le groupe de Jean Dalibard au Laboratoire), est étudié depuis longtemps dans l'hélium superfluide. Les condensats gazeux offrent cependant l'avantage d'être très bien isolés de leur environnement (contrairement à l'hélium superfluide exposé aux fluctuations thermiques de son récipient) et de pouvoir être soumis aux méthodes d'imagerie performantes de la physique atomique. Ils sont donc le système rêvé pour étudier et élucider totalement le processus de nucléation de vortex lors de la mise en rotation.

Ce problème de nucléation de vortex dans les gaz atomiques a tenu en haleine une bonne partie de la communauté internationale travaillant sur les condensats. Les résultats expérimentaux obtenus par l'équipe de Jean Dalibard contredisent en effet les prédictions théoriques développées pour les gaz par directe analogie avec le cas de l'hélium superfluide. D'abord, la fréquence de rotation minimale conduisant à l'apparition d'un vortex est deux fois plus élevée dans l'expérience que dans les premières prédictions théoriques. Ensuite, la nucléation de vortex dans l'expérience se produit dans un petit intervalle de fréquences de rotation, alors que l'approche thermodynamique ne prédit pas de borne supérieure pour la fréquence de rotation.

Nous sommes parvenu à identifier un mécanisme de nucléation à l'œuvre dans les expériences de Jean Dalibard. Le mécanisme que nous proposons, au lieu d'être de nature thermodynamique comme dans le cas de l'hélium, est purement dynamique et repose sur une instabilité de type hydrodynamique se développant dans le gaz sous l'effet du potentiel tournant appliqué. Nous avons dérivé, à partir de l'équation de Gross-Pitaevskii sur la fonction du condensat, des équations hydrodynamiques approchées, similaires à celles d'un fluide classique sans viscosité, et reproduisant de façon fort satisfaisante les résultats expérimentaux [40]. Ce mécanisme explique immédiatement pourquoi la nucléation de vortex se produit dans un petit intervalle de fréquence de rotation : l'instabilité dynamique se déclenche seulement si la perturbation tournante appliquée est suffisamment proche de résonance avec un mode propre du condensat. Une conclusion importante de notre étude

est que la valeur de la fréquence de nucléation des vortex n'est pas universelle, mais dépend explicitement du procédé de mise en rotation du gaz.

3.3.3 Formation du réseau de vortex dans un condensat de Bose-Einstein en rotation

Après avoir identifié le mécanisme de nucléation des vortex, il nous restait à démontrer que les vortex ainsi produits pouvaient bien s'arranger en un réseau stationnaire au bout d'un certain temps d'évolution. En effet, plusieurs auteurs ont contesté la possibilité que notre mécanisme d'instabilité dynamique puisse seul expliquer la formation d'un réseau, et ont affirmé qu'un phénomène supplémentaire devait être identifié. En particulier, un consensus s'était établi entre différents groupes, selon lequel l'équation de Gross-Pitaevskii seule ne pouvait expliquer la cristallisation du réseau de vortex, cette équation devant alors être complétée par un terme d'amortissement phénoménologique non hamiltonien.

Nous avons donc effectué une intégration numérique complète de l'équation de Gross-Pitaevskii à trois dimensions, sans aucun terme dissipatif ajouté, dans un potentiel harmonique anisotrope dans le plan $x - y$ et dont la vitesse de rotation est progressivement accrue jusqu'à une valeur limite. Aux fréquences de rotation inférieures à la valeur critique prédite analytiquement, aucun vortex n'entre dans le condensat. Aux fréquences de rotation supérieures, la fonction d'onde devient turbulente, des vortex entrent brutalement dans le condensat et, au bout d'un certain temps, s'arrangent en un réseau triangulaire, avec de légères fluctuations résiduelles de la position des vortex.

Une équation conservative et invariante par renversement du temps, comme l'équation de Gross-Pitaevskii, peut donc bien prédire la formation d'un réseau ordonné de vortex, le point clé étant que l'instabilité dynamique crée une composante turbulente du champ, en peuplant des modes d'énergie élevée qui peuvent ensuite jouer le rôle d'un réservoir vis-à-vis du condensat et lui ôter de l'énergie. Un autre point important est que le champ $\psi(\mathbf{r}, t)$ solution de l'équation de Gross-Pitaevskii ne représente plus un condensat pur ; la fonction de cohérence du premier ordre doit maintenant être définie comme la moyenne temporelle de $\psi^*(\mathbf{r}, t)\psi(\mathbf{r}', t)$, si bien que la partie bruitée du champ ne contribue pas au mode du condensat.

Nous avons également étudié la formation du réseau de vortex pour une température initiale non nulle du gaz, à l'aide des techniques de champ classique mentionnées au 3.2.3 : on intègre encore l'équation de Gross-Pitaevskii, mais avec un champ initialement bruité. Nous trouvons dans ce cas que l'apparition des vortex se fait suivant le scénario thermodynamique de type Landau, supposant que le gaz est à l'équilibre thermique dans le référentiel tournant : lorsque le condensat sans vortex n'est plus un minimum local d'énergie à la fréquence de rotation considérée, on constate numériquement qu'un vortex entre lentement dans le condensat en spiralant jusqu'au centre du piège ; un second vortex peut ensuite rejoindre le premier et former un 'réseau' à deux vortex ; puis un troisième vortex entre, etc. Notons que ce scénario thermodynamique n'a pas encore été observé expérimentalement, probablement à cause d'une anisotropie non tournante du piège capable d'empêcher la mise en rotation du nuage non condensé. Ce travail a fait l'objet d'une publication [51].

3.3.4 Condensats stationnaires avec un vortex dans un piège très allongé

Dans l'expérience de Jean Dalibard au Laboratoire, le condensat avec vortex est piégé dans un potentiel harmonique de deux ordres de grandeur moins raide le long de l'axe de rotation z que dans le plan transverse. Il a été découvert numériquement par deux chercheurs espagnols, Perez-Garcia et Garcia-Ripoll, que la solution de l'équation de Gross-Pitaevskii d'énergie minimale dans le référentiel tournant n'est alors pas un vortex droit, mais un vortex courbé.

Nous avons donc étudié la configuration d'équilibre d'un vortex unique dans un condensat cigare. Nous avons appliqué d'abord la très efficace méthode du gradient conjugué pour confirmer les prédictions de Perez-Garcia et Garcia-Ripoll et pour construire le diagramme de phase complet de la ligne de vortex en fonction du rapport d'aspect du condensat et de la fréquence de rotation. Nous avons ensuite écrit une fonctionnelle énergie approchée dépendant seulement de la forme de la ligne de vortex, en collaboration avec un groupe de mathématiciens appliqués de l'Université de Paris 6.

Cette fonctionnelle énergie nous a permis d'obtenir une prédiction analytique de la fréquence critique de rotation au-delà de laquelle le vortex courbé apparaît, en excellent accord avec le calcul numérique, et d'expliquer l'origine physique de la courbure de la ligne. Nous avons montré en effet qu'un condensat cigare peut être vu approximativement comme la superposition continue de condensats à deux dimensions, chacun correspondant à une tranche du condensat tridimensionnel parallèle au plan $x - y$ et ayant donc une densité dépendant de la cote z. Or l'on sait qu'à deux dimensions, le cœur du vortex, pour minimiser son énergie, se place soit à l'infini (pour des fréquences de rotation Ω inférieures à une valeur critique Ω_c^{2D}) soit sur l'axe de rotation (pour $\Omega > \Omega_c^{2D}$). Une propriété importante de la fréquence critique Ω_c^{2D} est qu'elle est une fonction décroissante de la densité : les tranches 2D de cote z proche de 0 ont une faible fréquence critique de rotation, les tranches 2D proches des extrémités du cigare ont une fréquence critique élevée. Nous comprenons ainsi pourquoi la ligne de vortex minimisant l'énergie à 3D est en forme de fer à cheval : la ligne se trouve sur l'axe de rotation dans la zone où Ω est supérieure à la fréquence critique locale Ω_c^{2D} (zone de faible $|z|$) et part à l'infini radialement dans la zone où Ω est inférieure à la fréquence critique locale.

De plus, notre fonctionnelle simplifiée nous a permis de découvrir un point selle de l'énergie correspondant à une ligne de vortex stationnaire mais non minimum local de l'énergie dans le référentiel tournant. Nous avons montré que ce point selle est cependant un minimum de l'énergie à moment cinétique total fixé, ce qui une illustration marquante de la non équivalence de deux ensembles thermodynamiques, l'un à vitesse de rotation fixée (ensemble 'grand canonique' supposant le couplage du condensat à un réservoir de moment cinétique) et l'autre à moment cinétique fixé (ensemble 'canonique' décrivant un condensat isolé c'est-à-dire dans un environnement invariant par rotation). Ce travail a fait l'objet d'une publication [46].

Depuis, le vortex courbé a été observé expérimentalement dans le groupe de Jean Dalibard, révélant en particulier l'existence de la branche 'point selle'.

3.4 Au-delà du champ moyen : Monte-Carlo quantique

3.4.1 Distribution de paires dans un condensat de Bose-Einstein

Les propriétés statiques à un corps des condensats sont maintenant assez bien connues expérimentalement (mesures de la densité dans l'espace des positions, dans l'espace des impulsions). Les distributions à deux corps n'ont encore été étudiées que partiellement.

Nous avons développé des méthodes simples partant d'approximations de type champ moyen (approche de Hartree-Fock, approche de Bogoliubov) pour déterminer la distribution à deux corps des atomes, en fonction de la température. L'effet du piégeage dans un potentiel harmonique est inclus par une approximation de densité locale [27].

Les expressions analytiques obtenues ont été comparées à un calcul de type Monte-Carlo quantique, virtuellement exact. L'accord est très bon, et constitue à basse température un test sérieux de l'approche de Bogoliubov [27].

3.4.2 De nouvelles méthodes Monte-Carlo quantiques

Il existe une méthode bien connue en physique statistique, la méthode Monte-Carlo quantique (Path Integral Monte Carlo) pour déterminer de manière exacte les propriétés à l'équilibre thermodynamique d'un système de bosons en interaction. Cette méthode est basée sur une formulation du problème en première quantification dans la représentation position : elle consiste essentiellement à échantillonner la distribution en position des N bosons.

Nous avons développé une nouvelle méthode Monte-Carlo quantique, basée sur une formulation totalement différente : il s'agit d'une méthode de champ stochastique formulable directement en seconde quantification et échantillonnant l'opérateur densité à N corps par des états de Hartree-Fock ayant une évolution stochastique continue de type mouvement brownien [41]. Cette méthode repose sur le fait que l'état d'équilibre thermodynamique dans l'ensemble canonique à la température T peut être vu comme le résultat d'une évolution du système en temps imaginaire pendant une 'durée' $\beta = 1/k_B T$. Il nous a suffi alors de généraliser au temps imaginaire la reformulation exacte en termes de mouvement brownien d'états de Hartree-Fock que nous avions donnée du problème à N corps pour l'évolution en temps réel [36], et dont nous avons approfondi depuis la remarquable propriété d'admettre un bruit statistique fini à tout temps fini [48].

Les avantages de cette nouvelle approche sur la méthode Monte-Carlo quantique traditionnelle sont doubles :

- la formulation directe en seconde quantification rend notre approche applicable aussi bien aux bosons qu'aux fermions, comme montré par Philippe Chomaz et Olivier Juillet (LPC/ISMRA et GANIL). La méthode traditionnelle n'est au contraire pas adaptée au problème fermionique.
- l'échantillonnage dans l'espace de Hilbert plutôt que dans l'espace des positions permet de se libérer de la contrainte d'avoir un Hamiltonien avec des éléments de matrice réels en représentation position, ce qui permet directement de traiter de manière exacte les systèmes en rotation.

Cette nouvelle approche, plus générale, est cependant moins performante que la méthode Monte-Carlo traditionnelle dans le cas spécifique de bosons avec un Hamiltonien réel en point de vue position : dans ce cas, la complexité de la méthode traditionnelle n'est plus exponentielle mais probablement polynômiale en le nombre de particules.

Nous avons appliqué notre approche à des modèles simples à une dimension [41], par exemple pour déterminer de manière exacte la distribution de probabilité du nombre de particules dans un condensat de Bose-Einstein, en particulier au voisinage de la température de transition [47], mais aussi pour tester la superfluidité du gaz de Bose à une dimension [52].

Récemment, certaines expériences ont mis en évidence des phases de bosons dites fortement corrélées, en ce sens que des corrélations très fortes existent entre les positions des bosons. Citons l'observation de la transition d'un superfluide à un isolant de Mott pour un gaz de Bose dans un réseau optique, dans le groupe de T. Hänsch, ou l'obtention d'un gaz de bosons impénétrables à une dimension, ce que l'on appelle le gaz de Tonks-Girardeau. Notre méthode Monte-Carlo, basée sur un ansatz de Hartree-Fock stochastique, est peu performante dans le cas d'une phase de Mott et inapplicable dans le cas de bosons impénétrables (le potentiel d'interaction étant alors non borné). Dans le cas d'une phase de Mott, on sait qu'une théorie de champ moyen basée sur la version bosonique de l'ansatz de Gutzwiller donne de bons résultats. Nous avons donc développé une nouvelle reformulation exacte du problème à N corps en termes d'un ansatz de Gutzwiller stochastique. Nous avons démontré son efficacité sur un modèle sur réseau à 1D, incluant le cas de bosons impénétrables [50].

3.5 En dimensionalité réduite

3.5.1 Condensats de Bose-Einstein solitoniques à une dimension : au-delà du champ moyen

A l'époque de ce travail, les condensats de Bose-Einstein avec interactions effectives attractives entre les atomes (cas d'une longueur de diffusion négative) avaient été peu étudiés expérimentalement. Ils nous semblaient posséder des propriétés intéressantes à une dimension (le système devient quasi 1D selon z dans le cas d'un confinement fort des atomes dans le plan $x-y$), régime que nous avons donc étudié avec Christopher Herzog [37].

Ainsi, à température nulle, le condensat serait l'équivalent pour les ondes de matière du soliton optique bien connu dans les fibres ; ce serait une sorte de super-atome, état lié à N atomes.

Nous avons donné d'abord une description du soliton dans un point de vue brisure de symétrie, la symétrie brisée étant l'invariance par translation spatiale. Puis, tirant parti de l'intégrabilité du problème à N corps dans un système homogène unidimensionnel avec des interactions en delta de Dirac, nous avons déterminé le spectre exact du hamiltonien du gaz ; nous trouvons que les états excités du système sont formés d'un nombre quelconque de solitons (composés chacun d'un nombre arbitraire d'atomes). Ces états excités constituent une généralisation originale de l'ansatz de Bethe au cas de vecteurs d'onde complexes et permettent de tester la théorie à symétrie brisée [37].

3.5.2 Condensats de Bose-Einstein solitoniques à une dimension : la première observation expérimentale

Les solitons atomiques, prévus depuis longtemps théoriquement, ont été observés pour la première fois en 2002, dans le groupe de Christophe Salomon au Laboratoire [42]. Cette première a eu lieu seulement six ans après l'obtention du premier condensat à interactions

attractives car la mise en évidence probante du soliton était considérée comme très difficile expérimentalement : le soliton a typiquement une taille bien inférieure à la résolution (quelques μm) du système optique standard utilisé pour faire une image du condensat.

Notre contribution à ce travail est d'avoir proposé une signature incontestable de la présence d'un soliton : l'absence d'étalement du paquet d'ondes en présence d'un potentiel harmonique anti-piégeant suivant l'axe z. Dans le cas d'interactions répulsives ou nulles entre les atomes, la taille du nuage croît exponentiellement en temps, avec un exposant parfaitement connu. L'absence de croissance exponentielle de la taille du nuage, facile à mettre en évidence expérimentalement (il suffit d'attendre assez longtemps !), démontre au contraire que le gaz est dans un état lié collectif.

D'un point de vue plus fondamental, la dynamique d'un condensat solitonique dans un potentiel harmonique anti-piégeant présente des propriétés intéressantes, qui n'avaient à notre connaissance pas été étudiées dans la littérature :

- une excitation du condensat est amortie exponentiellement en temps par émission de particules hors du soliton (et non pas comme l'inverse du temps pour un soliton en l'absence de potentiel extérieur). Ceci permet en pratique d'obtenir un condensat presque pur, débarrassé de son 'nuage thermique'
- le soliton subit une lente évaporation quantique de particules, due au fait que le potentiel extérieur tend vers $-\infty$ à l'infini. Le soliton maigrit, puis explose brutalement lorsque les forces attractives internes ne peuvent plus compenser le potentiel répulsif.

Le travail correspondant a fait l'objet de la publication [45].

3.5.3 Extension de la méthode de Bogoliubov aux quasi-condensats

Dans le cas d'un gaz de Bose presque totalement condensé, donc à basse température et faible interaction, la méthode de Bogoliubov permet de prendre en compte de façon systématique les corrections à l'équation de Gross-Pitaevskii, par développement en puissances de la fraction non condensée.

Cependant, dans le cas d'un gaz soumis à un confinement fort selon une ou plusieurs directions de l'espace, la dimensionalité effective du système est réduite et l'on peut ne pas avoir de condensat, même si le gaz est dégénéré, contrairement au cas 3D. Il reste cependant un petit paramètre, l'amplitude des fluctuations de la densité : c'est le régime dit des quasi-condensats. L'idée, bien présente déjà dans la littérature, est alors d'introduire le module et la phase de l'opérateur champ, et de développer le module en puissances des fluctuations de densité sans supposer que les fluctuations de la phase soient petites. La mise en œuvre brutale de cette approche conduit cependant à des divergences ultraviolettes, éliminées au moyen d'une coupure ; certaines observables dépendent alors de cette coupure non physique.

Nous avons mis en œuvre cette approche avec soin. Les positions des atomes sont discrétisées sur un réseau. Le pas du réseau doit être plus petit que la longueur d'onde de de Broglie et la longueur de relaxation pour conduire aux mêmes propriétés que dans l'espace physique continu. Le pas doit être cependant assez grand pour que le nombre moyen d'atomes par nœud soit $\gg 1$, afin de permettre une définition manipulable de l'opérateur phase du champ quantique ! L'interaction sur site doit être choisie avec soin de façon à reproduire la longueur de diffusion du vrai potentiel.

Nous avons abouti ainsi à une approche de Bogoliubov généralisée au cas des quasi-condensats, à la fois élémentaire et rigoureuse. Nous avons testé nos prédictions à 1D, en les comparant avec succès à la méthode relativement impénétrable d'intégrale fonctionnelle

de Popov et aux résultats exacts obtenus à partir de l'ansatz de Bethe. Notre approche est la première à proposer une formule explicite pour la fonction de cohérence du premier ordre valable en dimensions un, deux et trois, indépendante de toute coupure, exempte de toute divergence (infrarouge ou ultraviolette) et redonnant la prédiction habituelle de Bogoliubov en dimension 3.

Ce travail, constituant une partie de la thèse de Christophe Mora, a fait l'objet d'une publication [49].

Nous avons ensuite développé une extension de cette théorie des quasi-condensats au cas d'un gaz sur un tore à 1D, pour lequel il peut exister plusieurs quasi-condensats correspondant à des nombres d'enroulement différents de la phase. L'accord avec le calcul Monte-Carlo quantique est remarquable en ce qui concerne la fraction superfluide du gaz.

La prise en compte des nombres d'enroulement joue un rôle crucial dans la compréhension du caractère superfluide ou pas du gaz de Bose à 1D, sujet de points de vue fortement divisés, certains auteurs concluant à la superfluidité, d'autres non. Nous avons réalisé que l'on est tenté de conclure à la superfluidité du gaz si l'on raisonne pour une valeur fixée du nombre d'enroulement de la phase, et de conclure à l'absence de superfluidité si l'on autorise le peuplage thermique de plusieurs nombres d'enroulement.

Pour clarifier le débat, nous avons enrichi le critère habituel de superfluidité. Ce critère considère l'impulsion moyenne du gaz à l'équilibre thermique dans un repère en mouvement. A 1D, une même valeur moyenne peut cependant être obtenue de façons très variables : comme la somme de contributions très voisines pour différentes réalisations expérimentales, ou comme la somme de contributions variant considérablement d'une réalisation à l'autre. Nous avons donc calculé, à l'aide de la méthode de Bogoliubov étendue, la distribution de probabilité de l'impulsion totale du gaz, qui permet de révéler la présence de courants métastables individuellement superfluides, dans le régime de quasi-condensat, et donc de conclure.

Ceci a fait l'objet d'une publication [52].

Chapitre 4

Les travaux sur les gaz de fermions

Les numéros entre crochets font référence à la liste de mes publications, fournie en fin de document.

4.1 Théorie BCS pour des atomes piégés

À l'époque de ce travail (commencé en 1997), l'expérience dirigée par Christophe Salomon au Laboratoire sur l'atome de lithium 6 (isotope fermionique) en était à ses débuts, mais l'intérêt de chercher à observer la transition BCS, c'est-à-dire la condensation de paires de Cooper d'atomes en présence d'interactions effectives attractives, était déjà clair.

Nous avons donc déterminé la température de transition BCS pour un gaz d'atomes piégés dans le régime d'interaction faible [30]. La nouveauté étant bien entendu due au fait que les atomes étaient piégés, et non pas répartis uniformément dans l'espace libre.

Le calcul était théoriquement intéressant, car il fallait prendre en compte l'interaction entre les atomes d'une manière conduisant à une théorie BCS exempte de divergence ; le seul paramètre microscopique pertinent *a priori* dans le cas atomique est la longueur de diffusion, à l'exclusion d'autres longueurs existant dans le cas des supraconducteurs et fournissant des coupures naturelles dans les intégrales divergentes ; de plus, le caractère inhomogène spatialement rendait les techniques de renormalisation habituelles délicates à mettre en œuvre.

Nous sommes parvenu à une formulation régulière de la théorie BCS à l'aide du modèle du pseudo-potentiel de Fermi, introduit à l'origine en physique nucléaire. Ce modèle est excellent dans le cas d'une interaction ayant une longueur de diffusion beaucoup plus grande que la portée du potentiel (cas attendu expérimentalement).

Nous avons pu ainsi faire un calcul entièrement quantique de la température de transition BCS, en prenant en compte le caractère discret des niveaux d'énergie vibrationnels des atomes dans le piège. Ceci nous a permis de tester les approximations semi-classiques (de densité locale) et de confirmer le caractère non totalement irréaliste expérimentalement de la température à atteindre. Nous reviendrons sur ce point plus bas.

4.2 Signature d'une transition BCS dans un gaz d'atomes fermioniques dans le régime de Knudsen

A la fin des années 90, il était déjà clair qu'un des défis expérimentaux à venir serait l'observation de la transition BCS dans un gaz d'atomes fermioniques, c'est-à-dire

la condensation de paires de fermions de composantes de spin opposées sous l'effet d'interactions attractives et d'une basse température. Nous avons donc recherché des effets physiques caractéristiques de la transition BCS pour des atomes neutres, qui permettent à la fois de tester la théorie BCS et de mettre en évidence expérimentalement la transition de phase correspondante.

Nous avons identifié un tel effet dans le régime de Knudsen (*collisionless* en anglais) où le taux d'amortissement des modes d'excitation du gaz est bien plus faible que leur fréquence propre : la présence d'un condensat de paires dans un système homogène spatialement conduit à l'apparition dans le spectre d'excitation du gaz d'une branche de type phonon, c'est-à-dire avec une relation de dispersion linéaire aux faibles vecteurs d'onde. L'existence de cette branche de phonon, dite de Bogoliubov, avait été prédite depuis longtemps par un argument de symétrie général pour un état BCS de particules neutres. Nous avons vérifié qu'une telle branche perdure en présence d'un confinement harmonique suffisamment faible (le quantum d'oscillation des atomes dans le piège harmonique doit être très inférieur à $k_B T_c$ où T_c est la température de transition BCS), et que sa présence est détectable par diffusion d'un faisceau laser ou de particules, méthodes d'imagerie bien rodées sur les condensats de Bose-Einstein. Ce travail a fait l'objet de la publication [38]. Cette signature proposée s'est cependant révélée non pertinente pour les expériences en cours sur les fermions au voisinage d'une résonance de Feshbach car le gaz est alors dans le régime hydrodynamique, même à basse température, si bien que le gaz présente une branche acoustique même à une température supérieure à la température critique.

4.3 Méthodes de refroidissement d'un gaz d'atomes fermioniques

Les expériences sur les gaz de fermions ont effectué des progrès considérables ces dernières années. Le premier outil ayant permis ces progrès est le refroidissement des gaz fermioniques bien en dessous de leur température de dégénérescence, grâce au refroidissement par évaporation conjoint avec un gaz de Bose (*sympathetic cooling* en anglais) : on met en contact thermique les fermions avec les bosons, et l'on refroidit les bosons par évaporation. Ceci permet de contourner le fait que le taux de collision entre fermions est très fortement réduit à basse température, et ceci conduit à des températures de l'ordre d'un dixième de la température de Fermi.

Nous nous sommes interrogé sur les limites d'un tel refroidissement conjoint. Un mécanisme de chauffage parasite des fermions, proposé qualitativement par E. Timmermans, est la perte de fermions due aux collisions avec le gaz résiduel (le vide n'étant jamais parfait dans une expérience). Chaque perte crée un trou dans la mer de Fermi, ce qui augmente l'énergie totale du gaz d'une quantité de l'ordre de l'énergie de Fermi. Dans le cas d'un système homogène spatialement, nous avons donc étudié quantitativement ce phénomène, à l'aide d'équations de type équation de Boltzmann (sur les nombres d'occupation moyens) et d'équations de type équation maîtresse (sur la distribution de probabilité de l'ensemble des nombres d'occupation), et ceci en présence de refroidissement conjoint par des bosons. Nous trouvons une température limite dépendant simplement du rapport du taux de perte et du taux de collision entre un boson et un fermion [54], et conduisant à des valeurs plus faibles que les limites expérimentales actuelles, les expériences étant effectuées il est vrai dans un piège harmonique. Ceci laisse cependant espérer qu'il ne soit pas nécessaire de réduire fortement les pertes (ce qui aurait pu requérir un environnement cryogénique et rendre les expériences beaucoup plus lourdes) et suggère

que les limites actuelles du refroidissement sont d'ordre technique plus que fondamental.

En l'absence de pertes, nous prédisons une température minimale essentiellement nulle. Ceci était en contradiction avec l'idée intuitive suivante, présente dans la littérature, que le refroidissement conjoint s'arrête lorsque la capacité calorifique du gaz refroidi par évaporation devient inférieure à celle du gaz de fermions. Or la capacité calorifique des bosons chute lorsque ceux-ci se condensent de Bose ; un condensat de Bose-Einstein, ayant une capacité calorifique nulle, ne permettrait donc pas de refroidir du tout les fermions !

Nous avons montré sur un modèle simple exactement soluble que l'idée intuitive est en fait incorrecte parce que basée sur un raisonnement de pur équilibre thermodynamique sur un système isolé : un condensat est en fait le meilleur des réfrigérants, à condition que l'on évapore en permanence les excitations créées par son contact thermique avec les fermions, évaporation bien effectuée dans les expériences mais 'oubliée' dans l'idée intuitive [56].

Comme nous le disions, les limites du refroidissement conjoint des fermions par les bosons semble provenir de difficultés de mise en œuvre pratique de cette technique. Nous avons réfléchi à une autre méthode de refroidissement, plus facile à mettre en œuvre, et utilisant le deuxième outil à la base du succès récent des expériences sur les fermions : la résonance de Feshbach, qui permet, par simple balayage de la valeur d'un champ magnétique, de faire varier la longueur de diffusion virtuellement de $-\infty$ à $+\infty$. Nous avons proposé de partir d'une longueur de diffusion positive, auquel cas les fermions forment des dimères bosoniques que l'on sait condenser de Bose et refroidir par évaporation à une température T_1 ; il reste alors à changer lentement le signe de la longueur de diffusion pour transformer adiabatiquement (donc à entropie constante) le condensat de dimères en un gaz de fermions avec des interactions faiblement attractives, de température T_2. Comme l'entropie d'un gaz de Fermi varie linéairement en température, alors que celui d'un gaz de bosons varie cubiquement, on trouve que $T_2 \propto T_1^3$. Une réduction d'un facteur deux sur la température du condensat moléculaire diminue la température finale du gaz de Fermi attractif d'un facteur huit. On peut ainsi espérer atteindre des valeurs de T_2 de l'ordre d'un centième de la température de Fermi, ce qui devrait permettre d'observer enfin la condensation de paires de Cooper dans le régime BCS d'interactions faibles [55].

4.4 Premières études théoriques d'un gaz dégénéré d'atomes fermioniques en interaction forte

Un résultat vraiment marquant des expériences sur les gaz de fermions est la possibilité de préparer le gaz de manière stable à basse température dans le régime d'interaction forte, c'est-à-dire $k_F|a| > 1$, où k_F est le vecteur d'onde de Fermi et a la longueur de diffusion entre deux atomes de composantes de spin opposées. Juste à la résonance de Feshbach, on a en théorie $k_F|a| = +\infty$; c'est le régime universel dit du gaz quantique unitaire. Ces gaz de fermions interagissent alors plus fortement que les nucléons d'une étoile à neutrons, pour laquelle $k_F|a| < 1$!

Les premiers résultats expérimentaux étaient surprenants. De fortes pertes d'atomes étaient détectées et étaient maximales pour une valeur du champ magnétique différente de la position théorique de la résonance de Feshbach. Au delà de cette valeur de perte maximale, le gaz redevenait stable, mais avait des interactions effectives attractives, alors que la longueur de diffusion était positive. Les tentatives d'explication par des calculs de champ moyen échouèrent.

Nous avons alors exhibé un modèle très simple, sans prétention au quantitatif, de deux particules en interaction dans une boîte sphérique aux parois impénétrables et de

rayon égal à la distance moyenne entre les particules dans le gaz [53]. On prend ainsi en compte de façon exacte les corrélations à deux corps, l'effet des $N-2$ autres particules étant modélisé par la boîte. Nous avons alors expliqué les résultats expérimentaux très simplement, en montrant que deux branches d'état macroscopique du gaz interviennent, chaque branche variant continûment lorsque $-1/(k_F a)$ passe de $-\infty$ à $+\infty$ (ce qui correspond à un balayage du champ magnétique de la partie $a > 0$ de la résonance à la partie $a < 0$, a étant infini juste à la résonance). La branche fondamentale relie continûment le condensat moléculaire au condensat BCS de paires de Cooper. La branche supérieure contient, du côté $-1/(k_F a) \to -\infty$, le gaz de Fermi faiblement répulsif, point de départ de l'expérience. Lorsqu'on augmente a vers $+\infty$, le taux de collision à trois corps augmente fortement, et conduit à la formation de dimères : le gaz passe ainsi de la première branche excitée à la branche fondamentale, pour une valeur de a finie. Les 'pertes' sont en fait une transformation des atomes en molécules, ces dernières n'étant pas visibles dans les premières expériences. Sur la branche fondamentale, notre modèle donne une pression du gaz inférieure à la pression de Fermi du gaz parfait, alors qu'elle était supérieure à la pression de Fermi sur la branche supérieure. Ceci explique le passage d'interactions effectives répulsives à des interactions effectives attractives dans l'expérience, pour une valeur positive de a.

Nous avons commencé à réfléchir au gaz quantique unitaire, cas limite particulièrement intéressant car universel : dans le cas d'un système homogène de température nulle, la seule échelle de longueur est alors la distance moyenne entre particules, si bien que la gaz a un potentiel chimique égal à celui du gaz parfait de même densité, à un facteur numérique près, pour l'instant inconnu mais majoré par des calculs variationnels et Monte-Carlo à structure nodale imposée. Dans le cas d'un piégeage harmonique isotrope, nous avons trouvé que l'évolution du gaz quantique unitaire due à un changement de raideur du piège est donnée de façon exacte (au niveau de l'équation de Schrödinger à N corps) par une transformation de jauge et un changement d'échelle. Ceci permet de montrer que, dans un temps de vol, le profil de densité du gaz subit exactement un changement d'échelle. C'est important pour les expériences : le temps de vol peut ainsi être utilisé comme une loupe parfaite (sans aberration). Ceci a aussi d'intéressantes conséquences sur la nature du spectre à N corps, et a fait l'objet de la publication [58].

Enfin, afin d'identifier les observables pouvant révéler la formation d'un condensat de paires du côté $a < 0$ de la résonance, nous avons utilisé la variante fermionique de notre algorithme de Monte-Carlo quantique, développée par Philippe Chomaz et Olivier Juillet (LPC/ISMRA et GANIL), pour étudier un gaz de fermions à 1D en interaction forte. Nous montrons ainsi que la fonction de distribution de paires de particules de spins opposés, proposée dans la littérature comme indicateur de la transition, ne permet en fait pas de conclure. Nous avons identifié comme meilleure observable la fonction de cohérence de paires de fermions du premier ordre. Nous avons retrouvé les résultats du Monte-Carlo par un développement perturbatif à l'ordre trois, facile à utiliser dans le cas 3D (contrairement au Monte-Carlo) [57].

Chapitre 5

Reproduction d'articles représentatifs

5.1 Sur la méthode des fonctions d'onde Monte-Carlo

Cette article [11] illustre bien la motivation de nos premiers travaux, généraux et formels, sur la méthode des fonctions d'onde Monte-Carlo, motivation qui était d'aboutir à une description du refroidissement laser à gradients de polarisation non plus seulement qualitative (comme les modèles simples exhibant l'effet Sisyphe) mais totalement quantitative et directement comparable aux expériences à trois dimensions.

À l'époque, il semblait bien clair que le formalisme de l'équation pilote sur l'opérateur densité atomique, traitant quantiquement aussi bien les variables atomiques internes (de spin) que les variables atomiques externes (mouvement du centre de masse de l'atome) devait apporter la bonne réponse. Le problème était de résoudre cette équation pilote : une intégration numérique directe était inaccessible (par cinq ordres de grandeur sur les capacités des ordinateurs de l'époque), et les approches semi-classiques tridimensionnelles (suivies en particulier par Klaus Mølmer et Juha Javanainen) étaient d'une validité non clairement établie et conduisaient à des calculs en principe faisables mais extrêmement lourds et qui n'ont en fait jamais abouti.

Une fois le formalisme général de la méthode Monte-Carlo développé, il nous restait à l'implémenter numériquement pour le cas du refroidissement laser. Le programme fut écrit en quelques semaines, mais les temps de calcul restaient longs à l'époque, et nécessitèrent quand même l'utilisation d'un ordinateur massivement parallèle de la NASA (celui utilisé en particulier pour simuler la collision de la comète de Schumaker Levy 9 avec Jupiter) et de plusieurs ordinateurs CRAY, dont celui de l'IDRIS. L'accord avec les expériences étant parfait, ces simulations annoncèrent la fin de nos études théoriques sur le refroidissement laser, qui commençait ainsi à devenir un outil plus qu'un objet d'étude.

Nous avons étendu ces calculs Monte-Carlo au cas des mélasses grises, puis ensuite au piège magnéto-optique. Nous avons développé un formalisme efficace permettant de calculer la taille du nuage dans un tel piège dissipatif, mais les tailles obtenues, de l'ordre de quelques micromètres, se sont révélées bien plus faibles que celles observées expérimentalement, probablement à cause de la diffusion multiple de la lumière responsable d'une interaction effective répulsive entre atomes. Ceci constituait une porte d'entrée dans le problème à N corps, dans lequel nous nous sommes engagé par la suite, mais pour nous consacrer aux condensats de Bose-Einstein.

VOLUME 74, NUMBER 19 PHYSICAL REVIEW LETTERS 8 MAY 1995

Monte Carlo Wave-Function Analysis of 3D Optical Molasses

Yvan Castin[1] and Klaus Mølmer[2]

[1]*Laboratoire Kastler Brossel, Ecole Normale Superieure et Université Paris 6, 24 Rue Lhomond, F-75231 Paris Cedex 05, France**

[2]*Institute of Physics and Astronomy, Aarhus University, DK-8000 Århus C, Denmark*

(Received 27 October 1994)

A full quantum treatment of laser cooling in three dimensions is performed. It is based on a recently developed Monte Carlo wave-function technique, which reduces an otherwise unmanageable density matrix problem by at least a factor of 10^4 in computing requirements. For different atomic transitions and temporal phases of the laser beams, our calculated mean kinetic energies are in good agreement with experimental results. Momentum distributions are shown to develop escape lines when the optical molasses is close to disintegration. Spatial distributions are also calculated and discussed.

PACS numbers: 32.80.Pj, 42.50.Vk, 42.60.–v

By laser cooling it is possible to obtain samples of atoms with kinetic energies in the microkelvin range [1,2]. The underlying mechanisms have been identified in one-dimensional (1D) models [3,4] in which the atomic center-of-mass motion, subject to fluctuating radiative forces, is treated classically. This led to the scaling law for the atomic mean kinetic energy $E_K \propto \hbar|\delta|s$, where δ denotes the (negative) detuning of the laser frequency with respect to the atomic transition frequency $\delta = \omega_L - \omega_A$. We have introduced the saturation parameter $s = 2|\Omega|^2/(4\delta^2 + \Gamma^2)$, where Γ is the decay rate of the excited state and Ω is the Rabi frequency (atom-laser coupling amplitude). The same scaling laws are found when this semiclassical analysis is applied to cooling in three dimensions [5–8], and in treatments taking proper account of spatial localization, even quantitative agreement with experiments is observed [7].

This treatment does not apply in too weak laser fields, where the measured temperatures increase abruptly after going through a minimum. A quantum formulation of the problem leads [9], in the limit of large detunings, to a universal law for the mean kinetic energy,

$$E_K/E_{\mathrm{Rec}} = f(\hbar|\delta|s/2E_{\mathrm{Rec}}), \tag{1}$$

where the recoil energy, $E_{\mathrm{Rec}} = (\hbar k)^2/2M$, has been introduced, with k being the laser wave number and M the atomic mass. The function f depends only on the angular momentum quantum numbers of the atomic transition and on the laser configuration, and it leads to a minimum energy proportional to E_{Rec}. The function f and the minimum kinetic energies were determined in 1D [10] and in 2D [11].

In this Letter we report on quantum calculations performed in 3D laser cooling. The conventional starting point for such a calculation is the master equation for the atomic density matrix ρ, representing the quantum states of the electronic and center-of-mass degrees of freedom. The number of elements of ρ is proportional to the square of the number of points in a grid covering the center-of-mass momentum range. For example, for $|p_i| \leq 20\hbar k$, $i = x, y, z$, and a discretization of $\hbar k$ we get $(2 \times 20 + 1)^6 \simeq 5 \times 10^9$ elements, a number which should be multiplied by the number of matrix elements relative to the atomic electronic states. A direct integration, like the one in 2D [12] can therefore not be performed. A reduction to rate equations for the diagonal elements of ρ in a proper basis was applied in 1D and 2D [10,11]. In 3D the condition for this approximation is not fulfilled for typical experimental parameters.

With this type of problem in mind we have recently developed a general formulation of dissipative problems in quantum optics replacing the density matrix by stochastic wave functions [13–15]. Inspired by other problems in quantum mechanics and quantum optics, other authors have developed similar formulations [16–19].

We now outline our application of this method to 3D laser cooling. The time evolution of a single stochastic wave function is characterized by intervals of Hamiltonian evolution interrupted by random quantum jumps accounting for the spontaneous emission of photons. We introduce the ground and excited state components of the atomic state vector $|\psi_g\rangle$ and $|\psi_e\rangle$, obeying the coupled linear equations

$$i\hbar \frac{d}{dt}|\psi_e\rangle = \left(\frac{\vec{p}^2}{2M} - \hbar\delta - i\hbar\Gamma/2\right)|\psi_e\rangle + V^{(+)}|\psi_g\rangle, \tag{2}$$

$$i\hbar \frac{d}{dt}|\psi_g\rangle = \frac{\vec{p}^2}{2M}|\psi_g\rangle + V^{(-)}|\psi_e\rangle. \tag{3}$$

Here, $\vec{p}$ denotes the atomic momentum operator, and Γ enters explicitly as a damping term in the evolution of $|\psi_e\rangle$. Equations (2) and (3) are obtained in a rotating frame where the atom-laser interaction is written in the rotating wave approximation as $V = -\vec{D}^{(+)} \cdot \vec{E}_L^{(+)} +$ H.c., with $\vec{D}^{(+)}$ being the raising part of the atomic dipole operator and $\vec{E}_L^{(+)}$ the amplitude of the positive frequency component of the laser electric field.

The state vector also undergoes quantum jumps at instants chosen according to the current spontaneous

 0031-9007/95/74(19)/3772(4)$06.00

emission rate $dP/dt = \Gamma\langle\psi_e|\psi_e\rangle/\langle\psi|\psi\rangle$. The emission of a photon with a polarization $\vec{\varepsilon}_S$ and a wave vector $\vec{k}_S$ corresponds to a change of the state vector

$$|\psi\rangle \longrightarrow |\psi\rangle_{\vec{k}_S,\vec{\varepsilon}_S} = (\vec{\varepsilon}_S^{\,*} \cdot \vec{D}^{(-)}) e^{-i\vec{k}_S\cdot\vec{R}} |\psi_e\rangle, \qquad (4)$$

and it has a relative probability $\| |\psi\rangle_{\vec{k}_S,\vec{\varepsilon}_S} \|^2$. The exponential factor containing the position operator $\vec{R}$ of the atom translates the atomic momentum by the recoil momentum $-\hbar\vec{k}_S$, the operator $\vec{\varepsilon}_S^{\,*} \cdot \vec{D}^{(-)}$ projects the atom onto the ground state, and the evolution proceeds from here according to Eqs. (2) and (3). Although the calculations can be performed with the exact dipole pattern for spontaneous emission [14], we have simplified to emission of photons along the coordinate directions $\vec{e}_x$, $\vec{e}_y$, and $\vec{e}_z$, only. This is justified by the widths of the calculated distributions being several $\hbar k$.

To identify the optimum laser cooling we shall use the fact [1,2] that polarization gradient cooling is most efficient at low saturation $s \ll 1$, to adiabatically eliminate the excited state. Neglecting $\vec{p}^{\,2}/2M$ as compared to $\hbar\Gamma/2$ and putting $d|\psi_e\rangle/dt = 0$ in Eq. (2), we obtain $|\psi_e\rangle = (\hbar\delta + i\hbar\Gamma/2)^{-1} V^{(+)} |\psi_g\rangle$. When inserted into Eq. (3), this introduces the effective ground state potential operator $(\hbar\delta + i\hbar\Gamma/2)^{-1} V^{(-)} V^{(+)}$. Since V is proportional to $\hbar\Omega$, we have, in this way, made appear frequencies $\sim|\delta|s$ (light shifts) and damping rates $\sim\Gamma s$ (optical pumping rates), which we require to be much smaller than Γ for consistency with the elimination of $|\psi_e\rangle$. This procedure removes the short times $1/\delta$ and $1/\Gamma$, so that time steps, longer by a factor $\sim 1/s$, may be applied in the integration of Eq. (3).

We now take the laser configuration to be a superposition of fields propagating along the coordinate axes. We expand the center-of-mass components of the wave function on a set of states with momenta $\vec{p} = \vec{p}_0(t) + \hbar k(n_x, n_y, n_z)$, where n_x, n_y, and n_z are integers. Indeed, an initial momentum eigenstate will, at any later times, have an exact expansion on these states, and with the simplified emission pattern described above, $\vec{p}_0(t)$ can be set to 0 at all times. In practice, we have to limit the momentum grid, and we consider it sufficient to take $-20 \le n_x, n_y, n_z \le 20$ for calculations of momentum distributions with $p_{i,\mathrm{rms}} \le 7\hbar k$, $i = x, y, z$, the maximum considered in this paper.

The integration of Eq. (3) with $|\psi_e\rangle = (\hbar\delta + i\hbar\Gamma/2)^{-1} V^{(+)} |\psi_g\rangle$ follows a splitting technique. To obtain the wave function $|\psi_g(t + dt)\rangle$ from the value at time t, we first multiply components of momentum $\vec{p}$ by the kinetic energy phase factor $\exp(-i\vec{p}^{\,2} dt/2M\hbar)$. Second, we approximate the propagation due to V by a fourth order Taylor expansion in powers of dt, requiring $|\delta|sdt < 1$. The first neglected terms due to the splitting are proportional to $[\vec{p}^{\,2}/2M, V^{(-)}V^{(+)}/(\hbar\delta + i\hbar\Gamma/2)](dt/\hbar)^2 \sim (kpdt/M)\,|\delta|sdt$, and this puts an additional criterion on the maximum allowable time step dt. In our calculations we applied a time step of $dt = 0.025(\Gamma s)^{-1}$.

The Monte Carlo wave-function method is a simulation technique, and the restriction to a finite number of state vectors leads to error bars on our results. Suppose that at time t, n independent wave functions $|\psi_i(t)\rangle$ have been evolved, and that the expectation values $a_i(t) = \langle\psi_i|A|\psi_i\rangle/\langle\psi_i|\psi_i\rangle$ of an atomic operator A have been calculated for the n wave functions. The sample mean of the a_i's, $\langle a\rangle = (\sum_{i=1}^{n} a_i)/n$, then gives an approximation to the exact mean value, $\mathrm{Tr}[\rho(t)A]$, with a statistical error estimated by $\delta a/\sqrt{n}$, where $(\delta a)^2$ is the sample variance of the a_i's [14]. The statistical error will therefore be represented in our figures by error bars with a half-width $\delta a/\sqrt{n}$.

Here, the atomic density matrix $\rho(t)$ converges to a steady state ρ^{st} within a time τ of order the relaxation time of the mean kinetic energy. In the Monte Carlo simulation, the wave functions have no steady state, so that each expectation value $a_i(t)$ keeps fluctuating with time. In the derivation of steady-state mean values, one may, however, replace the variables $a_i(t)$ by their time average $\bar{a}_i$ on a time interval $\gg\tau$. An approximation of $\mathrm{Tr}(\rho^{\mathrm{st}}A)$ is then derived from the sample mean of the $\bar{a}_i$'s, with a statistical error $\delta\bar{a}/\sqrt{n}$, where $(\delta\bar{a})^2$ is the sample variance of the $\bar{a}_i$'s. For the interaction times considered, this time averaging procedure leads to $\delta\bar{a} \sim \delta a/3$, for $A = \vec{p}^{\,2}$, mimicking an increase in the number of wave functions by a factor of 9.

Measurements of temperatures in 3D optical molasses have been performed on $j_g \rightarrow j_e = j_g + 1$ atomic transitions, with $j_g = 2$ and $j_g = 3$ in two isotopes of Rb [2] and with $j_g = 4$ in Cs [1]. We present results for these three types of transitions, and for $j_g = 1$. Also, we restrict ourselves to one closely investigated laser configuration, the so-called lin $\perp$ lin configuration, defined by the electric field

$$\vec{E}_L^{(+)}(\vec{r}) = \frac{E_0}{2}\,[e^{i\phi_x}(\vec{e}_y e^{ikx} + \vec{e}_z e^{-ikx}) + e^{i\phi_y}(\vec{e}_z e^{iky} + \vec{e}_x e^{-iky}) + e^{i\phi_z}(\vec{e}_x e^{ikz} + \vec{e}_y e^{-ikz})]. \qquad (5)$$

The amplitude E_0 is included in the Rabi frequency $\Omega = dE_0/\hbar$, where d is the atomic dipole moment.

In Fig. 1 the mean steady-state kinetic energy of the atoms E_K is shown as a function of the parameter $\hbar|\delta|s/2$, for laser phases $(0, 0, 0)$ and a detuning of $\delta = -5\Gamma$. We recover the characteristic functional dependence of E_K described in the introduction. For a large light shift, $E_K \simeq a\hbar|\delta|s/2 + bE_{\mathrm{Rec}}$. For decreasing values of the light shift, E_K goes through a minimum and then increases sharply, indicating the existence of a threshold for polarization gradient cooling to be effective. We note the dependence of E_K on the angular momentum j_g, the largest values of j_g giving rise to the coldest atomic distributions. The slope a and the minimum mean kinetic energy are given in Table I, as functions of j_g, together with experimental values for $j_g > 1$. The number of Monte Carlo wave functions ranges from 6

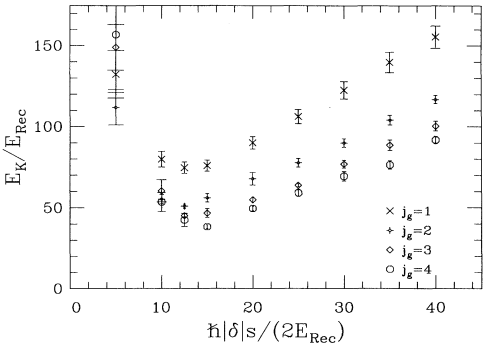

FIG. 1. Mean kinetic energy as a function of light shift for the atomic transitions $j_g \rightarrow j_e = j_g + 1$, $j_g = 1, 2, 3$, and 4. The laser field configuration is given by (5) with $\phi_x = \phi_y = \phi_z = 0$, and the atom-laser detuning is $\delta = -5\Gamma$.

to 12. In the affine regime, the points were obtained with an interaction time of $400(\Gamma s)^{-1}$, with the temporal average performed over the last $200(\Gamma s)^{-1}$, whereas close to threshold, relaxation times get longer and interaction times up to $800(\Gamma s)^{-1}$ were considered. The calculation per point required the equivalent of 10 to 50 h on a Cray C90 computer. In the experiments quoted above, the phases of the six laser beams were not controlled. In order to validate our comparison with the measurements we have extended our $j_g = 2$ calculations to the phase $(0, \pi/3, 2\pi/3)$. Within our error bars the minimum kinetic energy and the slopes are the same as in Fig. 1.

The Monte Carlo wave functions provide much more information than shown in Fig. 1. An aspect of laser cooling which has received much interest [20,21] is the possibility to form spatially periodic atomic distributions. In Figs. 2(a) and 2(b) we show position distributions calculated for two different sets of phases. We interpret the observed localization in terms of the spatial variation of the laser fields. In the case of vanishing phases, the electric field on the line $x = y = z$ is linearly polarized. The maximum intensity is obtained on this line at $(x, y, z) = (0, 0, 0)$ and at $(\lambda/2, \lambda/2, \lambda/2)$. But, because circularly polarized light interacts more strongly with $j_g > 0 \rightarrow j_e = j_g + 1$ transitions (Clebsch-Gordan coefficients), it may be advantageous for the atoms to localize at a distance from this line, where a larger fraction of circularly polarized light is present. This qualitatively explains the doughnut-shaped distributions shown in Fig. 2(a), a shape also obtained in semiclassical calculations [7]. The

TABLE I. Results of Fig. 1 ("calc," vanishing phases) and experimental results ("meas," uncontrolled phases) for the minimum kinetic energy and for the slope a (see text).

j_g	E_K^m/E_{Rec}(calc)	E_K^m/E_{Rec}(meas)	a(calc)	a(meas)
1	74.7 ± 3.5	···	3.3 ± 0.5	···
2	51.0 ± 1.4	50 ± 5	2.6 ± 0.2	2.3 ± 0.2
3	45.1 ± 1.1	50 ± 5	2.5 ± 0.2	2.1 ± 0.2
4	38.3 ± 1.2	40 ± 10	2.1 ± 0.2	2.1 ± 0.5

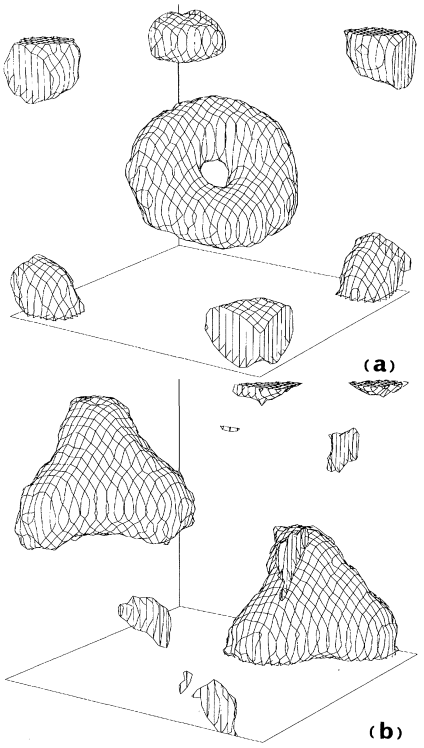

FIG. 2. Atomic position distributions in the cell $-\lambda/2 < x, y, z < \lambda/2$, for a $j_g = 2 \rightarrow j_e = 3$ transition, with $\hbar|\delta|s/2E_{Rec} = 30$ and $\delta = -5\Gamma$. The probability of finding the atom within the surfaces of constant density shown is 1/4. The corresponding enclosed volume is 6% for (a) (vanishing phases) and 8% for (b) [phases $(0, \pi/3, 2\pi/3)$].

situation for the case of $(\phi_x, \phi_y, \phi_z) = (0, \pi/3, 2\pi/3)$ is completely different. Now, the maximum intensity is obtained in the points $(x, y, z) = (\lambda/6, 2\lambda/3, \lambda/6)$ and $(2\lambda/3, \lambda/6, 2\lambda/3)$, where the light is circularly polarized. It follows that the optically induced potential wells have absolute minima here and, indeed, atoms are localized around these points; see Fig. [2(b)].

Also, fast atoms may localize within the plane perpendicular to their velocity. For example, for the set of phases $(0, \pi/3, 2\pi/3)$ we have identified lines through the points of maximum intensity and with direction $(1, 1, 1)$, where the light has a constant circular polarization [orthogonal to $(1, 1, 1)$], and where the localization of atoms with high velocities along $(1, 1, 1)$ is likely to occur. As the polarization is constant here we expect a less efficient cooling of these atoms and therefore an anisotropy in the momentum distribution. In a two-dimensional optical lattice this anisotropy leads to escape channels for the atoms for sufficiently small light shifts $\hbar|\delta|s$ [12].

Below the value of light shifts leading to the minimum kinetic energy we get a momentum distribution as exem-

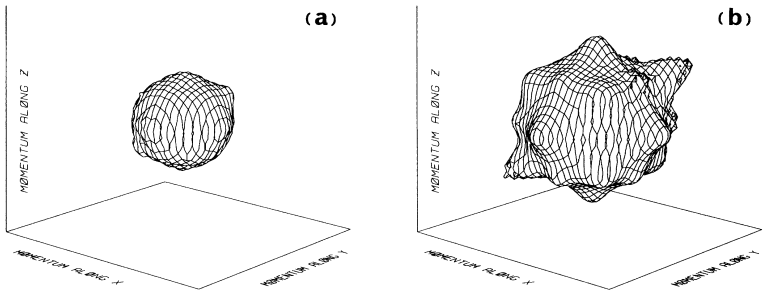

FIG. 3. Momentum distribution for a $j_g = 2 \rightarrow j_e = 3$ transition, with $\hbar|\delta|s/2E_{\mathrm{Rec}} = 5$ and $\delta = -5\Gamma$, and for the phases $(0, \pi/3, 2\pi/3)$. The plotted isodensity surfaces correspond to 1/15 (a) and 1/50 (b) of the maximal density. Similar results are obtained for vanishing phases.

plified in Fig. 3. The central part of the distribution is essentially isotropic; in an intermediate range [Fig. 3(a)] we recover the expected anisotropy along $(1, 1, 1)$ giving rise to a lemon-shaped isodensity surface, and in the far wings [Fig. 3(b)] further escape lines are visible. In fact, escape lines may exist in all directions $\vec{n}$ with transverse cooling, i.e., orthogonal to two Fourier components $\vec{k}_a - \vec{k}_b$, $\vec{k}_{a'} - \vec{k}_{b'}$ of $V^{(-)}V^{(+)}$, the $\vec{k}$'s being wave vectors of the laser beams. The relative importance of the escape lines, however, is difficult to assess when they are not associated to constant circular polarization.

In conclusion, we have shown that the Monte Carlo wave-function method applies successfully to the problem of 3D laser cooling. Mean kinetic energies in good agreement with the experimental values have been obtained, and we have discussed features of the cooled distributions which have not yet been measured. The low level of statistical uncertainty on our results was beyond our expectations and strongly relies on the time averaging procedure. This brings promises for further applications within this field, and we are currently investigating nonperiodic problems, appearing in connection with spatial diffusion and neutral atom traps.

We would like to thank Jean Dalibard and Kirstine Berg-Sørensen for fruitful interactions during the setup of the calculations. Allocation of time on Cray C90 computers by the French IDRIS and the Danish SNF, and access to a MasPar computer provided by the HPCC program at NASA Goddard Space Flight Center are gratefully acknowledged. Part of this work was done at NIST in Gaithersburg, and one of us (Y. C.) is particularly grateful to P. D. Lett, W. D. Phillips, C. Clark, and J. Devaney for their assistance. The Japanese NEDO is acknowledged for financial support.

*Unité de recherche de l'Ecole Normale Supérieure et de l'Université Paris 6, associée au CNRS.

[1] C. Salomon, J. Dalibard, W. D. Phillips, A. Clarion, and S. Guellati, Europhys. Lett. **12**, 683 (1990).
[2] C. Gerz, T. W. Hodapp, P. Jessen, K. M. Jones, W. D. Phillips, C. I. Westbrook, and K. Mølmer, Europhys. Lett. **21**, 661 (1993).
[3] P. J. Ungar, D. S. Weiss, E. Riis, and S. Chu, J. Opt. Soc. Am. B **6**, 2058 (1989).
[4] J. Dalibard and C. Cohen-Tannoudji, J. Opt. Soc. Am. B **6**, 2023 (1989).
[5] K. Mølmer, Phys. Rev. A **44**, 5820 (1991).
[6] J. Javanainen, Phys. Rev. A **46**, 5819 (1992).
[7] J. Javanainen, J. Phys. B **27**, L47 (1994).
[8] K. Mølmer and C. I. Westbrook, Laser Physics **4** (1994), special issue on cooling and trapping.
[9] Y. Castin, K. Berg-Sørensen, K. Mølmer, and J. Dalibard, in *Fundamentals of Quantum Optics III,* LNIP 420, edited by F. Ehlothzky (Springer-Verlag, Berlin, 1993).
[10] Y. Castin and J. Dalibard, Europhys. Lett. **14**, 761 (1991).
[11] K. Berg-Sørensen, Y. Castin, K. Mølmer, and J. Dalibard, Europhys. Lett. **22**, 663 (1993).
[12] Y. Castin, K. Berg-Sørensen, J. Dalibard, and K. Mølmer, Phys. Rev. A **50**, 5092 (1994).
[13] J. Dalibard, Y. Castin, and K. Mølmer, Phys. Rev. Lett. **68**, 580 (1992).
[14] K. Mølmer, Y. Castin, and J. Dalibard, J. Opt. Soc. Am. B **10**, 524 (1993).
[15] Y. Castin, J. Dalibard, and K. Mølmer, in *Proceedings of the Thirteenth International Conference on Atomic Physics* (ICAP 13) edited by H. Walther, T. W. Hänsch, and B. Neizert (AIP, New York, 1993).
[16] R. Dunn, P. Zoller, and H. Ritsch, Phys. Rev. A **45**, 315 (1992).
[17] H. J. Carmichael, *An Open Systems Approach to Quantum Optics,* LNIP m18, edited by W. Beiglböck (Springer, New York, 1993).
[18] N. Gisin and I. Percival, Phys. Lett. A **167**, 315 (1992); J. Phys. A **25**, 5677 (1992).
[19] G. C. Hegerfeldt and T. S. Wilser, in *Proceedings of the II International Wigner Symposium, Goslar, 1991,* edited by H. D. Döbner, W. Scherer, and F. Schröck (World Scientific, Singapore, 1992).
[20] G. Grynberg, B. Lounis, P. Verkerk, J.-Y. Courtois, and C. Salomon, Phys. Rev. Lett. **70**, 2249 (1993).
[21] A. Hemmerich, C. Zimmermann, and T. W. Hänsch, Phys. Rev. Lett. **72**, 625 (1994).

5.2 Sur les approches à la Bogoliubov

Ce travail [49] illustre bien le fait que l'approche de Bogoliubov, développée dans les années 1950 pour étudier les condensats gazeux presque purs, peut en fait avoir une portée plus considérable puisqu'on peut l'étendre au cas où il n'y a pas de condensat du tout (ce qui arrive souvent en dimensionalité réduite), à condition toutefois que le gaz soit dégénéré, en interaction faible et présente de faibles fluctuations de densité (régime dit des quasi-condensats).

Cette possibilité d'étendre l'approche de Bogoliubov, qui a constitué le sujet de thèse de Christophe Mora sous ma direction, était pressentie par la communauté mais à notre connaissance jamais explicitée. La sagesse collective enseignait simplement qu'il suffit d'écrire l'opérateur champ en point de vue module et phase :

$$\hat{\psi}(\mathbf{r}) = e^{i\hat{\theta}(\mathbf{r})}\sqrt{\hat{\rho}(\mathbf{r})}$$

où l'opérateur donnant la densité au point $\mathbf{r}$ considéré est parfaitement bien défini, $\hat{\rho}(\mathbf{r}) \equiv \hat{\psi}^\dagger(\mathbf{r})\hat{\psi}(\mathbf{r})$, et où le mythique opérateur phase $\hat{\theta}(\mathbf{r})$ n'est pas construit explicitement mais est supposé être hermitien et obéir à la relation de commutation :

$$[\hat{\theta}(\mathbf{r}), \hat{\rho}(\mathbf{r}')] = -i\delta(\mathbf{r} - \mathbf{r}').$$

Il reste alors, disait la sagesse collective, à développer le Hamiltonien en puissances de $\delta\hat{\rho} = \hat{\rho} - \langle\hat{\rho}\rangle$ jusqu'au second ordre, puis de diagonaliser le Hamiltonien quadratique correspondant par une transformation de Bogoliubov. Ceci a effectivement l'air justifié dès que $\delta\hat{\rho} \ll \langle\hat{\rho}\rangle$, c'est-à-dire lorsque les fluctuations de densité sont assez faibles, ce qui ne suppose pas nécessairement que l'on ait un condensat de Bose-Einstein. Néanmoins, de nombreuses divergences ultraviolettes apparaissaient, si bien qu'il fallait mettre une coupure en énergie dont les valeurs moyennes d'observables dépendaient.

En examinant cette procédure formelle, on tombe immédiatement sur deux obstacles majeurs, qui sont non pas d'ordre purement mathématique mais qui, comme nous l'avons montré, ont une origine physique profonde :

- les fluctuations de $\delta\hat{\rho}$ sont en fait infinies, en tout point où il peut y avoir des particules ($\langle\hat{\rho}\rangle \neq 0$), et ceci quel que soit l'état du système !
- l'opérateur phase $\hat{\theta}$ défini comme plus haut n'existe pas !

L'article reproduit ci-après montre comment surmonter ces deux obstacles et arrive à une théorie des quasi-condensats exempte de divergences et de dépendances en une coupure. Autre aspect important : le formalisme présenté donne des prédictions équivalentes à notre approche de Bogoliubov sans brisure de symétrie, dans le cas où un condensat est présent, et permet en particulier de calculer la première correction à l'équation de Gross-Pitaevskii sur la fonction d'onde du condensat. Ce qui nous permet de faire l'économie d'une inclusion de [23] dans ce mémoire.

Nous avions développé à l'origine ce formalisme adapté aux quasi-condensats pour prédire les propriétés de cohérence d'un laser à atomes. Mais une application inattendue de ce formalisme serait de calculer la première correction à l'approximation de Bogoliubov, en dimension un en particulier.

PHYSICAL REVIEW A **67**, 053615 (2003)

Extension of Bogoliubov theory to quasicondensates

Christophe Mora
Laboratoire de Physique Statistique, École Normale Supérieure, 24 rue Lhomond, 75231 Paris Cedex 5, France

Yvan Castin
Laboratoire Kastler Brossel, École Normale Supérieure, 24 rue Lhomond, 75231 Paris Cedex 5, France

(Received 20 December 2002; published 30 May 2003)

We present an extension of the well-known Bogoliubov theory to treat low-dimensional degenerate Bose gases in the limit of weak interactions and low density fluctuations. We use a density-phase representation and show that a precise definition of the phase operator requires a space discretization in cells of size *l*. We perform a systematic expansion of the Hamiltonian in terms of two small parameters, the relative density fluctuations inside a cell and the phase change over a cell. The resulting macroscopic observables can be computed in one, two, and three dimensions with no ultraviolet or infrared divergence. Furthermore, this approach exactly matches Bogoliubov's approach when there is a true condensate. We give the resulting expressions for the equation of state of the gas, the ground state energy, and the first order and second order correlation functions of the field. Explicit calculations are done for homogeneous systems.

DOI: 10.1103/PhysRevA.67.053615 PACS number(s): 03.75.Hh

INTRODUCTION

Recent progress in the realization of low-dimensional Bose gases in the quantum degenerate regime offers new perspectives for comparison with theoretical treatments. In atomic Bose gases, low-dimensional systems are achieved by creating anisotropic trapping potentials. Bose-Einstein condensates of reduced dimensionality, that is, with the atomic motion frozen in the harmonic oscillator ground state along one or two directions, have been produced [1,2].

Low-dimensional Bose gases with repulsive interactions were the subject of early theoretical studies. In the thermodynamic limit for spatially homogeneous systems, the Mermin-Wagner-Hohenberg theorem [3,4] excludes the formation of a Bose-Einstein condensate at finite temperature. This is physically due to large phase fluctuations which restrict the coherence length of the bosonic field to a finite value. One expects, however, that strong enough repulsive interactions between the particles strongly reduce the density fluctuations of the gas in contrast to the noninteracting case [5,6]. In this context, Popov introduced a long time ago the concept of a *quasicondensate* [7]. This concept has been extended to trapped gases [8–10]. The recent observation of large phase fluctuations for a degenerate Bose gas in a highly anisotropic cigar shaped trap has brought qualitative experimental confirmation of the theory in a quasi-one-dimensional geometry [11,12].

It turns out that the theory of quasicondensates has not yet reached the maturity of the theory for condensates. In the case of regular three-dimensional (3D) Bose-Einstein condensation in the weakly interacting regime, the Bogoliubov theory [13], based on a systematic expansion in a small parameter, gives a very precise description of the state of the gas. The intuitive idea of the Bogoliubov theory is to use the existence of a single macroscopically occupied mode ϕ_0 of the field, the mode of the condensate. We recall here the U(1)-symmetry preserving version of the theory [14,15]. One first splits the bosonic field operator as $\hat{\psi}=\phi_0\hat{a}_0+\delta\hat{\psi}$, where $\hat{a}_0$ annihilates a particle in the condensate mode and $\delta\hat{\psi}$ accounts for quantum and thermal fluctuations in the other modes. Then one uses the assumption $|\delta\hat{\psi}|\ll|\hat{a}_0|$ to solve the field equations of motion perturbatively. This approach is not suitable for a quasicondensate as there is no single macroscopically occupied field mode. Fortunately, in the case of weak density fluctuations, the Bogoliubov idea can still be adapted in a quantum phase-density representation of the field operator. One writes the field operator $\hat{\psi}$ as $\exp(i\hat{\theta})\hat{\rho}^{1/2}$ where $\hat{\theta}$ and $\hat{\rho}$ are position dependent operators, giving the phase and the density. One then splits the operator giving the density as $\rho_0+\delta\hat{\rho}$, where ρ_0 is a *c* number and $\delta\hat{\rho}$ are fluctuations, and one uses the fact that $|\delta\hat{\rho}|\ll\rho_0$. This idea has already been used in the literature [16] but to our knowledge without a precise definition of the phase operator, a well-known delicate point of quantum field theory [17,18]. As a consequence of the nonrigorous definition of the phase, divergences appear in the theory [16]: one has to introduce an arbitrary energy cutoff, so that predictions in 1D at zero temperature are made within a logarithmic accuracy only, and in 3D there is no full equivalence with the Bogoliubov theory. Another approach based on the current-density operator rather than on the phase operator was given by Schwartz [19]: an expansion of the Hamiltonian in terms of weak density and current fluctuations is performed relating the correlation function of the field to the static structure factor. It is subject to the same divergence problem in 2D and 3D in the absence of an energy cutoff if one calculates the structure factor in the Bogoliubov approximation.

A possibility to circumvent these difficulties is to rely on the path integral formulation of quantum field theory, which involves a functional integral over a classical field, for which the phase is perfectly well defined. This is the approach used by Popov, but with the introduction of an energy cutoff much smaller than the chemical potential of the gas, so that the physics at length scales smaller than the healing length is not

accurately described. This functional integral has recently been considered: it can lead to a cutoff independent formalism for quasicondensates [20,21] and it reproduces the same results as the Bogoliubov theory for a 3D condensate [22].

In this paper, we propose an improved Bogoliubov approach to treat quasicondensates in the phase-density formalism for a weakly interacting Bose gas. This approach is based on a lattice model, that is, with discrete spatial modes, which allows us to give a careful definition of the phase operator of the field and to introduce from the start an energy cutoff. It uses a systematic expansion in powers of the density fluctuations and of the spatial phase gradient and leads to simple expressions for the first and second order spatial correlation functions of the bosonic field that do not depend on the energy cutoff and that exactly reproduce in 3D the predictions of the Bogoliubov theory. We also use this formalism to determine the equation of state of the gas to the lowest nonvanishing order in the thermal and quantum excitations.

In Sec. I, we construct a discretized space model in order to define in a precise way the operators giving the phase and the density. We give the physical implications of the space discretization, restricting this approach to highly degenerate and weakly interacting Bose systems. In Sec. II, we derive a quadratic approximation to the Hamiltonian, that is, we derive approximate linear equations of motion for the density fluctuations and the phase operators. We recover to the lowest order the Gross-Pitaevskii equation for the quasicondensate density and we recover the Bogoliubov spectrum for the excitations. We also push the expansion to the next order, by producing a cubic correction to the quadratic Hamiltonian, including the interaction between the quasicondensate and the excitations. We show that inclusion of this correction is necessary to get a consistent theory and to establish the full equivalence between our approach and the number conserving Bogoliubov theory. In Sec. III, we present a few applications of our formalism: we give general formulas for the equation of state and the ground state of the gas, and for the first and second order correlation functions g_1 and g_2 of the field operator. In Sec. IV, we apply our formal results to the homogeneous Bose gas in various dimensions of space. This allows us to derive simply the validity condition of the method and to compare our results with existing results in the literature.

I. CONSTRUCTION OF A DISCRETE PHASE-DENSITY REPRESENTATION

A. Why discretize the real space?

In previous studies of quasicondensates the basic tools of the theory are an operator

$$\hat{\rho}(\mathbf{r}) = \hat{\psi}^\dagger(\mathbf{r})\,\hat{\psi}(\mathbf{r}) \tag{1}$$

giving the density in $\mathbf{r}$ and an operator $\hat{\theta}(\mathbf{r})$ giving the phase of $\hat{\psi}(\mathbf{r})$, the field operator in $\mathbf{r}$, the position $\mathbf{r}$ being a continuous variable [23]. A small parameter of the theory characterizing the regime of quasicondensates is then that the density fluctuations, that is, the fluctuations of $\hat{\rho}(\mathbf{r})$, are small in relative values:

$$\mathrm{var}[\hat{\rho}(\mathbf{r})] \equiv \langle \hat{\rho}(\mathbf{r})^2 \rangle - \langle \hat{\rho}(\mathbf{r}) \rangle^2 \ll \langle \hat{\rho}(\mathbf{r}) \rangle^2. \tag{2}$$

However, one finds that the expectation value of $\hat{\rho}(\mathbf{r})^2$ is infinite at every point with a nonvanishing mean density $\rho(\mathbf{r}) = \langle \hat{\rho}(\mathbf{r}) \rangle$:

$$\langle \hat{\rho}(\mathbf{r})^2 \rangle = \delta(\mathbf{0})\,\rho(\mathbf{r}) + \langle \hat{\psi}^\dagger(\mathbf{r})\,\hat{\psi}^\dagger(\mathbf{r})\,\hat{\psi}(\mathbf{r})\,\hat{\psi}(\mathbf{r}) \rangle, \tag{3}$$

where $\delta(\mathbf{0})$, the value of the Dirac distribution at the origin, is infinite, and the second term on the right-hand side, giving the probability density of finding two atoms at the same point of space, is finite in any realistic model. Mathematically, this divergence is due to the use of the bosonic commutation relations of the field operators $\hat{\psi}(\mathbf{r})$ and $\hat{\psi}^\dagger(\mathbf{r})$ at the same point of space to put the atomic field product in normal order.

In order to have small, and therefore finite, density fluctuations, one is forced to discretize the space, that is, to collect the particles in little boxes at the nodes of a spatial grid. Each little box has equal length l along each dimension of space and is parametrized by the position $\mathbf{r}$ of its center. The field operator $\hat{\psi}(\mathbf{r})$ has the effect of removing a particle in the box at position $\mathbf{r}$ and it now satisfies the bosonic commutation relations

$$[\hat{\psi}(\mathbf{r}), \hat{\psi}^\dagger(\mathbf{r}')] = \frac{\delta_{\mathbf{r},\mathbf{r}'}}{l^D}, \tag{4}$$

where $\delta_{\mathbf{r},\mathbf{r}'}$ is the discrete Kronecker delta function and D is the dimension of space. The variance of the operator giving the density is now finite:

$$\mathrm{var}[\hat{\rho}(\mathbf{r})] = \langle \hat{\psi}^\dagger(\mathbf{r})\,\hat{\psi}^\dagger(\mathbf{r})\,\hat{\psi}(\mathbf{r})\,\hat{\psi}(\mathbf{r}) \rangle - \rho^2(\mathbf{r}) + \frac{\rho(\mathbf{r})}{l^D}. \tag{5}$$

In the validity domain of the theoretical approach of this paper, this variance will be much smaller than $\rho^2(\mathbf{r})$ because both the sum of the first two terms and the last term in the right-hand side are small:

$$|\langle \hat{\psi}^\dagger(\mathbf{r})\,\hat{\psi}^\dagger(\mathbf{r})\,\hat{\psi}(\mathbf{r})\,\hat{\psi}(\mathbf{r}) \rangle - \rho^2(\mathbf{r})| \ll \rho^2(\mathbf{r}), \tag{6}$$

$$\rho(\mathbf{r})\,l^D \gg 1. \tag{7}$$

B. The phase operator

In the usual continuous space theories, a Hermitian field phase operator $\hat{\theta}(\mathbf{r})$ is introduced subject to the following commutation relation with the operator giving the density:

$$[\hat{\rho}(\mathbf{r}), \hat{\theta}(\mathbf{r}')] = i\,\delta(\mathbf{r} - \mathbf{r}'). \tag{8}$$

In our discrete model the desired commutation relation is modified into

$$[\hat{\rho}(\mathbf{r}),\hat{\theta}(\mathbf{r}')]=i\frac{\delta_{\mathbf{r},\mathbf{r}'}}{l^D}. \tag{9}$$

First we recall briefly that there actually exists no Hermitian operator $\hat{\theta}(\mathbf{r})$ satisfying strictly the above commutation relation. From the identity (9) one can indeed show that the operator

$$T(\alpha)\equiv e^{-i\alpha\hat{\theta}(\mathbf{r})}, \tag{10}$$

where α is any real number, is a translation operator for the density [24]:

$$T(\alpha)^\dagger\hat{\rho}(\mathbf{r})T(\alpha)=\hat{\rho}(\mathbf{r})+\frac{\alpha}{l^D}. \tag{11}$$

This identity contradicts two fundamental properties of $\hat{\rho}(\mathbf{r})$, the positiveness and the discreteness of its spectrum [25].

We now proceed with the construction of a phase operator $\hat{\theta}(\mathbf{r})$ approximately satisfying the commutation relation (9). The key ingredients allowing such an approximate construction are (i) to be in the limit of a large occupation number of the considered box of the lattice, and (ii) to construct the operator $e^{i\hat{\theta}}$ first, which, according to Eq. (11) taken with $\alpha=-1$, simply reduces the number of particles in the considered box by 1.

In each spatial box we introduce the basis of Fock states $|n,\mathbf{r}\rangle$ with exactly n particles in the box. In this basis the field operators have the following matrix elements:

$$\hat{\psi}(\mathbf{r}')|n,\mathbf{r}\rangle=\frac{\delta_{\mathbf{r},\mathbf{r}'}}{l^{D/2}}\sqrt{n}|n-1,\mathbf{r}\rangle,$$

$$\hat{\psi}^\dagger(\mathbf{r}')|n,\mathbf{r}\rangle=\frac{\delta_{\mathbf{r},\mathbf{r}'}}{l^{D/2}}\sqrt{n+1}|n+1,\mathbf{r}\rangle \tag{12}$$

as a consequence of the commutation relation (4). The atomic density $\hat{\rho}$ defined by $\hat{\rho}(\mathbf{r})=\hat{\psi}^\dagger(\mathbf{r})\hat{\psi}(\mathbf{r})$ is diagonal in the Fock state basis:

$$\hat{\rho}(\mathbf{r}')|n,\mathbf{r}\rangle=\delta_{\mathbf{r},\mathbf{r}'}\frac{n}{l^D}|n,\mathbf{r}\rangle. \tag{13}$$

We then introduce the operator $\hat{A}$ defined by

$$\hat{\psi}(\mathbf{r})\equiv\hat{A}(\mathbf{r})\sqrt{\hat{\rho}(\mathbf{r})}. \tag{14}$$

In the Fock space $\hat{A}(\mathbf{r})$ reduces by 1 the number of particles n in the box $\mathbf{r}$:

$$\hat{A}(\mathbf{r}')|n,\mathbf{r}\rangle=(1-\delta_{n,0})\,\delta_{\mathbf{r},\mathbf{r}'}|n-1,\mathbf{r}\rangle. \tag{15}$$

Note that its action on the vacuum state of the box gives zero. For each box $\mathbf{r}$, the definition of $\hat{A}$ leads to the exact relations

$$\hat{A}\hat{A}^\dagger=I,\quad \hat{A}^\dagger\hat{A}=I-|0\rangle\langle 0|,\quad \text{and}\quad [\hat{A},\hat{A}^\dagger]=|0\rangle\langle 0|, \tag{16}$$

where I is the identity operator and $|0\rangle$ is the zero-particle state or vacuum state in the box of center $\mathbf{r}$. We find that the operator $\hat{A}$ is almost unitary, i.e., it is effectively unitary for a physical state of the system with a negligible probability of having an empty box. In what follows, we assume that this condition is satisfied, so that the projector $|0\rangle\langle 0|$ can be neglected:

$$\text{occupation probability of } |n=0,\mathbf{r}\rangle\ll 1. \tag{17}$$

In this case, we write the approximately unitary operator $\hat{A}$ as

$$\hat{A}(\mathbf{r})\simeq e^{i\hat{\theta}(\mathbf{r})}\quad\text{with}\quad \hat{\theta}^\dagger(\mathbf{r})\simeq\hat{\theta}(\mathbf{r}), \tag{18}$$

which amounts to writing the field operator as

$$\hat{\psi}(\mathbf{r})\simeq e^{i\hat{\theta}(\mathbf{r})}\sqrt{\hat{\rho}(\mathbf{r})}. \tag{19}$$

This should be understood as a formal writing, allowing us, for example, to recover the matrix elements of $\hat{A}$ and therefore of the field operator $\hat{\psi}$ from the commutation relation (9). We summarize below all the commutation relations of our phase-density representation:

$$[\hat{\rho}(\mathbf{r}),\hat{\theta}(\mathbf{r}')]\simeq\frac{i\,\delta_{\mathbf{r},\mathbf{r}'}}{l^D},\quad [\hat{\rho}(\mathbf{r}),\hat{\rho}(\mathbf{r}')]=0,$$

$$[\hat{\theta}(\mathbf{r}),\hat{\theta}(\mathbf{r}')]\simeq 0. \tag{20}$$

We come back to the constraint (17) at the basis of the construction of $\exp(i\hat{\theta})$. A sufficient condition to have a low probability for zero particle occupation in a box is obtained for a large mean number of particles in the box and with small relative particle number fluctuations. This is the regime that we wish to consider in this paper. We are therefore back to the discussion of the previous subsection and to the conditions (6),(7) for weak density fluctuations. In particular, the construction of the operator $\exp(i\hat{\theta})$ becomes problematic in the limit $l\to 0$, that is, in the continuous model.

C. How to choose the grid spacing *l*

Working on a grid can also be seen as performing a coarse-grain average over all physical quantities on a scale l. This averaging suppresses the short wavelength modes (shorter than l) and thus introduces an energy cutoff:

$$E_{\text{cut}}\simeq\frac{\hbar^2}{ml^2}. \tag{21}$$

This cutoff is of no physical consequence if all characteristic energies (μ, k_BT) are smaller, i.e., l is smaller than the corresponding characteristic lengths. This leads, for instance, to the following restrictions for l:

$$l<\xi \quad \text{and} \quad l<\lambda, \tag{22}$$

where

$$\xi=\frac{\hbar}{\sqrt{m\mu}} \tag{23}$$

is the healing length, and

$$\lambda=\sqrt{\frac{2\pi\hbar^2}{mk_BT}} \tag{24}$$

is the thermal de Broglie wavelength. These two restrictions, combined with Eq. (7), impose

$$\rho\lambda^D\gg 1, \tag{25}$$

$$\rho\xi^D\gg 1. \tag{26}$$

These are conditions of validity for our discrete model.

The first one, Eq. (25), is the quantum degeneracy regime occurring at sufficiently low temperatures. The second restriction, Eq. (26), corresponds to the regime of weakly interacting systems. Its dependence on the density varies according to the dimension of space. In 1D and 3D, the mean field prediction for the chemical potential is $\mu\simeq g\rho$, where g is a constant characterizing the interaction potential, the so-called coupling constant. In 1D, Eq. (26) is the high-density limit where a mean field theory is valid; we recall that the small density limit $\rho\,\xi=\hbar\sqrt{\rho/mg}\ll 1$ corresponds to the strongly interacting (or strongly correlated) Tonks gas regime. In 3D, the effective coupling constant g is related to the s-wave scattering length a of the interaction potential, $g=4\pi\hbar^2a/m$, so that $\rho\xi^3\propto 1/\sqrt{\rho a^3}\gg 1$: one recovers the usual small gaseous parameter $\sqrt{\rho a^3}$. In 2D, the chemical potential scales as $\hbar^2\rho/[m\ln(1/\rho a^2)]$ where a is the scattering length of the 2D interaction potential, so that the condition $\rho\xi^2\gg 1$ results in a low-density condition, $\ln(1/\rho a^2)\gg 1$.

II. PERTURBATIVE TREATMENT OF A MODEL HAMILTONIAN

A. Model Hamiltonian

In our lattice model, we represent the binary interaction potential among the particles by a discrete δ potential:

$$V(\mathbf{r}_1-\mathbf{r}_2)=\frac{g_0}{l^D}\delta_{\mathbf{r}_1,\mathbf{r}_2}, \tag{27}$$

where g_0 is the bare coupling constant. Note that g_0 in general differs from the effective coupling constant g, and we shall come back to this point in Sec. IV A. With this model potential, the grand canonical Hamiltonian is

$$H=\sum_{\mathbf{r}} l^D\left[-\frac{\hbar^2}{2m}\hat{\psi}^\dagger(\mathbf{r})\Delta\hat{\psi}(\mathbf{r})+[U(\mathbf{r})-\mu]\hat{\psi}^\dagger(\mathbf{r})\hat{\psi}(\mathbf{r})+\frac{g_0}{2}\hat{\psi}^\dagger(\mathbf{r})\hat{\psi}^\dagger(\mathbf{r})\hat{\psi}(\mathbf{r})\hat{\psi}(\mathbf{r})\right], \tag{28}$$

where $U(\mathbf{r})$ is an external trapping potential and where the Laplacian is a symmetric operator coupling the different neighboring boxes:

$$\Delta f(\mathbf{r})=\sum_j \frac{f(\mathbf{r}+l\mathbf{e}_j)+f(\mathbf{r}-l\mathbf{e}_j)-2f(\mathbf{r})}{l^2}. \tag{29}$$

The $\mathbf{e}_j$ are the unitary vectors and j the different orthogonal space directions (for example, $j=x,y,z$ in 3D). As usual we take periodic boundary conditions inside a rectangular box with lengths integer multiples of l.

We now rewrite the Hamiltonian in the density-phase representation, that is, in term of the operators $\hat{\rho}$ and $\hat{\theta}$ giving the density and the phase as defined in the previous section. The contributions of the trapping potential and of the interaction potential to the Hamiltonian are local in real space and therefore include the operator $\hat{\rho}$ only:

$$H_{\rm pot}=\sum_{\mathbf{r}} l^D\hat{\rho}(\mathbf{r})\left[U(\mathbf{r})-\mu+\frac{g_0}{2}\left(\hat{\rho}(\mathbf{r})-\frac{1}{l^D}\right)\right], \tag{30}$$

where we have used the bosonic commutation relation (4) to exchange one of the $\hat{\psi}^\dagger$ with $\hat{\psi}$ in the interaction term. The kinetic energy term involves the phase operator explicitly:

$$H_{\rm kin}=-\frac{\hbar^2}{2ml^2}\sum_{\mathbf{r}} l^D\sum_j \sqrt{\hat{\rho}}\left(e^{i(\hat{\theta}_{+j}-\hat{\theta})}\sqrt{\hat{\rho}_{+j}}+e^{i(\hat{\theta}_{-j}-\hat{\theta})}\sqrt{\hat{\rho}_{-j}}-2\sqrt{\hat{\rho}}\right), \tag{31}$$

where we have introduced the notation $\hat{\theta}_{\pm j}=\hat{\theta}(\mathbf{r}\pm l\mathbf{e}_j)$ and $\hat{\rho}_{\pm j}=\hat{\rho}(\mathbf{r}\pm l\mathbf{e}_j)$. A remarkable property of this formulation, to be used below, is that it involves only the difference of two phase operators between two neighboring points of the lattice.

B. Hamiltonian quadratization and cubization

We now expand the Hamiltonian to third order in powers of two small parameters. As already discussed in Sec. I A the regime of quasicondensates that we are interested in corresponds to small relative fluctuations $\delta\hat{\rho}$ of the density. In the zeroth order approach totally neglecting the density fluctuations, the density is set to a deterministic value ρ_0, as we shall see. The second order expansion allows us to describe the density fluctuations:

$$\hat{\rho}(\mathbf{r})=\rho_0(\mathbf{r})+\delta\hat{\rho}(\mathbf{r}). \tag{32}$$

The third order expansion allows us to calculate the mean value of $\delta\hat{\rho}(\mathbf{r})$.

The first small parameter of the systematic expansion used in this paper is therefore given by

$$\epsilon_1 = \frac{|\delta\hat{\rho}|}{\rho_0} \ll 1, \tag{33}$$

where $|\delta\hat{\rho}|$ is the typical value of the operator $\delta\hat{\rho}$ in the physical state of the system. Mathematically, this allows us to expand $\sqrt{\hat{\rho}}$ as

$$\hat{\rho}^{1/2} = \rho_0^{1/2} + \frac{1}{2}\frac{\delta\hat{\rho}}{\rho_0^{1/2}} - \frac{1}{8}\frac{\delta\hat{\rho}^2}{\rho_0^{3/2}} + \frac{1}{16}\frac{\delta\hat{\rho}^3}{\rho_0^{5/2}} \cdots . \tag{34}$$

The second small parameter of the expansion is given by

$$\epsilon_2 = |l\nabla\hat{\theta}| \ll 1. \tag{35}$$

Here ∇ represents the gradient on the lattice:

$$\nabla f(\mathbf{r}) = \sum_j \frac{f(\mathbf{r}+l\mathbf{e}_j) - f(\mathbf{r}-l\mathbf{e}_j)}{2l}\mathbf{e}_j, \tag{36}$$

where f is an arbitrary function. Physically, the existence of the small parameter ϵ_2 is reasonable: it is at the basis of our hypothesis that the continuous quantum field problem can be well approximated by a discrete lattice model, provided that l is small enough (see Sec. I C). Mathematically, this second small parameter allows us to expand the exponentials of the phase differences in Eq. (31):

$$e^{i(\hat{\theta}_{+j} - \hat{\theta})} = 1 + i(\hat{\theta}_{+j} - \hat{\theta}) - \frac{1}{2}(\hat{\theta}_{+j} - \hat{\theta})^2 \cdots . \tag{37}$$

From the fact that the discretization length l is on the order of the smaller of the two macroscopic length scales ξ and λ [see Eq. (22)], it will be checked later that the parameters ϵ_1 and ϵ_2, though of apparently different physical origin, can be chosen to be of the same order of magnitude,

$$\epsilon_1 \sim \epsilon_2 \sim \frac{1}{\sqrt{\rho_0 l^D}}, \tag{38}$$

and can therefore be treated mathematically as infinitesimals of the same order. The mathematical details of the expansion

$$H = H_0 + H_1 + H_2 + H_3 + \cdots \tag{39}$$

are given in Appendix A; we present here only the results:

$$H_0 = \sum_{\mathbf{r}} l^D \left[-\frac{\hbar^2}{2m}\sqrt{\rho_0}\Delta\sqrt{\rho_0} + \frac{g_0}{2}\rho_0^2 + [U(\mathbf{r}) - \mu]\rho_0 \right],$$

$$H_1 = \sum_{\mathbf{r}} l^D \left[-\frac{\hbar^2}{2m\sqrt{\rho_0}}\Delta\sqrt{\rho_0} + U(\mathbf{r}) - \mu + g_0\rho_0 \right]\delta\hat{\rho},$$

$$H_2 = E_2[\rho_0] + \sum_{\mathbf{r}} l^D \left[-\frac{\hbar^2}{2m}\frac{\delta\hat{\rho}}{2\sqrt{\rho_0}}\Delta\left(\frac{\delta\hat{\rho}}{2\sqrt{\rho_0}}\right) + \frac{\hbar^2\delta\hat{\rho}^2}{8m\rho_0^{3/2}}\Delta\sqrt{\rho_0} + \frac{g_0}{2}\delta\hat{\rho}^2 + \frac{\hbar^2}{2m}\sum_j \sqrt{\rho_0(\mathbf{r})\rho_0(\mathbf{r}+l\mathbf{e}_j)}\frac{[\hat{\theta}(\mathbf{r}+l\mathbf{e}_j) - \hat{\theta}(\mathbf{r})]^2}{l^2} \right],$$

$$H_3 = -\frac{g_0}{2}\sum_{\mathbf{r}} \delta\hat{\rho} + \frac{\hbar^2}{4ml^2}\sum_{\mathbf{r},j} l^D(\hat{\theta}_{+j} - \hat{\theta})\left(\frac{\rho_{0,+j}^{1/2}}{\rho_0^{1/2}}\delta\hat{\rho} + \frac{\rho_0^{1/2}}{\rho_{0,+j}^{1/2}}\delta\hat{\rho}_{+j}\right)(\hat{\theta}_{+j} - \hat{\theta}) + \frac{\hbar^2}{8m}\sum_{\mathbf{r}} \frac{\delta\hat{\rho}}{\rho_0}(\rho_0^{-1/2}\Delta\rho_0^{1/2} - \rho_0^{1/2}\Delta\rho_0^{-1/2})$$
$$- \frac{\hbar^2}{16m}\sum_{\mathbf{r}} l^D\left[\frac{\delta\hat{\rho}^3}{\rho_0^{5/2}}\Delta\sqrt{\rho_0} - \frac{\delta\hat{\rho}^2}{\rho_0^{3/2}}\Delta\left(\frac{\delta\hat{\rho}}{\sqrt{\rho_0}}\right)\right]. \tag{40}$$

The quantity E_2 in H_2 is a c-number functional of the density ρ_0, given in Appendix A, which therefore has no contribution to the dynamics of the quantum field.

C. Iterative solution for the quadratic Hamiltonian

We now solve perturbatively, order by order, the Hamiltonian problems defined by H_0, H_0+H_1, and $H_0+H_1+H_2$. To zeroth order in $\epsilon_{1,2}$, the Hamiltonian is a c number. As the chemical potential is fixed in our approach, H_0 is minimized for a density profile $\rho_0(\mathbf{r})$ such that $\sqrt{\rho_0}$ solves the discrete version of the Gross-Pitaevskii equation:

$$\left[-\frac{\hbar^2}{2m}\Delta + U(\mathbf{r}) - \mu + g_0\rho_0\right]\sqrt{\rho_0} = 0. \tag{41}$$

This density profile constitutes the zeroth order approxima-

tion to the density ρ. It contains a number of particles that we call N_0:

$$N_0 \equiv \sum_{\mathbf{r}} l^D \rho_0(\mathbf{r}). \tag{42}$$

Note that N_0 coincides with the mean total number of particles N only to lowest order in the theory. Equation (41) defines ρ_0 and therefore N_0 as functions of the chemical potential μ. It will, however, turn out to be more convenient to parametrize the theory in terms of N_0 rather than in terms of μ. We will therefore consider μ and ρ_0 as functions of N_0:

$$\mu = \mu_0(N_0), \tag{43}$$

$$\rho_0(\mathbf{r}) = \rho_0(\mathbf{r}; N_0). \tag{44}$$

μ_0 is therefore the Gross-Pitaevskii prediction for the chemical potential of a gas of N_0 particles.

For the choice of density profile (41), the first order correction H_1 to the Hamiltonian vanishes. We therefore now have to solve the Hamiltonian problem defined by H_2, in order to determine the lowest-order approximation to the density fluctuation $\delta\hat{\rho}$ and the phase $\hat{\theta}$. It is instructive to write the corresponding Heisenberg equations of motion, which are linear (and therefore trivially solvable) since H_2 is quadratic. As $\hat{\theta}$ and $\delta\hat{\rho}$ are two canonically conjugate variables, the equations of motion are

$$\begin{aligned}\hbar\partial_t\hat{\theta} &\simeq -\frac{1}{l^D}\frac{\partial H_2}{\partial \delta\hat{\rho}(\mathbf{r})} = \frac{\hbar^2}{2m\sqrt{\rho_0}}\left[\Delta\left(\frac{\delta\hat{\rho}}{2\sqrt{\rho_0}}\right) - \delta\hat{\rho}\frac{\Delta\sqrt{\rho_0}}{2\rho_0}\right] \\ &\quad - g_0\delta\hat{\rho}, \\ \hbar\partial_t\delta\hat{\rho}(\mathbf{r}) &\simeq \frac{1}{l^D}\frac{\partial H_2}{\partial\hat{\theta}(\mathbf{r})} = -\frac{\hbar^2}{m}\sqrt{\rho_0}[\Delta(\hat{\theta}\sqrt{\rho_0}) - \hat{\theta}\Delta\sqrt{\rho_0}].\end{aligned} \tag{45}$$

An important difference of these equations from the so-called quantum hydrodynamics equations for $\delta\hat{\rho}$ and $\hat{\theta}$ is that our formalism keeps the so-called quantum pressure term for $\partial_t\hat{\theta}$, whereas it is usually neglected in the literature [23]. This allows our treatment to have a cutoff energy larger than μ, whereas the usual treatment is restricted to energy modes much below μ.

Furthermore, one can simplify these equations using the Gross-Pitaevskii equation (41) to eliminate $\Delta\sqrt{\rho_0}$:

$$\hbar\partial_t\hat{\theta} = -\frac{1}{2\sqrt{\rho_0}}\left[-\frac{\hbar^2}{2m}\Delta + U + 3g_0\rho_0 - \mu\right]\left(\frac{\delta\hat{\rho}}{\sqrt{\rho_0}}\right), \tag{46}$$

$$\hbar\partial_t\delta\hat{\rho}(\mathbf{r}) = 2\sqrt{\rho_0}\left[-\frac{\hbar^2}{2m}\Delta + U + g_0\rho_0 - \mu\right](\hat{\theta}\sqrt{\rho_0}). \tag{47}$$

This gives the idea of a very simple canonical transformation which, remarkably, maps our equations for a quasicondensate (46),(47) into the equations for the Bogoliubov modes of a condensate: the field

$$\hat{B} = \frac{\delta\hat{\rho}}{2\sqrt{\rho_0}} + i\sqrt{\rho_0}\hat{\theta} \tag{48}$$

has bosonic commutation relations

$$[\hat{B}(\mathbf{r}), \hat{B}^\dagger(\mathbf{r}')] = \frac{\delta_{\mathbf{r},\mathbf{r}'}}{l^D} \tag{49}$$

and it obeys the standard Bogoliubov equations

$$i\hbar\partial_t\begin{pmatrix}\hat{B}\\ \hat{B}^\dagger\end{pmatrix} = \mathcal{L}_{\mathrm{GP}}\begin{pmatrix}\hat{B}\\ \hat{B}^\dagger\end{pmatrix} \equiv \begin{pmatrix} -\frac{\hbar^2}{2m}\Delta + U - \mu + 2g_0\rho_0 & g_0\rho_0 \\ -g_0\rho_0 & -\left(-\frac{\hbar^2}{2m}\Delta + U - \mu + 2g_0\rho_0\right)\end{pmatrix}\begin{pmatrix}\hat{B}\\ \hat{B}^\dagger\end{pmatrix}. \tag{50}$$

This mapping can be readily extended to the Hamiltonian H_2, which is expected to be canonically equivalent to the Bogoliubov Hamiltonian:

$$\begin{aligned}H_2 = l^D\sum_{\mathbf{r}} &\hat{B}^\dagger\left(-\frac{\hbar^2}{2m}\Delta + U + g_0\rho_0 - \mu\right)\hat{B} \\ &+ g_0\rho_0\left[\hat{B}^\dagger\hat{B} + \frac{1}{2}(\hat{B}^2 + \hat{B}^{\dagger 2})\right].\end{aligned} \tag{51}$$

We have checked that the identity (51) indeed holds by replacing $\hat{B}$ by its expression (48) in terms of $\delta\hat{\rho}$ and $\hat{\theta}$, and by using the value of the commutators (20) and the fact that $\sqrt{\rho_0}$ solves the Gross-Pitaevskii equation. Remarkably, the energy functional $E_2[\rho_0]$ is exactly compensated by the contribution of the commutators.

This mapping therefore allows us to reuse the standard diagonalization of the Bogoliubov Hamiltonian. We recall here briefly the procedure described in [15,27]. One intro-

duces the normal eigenmodes (u_s, v_s) of the Bogoliubov operator $\mathcal{L}_{\rm GP}$ with an energy ϵ_s, normalizable as

$$\sum_{\mathbf{r}} l^D[|u_s(\mathbf{r})|^2 - |v_s(\mathbf{r})|^2] = 1. \tag{52}$$

Then (v_s^*, u_s^*) is an eigenmode of $\mathcal{L}_{\rm GP}$ with the energy $-\epsilon_s$. To form a complete family of vectors one has to further introduce the zero-energy mode of $\mathcal{L}_{\rm GP}$, given by $(\phi_0, -\phi_0)$, and the anomalous mode (ϕ_a, ϕ_a) with

$$\phi_0 = \sqrt{\rho_0/N_0} \quad \text{and} \quad \phi_a = \sqrt{N_0}\partial_{N_0}\sqrt{\rho_0}. \tag{53}$$

The corresponding normalization of the anomalous mode is such that the scalar product of ϕ_0 and ϕ_a is 1/2. With these definitions, one introduces the components of $(\hat{B}, \hat{B}^\dagger)$ on the zero-energy mode, on the anomalous mode and on the regular (u_s, v_s) modes:

$$\begin{pmatrix} \hat{B} \\ \hat{B}^\dagger \end{pmatrix} = -i\sqrt{N_0}\hat{Q}\begin{pmatrix} \phi_0 \\ -\phi_0 \end{pmatrix} + \frac{\hat{P}}{\sqrt{N_0}}\begin{pmatrix} \phi_a \\ \phi_a \end{pmatrix} + \sum_s \hat{b}_s\begin{pmatrix} u_s \\ v_s \end{pmatrix} + \hat{b}_s^\dagger\begin{pmatrix} v_s^* \\ u_s^* \end{pmatrix}. \tag{54}$$

$\hat{Q}$ is a collective coordinate representing the quantum phase of the field and $\hat{P}$ is its conjugate momentum

$$[\hat{P}, \hat{Q}] = -i. \tag{55}$$

Physically $\hat{P}$ corresponds to fluctuations in the total number of particles, as expected, and as shown in more detail later [see Eq. (67)]. The operators $\hat{b}_s$ are bosonic annihilation operators with the usual commutation relations $[\hat{b}_s, \hat{b}_{s'}] = \delta_{s,s'}$. They commute with $\hat{P}$ and $\hat{Q}$. The inverse formulas giving $\hat{b}_s$, $\hat{Q}$, and $\hat{P}$ in terms of $\hat{B}$ can be found, for example, in [15]. Equation (54) results in the following modal expansion for the density fluctuations and the phase operators:

$$\hat{\theta}(\mathbf{r}) = \sum_s \theta_s(\mathbf{r})\hat{b}_s + \theta_s^*(\mathbf{r})\hat{b}_s^\dagger - \hat{Q},$$

$$\delta\hat{\rho}(\mathbf{r}) = \sum_s \delta\rho_s(\mathbf{r})\hat{b}_s + \delta\rho_s^*(\mathbf{r})\hat{b}_s^\dagger + \hat{P}\partial_{N_0}\rho_0, \tag{56}$$

where

$$\theta_s(\mathbf{r}) = \frac{u_s(\mathbf{r}) - v_s(\mathbf{r})}{2i\sqrt{\rho_0(\mathbf{r})}},$$

$$\delta\rho_s(\mathbf{r}) = \sqrt{\rho_0(\mathbf{r})}[u_s(\mathbf{r}) + v_s(\mathbf{r})]. \tag{57}$$

By construction, this modal expansion, when inserted into the quadratic Hamiltonian H_2, results in

$$H = \sum_s \epsilon_s \hat{b}_s^\dagger \hat{b}_s + \frac{1}{2}\hat{P}^2\mu_0' + \tilde{E}_2[\rho_0], \tag{58}$$

where $\mu_0' = d\mu_0/dN_0$. This is the sum of uncoupled harmonic oscillators, plus a massive free degree of freedom corresponding to the unbound phase variable $\hat{Q}$. The effective mass of the phase variable is given by $1/\mu_0'$. The energy functional $\tilde{E}_2[\rho_0]$ will be calculated in Sec. III B, where it will be shown that it leads to exactly the same ground state energy as the number conserving Bogoliubov theory. This shows that the Bogoliubov theory can be used to calculate the ground state energy even for, e.g., 1D quasicondensates, a fact commonly used in the literature [28,29] but which looks rather heuristic in the absence of justification.

D. Effect of cubic Hamiltonian corrections on the density

The physics contained in the cubic term H_3 of the Hamiltonian is very rich. It includes interaction effects between the Bogoliubov modes of the previous section, allowing a generalization to quasicondensates of the theory of energy shifts and Beliaev-Landau damping usually put forward for Bose-Einstein condensates [30–32].

We are more modest here. Our motivation to include the cubic corrections is that the quadratic Hamiltonian H_2 brings actually no correction to the zeroth order approximation ρ_0 to the mean density, since the mean value of $\delta\hat{\rho}$ vanishes at the level of the second order theory. This is highly nonsatisfactory as it brings some inconsistency into the calculation of an observable like g_1, the first order correlation function of the field: to get a nontrivial prediction for g_1 one has to include terms quadratic in the phase operator, which are second order in ϵ_2, which forces us to also include second order corrections to the mean density, as will become very explicit in Sec. III.

We therefore calculate the first order correction to the equations of motion of $\delta\hat{\rho}$ and $\hat{\theta}$ due to the cubic Hamiltonian term H_3, and we take the average over the quantum state corresponding to the density operator at thermal equilibrium for the Hamiltonian H_2. This gives source terms to add to the equations for the mean density and phase derived from H_2. We leave the details of the calculations to Appendix B and give the result directly:

$$\hbar\partial_t\langle\delta\hat{\rho}\rangle_3 = \rho_0^{1/2}\left[-\frac{\hbar^2}{2m}\Delta + U + g_0\rho_0 - \mu\right](2\rho_0^{1/2}\langle\hat{\theta}\rangle_3), \tag{59}$$

$$-2\hbar\sqrt{\rho_0}\partial_t\langle\hat{\theta}\rangle_3 = \left[-\frac{\hbar^2}{2m}\Delta + U + 3g_0\rho_0 - \mu\right]\times\left(\frac{\langle\delta\hat{\rho}\rangle_3 - \langle\hat{B}^\dagger\hat{B}\rangle_2}{\rho_0^{1/2}}\right) + g_0\rho_0^{1/2}\langle 4\hat{B}^\dagger\hat{B} + \hat{B}^2 + B^{\dagger 2}\rangle_2 - 2\langle\hat{P}^2\rangle_2\mu_0'\partial_{N_0}\sqrt{\rho_0}, \tag{60}$$

where the thermal average $\langle\cdots\rangle_2$ is taken with the unperturbed Hamiltonian H_2 and $\langle\cdots\rangle_3$ is taken with the perturbed Hamiltonian H_2+H_3 to first order in H_3. The expectation value of the "kinetic energy" of the unbound phase variable in Eq. (58) is equal to $k_BT/2$ according to the equipartition theorem so that

$$\langle\hat{P}^2\rangle_2=\frac{k_BT}{\mu_0'}. \tag{61}$$

At equilibrium the expectation values of $\partial_t\delta\hat{\rho}$ and $\partial_t\hat{\theta}$ vanish. This fact is obvious for $\partial_t\delta\hat{\rho}$; it is less obvious for $\partial_t\hat{\theta}$ because of the presence of the unbound variable $\hat{Q}$; we therefore produce a proof of that in Appendix C. We therefore have to solve Eqs. (59) and (60) with the left-hand side set to zero. The first equation (59) imposes the condition that the mean value of $\hat{\theta}$ is position independent, a trivial result. In the second equation, the operator acting on $\langle\delta\hat{\rho}\rangle_3$ is strictly positive so that it is invertible, and Eq. (60) determines the correction to the mean density in a unique way.

We now go through a sequence of transformations allowing us to get a physical understanding of the value of $\langle\delta\hat{\rho}\rangle_3$. The first step is to pull out the contribution of the "anomalous" terms $\hat{P}$, $\hat{Q}$ in the modal expansion (54):

$$\hat{B}(\mathbf{r})\equiv -i\sqrt{N_0}\hat{Q}\phi_0(\mathbf{r})+\frac{1}{\sqrt{N_0}}\hat{P}\phi_a(\mathbf{r})+\hat{B}_n. \tag{62}$$

We calculate the expectation values of Eq. (60) involving the operator $\hat{B}$, using the fact that all the crossed terms between the anomalous part and the operators b_s have a vanishing expectation value:

$$\langle\hat{B}^\dagger\hat{B}\rangle_2=\frac{\phi_a^2}{N_0}\langle\hat{P}^2\rangle_2+N_0\phi_0^2\langle\hat{Q}^2\rangle_2+\langle\hat{B}_n^\dagger\hat{B}_n\rangle_2-\phi_a\phi_0, \tag{63}$$

$$\langle\hat{B}^2\rangle_2+\langle\hat{B}^{\dagger 2}\rangle_2=2\frac{\phi_a^2}{N_0}\langle\hat{P}^2\rangle_2-2N_0\phi_0^2\langle\hat{Q}^2\rangle_2+\langle\hat{B}_n^2\rangle_2+\langle\hat{B}_n^{\dagger 2}\rangle_2. \tag{64}$$

The term $\phi_0\phi_a$ in Eq. (63) comes from the noncommutation of $\hat{P}$ and $\hat{Q}$ [see Eq. (55)]. The contributions of $\langle\hat{Q}^2\rangle_2$ in Eqs. (63) and (64), when inserted into Eq. (60), are shown to compensate exactly when one uses the fact that ϕ_0 solves the Gross-Pitaevskii equation. This was expected from the U(1) symmetry of the Hamiltonian: only differences of the phase operator at two points appear in the Hamiltonian, so that H does not depend on $\hat{Q}$ and the mean density does not depend on $\langle\hat{Q}^2\rangle_2$.

We therefore get an equation for $\langle\delta\hat{\rho}\rangle_3$ involving the expectation value of $\hat{P}^2$ as a source term, and which looks rather involved:

$$\begin{aligned}0=&\left[-\frac{\hbar^2}{2m}\Delta+U+3g_0\rho_0-\mu\right]\\&\times\left(\frac{\langle\delta\hat{\rho}\rangle_3-\phi_a^2N_0^{-1}\langle\hat{P}^2\rangle_2-(\langle\hat{B}_n^\dagger\hat{B}_n\rangle_2-\phi_0\phi_a)}{\rho_0^{1/2}}\right)\\&+g_0\rho_0^{1/2}\langle 4(\hat{B}_n^\dagger\hat{B}_n-\phi_0\phi_a)+\hat{B}_n^2+B_n^{\dagger 2}\rangle_2\\&+\langle\hat{P}^2\rangle_2[6g_0\rho_0^{1/2}\partial_{N_0}\sqrt{\rho_0}-2\mu_0']\partial_{N_0}\sqrt{\rho_0}.\end{aligned} \tag{65}$$

Fortunately the underlying physics is very simple and allows us to predict the effect of this source term on the mean density. One first identifies the physical meaning of $\hat{P}$ in Eq. (56). Using the well-known fact that the eigenmodes of $\mathcal{L}_{\mathrm{GP}}$ are orthogonal for the modified scalar product of signature $(1,-1)$, one has [15]

$$\langle\phi_0|u_s\rangle+\langle\phi_0|v_s\rangle\equiv\sum_{\mathbf{r}}l^D\phi_0(\mathbf{r})[u_s(\mathbf{r})+v_s(\mathbf{r})]=0, \tag{66}$$

so that the sum of $\delta\rho_s$ over all spatial nodes vanishes. As a consequence, the operator $\hat{N}$ giving the total number of particles in the gas is simply

$$\hat{N}\equiv\sum_{\mathbf{r}}l^D\hat{\rho}(\mathbf{r})=N_0+\hat{P}, \tag{67}$$

where we have used the identity

$$\sum_{\mathbf{r}}l^D\partial_{N_0}\rho_0(\mathbf{r})=\frac{d}{dN_0}\sum_{\mathbf{r}}l^D\rho_0(\mathbf{r})=\frac{dN_0}{dN_0}=1. \tag{68}$$

The source terms involving $\hat{P}$ therefore correspond to fluctuations in the total number of particles in the gas, due to the fact that we consider the grand canonical ensemble. The effect of these grand canonical fluctuations can be considered for the case of a pure quasicondensate at the order of the present calculation so it is easy to calculate it directly. In the grand canonical ensemble the probability that the quasicondensate has n particles is

$$\Pi_n\propto\exp[-\beta(E_0(n)-\mu n)], \tag{69}$$

where $E_0(n)$ is the Gross-Pitaevskii energy for the density profile $\rho_0(\mathbf{r};n)$:

$$E_0(n)=\sum_{\mathbf{r}}l^D\left[-\frac{\hbar^2}{2m}\sqrt{\rho_0(\mathbf{r};n)}\Delta\sqrt{\rho_0(\mathbf{r};n)}+U(\mathbf{r})\rho_0(\mathbf{r};n)+\frac{g_0}{2}\rho_0^2(\mathbf{r};n)\right]. \tag{70}$$

The corresponding mean grand canonical density is

$$\rho_{\mathrm{GC}}(\mathbf{r})=\int dn\,\Pi_n\rho_0(\mathbf{r};n), \tag{71}$$

where we treat n as a continuous variable. The zeroth order approximation $n=N_0$ for the number of particles in the quasicondensate is such that $E_0(n)-\mu n$ has a minimum:

$$\frac{d}{dn}[E_0(n)-\mu n]=\mu_0(n)-\mu=0 \quad \text{for} \quad n=N_0 \tag{72}$$

as shown in Eq. (43). The corresponding density profile is $\rho_0(\mathbf{r};N_0)$. The next order correction to that is obtained by expanding the n dependent density profile to second order in $n-N_0$ and by averaging over n:

$$\delta\rho_{\rm GC}(\mathbf{r})=\langle(n-N_0)\rangle\partial_{N_0}\rho_0(\mathbf{r};N_0) + \frac{1}{2}\langle(n-N_0)^2\rangle\partial_{N_0}^2\rho_0(\mathbf{r};N_0). \tag{73}$$

The second moment of $n-N_0$ is calculated to lowest nonvanishing order by a Gaussian approximation to Π_n:

$$E_0(n)-\mu n\simeq E_0(N_0)-\mu N_0+\frac{1}{2}\frac{d^2E_0}{dN_0^2}(n-N_0)^2 = \text{const}+\frac{1}{2}\mu_0'(n-N_0)^2. \tag{74}$$

This leads to

$$\langle(n-N_0)^2\rangle_{\rm Gauss}=\frac{k_BT}{\mu_0'}=\langle\hat{P}^2\rangle_2. \tag{75}$$

More care has to be taken in the calculation of the mean of $n-N_0$: the Gaussian approximation to Π_n gives a vanishing contribution, so that the cubic distortion to it has to be included:

$$E_0(n)-\mu n\simeq E_0(N_0)-\mu N_0+\frac{1}{2}\mu_0'(n-N_0)^2 + \frac{1}{6}\mu_0''(n-N_0)^3, \tag{76}$$

$$\Pi_n\propto\exp\left[-\frac{1}{2}\beta\mu_0'(n-N_0)^2\right]\left[1-\frac{1}{6}\beta\mu_0''(n-N_0)^3\right]. \tag{77}$$

We then get a nonvanishing mean value for $n-N_0$:

$$\langle(n-N_0)\rangle_{\rm distor}=-\frac{1}{6}\beta\mu_0''\langle(n-N_0)^4\rangle_{\rm Gauss} = -\frac{1}{2}\beta\mu_0''(\langle\hat{P}^2\rangle_2)^2. \tag{78}$$

We have therefore predicted in a very simple way the correction to the mean density due to grand canonical fluctuations:

$$\delta\rho_{\rm GC}(\mathbf{r})=\frac{1}{2}\langle\hat{P}^2\rangle_2\left[\partial_{N_0}^2\rho_0(\mathbf{r};N_0)-\frac{\mu_0''}{\mu_0'}\partial_{N_0}\rho_0(\mathbf{r};N_0)\right]. \tag{79}$$

How does this compare to the general formalism (65)? We need to obtain a partial differential equation for $\delta\rho_{\rm GC}$. We just take the second order derivative of the Gross-Pitaevskii equation (41) with respect to N_0 and we replace ρ_0 by $\sqrt{\rho_0}^2$ in the resulting equation and in Eq. (79). This leads to the remarkable identity

$$\left[-\frac{\hbar^2}{2m}\Delta+U+3g_0\rho_0-\mu\right]\left(\frac{\delta\rho_{\rm GC}-N_0^{-1}\phi_a^2\langle\hat{P}^2\rangle_2}{\rho_0^{1/2}}\right) = -\langle\hat{P}^2\rangle_2[6g_0\rho_0^{1/2}\partial_{N_0}\sqrt{\rho_0}-2\mu_0']\partial_{N_0}\sqrt{\rho_0}. \tag{80}$$

The right-hand side of this identity coincides with the source term of Eq. (65) involving $\hat{P}$. We have therefore successfully identified $\delta\rho_{\rm GC}$ as a piece of $\langle\delta\hat{\rho}\rangle_3$ and we are left with the simpler equation

$$0=\left[-\frac{\hbar^2}{2m}\Delta+U+3g_0\rho_0-\mu\right] \times\left(\frac{\langle\delta\hat{\rho}\rangle_3-\delta\rho_{\rm GC}-(\langle\hat{B}_n^\dagger\hat{B}_n\rangle_2-\phi_0\phi_a)}{\rho_0^{1/2}}\right) + g_0\rho_0^{1/2}\langle 4(\hat{B}_n^\dagger\hat{B}_n-\phi_0\phi_a)+\hat{B}_n^2+B_n^{\dagger 2}\rangle_2. \tag{81}$$

We are not totally satisfied yet since the operator $\hat{B}_n$ does not obey bosonic commutation relations when the system is not spatially homogeneous; in particular, the field $\hat{B}_n$ does not commute with itself when taken at two different points:

$$[\hat{B}_n(\mathbf{r}),\hat{B}_n(\mathbf{r}')]=\phi_a(\mathbf{r})\phi_0(\mathbf{r}')-\phi_a(\mathbf{r}')\phi_0(\mathbf{r}), \tag{82}$$

$$[\hat{B}_n(\mathbf{r}),\hat{B}_n^\dagger(\mathbf{r}')]=\frac{1}{l^D}\delta_{\mathbf{r},\mathbf{r}'}-\phi_0(\mathbf{r})\phi_a(\mathbf{r}') - \phi_0(\mathbf{r}')\phi_a(\mathbf{r}). \tag{83}$$

To circumvent this difficulty we split the field $\hat{B}_n$ into its component along the quasicondensate mode ϕ_0 and its orthogonal component:

$$\hat{B}_n(\mathbf{r})=\hat{\alpha}\phi_0(\mathbf{r})+\hat{\Lambda}(\mathbf{r}). \tag{84}$$

The Bogoliubov functions $u_s(\mathbf{r})$ and $v_s(\mathbf{r})$ can be chosen here to be real. The operator $\hat{\alpha}$ can then be written as

$$\hat{\alpha}=\sum_s\langle\phi_0|u_s\rangle(\hat{b}_s-\hat{b}_s^\dagger), \tag{85}$$

where we have used the property (66). This clearly shows that the operator $\hat{\alpha}$ is anti-Hermitian:

$$\hat{\alpha}^\dagger=-\hat{\alpha}. \tag{86}$$

The field $\hat{\Lambda}$ has the following expansion on $\hat{b}_s$:

$$\hat{\Lambda}(\mathbf{r})=\sum_s u_{s\perp}(\mathbf{r})\hat{b}_s+v_{s\perp}(\mathbf{r})\hat{b}_s^\dagger, \tag{87}$$

where the index $\perp$ indicates projection orthogonally to ϕ_0. This field now has the desired bosonic commutation relations

$$[\hat{\Lambda}(\mathbf{r}),\hat{\Lambda}(\mathbf{r}')]=0, \tag{88}$$

$$[\hat{\Lambda}(\mathbf{r}),\hat{\Lambda}^\dagger(\mathbf{r}')]=\frac{1}{l^D}\delta_{\mathbf{r},\mathbf{r}'}-\phi_0(\mathbf{r})\phi_0(\mathbf{r}'). \tag{89}$$

Note that $\hat{\alpha}$ does not commute with $\hat{\Lambda}$:

$$[\hat{\alpha},\hat{\Lambda}(\mathbf{r})]=\frac{1}{2}\phi_0(\mathbf{r})-\phi_a(\mathbf{r}). \tag{90}$$

We insert the splitting of $\hat{B}_n$ in Eq. (81). The terms quadratic in $\hat{\alpha}$ cancel exactly, in the same way the terms in $\hat{Q}^2$ canceled. The terms linear in $\hat{\alpha}$ can all be expressed in terms of the expectation value of an anticommutator $\langle\{\hat{\alpha},\hat{\Lambda}\}\rangle_2$ using the commutation relation (90) and the fact that $\langle\hat{\alpha}\hat{\Lambda}\rangle_2$ is a real quantity. Furthermore, using the techniques of Appendix E of [26], as shown here in Appendix D, one obtains a simple partial differential equation for the anticommutator:

$$\left[-\frac{\hbar^2}{2m}\Delta+U+g_0\rho_0-\mu\right]\langle\{\hat{\alpha},\hat{\Lambda}(\mathbf{r})\}\rangle_2 = -\sum_{\mathbf{r}'} l^D g_0\rho_0(\mathbf{r}')\phi_0(\mathbf{r}')\langle\{\hat{\Lambda}(\mathbf{r}')+\hat{\Lambda}^\dagger(\mathbf{r}'),\hat{\Lambda}(\mathbf{r})\}\rangle_2. \tag{91}$$

Remarkably, this allows us to eliminate completely the operator $\hat{\alpha}$ in Eq. (81). We finally get an equation for the correction to the mean density involving the operator $\hat{\Lambda}$ only:

$$0=\left[-\frac{\hbar^2}{2m}\Delta+U+3g_0\rho_0-\mu\right]\left(\frac{\langle\delta\hat{\rho}\rangle_3-\delta\rho_{\mathrm{GC}}-\langle\hat{\Lambda}^\dagger\hat{\Lambda}\rangle_2}{\phi_0}\right)+S(\mathbf{r}), \tag{92}$$

where we have introduced the source term

$$S(\mathbf{r})\equiv g_0N_0\phi_0(\mathbf{r})\langle 4\hat{\Lambda}^\dagger(\mathbf{r})\hat{\Lambda}(\mathbf{r})+\hat{\Lambda}^2(\mathbf{r})+\hat{\Lambda}^{\dagger 2}(\mathbf{r})-\phi_0^2(\mathbf{r})\rangle_2 - \sum_{\mathbf{r}'} l^D g_0\rho_0(\mathbf{r}')\phi_0(\mathbf{r}')\langle\{\hat{\Lambda}(\mathbf{r}')+\hat{\Lambda}^\dagger(\mathbf{r}'),\hat{\Lambda}(\mathbf{r})\}\rangle_2. \tag{93}$$

It will be convenient to introduce the function $\chi(\mathbf{r})$ defined in a unique way by

$$0=\left[-\frac{\hbar^2}{2m}\Delta+U+3g_0\rho_0-\mu\right]\chi(\mathbf{r})+\frac{1}{2}S(\mathbf{r}). \tag{94}$$

We then obtain the following final expression for the correction to the mean density due to the cubic Hamiltonian terms H_3:

$$\langle\delta\hat{\rho}\rangle_3(\mathbf{r})=\delta\rho_{\mathrm{GC}}(\mathbf{r})+2\phi_0(\mathbf{r})\chi(\mathbf{r})+\langle\hat{\Lambda}^\dagger(\mathbf{r})\hat{\Lambda}(\mathbf{r})\rangle_2. \tag{95}$$

In the particular case where the gas is Bose condensed, our general theory for quasicondensates also applies, of course. One then expects that the result (95) has already been obtained for the condensate and can be given a clear physical interpretation. This expectation is totally justified: as shown in Appendix E, the component of $\chi(\mathbf{r})/N_0$ orthogonal to ϕ_0 is the correction given in [15] to the Gross-Pitaevskii condensate wave function ϕ_0 due to the interaction with the noncondensed particles; the component of χ along ϕ_0 describes the condensate depletion, and $\langle\hat{\Lambda}^\dagger\hat{\Lambda}\rangle_2$ is the mean density of noncondensed particles.

III. APPLICATIONS OF THE FORMALISM: GENERAL FORMULAS

A. Equation of state

What is referred to as the *equation of state* of the gas is the expression of the chemical potential as a function of the mean total number of particles N and the temperature T. It is useful in particular to predict properties of an inhomogeneous gas within the local density approximation.

We therefore now have to calculate μ for the quasicondensate. This is equivalent to a calculation of N_0 as μ and N_0 are by definition related through Eq. (43). To lowest order of the theory one assumes a pure quasicondensate with a density profile $\rho(\mathbf{r})=\rho_0(\mathbf{r})$, where $\sqrt{\rho_0}$ solves the Gross-Pitaevskii equation (41). One therefore gets $N=N_0$ so that $\mu=\mu_0(N)$.

The first nonvanishing correction to the density profile is given by Eq. (95). By integrating Eq. (95) over space we get the corresponding correction for the mean total number of particles:

$$N\equiv N_0+\delta N, \tag{96}$$

$$\delta N\simeq\delta N_{\mathrm{GC}}+l^D\sum_{\mathbf{r}}2\phi_0(\mathbf{r})\chi(\mathbf{r})+l^D\sum_{\mathbf{r}}\langle\hat{\Lambda}^\dagger(\mathbf{r})\hat{\Lambda}(\mathbf{r})\rangle_2. \tag{97}$$

The contribution to δN due to our use of the grand canonical ensemble can be calculated exactly from a spatial integration of Eq. (79), using the same technique as in Eq. (68):

$$\delta N_{\mathrm{GC}}=-k_BT\frac{\mu_0''}{2\mu_0'^2}. \tag{98}$$

The contribution of the term involving χ can also be made explicit by multiplication of Eq. (94) by $\phi_a(\mathbf{r})$ defined in Eq. (53) and by spatial integration. The function $\phi_a(\mathbf{r})$ is indeed known [27] to solve the partial differential equation

$$\left[-\frac{\hbar^2}{2m}\Delta+U+3g_0\rho_0-\mu\right]\phi_a=N_0\mu_0'\phi_0(\mathbf{r}), \quad (99)$$

which can be checked easily, just by taking the derivative of Eq. (41) with respect to N_0. This leads to

$$l^D\sum_{\mathbf{r}} 2\phi_0(\mathbf{r})\chi(\mathbf{r})=-\frac{1}{N_0\mu_0'}\sum_{\mathbf{r}} l^D\phi_a(\mathbf{r})S(\mathbf{r}), \quad (100)$$

where the source term S is known explicitly [see Eq. (93)]. We now just have to replace N_0 by $N-\delta N$ in Eq. (43) and expand to first order in δN:

$$\mu=\mu_0(N-\delta N)\simeq\mu_0(N)-\delta N\mu_0'(N_0). \quad (101)$$

We obtain the following expression for μ:

$$\mu\simeq\mu_0(N)+k_BT\frac{\mu_0''}{2\mu_0'}-\mu_0'(N_0)\sum_{\mathbf{r}} l^D\langle\hat\Lambda^\dagger(\mathbf{r})\hat\Lambda(\mathbf{r})\rangle_2 + \frac{1}{N_0}\sum_{\mathbf{r}} l^D\phi_a(\mathbf{r})S(\mathbf{r}). \quad (102)$$

Equivalently, we can replace the source term by its explicit expression to get

$$\mu\simeq\mu_0(N)+k_BT\frac{\mu_0''}{2\mu_0'}-\mu_0'(N_0)\left(\frac{1}{2}+\sum_{\mathbf{r}} l^D\langle\hat\Lambda^\dagger(\mathbf{r})\hat\Lambda(\mathbf{r})\rangle_2\right) + \sum_{\mathbf{r}} l^D g_0[\partial_{N_0}\rho_0(\mathbf{r})](2\langle\hat\Lambda^\dagger\hat\Lambda\rangle_2+\mathrm{Re}\langle\hat\Lambda^2\rangle_2) - \sum_{\mathbf{r}} l^D g_0\phi_0^3(\mathbf{r})\langle\{\hat\Lambda(\mathbf{r})+\hat\Lambda^\dagger(\mathbf{r}),\hat\gamma\}\rangle_2, \quad (103)$$

where we have introduced the operator

$$\hat\gamma=\sum_{\mathbf{r}} l^D\phi_a(\mathbf{r})\hat\Lambda(\mathbf{r}), \quad (104)$$

and we have used the identity

$$\mu_0'=\sum_{\mathbf{r}} l^D g_0\phi_0^2(\mathbf{r})\partial_{N_0}\rho_0(\mathbf{r};N_0) \quad (105)$$

obtained by performing the scalar product of both sides of Eq. (99) with ϕ_0. The application to spatially homogeneous systems will be given in Sec. IV; in this case both the operator $\hat\gamma$ and μ_0'' vanish.

B. Ground state energy

We now show that the ground state energy of a quasicondensate can be calculated with exactly the same Bogoliubov formula as for the ground state energy of a condensate.

We have to determine the ground state energy of H_2. We write it as the expectation value of Eq. (51) at zero temperature, that is here in the vacuum of the $\hat b_s$ and of $\hat P$:

$$\mathcal{E}_{\mathrm{ground}}(H_2)=l^D\sum_{\mathbf{r}}\left\langle\hat B^\dagger\left(-\frac{\hbar^2}{2m}\Delta+U+g_0\rho_0-\mu\right)\hat B\right\rangle_2 + g_0\rho_0\left\langle\left[\hat B^\dagger\hat B+\frac{1}{2}(\hat B^2+\hat B^{\dagger 2})\right]\right\rangle_2. \quad (106)$$

We reproduce the transformation of Sec. II D. We split $\hat B$ into an anomalous part involving $\hat P,\hat Q$, plus the contributions of the anti-Hermitian operator $\hat\alpha$ and of $\hat\Lambda$, the orthogonal component of the normal part. In the first expectation value of the right-hand side of Eq. (106) the operators $\hat Q$ and $\hat\alpha$ disappear as they come with the factor $\phi_0(\mathbf{r})$ in $\hat B$, and ϕ_0 solves the Gross-Pitaevskii equation (41). The expectation value of $\hat P^2$ in the ground state of H_2 also vanishes, so that

$$\left\langle\hat B^\dagger\left(-\frac{\hbar^2}{2m}\Delta+U+g_0\rho_0-\mu\right)\hat B\right\rangle_2 =\left\langle\hat\Lambda^\dagger\left(-\frac{\hbar^2}{2m}\Delta+U+g_0\rho_0-\mu\right)\hat\Lambda\right\rangle_2. \quad (107)$$

The same transformation is applied to the last expectation value in Eq. (106). Remarkably, the terms involving $\hat\alpha$ exactly cancel when one uses the relations (63), (64), (90), and (D5). This leads to

$$\left\langle\left[\hat B^\dagger\hat B+\frac{1}{2}(\hat B^2+\hat B^{\dagger 2})\right]\right\rangle_2 =-\frac{1}{2}\phi_0^2+\left\langle\left[\hat\Lambda^\dagger\hat\Lambda+\frac{1}{2}(\hat\Lambda^2+\hat\Lambda^{\dagger 2})\right]\right\rangle_2. \quad (108)$$

The expectation values involving $\hat\Lambda$ are readily calculated from the modal expansion (87):

$$\mathcal{E}_{\mathrm{ground}}(H_2)=-\frac{1}{2}\sum_{\mathbf{r}} l^D g_0\rho_0\phi_0^2 + \sum_s\langle v_{s\perp}|\left[\left(-\frac{\hbar^2}{2m}\Delta+U+2g_0\rho_0-\mu\right)|v_{s\perp}\rangle + g_0\rho_0|u_{s\perp}\rangle\right]. \quad (109)$$

As (u_s,v_s) is an eigenvector of $\mathcal{L}_{\mathrm{GP}}$, $(u_{s\perp},v_{s\perp})$ is an eigenvector of the operator $\mathcal{L}$ defined in [15] and this expression can be further simplified to

$$\mathcal{E}_{\mathrm{ground}}(H_2)=-\frac{1}{2}\sum_{\mathbf{r}} l^D g_0\rho_0\phi_0^2-\sum_s\epsilon_s\langle v_{s\perp}|v_{s\perp}\rangle. \quad (110)$$

The last step is to include the contribution of H_0 and to remove the $-\mu\hat{N}$ term from the grand canonical Hamiltonian. The ground state energy of the canonical Hamiltonian for N particles is therefore

$$E_{\text{ground}}(N) \simeq \mu N + E_0(N_0) - \mu N_0 + \mathcal{E}_{\text{ground}}(H_2), \quad (111)$$

where E_0 is the Gross-Pitaevskii energy (70). As we did in Sec. III A we replace N_0 by $N-\delta N$, where δN is calculated from H_3, and we expand $E_0(N-\delta N)$ to first order in δN:

$$\mu N + E_0(N_0) - \mu N_0 \simeq E_0(N) - \delta N(\mu_0(N) - \mu) \simeq E_0(N). \quad (112)$$

We recall that by definition $\mu = \mu_0(N_0)$. The first term in the right-hand side of Eq. (110) amounts to performing a small change in the Gross-Pitaevskii energy functional, expressing the fact that a given particle interacts in the gas with $N-1$ particles so that the mean field term should be proportional to $N-1$ rather than to N. The final expression for the ground state energy is

$$E_{\text{ground}}(N) \simeq N \sum_{\mathbf{r}} l^D \Big[-\frac{\hbar^2}{2m}\phi_0(\mathbf{r};N)\Delta\phi_0(\mathbf{r};N) + U(\mathbf{r})\phi_0^2(\mathbf{r};N) + \frac{1}{2}g_0(N-1)\phi_0^4(\mathbf{r};N)\Big] - \sum_s \epsilon_s \langle v_{s\perp}|v_{s\perp}\rangle. \quad (113)$$

This exactly coincides with the Bogoliubov result; see, e.g., Eq. (71) of [15].

C. Second order correlation function

The second order correlation function of the atomic field is defined as

$$g_2(\mathbf{r}) \equiv \langle \hat{\psi}^\dagger(\mathbf{r})\hat{\psi}^\dagger(\mathbf{0})\hat{\psi}(\mathbf{0})\hat{\psi}(\mathbf{r})\rangle, \quad (114)$$

where we have taken for simplicity one of the two points as the origin of the coordinates. To calculate g_2 with the formalism of this paper we have to express g_2 in terms of the operator $\hat{\rho}$ giving the density. This is achieved using the commutation relation (4) of the bosonic field $\hat{\psi}$:

$$g_2(\mathbf{r}) = \langle \hat{\rho}(\mathbf{r})\hat{\rho}(\mathbf{0})\rangle - \frac{\delta_{\mathbf{r},\mathbf{0}}}{l^D}\langle\hat{\rho}(\mathbf{0})\rangle. \quad (115)$$

We then insert the splitting (32) of $\hat{\rho}$ in terms of the quasicondensate density ρ_0 and the fluctuations $\delta\hat{\rho}$:

$$g_2(\mathbf{r}) = \rho_0(\mathbf{r})\rho_0(\mathbf{0}) + \rho_0(\mathbf{0})\langle\delta\hat{\rho}(\mathbf{r})\rangle + \rho_0(\mathbf{r})\langle\delta\hat{\rho}(\mathbf{0})\rangle + \langle\delta\hat{\rho}(\mathbf{r})\delta\hat{\rho}(\mathbf{0})\rangle - \frac{\delta_{\mathbf{r},\mathbf{0}}}{l^D}[\rho_0(\mathbf{0}) + \langle\delta\hat{\rho}(\mathbf{0})\rangle]. \quad (116)$$

This expression for g_2 is still exact. We now perform approximations consistent with an expansion of g_2 up to second order in the small parameters $\epsilon_{1,2}$. The expectation value of the term quadratic in $\delta\hat{\rho}$ is calculated within the thermal equilibrium for the quadratic Hamiltonian H_2. The expectation value of $\delta\hat{\rho}$ is evaluated in Sec. II D by inclusion of the cubic perturbation H_3. The contribution of $\delta\hat{\rho}$ in the last term of Eq. (116) is negligible as it is ϵ_1^4 times smaller than the leading term in g_2. We therefore obtain the explicit expression

$$g_2(\mathbf{r}) \simeq \rho_0(\mathbf{r})\rho_0(\mathbf{0}) + \rho_0(\mathbf{0})\langle\delta\hat{\rho}(\mathbf{r})\rangle_3 + \rho_0(\mathbf{r})\langle\delta\hat{\rho}(\mathbf{0})\rangle_3 + \langle\delta\hat{\rho}(\mathbf{r})\delta\hat{\rho}(\mathbf{0})\rangle_2 - \frac{\delta_{\mathbf{r},\mathbf{0}}}{l^D}\rho_0(\mathbf{0}). \quad (117)$$

This formulation, however, is not the optimal one as the last term in $1/l^D$ gives the wrong impression that $g_2(0)$ strongly depends on the discretization length l in the continuous limit $l\to 0$. In fact, this strong dependence exactly compensates a term in $1/l^D$ in the density fluctuations $\langle\delta\hat{\rho}^2(\mathbf{0})\rangle$ coming from the fact that $\delta\hat{\rho}^2(\mathbf{0})$ is a product of field operators not in normal order. To reveal this fact we express $\delta\hat{\rho}$ in terms of the operator $\hat{\Lambda}$ of Eq. (87):

$$\delta\hat{\rho}(\mathbf{r}) = \sqrt{\rho_0(\mathbf{r})}[\hat{\Lambda}(\mathbf{r}) + \hat{\Lambda}^\dagger(\mathbf{r})] + \hat{P}\,\partial_{N_0}\rho_0(\mathbf{r};N_0), \quad (118)$$

and we put the resulting expression in normal order with respect to the field $\hat{\Lambda}$ using the bosonic commutation relation (89):

$$\delta\hat{\rho}(\mathbf{r})\delta\hat{\rho}(\mathbf{0}) = :\delta\hat{\rho}(\mathbf{r})\delta\hat{\rho}(\mathbf{0}): + \frac{\delta_{\mathbf{r},\mathbf{0}}}{l^D}\rho_0(\mathbf{0}) - N_0\phi_0^2(\mathbf{r})\phi_0^2(\mathbf{0}), \quad (119)$$

where $::$ is the standard notation to represent normal order. The spurious term in $1/l^D$ is then exactly canceled:

$$g_2(\mathbf{r}) = N_0(N_0-1)\phi_0^2(\mathbf{r})\phi_0^2(\mathbf{0}) + \rho_0(\mathbf{0})\langle\delta\hat{\rho}(\mathbf{r})\rangle_3 + \rho_0(\mathbf{r})\langle\delta\hat{\rho}(\mathbf{0})\rangle_3 + \langle:\delta\hat{\rho}(\mathbf{r})\delta\hat{\rho}(\mathbf{0}):\rangle_2. \quad (120)$$

This expression allows a proof of the equivalence with the prediction for g_2 in the Bogoliubov theory. We do not present the calculations here, as they are a straightforward application of Appendix E. Finally, we give a last alternative expression for g_2 equivalent to Eq. (120) at the present order:

$$g_2(\mathbf{r}) = (1-1/N)\rho(\mathbf{0})\rho(\mathbf{r}) + \langle:\delta\hat{\rho}(\mathbf{r})\delta\hat{\rho}(\mathbf{0}):\rangle_2, \quad (121)$$

where N is the mean total number of particles and ρ is the mean total density:

$$\rho(\mathbf{r}) = \rho_0(\mathbf{r}) + \langle\delta\hat{\rho}(\mathbf{r})\rangle_3. \quad (122)$$

D. First order correlation function

The first order correlation function of the field is defined as

$$g_1(\mathbf{r}) \equiv \langle \hat{\psi}^\dagger(\mathbf{r})\hat{\psi}(\mathbf{0})\rangle = \langle \sqrt{\hat{\rho}(\mathbf{r})}e^{i[\hat{\theta}(\mathbf{0})-\hat{\theta}(\mathbf{r})]}\sqrt{\hat{\rho}(\mathbf{0})}\rangle. \tag{123}$$

As previously done we perform the calculation up to second order in the small parameters $\epsilon_{1,2}$. We therefore expand $\sqrt{\hat{\rho}}$ up to second order in $\delta\hat{\rho}$ using Eq. (34). Note that we do not expand the exponential in $\hat{\theta}(\mathbf{0})-\hat{\theta}(\mathbf{r})$, contrary to what we did in the Hamiltonian: as $\mathbf{r}$ and $\mathbf{0}$ are not neighboring points of the lattice anymore, the phase difference of the field can be arbitrarily large. The expansion in $\delta\hat{\rho}$ gives rise to six terms:

$$\begin{aligned} g_1(\mathbf{r}) = \rho_0^{1/2}(\mathbf{r})\rho_0^{1/2}(\mathbf{0})\Big[& \langle e^{i\Delta\theta}\rangle + \frac{1}{2}\langle \delta\tilde{\rho}(\mathbf{r})e^{i\Delta\theta} + e^{i\Delta\theta}\delta\tilde{\rho}(\mathbf{0})\rangle \\ & - \frac{1}{8}\langle \delta\tilde{\rho}^2(\mathbf{r})e^{i\Delta\theta} + e^{i\Delta\theta}\delta\tilde{\rho}^2(\mathbf{0}) \\ & - 2\,\delta\tilde{\rho}(\mathbf{r})e^{i\Delta\theta}\delta\tilde{\rho}(\mathbf{0})\rangle\Big], \end{aligned} \tag{124}$$

where we have introduced the following notation to simplify the writing:

$$\Delta\theta \equiv \hat{\theta}(\mathbf{0}) - \hat{\theta}(\mathbf{r}) \tag{125}$$

$$\delta\tilde{\rho}(\mathbf{r}) \equiv \frac{\delta\hat{\rho}(\mathbf{r})}{\rho_0(\mathbf{r})}. \tag{126}$$

We calculate the expectation values in this expression in two steps, first using the thermal equilibrium distribution for H_2, and then including the corrections due to H_3.

The thermal expectation values corresponding to the quadratic Hamiltonian H_2 are evaluated using Wick's theorem. One first expands the exponential in powers of $\Delta\theta$, one calculates the expectation value of each term, and then one performs an exact resummation of the resulting series. This leads to the simple identities

$$\langle e^{i\Delta\theta}\rangle_2 = e^{-\langle(\Delta\theta)^2\rangle_2/2}, \tag{127}$$

$$\langle \delta\tilde{\rho}(\mathbf{r})e^{i\Delta\theta}\rangle_2 = e^{-\langle(\Delta\theta)^2\rangle_2/2}\langle \delta\tilde{\rho}(\mathbf{r})i\Delta\theta\rangle_2, \tag{128}$$

$$\begin{aligned} \langle \delta\tilde{\rho}^2(\mathbf{r})e^{i\Delta\theta}\rangle_2 = {} & e^{-\langle(\Delta\theta)^2\rangle_2/2} \\ & \times[\langle \delta\tilde{\rho}^2(\mathbf{r})\rangle_2 + (\langle \delta\tilde{\rho}(\mathbf{r})i\Delta\theta\rangle_2)^2], \end{aligned} \tag{129}$$

$$\begin{aligned} \langle \delta\tilde{\rho}(\mathbf{r})e^{i\Delta\theta}\delta\tilde{\rho}(\mathbf{0})\rangle_2 = {} & e^{-\langle(\Delta\theta)^2\rangle_2/2}[\langle \delta\tilde{\rho}(\mathbf{r})\delta\tilde{\rho}(\mathbf{0})\rangle_2 \\ & + \langle \delta\tilde{\rho}(\mathbf{r})i\Delta\theta\rangle_2\langle i\Delta\theta\delta\tilde{\rho}(\mathbf{0})\rangle_2]. \end{aligned} \tag{130}$$

The expectation value of a product of the density fluctuation $\delta\hat{\rho}$ and of the phase variation $i\Delta\theta$ is particularly simple. In classical field theory this expectation value would obviously vanish, as there is no crossed term in H_2 between the density fluctuations and the phase. In the present quantum field theory this is not exactly the case as $\hat{\rho}$ and $\hat{\theta}$ do not commute. To show that, we use the fact that the Bogoliubov mode functions $u_s(\mathbf{r})$ and $v_s(\mathbf{r})$ can be chosen to be real, so that $\delta\hat{\rho}$ and $i\Delta\theta$ are linear combinations of $\hat{b}_s, \hat{b}_s^\dagger, \hat{P}$ with real coefficients. As a consequence,

$$\langle \delta\tilde{\rho}(\mathbf{r})i\Delta\theta\rangle_2 = \langle \delta\tilde{\rho}(\mathbf{r})i\Delta\theta\rangle_2^* = -\langle i\Delta\theta\delta\tilde{\rho}(\mathbf{r})\rangle. \tag{131}$$

This leads to

$$\langle \delta\tilde{\rho}(\mathbf{r})i\Delta\theta\rangle_2 = \frac{i}{2}\langle[\delta\tilde{\rho}(\mathbf{r}), \Delta\theta]\rangle_2 = \frac{1-\delta_{\mathbf{r},\mathbf{0}}}{2\rho_0(\mathbf{r})l^D}. \tag{132}$$

The same reasoning can be applied for the other expectation value:

$$\langle i\Delta\theta\delta\tilde{\rho}(\mathbf{0})\rangle_2 = \frac{1-\delta_{\mathbf{r},\mathbf{0}}}{2\rho_0(\mathbf{0})l^D}. \tag{133}$$

These expressions are second order in $\epsilon_{1,2}$. An important consequence is that the product of such crossed phase-density expectation values in Eqs. (129) and (130) is actually negligible at the present order of the calculation. The resulting form for g_1, at the level of H_2, is quite simple:

$$\begin{aligned} g_1(\mathbf{r})|_{H_2} = \rho_0^{1/2}(\mathbf{r})\rho_0^{1/2}(\mathbf{0})e^{-\langle(\Delta\theta)^2\rangle_2/2}\Big[& 1 - \frac{1}{8}\langle(\Delta\delta\tilde{\rho})^2\rangle_2 \\ & + \frac{1}{4}\mathcal{E}_{\text{scoria}}(\mathbf{r})\Big]. \end{aligned} \tag{134}$$

The notation $\Delta\delta\tilde{\rho}$ is similar to the one for the phase:

$$\Delta\delta\tilde{\rho} \equiv \delta\tilde{\rho}(\mathbf{0}) - \delta\tilde{\rho}(\mathbf{r}) \tag{135}$$

and $\mathcal{E}_{\text{scoria}}$ comes from the crossed expectation value of $\Delta\theta$ and $\delta\tilde{\rho}$:

$$\mathcal{E}_{\text{scoria}}(\mathbf{r}) \equiv (1-\delta_{\mathbf{r},\mathbf{0}})\left(\frac{1}{\rho_0(\mathbf{r})l^D} + \frac{1}{\rho_0(\mathbf{0})l^D}\right). \tag{136}$$

At this point we face the same apparent problem as in the calculation of g_2: $\mathcal{E}_{\text{scoria}}$ scales as $1/l^D$ and gives the wrong impression that our expression for g_1 will depend dramatically on l in the continuous limit $l\to 0$. As in the case of g_2, we solve this problem by expressing $\delta\hat{\rho}$ and $\hat{\theta}$ in terms of the field $\hat{\Lambda}$ and putting the operators $\hat{\Lambda}$ and $\hat{\Lambda}^\dagger$ in normal order. We use Eq. (118) for the expression for $\delta\hat{\rho}$. For the difference of two phase operators, $\hat{Q}$ and the anti-Hermitian operator $\hat{\alpha}$ cancel so that

$$\Delta\theta=\frac{1}{2i}(\Delta\tilde{\Lambda}-\Delta\tilde{\Lambda}^{\dagger}), \tag{137}$$

where we have introduced the notation

$$\tilde{\Lambda}(\mathbf{r})\equiv\frac{\hat{\Lambda}(\mathbf{r})}{\rho_0^{1/2}(\mathbf{r})}, \tag{138}$$

$$\Delta\tilde{\Lambda}\equiv\tilde{\Lambda}(\mathbf{0})-\tilde{\Lambda}(\mathbf{r}). \tag{139}$$

After some calculations we arrive at

$$\langle(\Delta\delta\tilde{\rho})^2\rangle_2=\langle:(\Delta\delta\tilde{\rho})^2:\rangle_2+\mathcal{E}_{\text{scoria}}(\mathbf{r}), \tag{140}$$

$$\langle(\Delta\theta)^2\rangle_2=\langle:(\Delta\theta)^2:\rangle_2+\frac{1}{4}\mathcal{E}_{\text{scoria}}(\mathbf{r}). \tag{141}$$

As $\mathcal{E}_{\text{scoria}}$ is second order in $\epsilon_{1,2}$, its exponential function can be expanded to first order. We then find as expected that all the $1/l^D$ terms exactly cancel:

$$g_1(\mathbf{r})|_{H_2}=\rho_0^{1/2}(\mathbf{r})\rho_0^{1/2}(\mathbf{0})e^{-\langle:(\Delta\theta)^2:\rangle_2/2}\left[1-\frac{1}{8}\langle:(\Delta\delta\tilde{\rho})^2:\rangle_2\right]. \tag{142}$$

The last step is to include the first order correction to g_1 coming from the cubic Hamiltonian H_3. One then has to calculate expectation values with the thermal equilibrium density operator $\exp[-\beta(H_2+H_3)]$ to first order in H_3. This thermal density operator can be viewed as the evolution operator during the imaginary time $-i\hbar\beta$ so that one can use first order time dependent perturbation theory to get

$$\langle\hat{O}\rangle_3\simeq\langle\hat{O}\rangle_2-\int_0^{\beta}d\tau\langle e^{\tau H_2}H_3e^{-\tau H_2}\hat{O}\rangle_2, \tag{143}$$

where $\hat{O}$ is an arbitrary operator of the gas and where we have used the fact that H_3 has a vanishing expectation value in the thermal equilibrium state for H_2. One is back to the calculation of expectation values of some operators in the thermal state corresponding to H_2. Wick's theorem can be applied. The resulting calculations are very similar to the ones leading to Eq. (142), but more involved, and are detailed in Appendix F. The same phenomenon occurs, that terms of a higher order than the present calculation can be neglected. One then gets

$$\langle e^{i\Delta\theta}\rangle_3\simeq e^{-\langle(\Delta\theta)^2\rangle_2/2}[1+\langle i\Delta\theta\rangle_3], \tag{144}$$

$$\langle\delta\tilde{\rho}(\mathbf{r})e^{i\Delta\theta}\rangle_3\simeq e^{-\langle(\Delta\theta)^2\rangle_2/2}[\langle\delta\tilde{\rho}(\mathbf{r})i\Delta\theta\rangle_2+\langle\delta\tilde{\rho}(\mathbf{r})\rangle_3]. \tag{145}$$

The first terms in the right-hand sides of Eqs. (144) and (145) already appeared at the level of H_2, and the second terms are corrections due to H_3 that we now take into account. There is no need to include H_3 corrections to the other terms of Eq. (124) since they are quadratic in $\delta\hat{\rho}$ and are therefore already of second order. The expectation values of the phase $\hat{\theta}$ and of the density fluctuations $\delta\hat{\rho}$ have been calculated in Sec. II D. It was found that the expectation value of the phase operator is space independent so that $\langle\Delta\theta\rangle_3$ vanishes. The expectation value of the density fluctuations including the effect of H_3 was given in Eq. (95) and is in general different from zero. Remarkably, the whole effect on the correlation function g_1 of the first order correction in H_3 is to replace $\rho_0(\mathbf{r})$ by the total mean density $\rho(\mathbf{r})$ defined in Eq. (122).

We write our final expression for the first order correlation function of the field, calculated consistently up to $\epsilon_{1,2}^2$:

$$g_1(\mathbf{r})=\sqrt{\rho(\mathbf{r})\rho(\mathbf{0})}\exp\left[-\frac{1}{2}\langle:(\Delta\theta)^2:\rangle_2-\frac{1}{8}\langle:(\Delta\delta\tilde{\rho})^2:\rangle_2\right]. \tag{146}$$

Note that we have inserted the contribution of the density fluctuations inside the exponential factor, which is allowed at the order of the present calculation since this contribution is of order $\epsilon_{1,2}^2$.

What happens in the regime where a true condensate is present? Both phase and density fluctuations are small, so that the exponential function in Eq. (146) can be expanded to first order. We then express $\Delta\theta$ and $\Delta\tilde{\rho}$ in terms of the operator $\hat{\Lambda}$ and the operator $\hat{P}$. Since the Bogoliubov theory is usually considered in the canonical ensemble we remove the terms corresponding to the grand canonical fluctuations of the particle number. We then recover exactly the Bogoliubov prediction:

$$g_1^{\text{Bog}}(\mathbf{r})=\Psi_c(\mathbf{r})\Psi_c(\mathbf{0})+\langle\hat{\Lambda}^{\dagger}(\mathbf{r})\hat{\Lambda}(\mathbf{0})\rangle, \tag{147}$$

where $\Psi_c(\mathbf{r})=\sqrt{N_0}\phi_0(\mathbf{r})+\chi(\mathbf{r})/\sqrt{N_0}$ is the condensate field. Amazingly, the general formula (146) for quasicondensates can be related to the Bogoliubov formula in the following very simple way:

$$g_1(\mathbf{r})=\sqrt{\rho(\mathbf{r})\rho(\mathbf{0})}\exp\left[\frac{g_1^{\text{Bog}}(\mathbf{r})}{\sqrt{\rho(\mathbf{r})\rho(\mathbf{0})}}-1\right]. \tag{148}$$

IV. EXPLICIT RESULTS FOR THE SPATIALLY HOMOGENEOUS CASE

In this section we apply our approach to a spatially homogeneous Bose gas. The quasicondensate density is then uniform:

$$\rho_0(\mathbf{r})=\frac{N_0}{L^D}=\frac{\mu}{g_0}. \tag{149}$$

The Bogoliubov equations (50) can then be exactly solved for any dimension of space and lead to $u_k(r)=\overline{u_k}e^{ikr}/L^{D/2}$ and $v_k(r)=\overline{v_k}e^{ikr}/L^{D/2}$ with

$$\overline{u_k}-\overline{v_k}=\left[\frac{\hbar^2k^2/2m+2\mu}{\hbar^2k^2/2m}\right]^{1/4}$$

and

$$\overline{u}_k+\overline{v}_k=\left[\frac{\hbar^2k^2/2m}{\hbar^2k^2/2m+2\mu}\right]^{1/4}. \tag{150}$$

The corresponding eigenenergies are given by

$$\epsilon_k=\left[\frac{\hbar^2k^2}{2m}\left(\frac{\hbar^2k^2}{2m}+2\mu\right)\right]^{1/2}. \tag{151}$$

A. Equation of state

From the general expression (103) for the chemical potential of the gas we arrive in the thermodynamic limit at

$$\mu=\rho g_0+g_0\int_{\mathcal{D}}\frac{d\mathbf{k}}{(2\pi)^D}[(\overline{u}_k+\overline{v}_k)^2n_k+\overline{v}_k(\overline{u}_k+\overline{v}_k)], \tag{152}$$

where $n_k=1/[\exp(\beta\epsilon_k)-1]$ is the mean occupation number of the Bogoliubov mode $\mathbf{k}$. $\mathcal{D}=[-\pi/l,\pi/l]^D$ is the square domain of integration in the $\mathbf{k}$ space. The integral over the wave vector $\mathbf{k}$ does not contain any infrared divergence for any dimension of space. However, the long wave vector behavior given by

$$\overline{v}_k(\overline{u}_k+\overline{v}_k)\simeq-\frac{m\mu}{\hbar^2k^2} \tag{153}$$

gives rise to an integral convergent in 1D and divergent in 2D and 3D in the $l\to0$ limit. This gives the impression that the result depends strongly on l. The solution of this paradox comes from the link between the bare coupling constant g_0 of the model potential in the discretized space and the low-energy two-body scattering properties of the exact potential in the continuous space. This gives to g_0 in two and three dimensions a dependence in l so that our expression for μ does not depend on l anymore in the $l\to0$ limit. In one dimension, the bare coupling g_0 is simply equal to the actual coupling strength g for $l\to0$ and there is no divergence. At $T=0$, Eq. (152) leads to

$$\mu=g\rho\left(1-\frac{1}{\pi\rho\xi}\right), \tag{154}$$

where ξ is the healing length defined in Eq. (23). This agrees with the result of Lieb and Liniger in the weak interaction limit [28]. In three dimensions, we refer to the Appendix of [26] where the calculation has been done. One finds

$$g_0=\frac{g}{1-g\int_{\mathcal{D}}[d\mathbf{k}/(2\pi)^3](m/\hbar^2k^2)}. \tag{155}$$

g is the usual 3D coupling strength given by

$$g=\frac{4\pi\hbar^2a}{m}, \tag{156}$$

where a is the exact potential scattering length. A more explicit form of Eq. (155) is

$$g_0=\frac{g}{1-\mathcal{K}a/l}, \tag{157}$$

where $\mathcal{K}=2.442\ldots$. It has to be noted that the difference between g_0 and g is still small in the validity domain of our approach since it is a second order correction in $\epsilon_{1,2}$: taking $l\sim\xi$ one finds $a/l\sim1/\rho l^3$. Replacing the first factor g_0 in Eq. (152) with the formula (155) expanded up to second order in $\epsilon_{1,2}$ gives

$$\mu=\rho g+g_0\int_{\mathcal{D}}\frac{d\mathbf{k}}{(2\pi)^3}\left((\overline{u}_k+\overline{v}_k)^2n_k+\overline{v}_k(\overline{u}_k+\overline{v}_k)+\frac{m\mu}{\hbar^2k^2}\right). \tag{158}$$

One can then safely take the $l\to0$ limit. At $T=0$, the integration gives:

$$\mu=g\rho\left(1+\frac{32\sqrt{\pi}}{3}\sqrt{\rho a^3}\right) \tag{159}$$

which is the same result as Lee and Yang's [33]. In two dimensions, the low-energy two-body scattering of a general short range potential is described by a single length a also named the scattering length. In a continuous space, the T matrix can be calculated in the low-energy limit:

$$\langle\mathbf{k}|T(E+i\eta)|\mathbf{k}'\rangle\simeq-\frac{2\pi\hbar^2}{m[\ln(ak_0/2)+C-i\pi/2]}, \tag{160}$$

where $C=0.57721\ldots$ is the Euler constant, a is the scattering length, $E=\hbar^2k_0^2/m$, and $\eta\to0^+$. We can also calculate the T matrix for the discrete δ potential defined by Eq. (27), which can also be expressed as

$$V=\frac{g_0}{l^2}|\mathbf{r}=0\rangle\langle\mathbf{r}=0|. \tag{161}$$

The general scattering theory gives the relations between the T matrix, the propagator G, and the free propagator G_0:

$$T=V+VGV, \tag{162}$$

$$G=G_0+G_0VG. \tag{163}$$

Using these relations and Eq. (161) for the potential, we find

$$\langle\mathbf{k}|T_{\mathrm{grid}}(E+i\eta)|\mathbf{k}'\rangle=\frac{g_0}{1-g_0\langle\mathbf{r}=0|G_0(E+i\eta)|\mathbf{r}=0\rangle}. \tag{164}$$

The only term we need to calculate is the free propagator taken at the origin, which is conveniently performed with a Fourier transform:

$$\langle \mathbf{r}=0|G_0(E+i\eta)|\mathbf{r}=0\rangle=\int_{\mathcal{D}}\frac{d\mathbf{k}}{(2\pi)^2}\frac{1}{E+i\eta-\hbar^2k^2/m}. \tag{165}$$

We split the square $\mathcal{D}$ into a disk of radius π/l and the complementary domain. Integration over the complementary domain gives simply a constant term in the low-energy limit $E\ll\hbar^2/ml^2$:

$$J\equiv\frac{2\pi\hbar^2}{m}\int_{\mathcal{D}-\text{disk}}\frac{d\mathbf{k}}{(2\pi)^2}\frac{1}{E+i\eta-\hbar^2k^2/m}$$

$$\simeq-\frac{1}{2\pi}\int_{\mathcal{D}-\text{disk}}\frac{d\mathbf{k}}{k^2}=\frac{2G}{\pi}-\ln(2), \tag{166}$$

where $G=0.91596\ldots$ is the Catalan constant. The disk integration is straightforward and leads to the following expression for the T matrix:

$$\langle\mathbf{k}|T_{\text{grid}}(E+i\eta)|\mathbf{k}'\rangle=\frac{1}{1/g_0-(m/2\pi\hbar^2)\ln(lk_0/\pi)+im/4\hbar^2-(m/2\pi\hbar^2)J}. \tag{167}$$

We now take $T_{\text{grid}}=T$, where T is approximated by Eq. (160), in order to reproduce the low-energy scattering properties of the exact potential. This leads to

$$\frac{1}{g_0}=\frac{m}{2\pi\hbar^2}\left[\ln\left(\frac{l}{\pi a}\right)-C+\frac{2G}{\pi}\right]. \tag{168}$$

Note that the condition (26) has to be satisfied in our approach. In two dimensions, this gives $\hbar^2/mg_0\gg1$, or using Eq. (168)

$$\frac{1}{2\pi}\ln\left(\frac{l}{a}\right)\gg1. \tag{169}$$

We now show that the logarithmic dependence on l appearing in g_0, Eq. (168), exactly cancels the one appearing in the equation of state. Equation (152) can be rewritten as

$$\rho=\frac{\mu}{g_0}-\int_{\mathcal{D}}\frac{d\mathbf{k}}{(2\pi)^2}[(\overline{u_k}+\overline{v_k})^2n_k+\overline{v_k}(\overline{u_k}+\overline{v_k})]. \tag{170}$$

In the thermal part, one can immediately take the $l\to0$ limit. In order to calculate the integral corresponding to the $T=0$ case, we use the same technique as for the calculation of g_0: the integration is done on a disk domain of radius π/l and we keep as a correction the integration over the complementary domain. The complementary domain integration is done by using the high-wave-vector behavior of $\overline{v_k}(\overline{u_k}+\overline{v_k})$, Eq. (153). This leads to

$$-\int_{\mathcal{D}}\frac{d\mathbf{k}}{(2\pi)^2}\overline{v_k}(\overline{u_k}+\overline{v_k})=\frac{m\mu}{4\pi\hbar^2}\left[\ln\left(\frac{\pi^2\hbar^2}{ml^2\mu}\right)-1-2J\right]. \tag{171}$$

Using Eqs. (168) and (171) in Eq. (170), we arrive at an implicit equation of state:

$$\rho=\frac{m\mu}{4\pi\hbar^2}\ln\left(\frac{4\hbar^2}{a^2m\mu e^{2C+1}}\right)-\int\frac{d\mathbf{k}}{(2\pi)^2}(\overline{u_k}+\overline{v_k})^2n_k. \tag{172}$$

Remarkably, this is identical to the result (20.45) obtained by the functional integral method in [7]. At $T=0$, one can show from the condition $\rho\xi^2\gg1$ [see Eq. (26)] that the validity condition of our approach is $\ln(1/\rho a^2)\gg4\pi$. If one approximately inverts Eq. (172), neglecting constant terms and $\ln[\ln(1/\rho a^2)]$ with respect to $\ln(1/\rho a^2)$, one recovers Schick's formula [34].

B. Are density and gradient-of-phase fluctuations small?

As mentioned in Sec. II B, our approach relies in particular on two assumptions: the assumption that the relative density fluctuation ϵ_1 is small, and the assumption that the phase variation ϵ_2 between two neighboring points of the grid is small.

Let us consider first the relative density fluctuations. Because of Eq. (119), their mean square value can be separated into two parts:

$$\epsilon_1^2=\frac{\langle\delta\hat{\rho}^2(\mathbf{0})\rangle_2}{\rho_0^2}=\frac{1}{\rho_0l^D}+\frac{\langle:\delta\hat{\rho}^2(\mathbf{0}):\rangle_2}{\rho_0^2}, \tag{173}$$

where we have neglected $1/L^D$ with respect to $1/l^D$ in the thermodynamic limit. The second term in Eq. (173), involving the normal order, is expressed in terms of the $\overline{u_k},\overline{v_k}$ in the thermodynamic limit as

$$\frac{\langle:\delta\hat{\rho}^2(\mathbf{0}):\rangle_2}{\rho_0^2}=\frac{2}{\rho_0}\int_{\mathcal{D}}\frac{d\mathbf{k}}{(2\pi)^D}[(\overline{u_k}+\overline{v_k})^2n_k+\overline{v_k}(\overline{u_k}+\overline{v_k})], \tag{174}$$

where the integration domain is $\mathcal{D}=[-\pi/l,\pi/l]^D$. At zero temperature one introduces the change of variable $\mathbf{q}=\mathbf{k}\xi$ in the integral: one finds that Eq. (174) is of the order of $1/\rho_0\xi$ in 1D, of the order of $\ln(\xi/l)/\rho_0\xi^2$ in 2D, and of the order of $1/\rho_0\xi^2l$ in 3D. Since $l<\xi$ the second term in Eq. (173) is dominated by the first term, and one has indeed

$$\epsilon_1^2\simeq\frac{1}{\rho_0l^D}. \tag{175}$$

At finite temperature we have to calculate the thermal contribution to Eq. (174) involving the occupation number n_k.

At a temperature $k_BT<\mu$ we use the low-momentum expansion of $\overline{u_k}+\overline{v_k}$, and ϵ_k and we find that the thermal contribution is $(k_BT/\mu)^{D+1}(l/\xi)^D$ times smaller than $1/\rho_0l^D$.

At a temperature $k_BT>\mu$, that is, $\lambda<\xi$, the treatment depends on the dimension of space. In 1D the main contribution to the integral comes from the domain $\epsilon_k\sim\mu$, over which one can approximate the Bose formula by its low-energy limit k_BT/ϵ_k. This leads to a normal ordered fluctuation (174) of the order of $k_BT/(\mu\rho_0\xi)$. This is larger than $1/\rho_0\lambda$ so that the condition $l<\lambda$ then no longer implies that the first term $1/\rho_0 l$ in Eq. (173) is the dominant one. For convenience, one can however adjust l to a value such that

$$\frac{1}{\rho_0 l}\sim\frac{k_BT}{\mu}\frac{1}{\rho_0\xi}. \tag{176}$$

The condition for weak density fluctuations then becomes

$$\epsilon_1^2\sim\frac{k_BT}{\mu}\frac{1}{\rho_0\xi}\ll 1. \tag{177}$$

Using $\rho_0\simeq\rho$ and $\mu\simeq g\rho$ we recover the condition already obtained in [5] with a pure classical field approach. Note that this condition can be rewritten as $\xi\ll l_c$ where the coherence length of the field will be defined in Eq. (187). In 2D both the low-energy domain $\epsilon_k<k_BT$ and the high-energy domain $\epsilon_k>k_BT$ have important contributions. In the low-energy domain we approximate the Bose law by its low-energy limit. In the high-energy domain we keep the full Bose law but, ϵ_k being then larger than μ, we approximate $\overline{u_k}+\overline{v_k}$ by unity and ϵ_k by $\hbar^2k^2/2m$. This leads to a normal ordered fluctuation (174) of the order of $\ln(k_BT/\mu)k_BT/(\mu\rho_0\xi^2)$, a quantity that is larger than $1/\rho_0\lambda^2$. As in 1D we therefore adjust l so that

$$\epsilon_1^2\sim\frac{1}{\rho_0 l^2}\sim\frac{k_BT}{\mu}\ln\left(\frac{k_BT}{\mu}\right)\frac{1}{\rho_0\xi^2}. \tag{178}$$

In 3D the high-energy domain $\epsilon_k>k_BT$ gives the dominant contribution so that the normal ordered expectation value (174) scales as $1/\rho_0\lambda^3$. This is dominated by the first term in Eq. (173) so that the estimate (175) applies as soon as $l<\lambda,\xi$.

Let us consider now the condition that the mean squared phase change over a grid cell,

$$\epsilon_2^2=\langle(l\nabla\hat{\theta})^2\rangle_2=\frac{l^2}{2\rho_0}\int_{\mathcal{D}}\frac{d\mathbf{k}}{(2\pi)^D}k^2(\overline{u_k}-\overline{v_k})^2(n_k+1/2), \tag{179}$$

is much smaller than unity. The presence of the factor k^2 inside the integral, coming from the action of $\boldsymbol{\nabla}$, has the consequence that the contribution to the integral is dominated by the high energy domain. At zero temperature one can replace $\overline{u_k}-\overline{v_k}$ by unity since the integral is dominated by wave vectors $k\sim 1/l>1/\xi$. This leads to

$$\epsilon_2^2\sim\frac{1}{\rho_0 l^D} \tag{180}$$

whatever the dimension D.

At a temperature $k_BT<\mu$ we estimate the thermal contribution by replacing $\overline{u_k}-\overline{v_k}$ and ϵ_k by their low-momentum approximations: the thermal contribution is then $(l/\lambda)^{2+D}(\xi/\lambda)^D$ times smaller than the zero-temperature result (180) and is therefore negligible since $l<\xi<\lambda$.

At a temperature $k_BT>\mu$ we use the high-energy approximation, replacing $\overline{u_k}-\overline{v_k}$ by unity and ϵ_k by $\hbar^2k^2/2m$. Note that this works even in 1D because of the presence of the k^2 factor in the integral (179). This leads to a thermal contribution which is $(l/\lambda)^{2+D}$ times smaller than the zero-temperature contribution (180), and which is negligible since $l<\lambda$.

We conclude that the small parameter ϵ_2 of the theory, ensuring that there is a weak phase variation over a grid cell, is always given by Eq. (180) provided that the conditions (22), (25), and (26) are satisfied.

One may wonder if the corrections of the mean density due to the interaction H_3 between the Bogoliubov modes lead to an extra validity condition of our treatment. For the considered case of a spatially homogeneous gas it turns out that the answer to this question is no. One has indeed the remarkable identity in the thermodynamic limit

$$\frac{1}{\rho_0}\langle\delta\hat{\rho}(\mathbf{r})\rangle_3=-\frac{1}{2\rho_0^2}\langle:\delta\hat{\rho}(\mathbf{r})^2:\rangle_2. \tag{181}$$

If the relative density fluctuations are weak, the relative correction to the density will also be weak.

To end this subsection we discuss briefly the second order correlation function of the field $g_2(\mathbf{r})$. Restricting the general formula (121) to the spatially homogeneous case in the thermodynamic limit, we obtain

$$g_2(\mathbf{r})=\rho^2+2\rho\int_{\mathcal{D}}\frac{d\mathbf{k}}{(2\pi)^D}[(\overline{u_k}+\overline{v_k})^2n_k+\overline{v_k}(\overline{u_k}+\overline{v_k})]\cos(\mathbf{k}\cdot\mathbf{r}). \tag{182}$$

Limiting cases of this general formula can be compared to existing results in the literature. At zero temperature for a 1D Bose gas one gets for $r=0$,

$$g_2(0)=\rho^2\left(1-\frac{2}{\pi\rho\xi}\right). \tag{183}$$

This formula can be checked from [28]: the mean interaction energy per particle v is equal to $g_2(0)$ multiplied by $g/2\rho$, and v can be calculated in the weakly interacting regime by combining (3.29) of [28] (relating v to the derivative of the ground state energy with respect to g) and (4.2) of [28] (giving the ground state energy in the Bogoliubov approximation). This exactly leads to Eq. (183). This prediction for $g_2(0)$ also appears in [35].

C. First order correlation function

Because of the general formula (148) the first order correlation function of the field for the quasicondensate is immediately related to that of the Bogoliubov theory, here in the thermodynamic limit

$$\ln[g_1(\mathbf{r})/\rho] = \frac{g_1^{\mathrm{Bog}}(\mathbf{r})}{\rho} - 1 = -\frac{1}{\rho}\int \frac{d^D k}{(2\pi)^D}[(\overline{u_k^2}+\overline{v_k^2})n_k + \overline{v_k^2}] \times (1-\cos\,\mathbf{k}\cdot\mathbf{r}). \quad (184)$$

We have also taken here the continuous limit $l\to 0$, which does not lead to any divergence.

We concentrate our analysis on the 1D case and we make the link with existing results in the literature. These existing results deal with the asymptotic behavior of g_1 for large r, where r is the absolute value of the spatial coordinate. At zero temperature, we find for $r \gg \xi$:

$$g_1(r) \simeq \rho\left(\frac{r_1}{r}\right)^{1/2\pi\rho\xi}, \quad (185)$$

with $r_1 = e^{2-C}\xi/4 \simeq 1.037\xi$ where $C = 0.577\,21\ldots$ is Euler's constant [36]. This reproduces a result obtained in a nonexplicit way in [37]. At a finite temperature, g_1/ρ is the exponential of an integral of the form

$$\int_0^{+\infty} \frac{A(k)}{k^2}[1-\cos(kr)], \quad (186)$$

where the function $A(k)$ is a regular and even function of k, therefore behaving quadratically with k around $k=0$ [38]. Writing $A(k)$ as $[A(k)-A(0)]+A(0)$ and splitting the integral, accordingly one obtains for r much larger than both ξ and λ,

$$\ln[g_1(r)/\rho] = \frac{r}{l_c} + K + o(1/r^n), \quad (187)$$

where the coherence length $l_c = \rho\lambda^2/\pi$ coincides with the one of [39] and the constant K is given by

$$K = \int_0^{+\infty} \frac{A(k)-A(0)}{k^2}. \quad (188)$$

Since $A(k)$ is even one can show by repeated integration by parts that the remainder in Eq. (187) tends to 0 faster than any power law, contrary to what is stated in [39].

Of course our formula gives access to g_1 for any value of the distance. This is illustrated in Fig. 1 where we have plotted the logarithm of g_1 as function of r/ξ for various temperatures.

As a consequence, we can, for example, calculate the momentum distribution of the atoms:

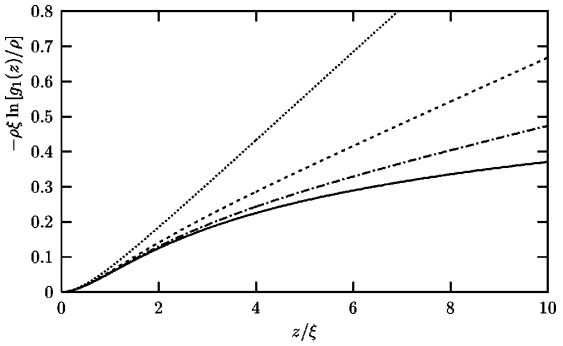

FIG. 1. First order correlation function of the field $g_1(z)$ for a repulsive 1D Bose gas in the thermodynamic limit. The different curves correspond to various ratios of the temperature to the chemical potential: $k_BT/\mu = 0$ (solid line), 1/15 (dot-dashed line), 1/8 (dashed line), 1/4 (dotted line). We plot the logarithm of $g_1(z)$ multiplied by the parameter $\rho\xi$, where ρ is the 1D spatial density and $\xi = \hbar/\sqrt{m\mu}$ is the healing length, so that we obtain a quantity depending only on z/ξ and k_BT/μ in the weakly interacting limit.

$$\Pi(p) = 2\int_0^{+\infty} dr\, g_1(r)\cos(pr/\hbar) \quad (189)$$

normalized here as $\int dp\,\Pi(p) = 2\pi\hbar\rho$ so that $\Pi(p)$ is dimensionless. This is illustrated in Fig. 2 where we have plotted the momentum distribution for various temperatures and for $\rho\xi = 10$. Using integration by parts we can show that the behavior of Π for large p is related to the fact that the third order derivative of g_1 in $r = 0^+$ does not vanish:

$$\Pi(p) \sim \frac{2\hbar^4 g_1^{(3)}(0^+)}{p^4} \quad \text{with} \quad g_1^{(3)}(0^+) = \mu^2 m^2/(2\hbar^4). \quad (190)$$

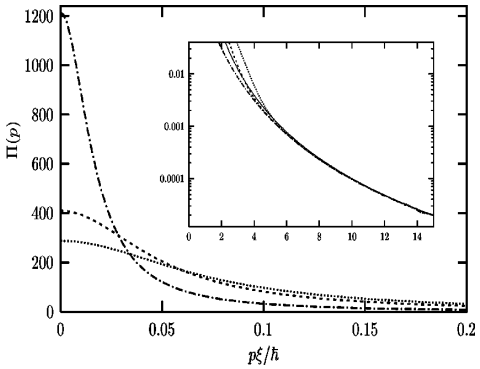

FIG. 2. Momentum distribution of a repulsive 1D Bose gas in the thermodynamic limit. $\Pi(p)$ is normalized as $\int dp\,\Pi(p) = 2\pi\hbar\rho$ where ρ is the 1D spatial density so that $\Pi(p)$ is dimensionless. We plot $\Pi(p)$ as a function of $p\xi/\hbar$ for various ratios of the temperature to the chemical potential: $k_BT/\mu = 1/3$ (dot-dashed lines), 1 (dashed lines), 10/7 (dotted lines). We have taken $\rho\xi = 10 \gg 1$ where $\xi = \hbar/\sqrt{m\mu}$ is the healing length. The solid line is the large p limit: $(\hbar/p\xi)^4$. The inset is a magnification.

This prediction, valid at zero or finite temperature, agrees with the weak interaction limit of a recently obtained exact result based on the Bethe ansatz [40]. At zero temperature we find that the momentum distribution diverges at $p=0$ as

$$\Pi(p)\sim\frac{\hbar\rho\pi\nu}{p}(r_1 p/\hbar)^{\nu}, \tag{191}$$

where $\nu=1/(2\pi\rho\xi)\ll 1$.

CONCLUSION

We have studied the thermal equilibrium of weakly interacting degenerate Bose gases in the regime of weak density fluctuations, the so-called quasicondensate regime. The method can be considered as a Bogoliubov method in the density-phase representation of the field operator.

In the first step one discretizes the real space in cells of size l: l is small enough that the macroscopic properties of the gas are not affected by the discretization, and l large enough that each cell contains on the average a large number of particles. The macroscopic occupation of each cell allows one to give a precise definition of the phase operator, following the method of Girardeau and Arnowitt [18].

In a second step one performs a systematic expansion of the full Hamiltonian in terms of two small parameters, the relative density fluctuations inside a cell and the phase change over a grid cell. This procedure leads to an exact expansion of the observables of the gas in the regime of weak interactions and low density fluctuations, in 1D, 2D, and 3D. In particular, it is free of any ultraviolet or infrared divergences and exactly matches the usual Bogoliubov predictions when the gas contains a true Bose-Einstein condensate.

As a first application of the general formalism, we have given in this paper formulas for the equation of state of the gas, the ground state energy, and the first order and second order correlation functions of the field. We have applied these formulas to the spatially homogeneous case in 1D, 2D, and 3D, recovering in this way known results, but obtaining also other results, like the full position dependence of the first order correlation function of the field.

ACKNOWLEDGMENTS

We acknowledge useful discussions with Iacopo Carusotto, Gora Shlyapnikov, Dimitri Gangardt, and Gordon Baym. Laboratoire Kastler Brossel is a research unit of Ecole Normale Supérieure and Université Paris 6, associated with CNRS.

APPENDIX A: EXPANSION OF THE HAMILTONIAN

As explained in Sec. II B we expand the Hamiltonian (28) up to third order in powers of the small parameters ϵ_1 and ϵ_2 defined in Eqs. (33) and (35). This will produce terms $H^{(n_1,n_2)}$ of order $\epsilon_1^{n_1}\epsilon_2^{n_2}$ with $n_1+n_2\leqslant 3$. The expansion of the potential energy part $H_{\rm pot}$ defined in Eq. (30) is very simple as it involves only the operator giving the density. The only point is to realize that the term $1/l^D$ is ϵ_1^2 times smaller than the zeroth order density ρ_0. This leads to

$$H_{\rm pot}^{(0,0)}=\sum_{\mathbf{r}} l^D\rho_0\left[U(\mathbf{r})-\mu+\frac{g_0}{2}\rho_0\right], \tag{A1}$$

$$H_{\rm pot}^{(1,0)}=\sum_{\mathbf{r}} l^D\delta\hat{\rho}[U(\mathbf{r})-\mu+g_0\rho_0], \tag{A2}$$

$$H_{\rm pot}^{(2,0)}=\sum_{\mathbf{r}} l^D\frac{g_0}{2}\left[\delta\hat{\rho}^2-\frac{\rho_0}{l^D}\right], \tag{A3}$$

$$H_{\rm pot}^{(3,0)}=-\sum_{\mathbf{r}}\frac{g_0}{2}\delta\hat{\rho}. \tag{A4}$$

The expansion of the kinetic energy part (31) is more complicated as it involves also the phase operator $\hat{\theta}$, which, furthermore, does not commute with $\delta\hat{\rho}$. An expression slightly more convenient than Eq. (31) can be given for the kinetic energy. Because of the periodic boundary conditions one can freely shift the summation variable in the term of Eq. (31) involving $\hat{\rho}_{-j}$, so that

$$H_{\rm kin}=-\frac{\hbar^2}{2ml^2}\sum_{\mathbf{r},j} l^D\{[\sqrt{\hat{\rho}}e^{i(\hat{\theta}_{+j}-\hat{\theta})}\sqrt{\hat{\rho}_{+j}}+\text{H.c.}]-2\hat{\rho}\}. \tag{A5}$$

The calculation to zeroth order in ϵ_2 can be done first easily: using the expansion (37) to zeroth order, we get from Eq. (31) to all orders in ϵ_1,

$$H_{\rm kin}^{(\leqslant+\infty,0)}=-\frac{\hbar^2}{2m}\sum_{\mathbf{r}} l^D\sqrt{\hat{\rho}}\Delta\sqrt{\hat{\rho}}. \tag{A6}$$

This involves a function of $\hat{\rho}$ only that it is easily expanded in powers of ϵ_1 using Eq. (34). A simplification occurs after summation over the lattice, as the matrix Δ is symmetric for the considered periodic boundary conditions:

$$\sum_{\mathbf{r}} u\Delta v=\sum_{\mathbf{r}}(\Delta u)v, \tag{A7}$$

where u and v are arbitrary functions on the lattice. This leads to

$$H_{\rm kin}^{(0,0)}=-\frac{\hbar^2}{2m}l^D\sum_{\mathbf{r}}\sqrt{\rho_0}\Delta\sqrt{\rho_0}, \tag{A8}$$

$$H_{\rm kin}^{(1,0)}=-\frac{\hbar^2}{2m}l^D\sum_{\mathbf{r}}\frac{\delta\hat{\rho}}{\sqrt{\rho_0}}\Delta\sqrt{\rho_0}, \tag{A9}$$

$$H_{\rm kin}^{(2,0)}=-\frac{\hbar^2}{2m}l^D\sum_{\mathbf{r}}\left[\frac{\delta\hat{\rho}}{4\sqrt{\rho_0}}\Delta\frac{\delta\hat{\rho}}{\sqrt{\rho_0}}-\frac{\delta\hat{\rho}^2}{4\rho_0^{3/2}}\Delta\sqrt{\rho_0}\right], \tag{A10}$$

$$H_{\rm kin}^{(3,0)} = -\frac{\hbar^2}{2m} l^D \sum_{\mathbf{r}} \left[\frac{1}{8} \frac{\delta\hat{\rho}^3}{\rho_0^{5/2}} \Delta\sqrt{\rho_0} - \frac{1}{8} \frac{\delta\hat{\rho}^2}{\rho_0^{3/2}} \Delta \frac{\delta\hat{\rho}}{\rho_0^{1/2}} \right]. \tag{A11}$$

The second order term of vanishing order in ϵ_1 is also immediately obtained:

$$H_{\rm kin}^{(0,2)} = \frac{\hbar^2}{2ml^2} l^D \sum_{\mathbf{r},j} \sqrt{\rho_0 \rho_{0,+j}} (\hat{\theta}_{+j} - \hat{\theta})^2. \tag{A12}$$

The last second order quantity to calculate is $H_{\rm kin}^{(1,1)}$, which is first order in ϵ_1 and first order in ϵ_2. There are four terms, two involving $\hat{\theta}_{+j}$ and two being their Hermitian conjugates. One can then collect the terms to form commutators:

$$H_{\rm kin}^{(1,1)} = -\frac{\hbar^2}{2ml^2} l^D \sum_{\mathbf{r},j} \frac{i}{2} \left(\frac{\rho_0}{\rho_{0,+j}} \right)^{1/2} [\hat{\theta}_{+j} - \hat{\theta}, \delta\hat{\rho}_{+j}] - \frac{i}{2} \left(\frac{\rho_{0,+j}}{\rho_0} \right)^{1/2} [\hat{\theta}_{+j} - \hat{\theta}, \delta\hat{\rho}]. \tag{A13}$$

$$= -\frac{\hbar^2}{4ml^2} \sum_{\mathbf{r},j} \left[\left(\frac{\rho_{0,+j}}{\rho_0} \right)^{1/2} + \left(\frac{\rho_0}{\rho_{0,+j}} \right)^{1/2} \right], \tag{A14}$$

where we have used the commutation relation of $\hat{\rho}$ and $\hat{\theta}$ [see Eq. (20)].

We collect all the second order c-number contributions to the Hamiltonian H in a single energy functional of the density profile of the quasicondensate,

$$E_2[\rho_0] = -\frac{g_0}{2} \sum_{\mathbf{r}} \rho_0 - \frac{\hbar^2}{4ml^2} \sum_{\mathbf{r},j} \left[\left(\frac{\rho_{0,+j}}{\rho_0} \right)^{1/2} + \left(\frac{\rho_0}{\rho_{0,+j}} \right)^{1/2} \right]. \tag{A15}$$

The technique used to calculate $H_{\rm kin}^{(1,1)}$ can be extended to the calculation of $H_{\rm kin}^{(2,1)}$. There are now three terms and their Hermitian conjugates. Two of these terms, when combined with their Hermitian conjugates, form a commutator that is calculated according to Eq. (20). The third term and its Hermitian conjugate involve the expression

$$\delta\hat{\rho}(\hat{\theta}_+ - \hat{\theta})\delta\hat{\rho}_+ - \delta\hat{\rho}_+(\hat{\theta}_+ - \hat{\theta})\delta\hat{\rho} = \delta\hat{\rho}[\hat{\theta}_+, \delta\hat{\rho}_+] - [\delta\hat{\rho}, \hat{\theta}]\delta\hat{\rho}_+, \tag{A16}$$

which is a sum of two commutators, easy to evaluate. This leads to

$$H_{\rm kin}^{(2,1)} = \frac{\hbar^2}{8m} \sum_{\mathbf{r}} \frac{\delta\hat{\rho}}{\rho_0} (\rho_0^{-1/2} \Delta \rho_0^{1/2} - \rho_0^{1/2} \Delta \rho_0^{-1/2}). \tag{A17}$$

To calculate $H_{\rm kin}^{(1,2)}$ we first evaluate

$$H_{\rm kin}^{(\leqslant+\infty,2)} = \frac{\hbar^2}{4ml^2} \sum_{\mathbf{r},j} l^D [\sqrt{\hat{\rho}} (\hat{\theta}_{+j} - \hat{\theta})^2 \sqrt{\hat{\rho}_{+j}} + \text{H.c.}] \tag{A18}$$

and we expand to first order in $\delta\hat{\rho}$, which leads to a sum of terms that are not individually Hermitian. We then use the commutation relation (20) to produce Hermitian terms, e.g.,

$$\delta\hat{\rho}(\hat{\theta}_{+j} - \hat{\theta})^2 = (\hat{\theta}_{+j} - \hat{\theta})\delta\hat{\rho}(\hat{\theta}_{+j} - \hat{\theta}) - \frac{i}{l^D}(\hat{\theta}_{+j} - \hat{\theta}). \tag{A19}$$

The last term of the right-hand side of this expression is anti-Hermitian and does not contribute to the final result

$$H_{\rm kin}^{(1,2)} = \frac{\hbar^2}{4ml^2} \sum_{\mathbf{r},j} l^D (\hat{\theta}_{+j} - \hat{\theta}) \left(\frac{\rho_{0,+j}^{1/2}}{\rho_0^{1/2}} \delta\hat{\rho} + \frac{\rho_0^{1/2}}{\rho_{0,+j}^{1/2}} \delta\hat{\rho}_{+j} \right) \times (\hat{\theta}_{+j} - \hat{\theta}). \tag{A20}$$

Finally, $H_{\rm kin}^{(0,1)}$ and $H_{\rm kin}^{(0,3)}$ vanish as the odd order expansion of $\exp[i(\hat{\theta}_{+j} - \hat{\theta})]$ is anti-Hermitian.

APPENDIX B: CORRECTIONS TO THE EQUATIONS OF MOTION DUE TO H_3

The Hamiltonian H_3 gives rise to quadratic corrections to the equations of motion for $\delta\hat{\rho}$ and $\hat{\theta}$. In this appendix, these corrections are calculated explicitly and the thermal average is taken over the equations of motion with the Hamiltonian $H_2 + H_3$ for the linear part and the Hamiltonian H_2 for the quadratic corrections. This allows us to calculate the first correction to the mean density due to H_3.

The corrections to the equation of motion for the density fluctuations are given by

$$\hbar\,\partial_t \delta\hat{\rho}|_{H_3} = \frac{\hbar^2}{4ml^2} \sum_j \left[\left\{ \hat{\theta} - \hat{\theta}_{+j}, \left(\frac{\rho_{0,+j}}{\rho_0} \right)^{1/2} \delta\hat{\rho} + \left(\frac{\rho_0}{\rho_{0,+j}} \right)^{1/2} \delta\hat{\rho}_{+j} \right\} + (+j \leftrightarrow -j) \right], \tag{B1}$$

where $\{A,B\}$ stands for the anticommutator $AB + BA$ of two operators. When we take the average with the Hamiltonian H_2, we use the explicit modal expansion of $\delta\hat{\rho}$ and $\hat{\theta}$ given by Eq. (56). The operator $\hat{Q}$ disappears since Eq. (B1) involves only differences of $\hat{\theta}$. Terms with $\hat{P}$ also disappear since $\langle \hat{P} \rangle_2 = 0$. The expectation value of the product $\hat{\theta}(\mathbf{r})\delta\hat{\rho}(\mathbf{r}')$, where $\hat{\theta}$ is written without $\hat{Q}$ and $\delta\hat{\rho}$ is written without $\hat{P}$, is actually purely imaginary: as u_s and v_s can be chosen to be real, $\theta_s^* = -\theta_s$ [see Eq. (57)]. Since $\partial_t \langle \delta\hat{\rho} \rangle$ is real, all imaginary contributions to it have to cancel so that the corrections to the motion of $\langle \delta\hat{\rho} \rangle$ due to H_3 finally vanish when we take the thermal average:

$$\hbar\,\partial_t \langle \delta\hat{\rho} \rangle|_{H_3} = 0. \tag{B2}$$

The corrections to the equation of motion for $\hat{\theta}$ are more involved:

$$\hbar\partial_t\hat{\theta}|_{H_3}=\frac{1}{2\sqrt{\rho_0}}\Bigg[-\frac{\hbar^2}{4m\rho_0}\delta\hat{\rho}\Delta\left(\frac{\delta\hat{\rho}}{\sqrt{\rho_0}}\right)+\frac{3\hbar^2}{8m\rho_0^2}\delta\hat{\rho}^2\Delta(\sqrt{\rho_0})-\frac{\hbar^2}{8m}\Delta\left(\frac{\delta\hat{\rho}^2}{\rho_0^{3/2}}\right)-\frac{\hbar^2}{2ml^2}\times\sum_j\left[\sqrt{\rho_{0,+j}}(\hat{\theta}_{+j}-\hat{\theta})^2+\sqrt{\rho_{0,-j}}(\hat{\theta}_{-j}-\hat{\theta})^2\right]+\frac{g_0\sqrt{\rho_0}}{l^D}-\frac{\hbar^2}{4ml^D\sqrt{\rho_0}}(\rho_0^{-1/2}\Delta\rho_0^{1/2}-\rho_0^{1/2}\Delta\rho_0^{-1/2})\Bigg]. \quad \text{(B3)}$$

Fortunately, we can use the linear equations of motion (46),(47) to significantly simplify the above equation of motion. We rewrite the first term in square brackets of Eq. (B3) as

$$-\frac{\hbar^2}{4m\rho_0}\delta\hat{\rho}\Delta\left(\frac{\delta\hat{\rho}}{\sqrt{\rho_0}}\right)=-\frac{\delta\hat{\rho}}{2\rho_0}\left[(U-\mu+3g_0\rho_0)\left(\frac{\delta\hat{\rho}}{\sqrt{\rho_0}}\right)+2\sqrt{\rho_0}\hbar\partial_t\hat{\theta}\right]. \quad \text{(B4)}$$

The second term in square brackets of Eq. (B3) gives, as $\sqrt{\rho_0}$ solves the Gross-Pitaevskii equation,

$$\frac{3\hbar^2}{8m\rho_0^2}\delta\hat{\rho}^2\Delta(\sqrt{\rho_0})=\frac{3\delta\hat{\rho}^2}{4\rho_0^{3/2}}(U-\mu+g_0\rho_0). \quad \text{(B5)}$$

The sum of Eqs. (B4) and (B5) and the third term in square brackets of Eq. (B3) leads to

$$\frac{1}{4}\left(-\frac{\hbar^2\Delta}{2m}+U-\mu+g_0\rho_0\right)\left(\frac{\delta\hat{\rho}^2}{\rho_0^{3/2}}\right)-g_0\frac{\delta\hat{\rho}^2}{\sqrt{\rho_0}}-\hbar(\partial_t\hat{\theta})\frac{\delta\hat{\rho}}{\sqrt{\rho_0}}. \quad \text{(B6)}$$

To rewrite the fourth term in square brackets of Eq. (B3), it is convenient to use the following identity:

$$\begin{aligned}&\sum_j\sqrt{\rho_{0,+j}}(\hat{\theta}_{+j}-\hat{\theta})^2+\sqrt{\rho_{0,-j}}(\hat{\theta}_{-j}-\hat{\theta})^2\\&\quad+2\hat{\theta}[\sqrt{\rho_{0,+j}}(\hat{\theta}_{+j}-\hat{\theta})+\sqrt{\rho_{0,-j}}(\hat{\theta}_{-j}-\hat{\theta})]\\&=\sum_j\sqrt{\rho_{0,+j}}(\hat{\theta}^2_{+j}-\hat{\theta}^2)+\sqrt{\rho_{0,-j}}(\hat{\theta}^2_{-j}-\hat{\theta}^2)\\&=l^2[\Delta(\sqrt{\rho_0}\hat{\theta}^2)-\hat{\theta}^2\Delta(\sqrt{\rho_0})],\end{aligned} \quad \text{(B7)}$$

leading to

$$\sum_j\sqrt{\rho_{0,+j}}(\hat{\theta}_{+j}-\hat{\theta})^2+\sqrt{\rho_{0,-j}}(\hat{\theta}_{-j}-\hat{\theta})^2=l^2[\hat{\theta}^2\Delta\sqrt{\rho_0}-2\hat{\theta}\Delta(\sqrt{\rho_0}\hat{\theta})+\Delta(\sqrt{\rho_0}\hat{\theta}^2)]. \quad \text{(B8)}$$

Using this equality, the Gross-Pitaevskii equation (41), and the equation of motion (47), the fourth term in square brackets of Eq. (B3) can be written as

$$-\frac{\hbar^2}{2ml^2}\sum_j\left[\sqrt{\rho_{0,+j}}(\hat{\theta}_{+j}-\hat{\theta})^2+\sqrt{\rho_{0,-j}}(\hat{\theta}_{-j}-\hat{\theta})^2\right]=\left(-\frac{\hbar^2}{2m}\Delta+U-\mu+g_0\rho_0\right)(\sqrt{\rho_0}\hat{\theta}^2)-\hbar\hat{\theta}\frac{\partial_t\delta\hat{\rho}}{\sqrt{\rho_0}}. \quad \text{(B9)}$$

The sixth (and last) term in square brackets of Eq. (B3) can also be transformed using the Gross-Pitaevskii equation (41):

$$-\frac{\hbar^2}{4ml^D\sqrt{\rho_0}}(\rho_0^{-1/2}\Delta\rho_0^{1/2}-\rho_0^{1/2}\Delta\rho_0^{-1/2})=-\left(-\frac{\hbar^2}{2m}\Delta+U-\mu+g_0\rho_0\right)\left(\frac{1}{2l^D\sqrt{\rho_0}}\right). \quad \text{(B10)}$$

This leads finally to a rewriting of the thermal average of Eq. (B3) as

$$2\sqrt{\rho_0}\hbar\langle\partial_t\hat{\theta}\rangle|_{H_3}=\left(-\frac{\hbar^2}{2m}\Delta+U-\mu+g_0\rho_0\right)\times\left(\frac{\langle\delta\hat{\rho}^2\rangle_2}{4\rho_0^{3/2}}+\sqrt{\rho_0}\langle\hat{\theta}^2\rangle_2-\frac{1}{2l^D\sqrt{\rho_0}}\right)-g_0\frac{\langle\delta\hat{\rho}^2\rangle_2-\rho_0/l^D}{\sqrt{\rho_0}}-\frac{\hbar\partial_t\langle\hat{\theta}\delta\hat{\rho}\rangle_2}{\sqrt{\rho_0}}. \quad \text{(B11)}$$

The last term of this expression can be calculated using Eq. (56). The harmonic modes do not contribute since the expectation value of products of $\hat{b}_s$ and $\hat{b}_s^\dagger$ is time independent. We are left with

$$\partial_t\langle\hat{Q}\hat{P}\rangle_2=\partial_t\left\langle\hat{Q}(0)\hat{P}+t\frac{\mu_0'}{\hbar}\hat{P}^2\right\rangle_2=\frac{\mu_0'}{\hbar}\langle\hat{P}^2\rangle_2, \quad \text{(B12)}$$

which gives

$$-\frac{\hbar\partial_t\langle\hat{\theta}\delta\hat{\rho}\rangle_2}{\sqrt{\rho_0}}=2\mu_0'\langle\hat{P}^2\rangle_2\partial_{N_0}\sqrt{\rho_0}. \quad \text{(B13)}$$

As a conclusion, the quadratic correction to the first equation of motion can be written as in Eq. (60) if one uses the identities

$$\hat{B}^\dagger\hat{B}=\frac{\delta\hat{\rho}^2}{4\rho_0}+\rho_0\hat{\theta}^2-\frac{1}{2l^D},$$

$$\frac{\delta\hat{\rho}^2}{\sqrt{\rho_0}} = \sqrt{\rho_0}(\hat{B}+\hat{B}^\dagger)^2$$

$$= \sqrt{\rho_0}\left(2\hat{B}^\dagger\hat{B}+\hat{B}^2+\hat{B}^{\dagger 2}+\frac{1}{l^D}\right). \quad \text{(B14)}$$

APPENDIX C: THE MEAN VALUE OF $\partial_t\hat{\theta}$ VANISHES AT EQUILIBRIUM

As the field degree of freedom $\hat{Q}$, that is, the global phase of the field, is not subject to a restoring force in H_2, it is not totally obvious that the perturbation H_3 cannot set it into permanent motion. We therefore check this point explicitly here.

The first step is to calculate the mean value of $\hat{P}$ to first order in H_3. We approximate the unnormalized density operator of the gas at thermal equilibrium to first order in H_3 using perturbation theory:

$$\sigma = e^{-\beta(H_2+H_3)} = e^{-\beta H_2} - \int_0^\beta d\tau e^{-(\beta-\tau)H_2} H_3 e^{-\tau H_2} + \cdots. \quad \text{(C1)}$$

$\hat{P}$ commutes with H_2 and has a vanishing mean value in the thermal state corresponding to H_2 so that, to first order in H_3,

$$\langle\hat{P}\rangle_3 = -\langle\beta\hat{P}H_3\rangle_2. \quad \text{(C2)}$$

The Hamiltonian H_3 is a polynomial of degree 3 in $\hat{P}$:

$$H_3 = A_0 + A_1\hat{P} + A_2\hat{P}^2 + A_3\hat{P}^3, \quad \text{(C3)}$$

where the A_i are still operators with respect to the harmonic oscillator variables b_s. This leads to

$$\langle\hat{P}\rangle_3 = -\beta[\langle A_1\rangle_2\langle\hat{P}^2\rangle_2 + \langle A_3\rangle_2\langle\hat{P}^4\rangle_2]. \quad \text{(C4)}$$

From Wick's theorem, $\langle\hat{P}^4\rangle_2 = 3\langle\hat{P}^2\rangle_2^2$.

In the second step we calculate $\langle d\hat{Q}/dt\rangle$ to first order in H_3:

$$\langle d\hat{Q}/dt\rangle \simeq \langle\partial_{\hat{P}}(H_2+H_3)\rangle_3 \simeq \mu_0'\langle\hat{P}\rangle_3 + \langle A_1\rangle_2 + 3\langle A_3\rangle_2\langle\hat{P}^2\rangle_2, \quad \text{(C5)}$$

where the terms coming from $\partial_{\hat{P}}H_3$ are calculated in the thermal state for H_2 since they are already first order in the perturbation. From the value of $\langle\hat{P}\rangle_3$ obtained from Eq. (C4) and from Eq. (61) we obtain the desired result:

$$\langle d\hat{Q}/dt\rangle_3 = 0 \quad \text{(C6)}$$

to first order in H_3.

APPENDIX D: AN EQUATION FOR $\{\hat{\alpha},\hat{\Lambda}\}$

In this appendix, we derive the partial differential equation (91). We first note that $\hat{B}_n$, being a sum of eigenmodes of the operator $\mathcal{L}_{\rm GP}$, obeys the differential equation for the evolution governed by H_2:

$$i\hbar\partial_t\begin{pmatrix}\hat{B}_n\\ \hat{B}_n^\dagger\end{pmatrix} = \mathcal{L}_{\rm GP}\begin{pmatrix}\hat{B}_n\\ \hat{B}_n^\dagger\end{pmatrix}. \quad \text{(D1)}$$

We project this equation orthogonally to ϕ_0 and along ϕ_0, so that we get the quantum analog of Eqs. (E9) and (E10) of [26], with the simplification that $\phi_0(\mathbf{r})$ is real:

$$i\hbar\partial_t\begin{pmatrix}\hat{\Lambda}\\ \hat{\Lambda}^\dagger\end{pmatrix} = \begin{pmatrix}\mathcal{Q} & 0\\ 0 & \mathcal{Q}\end{pmatrix}\mathcal{L}_{\rm GP}\begin{pmatrix}\hat{\Lambda}\\ \hat{\Lambda}^\dagger\end{pmatrix} + (\hat{\alpha}+\hat{\alpha}^\dagger)\begin{pmatrix}\mathcal{Q}g_0\rho_0\phi_0\\ -\mathcal{Q}g_0\rho_0\phi_0\end{pmatrix}, \quad \text{(D2)}$$

$$i\hbar\frac{d\hat{\alpha}}{dt} = l^D\sum_{\mathbf{r}} g_0\rho_0\phi_0(\hat{B}_n+\hat{B}_n^\dagger)$$

$$= l^D\sum_{\mathbf{r}} g_0\rho_0\phi_0(\hat{\Lambda}+\hat{\Lambda}^\dagger). \quad \text{(D3)}$$

We have introduced the projection matrix

$$\langle\mathbf{r}|\mathcal{Q}|\mathbf{r}'\rangle = \delta_{\mathbf{r},\mathbf{r}'} - l^D\phi_0(\mathbf{r})\phi_0(\mathbf{r}'). \quad \text{(D4)}$$

As $\hat{\alpha}$ is anti-Hermitian, the source term in Eq. (D2) vanishes and one can replace $\hat{B}_n$ by $\hat{\Lambda}$ in Eq. (D3).

We use these two equations of motion to calculate the first order time derivative of $A(\mathbf{r}) \equiv \langle\{\hat{\alpha},\hat{\Lambda}(\mathbf{r})\}\rangle_2$. We do not give the intermediate result. As A is real here, we have the property

$$\langle\{\hat{\alpha},\hat{\Lambda}^\dagger(\mathbf{r})\}\rangle_2 = -\langle\{\hat{\alpha},\hat{\Lambda}(\mathbf{r})\}\rangle_2. \quad \text{(D5)}$$

As $\hat{\Lambda}$ is orthogonal to ϕ_0 one has

$$\mathcal{Q}A = A. \quad \text{(D6)}$$

All this leads to Eq. (91).

APPENDIX E: INTERPRETATION OF χ IN THE NUMBER CONSERVING BOGOLIUBOV APPROACH

We assume here that the gas is a quasipure condensate so that ϕ_0 is now the condensate wave function in the Gross-Pitaevskii approximation. We then show that $\chi(\mathbf{r})/N_0$, where χ is defined in Eq. (94), essentially coincides with the lowest order deviation of the exact condensate wave function from the Gross-Pitaevskii prediction ϕ_0. This deviation was calculated in [15].

We split χ into a component orthogonal to ϕ_0 and a component collinear to ϕ_0:

$$\chi(\mathbf{r}) = \gamma\phi_0(\mathbf{r}) + \chi_\perp(\mathbf{r}). \quad \text{(E1)}$$

The component γ has a simple physical interpretation: we sum Eq. (95) over $\mathbf{r}$ after multiplication by l^D. If we omit the grand canonical term (absent in the canonical treatment of [15]) we obtain

$$N = N_0 + 2\gamma + \delta N, \tag{E2}$$

where

$$\delta N \equiv l^D \sum_{\mathbf{r}} \langle \hat{\Lambda}^\dagger \hat{\Lambda} \rangle_2 \tag{E3}$$

exactly coincides with the mean number of noncondensed particles predicted in [15]. The physical interpretation of 2γ is then simple:

$$\delta N_0 \equiv 2\gamma \tag{E4}$$

is the correction to apply to the pure condensate prediction for the number of condensate particles in order to recover the correct Bogoliubov prediction. Applying to Eq. (94) the matrix $\mathcal{Q}$ (D4) projecting orthogonally to ϕ_0 we obtain

$$\left[-\frac{\hbar^2}{2m}\Delta + U + g_0\rho_0 - \mu \right] \chi_\perp + 2\mathcal{Q} g_0 \rho_0 \chi_\perp + \mathcal{Q}\left(2 g_0 \rho_0 \gamma \phi_0 + \frac{1}{2} S \right) = 0. \tag{E5}$$

We modify slightly the form of the source term S, eliminating the anticommutator:

$$\{\hat{\Lambda}^\dagger(\mathbf{r}'), \hat{\Lambda}(\mathbf{r})\} = 2\hat{\Lambda}^\dagger(\mathbf{r}')\hat{\Lambda}(\mathbf{r}) + \frac{1}{l^D}\langle \mathbf{r}| \mathcal{Q} |\mathbf{r}'\rangle. \tag{E6}$$

This leads to the system

$$\begin{pmatrix} \mathcal{Q} & 0 \\ 0 & \mathcal{Q} \end{pmatrix} \mathcal{L}_{\mathrm{GP}} \begin{pmatrix} \chi_\perp \\ \chi_\perp \end{pmatrix} + \begin{pmatrix} \mathcal{Q} S_{\mathrm{eff}} \\ -\mathcal{Q} S_{\mathrm{eff}} \end{pmatrix} = 0 \tag{E7}$$

with the effective source term

$$S_{\mathrm{eff}}(\mathbf{r}) = g_0 \rho_0(\mathbf{r}) \phi_0(\mathbf{r}) (\delta N_0 - 1) + g_0 N_0 \phi_0(\mathbf{r}) \times [2\langle \hat{\Lambda}^\dagger(\mathbf{r}) \hat{\Lambda}(\mathbf{r}) \rangle_2 + \langle \hat{\Lambda}^2(\mathbf{r}) \rangle_2] - l^D \sum_{\mathbf{r}'} g_0 \rho_0(\mathbf{r}') \phi_0(\mathbf{r}') \langle [\hat{\Lambda}(\mathbf{r}') + \hat{\Lambda}^\dagger(\mathbf{r}')] \hat{\Lambda}(\mathbf{r}) \rangle_2, \tag{E8}$$

where we used the fact that here $\langle \hat{\Lambda}^2 \rangle_2 = \langle \hat{\Lambda}^{\dagger 2} \rangle_2$ since the condensate wave function is real. Equation (E7) is the steady version of Eq. (95) of [15], which gives N times the correction to the condensate wave function, and the source term (E8) exactly coincides with the one of Eq. (96) of [15] if one realizes that $N = N_0$, so that $\delta N_0 = -\delta N$, in the systematic expansion used in [15].

APPENDIX F: CORRECTIONS TO g_1 DUE TO THE CUBIC HAMILTONIAN

We calculate the corrections to the first order correlation function due to H_3 using the perturbative formula (143). A first remark is that

$$H_3(\tau) \equiv e^{\tau H_2} H_3 e^{-\tau H_2} \tag{F1}$$

is still cubic in the operators $\hat{b}_s$, since one has

$$e^{\tau H_2} \hat{b}_s e^{-\tau H_2} = e^{-\tau \epsilon_s} \hat{b}_s, \tag{F2}$$

$$e^{\tau H_2} \hat{b}_s^\dagger e^{-\tau H_2} = e^{\tau \epsilon_s} \hat{b}_s^\dagger, \tag{F3}$$

where ϵ_s is the energy of the Bogoliubov mode s. The second step is to use Wick's theorem to calculate the expectation values in the thermal state corresponding to the Hamiltonian H_2. One can derive the general formulas

$$\langle A_1 A_2 A_3 e^{i\Delta\theta} \rangle_2 = [\langle A_1 A_2 A_3 i\Delta\theta \rangle_2 + \langle A_1 i\Delta\theta \rangle_2 \langle A_2 i\Delta\theta \rangle_2 \langle A_3 i\Delta\theta \rangle_2] \times e^{-\langle (\Delta\theta)^2 \rangle_2/2}, \tag{F4}$$

$$\langle A_1 A_2 A_3 A_4 e^{i\Delta\theta} \rangle_2 = \left\{ \langle A_1 A_2 A_3 A_4 \rangle_2 \left[1 + \frac{1}{2}\langle (\Delta\theta)^2 \rangle_2 \right] - \frac{1}{2}\langle A_1 A_2 A_3 A_4 (\Delta\theta)^2 \rangle_2 + \langle A_1 i\Delta\theta \rangle_2 \langle A_2 i\Delta\theta \rangle_2 \langle A_3 i\Delta\theta \rangle_2 \times \langle A_4 i\Delta\theta \rangle_2 \right\} e^{-\langle (\Delta\theta)^2 \rangle_2/2}, \tag{F5}$$

where the A_i are linear in $\delta\hat{\rho}$ and $\hat{\theta}$ and have a vanishing mean value. A last point is to realize that some of the terms obtained contain a larger number of factors equal to $\Delta\theta$ than other ones. Since $\Delta\theta$ scales as $1/\sqrt{\rho_0}$ [see, e.g., the expression of $\hat{\theta}$ in terms of the mode functions u_s, v_s in Eq. (57)], the terms with an excess of $\Delta\theta$ factors are higher order in the expansion and are therefore negligible. Note that, strictly speaking, this argument is correct provided that each factor $\langle A_i \Delta\theta \rangle_2$ remains bounded whatever the distance from $\mathbf{0}$ to $\mathbf{r}$. This can be checked to be indeed the case: from the form of H_3 one sees that A_i is either $\delta\hat{\rho}$ or the phase difference between two neighboring points of the grid. One can therefore use the approximate identities

$$\langle A_1 A_2 A_3 e^{i\Delta\theta} \rangle_2 \simeq \langle A_1 A_2 A_3 i\Delta\theta \rangle_2 e^{-\langle (\Delta\theta)^2 \rangle_2/2}, \tag{F6}$$

$$\langle A_1 A_2 A_3 A_4 e^{i\Delta\theta} \rangle_2 \simeq \langle A_1 A_2 A_3 A_4 \rangle_2 e^{-\langle (\Delta\theta)^2 \rangle_2/2}. \tag{F7}$$

This immediately leads to the identities (144) and (145).

[1] A. Görlitz, J. M. Vogels, A. E. Leanhardt, C. Raman, T. L. Gustavson, J. R. Abo-Shaeer, A. P. Chikkatur, S. Gupta, S. Inouye, T. P. Rosenband, D. E. Pritchard, and W. Ketterle, Phys. Rev. Lett. **87**, 130402 (2001).

[2] F. Schreck, L. Khaykovich, K. L. Corwin, G. Ferrari, T. Bourdel, J. Cubizolles, and C. Salomon, Phys. Rev. Lett. **87**, 080403 (2001).

[3] N. D. Mermin and H. Wagner, Phys. Rev. Lett. **22**, 1133 (1966).

[4] P. C. Hohenberg, Phys. Rev. **158**, 383 (1967).

[5] Y. Castin, R. Dum, E. Mandonnet, A. Minguzzi, and I. Carusotto, J. Mod. Opt. **47**, 2671 (2000).

[6] I. Carusotto and Y. Castin, J. Phys. B **34**, 4589 (2001).

[7] V. N. Popov, Theor. Math. Phys. **11**, 565 (1972); *Functional Integrals in Quantum Field Theory and Statistical Physics* (Reidel, Dordrecht, 1983), Chap. 6.

[8] D. S. Petrov, G. V. Shlyapnikov, and J. T. M. Walraven, Phys. Rev. Lett. **85**, 3745 (2000).

[9] D. S. Petrov, M. Holzmann, and G. V. Shlyapnikov, Phys. Rev. Lett. **84**, 2551 (2000).

[10] T.-L. Ho and M. Ma, J. Low Temp. Phys. **115**, 61 (1999).

[11] S. Dettmer, D. Hellweg, P. Ryytty, J. J. Arlt, W. Ertmer, K. Sengstock, D. S. Petrov, and G. V. Shlyapnikov, Phys. Rev. Lett. **87**, 160406 (2001).

[12] F. Gerbier, S. Richard, J. H. Thywissen, M. Hugbart, P. Bouyer, and A. Aspect, e-print cond-mat/0210206.

[13] N. Bogoliubov, J. Phys. (Moscow) **11**, 23 (1947).

[14] C. Gardiner, Phys. Rev. A **56**, 1414 (1997).

[15] Y. Castin and R. Dum, Phys. Rev. A **57**, 3008 (1998).

[16] S. I. Shevchenko, Sov. J. Low Temp. Phys. **18**, 223 (1992).

[17] D. F. Walls and G. J. Milburn, *Quantum Optics* (Springer-Verlag, Berlin, 1995), Chap. 28.

[18] M. Girardeau and R. Arnowitt, Phys. Rev. **113**, 755 (1959).

[19] M. Schwartz, Phys. Rev. A **10**, 1858 (1974).

[20] J. O. Andersen, U. Al Khawaja, and H. T. C. Stoof, Phys. Rev. Lett. **88**, 070407 (2002).

[21] U. Al Khawaja, J. O. Andersen, N. P. Proukakis, and H. T. C. Stoof, Phys. Rev. A **66**, 013615 (2002).

[22] U. Al Khawaja, J. O. Andersen, N. P. Proukakis, and H. T. C. Stoof, Phys. Rev. A **66**, 059902 (2002).

[23] W.-C. Wu and A. Griffin, Phys. Rev. A **54**, 4204 (1996).

[24] This can be seen by taking the derivative of Eq. (11) with respect to α.

[25] We note that the same problem of course arises in the continuous version of the theory; in the above reasoning one has to replace $\hat{\rho}(\mathbf{r})$ by the integral of $\hat{\rho}(\mathbf{r}')$ over a finite volume around the point $\mathbf{r}$.

[26] A. Sinatra, C. Lobo, and Y. Castin, J. Phys. B **35**, 3599 (2002).

[27] M. Lewenstein and Li You, Phys. Rev. Lett. **77**, 3489 (1996).

[28] E. H. Lieb and W. Liniger, Phys. Rev. **130**, 1605 (1963).

[29] M. Gaudin, *La Fonction d'Onde de Bethe* (Masson, Paris, 1983).

[30] V. Liu, Phys. Rev. Lett. **79**, 4056 (1997).

[31] L. P. Pitaevskii and S. Stringari, Phys. Lett. A **235**, 398 (1997).

[32] P. O. Fedichev and G. V. Shlyapnikov, Phys. Rev. A **58**, 3146 (1998).

[33] T. D. Lee and C. N. Yang, Phys. Rev. **105**, 1119 (1957).

[34] M. Schick, Phys. Rev. A **3**, 1067 (1971).

[35] D. M. Gangardt and G. V. Shlyapnikov, Phys. Rev. Lett. **90**, 010401 (2003).

[36] We have used the identity $\int_0^x du\ (1-\cos u)/u = \ln x + C - \mathrm{Ci}(x)$, where the cosine-integral function $\mathrm{Ci}(x)$ tends to zero in the limit $x \to +\infty$.

[37] V. N. Popov, JETP Lett. **31**, 526 (1980).

[38] The trick is to use the rewriting $-\rho A(k)/k^2 = (1+2\overline{v_k^2})(n_k + 1/2) - 1/2$ where $2n_k + 1 = \coth(\beta\epsilon_k/2)$ and $1 + 2\overline{v_k^2} = (\mu + \hbar^2 k^2/2m)/\epsilon_k$. It is then clear that $A(k)$ can be extended to the domain $k<0$ to form an even C^∞ function of k since one can extend ϵ_k as an odd C^∞ function of k.

[39] M. Schwartz, Phys. Rev. B **15**, 1399 (1977).

[40] M. Olshanii and V. Dunjko, e-print cond-mat/0210629.

5.3 Sur la phase relative de deux condensats

Ce travail [20] est le début d'une réflexion sur le concept de phase d'un champ atomique ; il est né de la confrontation brutale entre la communauté de la physique de la matière condensée et celle de physique atomique, à l'issue de l'observation de la condensation de Bose-Einstein gazeuse en 1995.

Illustrons l'origine de cette confrontation par un exemple extrême. Deux groupes expérimentaux préparent un condensat d'atomes de rubidium 87, l'un aux USA, l'autre en Europe. Quel est l'état quantique de l'ensemble de ces deux condensats ? C'est un état cohérent, de type Glauber, s'écrièrent les physiciens de la matière condensée (à de rares exceptions près) :

$$|\psi\rangle_{mc} \propto e^{\alpha \hat{a}^\dagger} e^{\beta \hat{b}^\dagger} |0\rangle$$

où α, β sont deux nombres complexes de phases inconnues, et $\hat{a}$, $\hat{b}$ annihilent une particule respectivement dans le condensat américain et dans le condensat européen. C'est évident, dirent-ils, car un condensat est lui-même décrit par un état cohérent, ce qui illustre la brisure de symétrie $U(1)$.

Surprenant, répondirent les physiciens des gaz atomiques, guidés par le bon sens. Comme le passage transatlantique d'atomes par effet tunnel semble négligeable, il est étrange de penser qu'un atome donné puisse être dans une superposition cohérente de deux états, l'un aux USA, l'autre en Europe ! Par ailleurs, il est bien clair qu'un état qui soit superposition cohérente d'états à nombres totaux de particules différents ne peut pas être préparé dans nos expériences de basse énergie ! Et les physiciens atomistes de proposer l'état

$$|\psi\rangle_{at} \propto (\hat{a}^\dagger)^{N_a} (\hat{b}^\dagger)^{N_b} |0\rangle$$

où les nombres de particules N_a et N_b sont des entiers.

L'article ci-après reproduit réconcilie les deux points de vue et résout le paradoxe, en prenant comme fil directeur une expérience de pensée, et en comparant les résultats obtenus pour les divers états quantiques proposés par les deux communautés. Mais il dépasse en fait ce débat à forte teneur philosophique, en proposant une méthode utilisable expérimentalement pour établir une relation de phase bien déterminée entre deux condensats, et en découvrant un effet purement quantique dans la dynamique de la phase, dû aux interactions et observé depuis.

PHYSICAL REVIEW A VOLUME 55, NUMBER 6 JUNE 1997

Relative phase of two Bose-Einstein condensates

Yvan Castin and Jean Dalibard
Laboratoire Kastler Brossel, 24 rue Lhomond, 75005 Paris, France
(Received 24 June 1996; revised manuscript received 21 January 1997)

We show that two independent Bose-Einstein condensates, each initially containing a well-defined number of atoms, will appear coherent in an experiment that measures the beat note between these condensates. We investigate the role played by atomic interactions within each condensate in the time evolution of their relative phase. [S1050-2947(97)03606-8]

PACS number(s): 03.75.Fi, 42.50.Gy, 05.30.Jp

Since the recent observations of the Bose-Einstein condensation (BEC) of a dilute atomic gas [1–3], the problem of the phase of an atomic sample has been raised with renewed interest. Theoretically, this phase appears naturally as a result of a broken symmetry in the theory of BEC [4,5]. At zero temperature, the atomic sample is described by a coherent state, i.e., an eigenstate of the annihilation operator for a particular state of the one-atom Hilbert space. A classical field $|\psi_0|e^{i\phi}$ with a well defined amplitude $|\psi_0|$ and phase ϕ is associated with this coherent state. Experimentally, however, one can, in principle, measure the exact number of trapped atoms. The condensate is then described by a Fock state (or number state), and no definite phase can be attributed to the gas. The question then arises of whether these two different descriptions lead to identical predictions for a given experimental setup.

To investigate this problem, we consider the following Gedanken experiment, using two trapped condensates of the same atomic species. The trapping potentials are isotropic and harmonic, except for a finite barrier in a given direction, through which the atoms can tunnel (Fig. 1). The phase between the two emerging beams can be probed by ''beating'' them together, i.e., by mixing them with a 50-50 atomic beam splitter [6].

If each condensate is in a coherent state with the same average number of atoms, the beams incident on the beam splitter are described by the two fields, $|\psi_0|e^{i\phi_A}$ and $|\psi_0|e^{i\phi_B}$. The intensities in the two outputs of the beam splitter are then

$$I_+ = 2|\psi_0|^2\cos^2\phi, \quad I_- = 2|\psi_0|^2\sin^2\phi, \tag{1}$$

where $\phi=(\phi_A-\phi_B)/2$. The recording of $I_\pm$ allows one to determine the absolute value of the relative phase 2ϕ. Note that ϕ is an unpredictable random variable, which takes a different value for any new realization of the experiment.

In a description of the system in terms of Fock states, one supposes that the system is initially in the state $|N_A,N_B\rangle$, i.e., there are $N_{A/B}$ particles in the condensates A/B. Our purpose is to show that the predictions corresponding to a statistical mixture of states $|N_A,N_B\rangle$ with a Poissonian distribution for $N_{A/B}$ are identical to Eq. (1). The notion of phase-broken symmetry is therefore not indispensable in order to understand the beating of two condensates [7]. On the other hand, it provides a simple way of analyzing such an experiment, while, as we see below, Fock states are more difficult to handle in such a situation.

The problem that we are facing here is analogous to the question raised by P. W. Anderson [8]: Do two superfluids that have never ''seen'' one another possess a definite relative phase? As pointed out in [4], the question is meaningless as long as no measurement is performed on the system. J. Javanainen and S. M. Yoo recently addressed a similar question by considering the spatial interferences of two condensates prepared in the state $|N,N\rangle$ and arriving on a given array of detectors [9]. He showed numerically that, after the detection of all the atoms of the two condensates, the count distribution on the set of detectors was similar to the one predicted from a phase broken symmetry state.

The paper is organized as follows. In the Sec. I, we address the simple particular case where all the detected particles are bunched in the same output channel of the beam splitter. In Sec. II, we present a general reasoning showing that the descriptions in terms of coherent or Fock states lead to identical predictions for any type of measurements performed on the system. In Sec. III, assuming an initial Fock state for the system, we investigate the buildup of a relative phase between the two condensates as the measurements proceed. In Sec. IV, we add a device, shifting the atomic phase in one of the channels of Fig. 1, in order to perform multichannel detection; we then recover analytically the numerical results of [9]. Finally, we include the effect of the atomic interactions on the distribution of the relative phase between the two condensates. We predict collapses and revivals for this distribution with time scales that should be experimentally accessible.

I. A PARTICULAR CASE: ALL THE DETECTIONS IN ONE CHANNEL

We assume that k atoms are detected on $D_\pm$. For simplicity we consider in this section the situation where all the k detections occur in the $(+)$ channel. If the system is initially in a coherent state, the probability for such a sequence (given that k atoms have been detected) is $\cos^{2k}\phi$. The average over the unknown relative phase 2ϕ gives

$$W_k = \int_{-\pi/2}^{\pi/2} \frac{d\phi}{\pi}\ \cos^{2k}\phi = \frac{(2k)!}{(2^k k!)^2} \underset{k\gg 1}{\sim} \frac{1}{\sqrt{\pi k}} \tag{2}$$

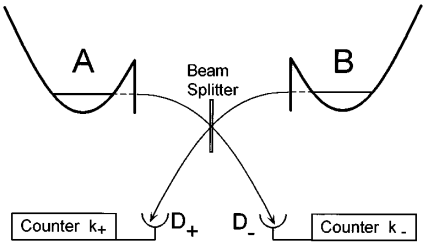

FIG. 1. A Gedanken experiment: atoms leaking from two trapped condensates, A and B, are detected in the output channels ($\pm$) of a 50-50 beam splitter.

For $k=100$, this probability of getting all counts in the ($+$) channel is $\sim 6\%$.

We suppose now that the system is in a Fock state and for simplicity we take $N_B=N_A \gg k$. A naive argument could consist of saying that since $k \ll N_A$, the probability of detecting the nth atom ($n \leqslant k$) in the ($+$) channel is nearly independent of the $n-1$ previous detection results. The probability of k detections in the ($+$) channel should then be 2^{-k}. This is obviously very different from the result W_k obtained from the coherent state point of view ($2^{-k}<10^{-30}$ for $k=100$).

However, the latter reasoning is wrong; the first detection of an atom in the ($+$) channel projects the atom in a state proportional to

$$(\hat{a}+\hat{b})|N_A,N_A\rangle \propto |\Psi\rangle = |N_A,N_A-1\rangle + |N_A-1,N_A\rangle, \quad (3)$$

where $\hat{a}$ ($\hat{b}$) annihilates a particle in the condensate A (B). To calculate the probability of detecting a second atom in the ($+$) channel, we have to compare the squared norm of the two vectors corresponding to a detection in the ($\pm$) channels:

$$(+):(\hat{a}+\hat{b})|\Psi\rangle = \sqrt{N_A-1}(|N_A-2,N_A\rangle + |N_A,N_A-2\rangle) + 2\sqrt{N_A}|N_A-1,N_A-1\rangle, \quad (4)$$

$$(-):(\hat{a}-\hat{b})|\Psi\rangle = \sqrt{N_A-1}(|N_A-2,N_A\rangle - |N_A,N_A-2\rangle). \quad (5)$$

For $N_A=1$, we recover the well-known interference effect leading to a bunching of the two bosons in a single output of the beam splitter [11]. For $N_A \gg 1$, the squared norms of these two vectors are in the ratio 3:1. This indicates that once a first atom has been detected in the ($+$) channel, the probability of detecting the second atom in the same channel is 3/4, while the probability of detecting this second atom in the ($-$) channel is only 1/4. This somewhat counterintuitive result shows clearly that the successive detection probabilities are strongly correlated in the case of an initial Fock state, even if the number of detected atoms is very small compared to the number of atoms present in the condensates. The reasoning can be extended to k detections (see Fig. 2) and we find that the probability of detecting respectively, $k_+=k$ and $k_-=0$ atoms in the two channels is

$$\mathcal{P}(k,0)=\frac{1}{2}\frac{3}{4}\cdots\frac{2k-1}{2k}, \quad (6)$$

which is equal to W_k for any k. Note that the explicit average over N_A and N_B is correctly omitted in this last calculation in the limit $\overline{N_A}=\overline{N_B} \gg 1$, where the Poissonian fluctuations have a negligible effect.

The predictions for an initial Fock state and for an initial coherent state with random phase are therefore equivalent, but the result for the coherent state is obtained in a much more straightforward and intuitive manner than for the Fock state.

II. ENSEMBLE AVERAGE WITH AND WITHOUT PHASE-BROKEN SYMMETRY

This equivalence between the Fock-state and the coherent state descriptions is actually not restricted to the particular detection scheme considered in this paper. It is a consequence of the identity of the density operators of the total system in those two descriptions. To prove this identity, we first consider the coherent state with well-defined phases ϕ_A and ϕ_B:

$$|\overline{N_A}^{1/2}e^{i\phi_A},\overline{N_B}^{1/2}e^{i\phi_B}\rangle \equiv \sum_{N_A,N_B} \frac{\overline{N_A}^{N_A/2}\ \overline{N_B}^{N_B/2}}{\sqrt{N_A!\ N_B!}} e^{i(N_A\phi_A+N_B\phi_B)}|N_A,N_B\rangle \times e^{-(\overline{N_A}+\overline{N_B})/2}, \quad (7)$$

where $\overline{N_A}$ and $\overline{N_B}$ are the mean number of particles in the condensates A and B. In the coherent-state description, the

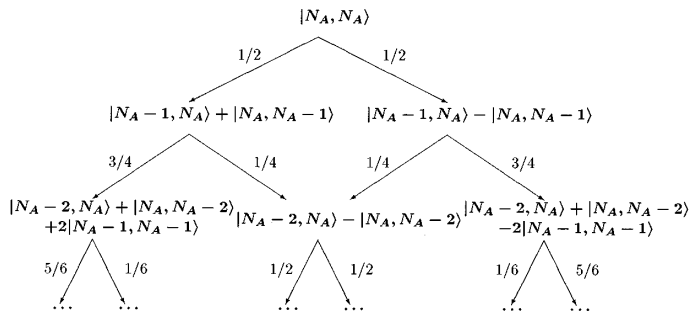

FIG. 2. Possible outcomes (and the corresponding branching ratios) of the first three detections in the output channels of the beam splitter. Initially, the system is in a Fock state, with the same numbers of particles $N_A \gg 1$ in the two condensates.

density operator ρ of the system is then obtained by a statistical average over the phases ϕ_A and ϕ_B:

$$\rho = \int_0^{2\pi}\int_0^{2\pi} \frac{d\phi_A}{2\pi}\frac{d\phi_B}{2\pi} |\overline{N_A}^{1/2} e^{i\phi_A}, \overline{N_B}^{1/2} e^{i\phi_B}\rangle \times \langle \overline{N_A}^{1/2} e^{i\phi_A}, \overline{N_B}^{1/2} e^{i\phi_B}|. \quad (8)$$

Using the explicit expression (7) of the coherent states, we find that all off-diagonal terms in the Fock-state basis are suppressed after the integration over ϕ_A, ϕ_B,

$$\rho = \sum_{N_A,N_B} \frac{\overline{N_A}^{N_A}\overline{N_B}^{N_B}}{N_A!\ N_B!} |N_A,N_B\rangle\langle N_A,N_B|\ e^{-(\overline{N_A}+\overline{N_B})}, \quad (9)$$

which coincides with the Poissonian statistical mixture considered in the Fock-state description [7,12].

From the identity of the density operators ρ we can conclude that no measurement (or no series of measurements) performed on the system can allow one to distinguish between the coherent state and the Fock-state descriptions. Indeed, in a sequence of measurements, the probability of getting a given set of results can always be expressed as the expectation value $\mathrm{Tr}(\hat{O}\rho)$ of an operator $\hat{O}$ [13]. For example, the probability that at least k atoms are detected and that the first k detections occur in the $(+)$ channel is obtained from (see Appendix)

$$\hat{O} = \frac{1}{2^k}(\hat{a}^\dagger + \hat{b}^\dagger)^k \frac{1}{(\hat{N}+1)\cdots(\hat{N}+k)}(\hat{a}+\hat{b})^k, \quad (10)$$

where $\hat{N} = \hat{a}^\dagger\hat{a} + \hat{b}^\dagger\hat{b}$. It is shown in the Appendix that $\mathrm{Tr}(\hat{O}\rho)$ is nearly equal to $\mathcal{P}(k,0)$. The difference between the two quantities is due to the fact that $\mathcal{P}(k,0)$ is a *conditional* probability that the first k detections occur in the $(+)$ channel, knowing that at least k particles have been detected. This difference is negligible in the limit where the mean numbers of atoms $\overline{N_A} = \overline{N_B}$ are much larger than k, since the probability that at least k detections occur after an arbitrarily long time approaches 1 in this case.

III. PROBABILITY OF A GENERAL (k_+,k_-) DETECTION RESULT

We now generalize the discussion of Sec. I to the general case of $k_\pm$ detected atoms in the $(\pm)$ channels for a fixed number of measurements $k = k_+ + k_-$. We first address the case of an initial coherent state. We then define the so-called phase states, which correspond to a well defined total number of particles and a well defined relative phase between the two condensates. Finally, starting from the system in a Fock state, we expand the state vector on those phase states as the measurements proceed, to show the emergence of a relative phase.

A. Case of an initial coherent state

We assume that the system is initially in the coherent state, Eq. (7). As the measurements proceed, the state of the system remains coherent, with the same relative phase $\phi = (\phi_A - \phi_B)/2$. Each count occurs with probabilities $\cos^2\phi$ and $\sin^2\phi$ in the $(+)$ and $(-)$ channels. Given that k particles have been detected, the distribution of counts in the $(\pm)$ channels is binomial and the probability for the result (k_+,k_-) is

$$\mathcal{P}(k_+,k_-,\phi) = \frac{k!}{k_+!\ \ k_-!}(\cos\phi)^{2k_+}(\sin\phi)^{2k_-}. \quad (11)$$

The number of counts k_+ in the $(+)$ channel has, therefore, a mean value $k\cos^2\phi$ and a standard deviation (shot noise) $\sigma[k_+] = \sqrt{k}|\cos\phi\,\sin\phi|$.

In the limit $k_\pm \gg 1$, using $\ln n! \sim n\ln n - n$ for $n \gg 1$, we find from Eq. (11) that $\mathcal{P}(k_+,k_-,\phi)$ is maximal for $k_-/k_+ = \tan^2\phi$, as expected from Eq. (1). In other words, for $k \gg 1$, the mean and most probable intensities coincide, since the shot noise on the signal in the two channels $(\pm)$ becomes negligible.

B. Phase states

For an initial state $|\Psi\rangle$ with a well-defined total number of particles N, the evolution due to the sequence of measurements is conveniently analyzed by expanding $|\Psi\rangle$ onto the overcomplete set of *phase states* $|\phi\rangle_N$ [4]:

$$|\phi\rangle_N = \frac{1}{\sqrt{2^N N!}}(\hat{a}^\dagger e^{i\phi} + \hat{b}^\dagger e^{-i\phi})^N|0\rangle, \quad (12)$$

where $|0\rangle$ stands for the vacuum. If the system is in a given state $|\phi\rangle_N$, there exists a well defined relative phase ϕ between A and B: if a device shifting the phase of the matter wave by 2ϕ were placed in front of the B input of the beam splitter, all the atoms would be detected in the $(+)$ output of the beam splitter.

Any state $|\Psi\rangle$ with N particles can be expanded in the set of phase states:

$$|\Psi\rangle = \int_{-\pi/2}^{\pi/2} \frac{d\phi}{\pi}\ c(\phi)\ |\phi\rangle_N, \quad (13)$$

where the phase amplitude $c(\phi)$ is obtained as

$$c(\phi) = 2^{N/2}\sum_{N_A=0}^{N}\left(\frac{N_A!\ \ (N-N_A)!}{N!}\right)^{1/2} e^{i(N-2N_A)\phi} \times \langle N_A, N-N_A|\Psi\rangle. \quad (14)$$

In what follows, we will use the quasiorthogonality of the phase states valid for large N and for $-\pi/2 \leqslant \phi,\phi' < \pi/2$:

$${}_N\langle\phi|\phi'\rangle_N = \cos^N(\phi-\phi') \simeq e^{-N(\phi'-\phi)^2/2} \simeq \sqrt{2\pi/N}\,\delta(\phi-\phi'). \quad (15)$$

As an illustration of the relevance of the phase states we now derive the probability $\mathcal{P}(k_+,k_-)$ for the system in the initial state $|N/2,N/2\rangle$. We show that it is approximately equal to the result obtained for a statistical mixture of coherent states, as expected from the general discussion of Sec. II.

Using the formula found in Eq. (A4) of the Appendix, we get as a starting point

$$\mathcal{P}(k_+,k_-)=\frac{(N-k)!}{2^k N!}\frac{k!}{k_+!\ k_-!}\times||(\hat{a}+\hat{b})^{k_+}(\hat{a}-\hat{b})^{k_-}|N/2,N/2\rangle||^2. \quad (16)$$

We expand the state vector over the set of phase states:

$$|N/2,N/2\rangle = c_0\int_{-\pi/2}^{\pi/2}\frac{d\phi}{\pi}\ |\phi\rangle_N, \quad (17)$$

$$c_0=2^{N/2}\frac{(N/2)!}{\sqrt{N!}}\sim(\pi N/2)^{1/4}. \quad (18)$$

We calculate first the action of the annihilation operators in Eq. (16) on the phase states:

$$(\hat{a}+\hat{b})^{k_+}(\hat{a}-\hat{b})^{k_-}|\phi\rangle_N = \left(\frac{N!\ 2^k}{(N-k)!}\right)^{1/2} e^{ik_-\pi/2}(\cos\phi)^{k_+}\ (\sin\phi)^{k_-}\ |\phi\rangle_{N-k}, \quad (19)$$

with $k=k_++k_-$. The quasiorthogonality [Eq. (15)] of the phase states in the limit of large N then gives

$$\mathcal{P}(k_+,k_-)\sim\frac{k!}{k_+!\ k_-!}\int_{-\pi/2}^{\pi/2}\frac{d\phi}{\pi}\ (\cos\phi)^{2k_+}\ (\sin\phi)^{2k_-} = \int_{-\pi/2}^{\pi/2}\frac{d\phi}{\pi}\mathcal{P}(k_+,k_-,\phi), \quad (20)$$

which shows the announced equivalence.

C. Emergence of the relative phase for an initial Fock state.

For an initial Fock state $|N/2,N/2\rangle$, which has a flat phase probability distribution $|c(\phi)|^2$, we now investigate the emergence of a relative phase between the two condensates during the sequence of measurements.

After a sequence of $(k_+,k_-=k-k_+)$ detections, the state of the system is obtained from Eqs. (17) and (19):

$$|\Psi(k_+,k_-)\rangle\propto(\hat{a}+\hat{b})^{k_+}(\hat{a}-\hat{b})^{k_-}|N/2,N/2\rangle \propto\int_{-\pi/2}^{\pi/2}d\phi\ (\cos\phi)^{k_+}(\sin\phi)^{k_-}|\phi\rangle_{N-k}. \quad (21)$$

For $k_\pm\gg1$, we use the stationary-phase method, which approximates the integrand $(\cos\phi)^{k_+}(\sin\phi)^{k_-}$ by a Gaussian around each of its maxima. The maxima in $[-\pi/2,\pi/2]$ are located in ϕ_0 and $-\phi_0$, with $0\leqslant\phi_0\leqslant\pi/2$ and

$$k_+=k\cos^2\phi_0, \quad (22)$$

$$k_-=k\sin^2\phi_0. \quad (23)$$

We get, for instance, for ϕ close to ϕ_0,

$$(\cos\phi)^{k_+}(\sin\phi)^{k_-}\simeq\exp\left[\frac{1}{2}\left(k_+\log\frac{k_+}{k}+k_-\log\frac{k_-}{k}\right)-k(\phi-\phi_0)^2\right]. \quad (24)$$

We obtain therefore:

$$|\Psi(k_+,k_-)\rangle\propto\int_{-\pi/2}^{\pi/2}d\phi\ [e^{-k(\phi-\phi_0)^2}+(-1)^{k_-}e^{-k(\phi+\phi_0)^2}]|\phi\rangle_{N-k}. \quad (25)$$

The interpretation of this result is quite clear: initially, the relative phase of the two condensates is indefinite, since the vector state of the system projects equally onto the various phase states [see Eq. (17)]. After $k\gg1$ detections, the system has evolved into a state where the phase ϕ is well defined; more precisely, the phase distribution is a double Gaussian, centered on ϕ_0 and $-\phi_0$, with a standard deviation of $1/\sqrt{2k}$. This ambiguity between ϕ_0 and $-\phi_0$ also arises in the determination of ϕ from Eq. (1).

To summarize, we have two different points of view on the system: for an initial coherent state, the measurement ''reveals'' the pre-existing phase through $\tan^2\phi=k_-/k_+$; for an initial Fock state, the detection sequence ''builds up'' the phase. A similar conclusion has been reached by a numerical analysis of quantum trajectories in the framework of continuous measurement theory [12]. It is not possible to favor one particular point of view, based on experimental results. If the same experimental sequence involving k detections is repeated, with the phase varying randomly from shot to shot in the coherent-state point of view, the predicted occurrence of a given result $k_+,k_-=k-k_+$ is identical in the two points of view.

IV. MOST PROBABLE MEASUREMENT SEQUENCES IN A MULTICHANNEL DETECTION SCHEME

In this section, we analyze the results of a multichannel experiment where a device shifting the atomic phase by an adjustable quantity 2γ is introduced in one of the input channels of the beam splitter, sketched in Fig. 1. Our analysis also applies to the case of spatial interferences between two condensates arriving simultaneously on an array of atom detectors [9].

We imagine that the phase shift γ is tuned successively to the L different values $\gamma_j=j\pi/2L, j=0,\ldots,Ł-1$. We assume, for simplicity, that exactly $k\gg1$ particles are detected for each value of γ. Our goal is to show that the signals in each $+$ and $-$ channel, $k_+(j)$ and $k_-(j)$, are equal (within shot noise) to $k\cos^2(\phi_0-\gamma_j)$ and $k\sin^2(\phi_0-\gamma_j)$, where the parameter ϕ_0, varying randomly for any new realization of the whole experiment, is the same for all channels.

As emphazised in Sec. II, the probability for a given set of results $\{k_\pm(j)\}$ is given by the average of an operator $\hat{O}$ over the density matrix of the system [Eq. (8)]. For the multichannel detection scheme considered here, the probability of observing this sequence, knowing that k counts have been ob-

tained in each channel, is obtained by a generalization of the result of the Appendix:

$$\mathcal{P}[\{k_+(j)\}]=\int_{-\pi/2}^{\pi/2}\frac{d\phi}{\pi}\prod_{j=0}^{L-1}\frac{k!}{k_+(j)!\;\;k_-(j)!}\times[\cos(\phi-\gamma_j)]^{2k_+(j)}[\sin(\phi-\gamma_j)]^{2k_-(j)}. \tag{26}$$

To demonstrate this result, we have used the operators $\hat{a}\pm e^{2i\gamma_j}\hat{b}$ associated with a count in the $(\pm)$ channel with a phase shift $2\gamma_j$.

We investigate first the case $L=1$ discussed in the preceding section, to identify a physically optimal parametrization of the problem. For $k\gg1, k_\pm>1$, we get an approximation of the right-hand side of Eq. (20) by using the stationary phase method for the integral [Eqs. (24) and (25)] and Stirling's formula for the binomial factor:

$$\frac{k!}{k_+!\;\;k_-!}\simeq\left(\frac{k}{2\pi k_+k_-}\right)^{1/2}\exp\left(-k_+\ln\frac{k_+}{k}-k_-\ln\frac{k_-}{k}\right). \tag{27}$$

This leads to

$$\mathcal{P}(k_+,k_-)\simeq\frac{1}{\pi\sqrt{k_+k_-}}. \tag{28}$$

The remaining slow variation with $k_\pm$ can be suppressed by characterizing the sequence of measurements by the angle ϕ_0, defined in Eq. (22), rather than by $k_\pm$; in the limit $k\gg1$ we treat ϕ_0 as a continuous variable, and the Jacobian for the change of variables $k_+\to\phi_0$ satisfactorily leads to a flat probability density for ϕ_0:

$$\widetilde{\mathcal{P}}(\phi_0)\equiv\mathcal{P}(k_+,k_-)\left|\frac{dk_+}{d\phi_0}\right|\simeq\frac{2}{\pi}. \tag{29}$$

We now generalize this calculation to an arbitrary value for the number of phase bins L. A sequence of kL detections (with k detection in each bin) $\{k_+(j), j=0,\ldots,L-1\}$ is characterized by the L angles θ_j, such that

$$k_+(j)=k\cos^2\theta_j,\quad \theta_j\in[0,\pi/2],\quad j=0,\ldots,L-1. \tag{30}$$

In the limit $k\gg1$, we consider the θ_j's as continuous variables; expanding the binomial factors in Eq. (26), using Eq. (27) as in the previous case $L=1$, we find for the probability density of the θ_j's

$$\begin{aligned}\widetilde{\mathcal{P}}(\theta_0,\ldots,\theta_{L-1})&\equiv\mathcal{P}(\{k_+(j)\})\prod_{j=0}^{L-1}\left|\frac{dk_+(j)}{d\theta_j}\right|\\&\simeq\left(\frac{2k}{\pi}\right)^{L/2}\int_{-\pi/2}^{\pi/2}\frac{d\phi}{\pi}\;\exp[kS(\theta_0,\ldots,\theta_{L-1},\phi)],\end{aligned} \tag{31}$$

where we have introduced

$$S(\theta_0,\ldots,\theta_{L-1},\phi)\equiv\sum_{j=0}^{L-1}\cos^2\theta_j\ln\left(\frac{\cos^2(\phi-\gamma_j)}{\cos^2\theta_j}\right)+\sin^2\theta_j\ln\left(\frac{\sin^2(\phi-\gamma_j)}{\sin^2\theta_j}\right). \tag{32}$$

We now look for the values $(\theta_0,\ldots,\theta_{L-1})$ maximizing $\widetilde{\mathcal{P}}(\theta_0,\ldots,\theta_{L-1})$. We note the position ϕ_0 of the absolute maximum of S [15] as a function of ϕ, for given $(\theta_0,\ldots,\theta_{L-1})$, and we perform the stationary-phase approximation in the integral [Eq. (31)]:

$$\widetilde{\mathcal{P}}(\theta_0,\ldots,\theta_{L-1})\simeq\frac{C}{\sqrt{|\partial_\phi^2S|_{\phi_0}}}\exp[kS(\theta_0,\ldots,\theta_{L-1},\phi_0)], \tag{33}$$

where the normalization factor C depends on k and L only. If one neglects the slow variations of the prefactor, the maximum of $\widetilde{\mathcal{P}}$ is obtained by maximizing S in Eq. (33) over the remaining variables $\theta_0,\ldots,\theta_{L-1}$. This is equivalent to a global maximization of S in Eq. (32) over all the variables. We find [16] that the maximal value of S is 0 and that it is obtained for the measurement sequences

$$k_+(j)=k\cos^2(\phi_0-\gamma_j),\quad j=0,\ldots,Ł-1,\quad -\pi/2\leqslant\phi_0<\pi/2. \tag{34}$$

The curve defined by Eq. (34) for the θ_j's is the straight line $\theta_j=\pm(\phi_0-\gamma_j)[\pi]$. Along this line the probability density is constant (and equal to $C/\sqrt{4L}$). Expanding S around the distributions [Eq. (34)], we find, after a rather involved calculation, that the probability density decreases away from this line as

$$\widetilde{\mathcal{P}}\simeq\frac{C}{\sqrt{4L}}\exp(-2kd^2), \tag{35}$$

where d is the Euclidian distance to the line.

These results can be understood in a simple and physical manner as follows. Assume that the system is initially in a coherent state [Eq. (7)], with a random relative phase $\phi_A-\phi_B\equiv2\phi_0$ uniformly distributed in $[-\pi,\pi[$. For a total number of $k\gg1$ counts, measured with a phase shift $2\gamma_j$ in the input channel B of the beam splitter, we use the results of Sec. III A, replacing ϕ by $\phi_0-\gamma_j$ in Eq. (11); we find that the probability distribution for the angle θ_j in Eq. (30) is strongly peaked around $\phi_0-\gamma_j$, with a standard deviation $1/\sqrt{4k}$, in agreement with Eqs. (34) and (35).

This exemplifies again the relevance of the coherent-state point of view in the description of the measured results for a single realization of the beating experiment.

V. ROLE OF ATOMIC INTERACTIONS: COLLAPSES AND REVIVALS

Up to now, we have neglected the time evolution of the system, except for the state projection consecutive to a detection on $D_\pm$. We now investigate the dynamics of the phase distribution $c(\phi,t)$ [Eq. (14)] for a state with N par-

ticles, including the effects of atomic interactions. We consider here the situation where no interaction takes place between A and B; this situation differs from the one in [10] where the two condensates are spatially overlapping and the interferences are modified by their mutual interactions.

In our case, the Fock states $|N_A,N_B\rangle$ are eigenstates of the total Hamiltonian, with an energy $E(N_A,N_B)$. To express the phase distribution at time t in terms of $c(\phi,0)$, we expand the initial state to the Fock states using Eqs. (12) and (13), we evolve the Fock states for the time t with the appropriate phase factors, and we calculate $c(\phi,t)$ from Eq. (14). This leads to

$$c(\phi,t)=\int_{-\pi/2}^{\pi/2}\frac{d\phi'}{\pi}\;K(\phi-\phi';t)c(\phi',0), \tag{36}$$

with

$$K(\phi;t)=\sum_{N_A=0}^{N} e^{i[(N_B-N_A)\phi-E(N_A,N_B)t/\hbar]}, \tag{37}$$

where $N_B=N-N_A$. Assuming a distribution of the Fock states peaked around $N_A=N_B=N/2$ with a width $\ll N$ [14], we expand

$$E(N_A,N_B)=E(N/2,N/2)+(\mu_B-\mu_A)(N_B-N_A)/2 +\hbar\kappa(N_B-N_A)^2+\cdots, \tag{38}$$

where $\mu_{A/B}$ are the chemical potentials for the condensates A/B. From Eq. (38), we find that the effect of the linear term is a mere phase drift, with a velocity $\dot{\phi}=(\mu_B-\mu_A)/(2\hbar)$. For an ideal gas, $\kappa=0$ and this drift is the only possible evolution, with $\dot{\phi}=(3/4)(\Omega_B-\Omega_A)$, where $\Omega_{A/B}$ are the trap oscillation frequencies.

When atomic interactions are present, $\kappa\neq 0$, and the $(N_B-N_A)^2$ term in $E(N_A,N_B)$ is responsible for a phase spreading analogous to the spreading of the wave function of a free massive particle. This phenomenon is similar to the ''phase diffusion'' predicted in [17]. If we replace the sum over N_A in Eq. (37) with an integral, we find that an initial Gaussian phase distribution remains Gaussian; the variance for ϕ calculated in $|c(\phi,t)|^2$ then evolves as

$$\Delta\phi_t^2=\Delta\phi_0^2+(\kappa t/\Delta\phi_0)^2. \tag{39}$$

Therefore, a state with a well- defined initial phase ($\Delta\phi_0\ll 1$) will be ''dephased'' in a time $\sim t_{\rm collapse}\equiv\Delta\phi_0/\kappa$. For times longer than $t_{\rm collapse}$, we have to keep the discrete sum over N_A in Eq. (37). We find that this phase collapse is followed by revivals occurring at times $t_j=\pi j/4\kappa$, j integer [18], with an average phase displaced by $\dot{\phi}t_j+j\pi/2$ from its initial value.

This discussion implies that the results derived in the first part of this paper are valid provided the measurement sequence is performed in a time short enough that the phase spreading or drift is small compared to the final phase width. As a typical situation, we consider a condensate in the Thomas-Fermi regime [19] for which

$$2\mu_i=\hbar\Omega_i(225\,N_i^2a^2m\Omega_i/\hbar)^{1/5},\quad i=A,B, \tag{40}$$

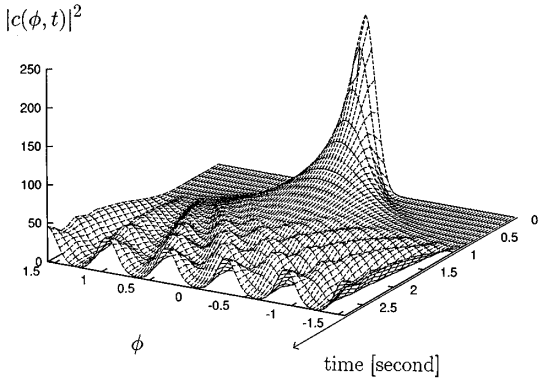

FIG. 3. Short time evolution of the phase probability distribution $|c(\phi,t)|^2$ for $N_A=N_B=10^4$ rubidium atoms. The scattering length is $a=10$ nm. The frequencies of the two traps are identical, $\Omega_{A/B}=2\pi\times 100$ Hz. The initial phase distribution $c(\phi,t=0)$ is real Gaussian, with $|c(\phi,t=0)|^2$ leading to a standard deviation $\Delta\phi_0=1/10$. Note the emergence of fractional revivals after the collapse of the wave packet.

where m is the atomic mass and a is the s-wave scattering length; this leads to $\hbar\kappa=(\mu_A+\mu_B)/(10N)$. Using $\Omega_i=2\pi\times 100$ Hz [1], we find $t_{\rm collapse}=\Delta\phi_0\times 18$ s for $N/2=10^4$ rubidium atoms ($a\sim 10$ nm). The phase collapse is followed by partial fractional revivals (see Fig. 3), a known phenomenon in quantum mechanics [20]. The first full revival occurs at a time ~ 14 s, with an average phase shifted by

$$\delta\phi=\frac{\pi}{2}+\frac{5\pi}{4}\,N\,\frac{\Omega_A^{6/5}-\Omega_B^{6/5}}{\Omega_A^{6/5}+\Omega_B^{6/5}}. \tag{41}$$

For $N\gg 1$, this shift is very sensitive to any asymmetry between the two traps.

To summarize, we have developed an approach to the problem of relative phase of two macroscopic entities that is based on microscopic measurements. In this way, quantitative predictions can be obtained about the phase distribution and its time evolution. This approach is complementary to the one dealing with a macroscopic variable, such as a Josephson current, connecting these two entities [4,21]. It can be extended to the case of more than two condensates in order to discuss the problem of an ''atomic phase standard'' [22]. We note, however, that the phase dynamics described above makes it difficult to establish a long-lived phase coherence between separate atomic samples.

ACKNOWLEDGMENTS

We are grateful to Claude Cohen-Tannoudji, Franck Laloë, and Christophe Salomon for useful discussions, and to Karl Berggren for a careful reading of an early version of the manuscript. This work is partially supported by the DRET, Collège de France, Ultimatech and the European Community. The Laboratoire Kastler Brossel is unité de Recherche de l'Ecole Normale Supérieure et de l'Université Pierre et Marie Curie, associée au CNRS.

APPENDIX A: PROBABILITY FOR A GIVEN DETECTION SEQUENCE

Consider first a single condensate A leaking with a loss rate Γ towards an ideal detector. As usual, in the continuous measurement theory [23,24] the state of the system undergoes a sequence of quantum jumps; the operator characterizing these jumps is $\sqrt{\Gamma}\hat{a}$, where $\hat{a}$ annihilates one particle in the condensate. Between these jumps, the evolution of the system is governed by the non-Hermitian Hamiltonian $-i\hbar\Gamma\hat{N}_A/2$, where $\hat{N}_A=\hat{a}^\dagger\hat{a}$. From [23], we find that the probability density that k counts occur at times $t_1\leqslant t_2\leqslant\cdots\leqslant t_k$ (with no additional count between $t=0$ and $t=t_k$) is given by

$$Q(t_1,\ldots,t_k)=\Gamma^k\,\mathrm{Tr}[\rho(0)e^{-\Gamma\hat{N}_A t_1/2}\hat{a}^\dagger\cdots e^{-\Gamma\hat{N}_A(t_k-t_{k-1})/2}\times\hat{a}^\dagger\hat{a}e^{-\Gamma\hat{N}_A(t_k-t_{k-1})/2}\cdots\hat{a}e^{-\Gamma\hat{N}_A t_1/2}]. \tag{A1}$$

The probability of getting at least k counts for an arbitrarly long measurement time is obtained after some algebra:

$$Q(k)=\int_0^{+\infty}dt_1\int_{t_1}^{+\infty}dt_2\ \ldots\int_{t_{k-1}}^{+\infty}dt_k\ Q(t_1,\ldots,t_k)=\mathrm{Tr}\left[\rho(0)(\hat{a}^\dagger)^k\frac{1}{(\hat{N}_A+1)\cdots(\hat{N}_A+k)}\hat{a}^k\right], \tag{A2}$$

which, in the present case of a single condensate, reduces to the expectation value of the projector onto the states with at least k particles.

This can be generalized to the case of two condensates A and B, with identical loss rates Γ and whose outputs are mixed on a 50-50 beam splitter (see Fig. 1). The measurement process now involves two types of quantum jumps, characterized by the two operators $\sqrt{\Gamma/2}(\hat{a}\pm\hat{b})$. The non-Hermitian Hamiltonian governing the evolution between the quantum jumps is given by $-i\hbar\Gamma\hat{N}/2$, with $\hat{N}=\hat{a}^\dagger\hat{a}+\hat{b}^\dagger\hat{b}$. We now define the probability density $Q(t_1\ \eta_1,\cdots,t_k\ \eta_k)$ that k counts occur at times $t_1\leqslant t_2\leqslant\ldots\leqslant t_k$ (with no additional count between $t=0$ and $t=t_k$) in the output channels $\eta_1=\pm,\ldots,\eta_k=\pm$:

$$\begin{aligned}Q(t_1\ \eta_1,\ldots,t_k\ \eta_k)&=(\Gamma/2)^k\mathrm{Tr}[\rho(0)e^{-\Gamma\hat{N}t_1/2}(\hat{a}^\dagger+\eta_1\hat{b}^\dagger)\cdots\\&\quad\times e^{-\Gamma\hat{N}(t_k-t_{k-1})/2}(\hat{a}^\dagger+\eta_k\hat{b}^\dagger)\\&\quad\times(\hat{a}+\eta_k\hat{b})e^{-\Gamma\hat{N}(t_k-t_{k-1})/2}\cdots\\&\quad\times(\hat{a}+\eta_1\hat{b})e^{-\Gamma\hat{N}t_1/2}].\end{aligned} \tag{A3}$$

From this expression, we can determine the probability $Q(k_+,k_-)$ of getting at least $k=k_++k_-$ counts for an arbitrarily long measurement time, the first k counts involving $k_\pm$ counts in the output channels $\pm$:

$$Q(k_+,k_-)=\frac{1}{2^k}\frac{k!}{k_+!\,k_-!}\mathrm{Tr}\left[\rho(0)(\hat{a}^\dagger+\hat{b}^\dagger)^{k_+}(\hat{a}^\dagger-\hat{b}^\dagger)^{k_-}\times\frac{1}{(\hat{N}+1)\cdots(\hat{N}+k)}(\hat{a}-\hat{b})^{k_-}(\hat{a}+\hat{b})^{k_+}\right]. \tag{A4}$$

The operator $\hat{O}$ introduced in Eq. (10) is readily obtained from this expression, with $k_+=k,k_-=0$.

We now calculate the probability $Q(k_+,k_-)$ when the system is in the coherent state Eq. (7), assuming $\overline{N_A}=\overline{N_B}$. The action of the annihilation and creation operators in Eq. (A4) is easily obtained and we are left with

$$Q(k_+,k_-)=(2\overline{N_A})^k\frac{k!}{k_+!\,k_-!}(\cos\phi)^{2k_+}(\sin\phi)^{2k_-}\times\left\langle\frac{1}{(\hat{N}+1)\cdots(\hat{N}+k)}\right\rangle, \tag{A5}$$

where $\phi=(\phi_A-\phi_B)/2$ and where the average $\langle\cdots\rangle$ is taken in the coherent state. Since the total number of particles has a Poissonian distribution with a mean value $\overline{N_A}+\overline{N_B}=2\overline{N_A}$, this average is given by

$$\begin{aligned}\left\langle\frac{1}{(\hat{N}+1)\ldots(\hat{N}+k)}\right\rangle&=\sum_{N=0}^{\infty}\frac{1}{(N+1)\ldots(N+k)}\frac{1}{N!}(2\overline{N_A})^N e^{-2\overline{N_A}}\\&=\frac{1}{(2\overline{N_A})^k}[1-\Pi(k,\overline{N_A})],\end{aligned} \tag{A6}$$

where we have introduced

$$\Pi(k,\overline{N_A})=e^{-2\overline{N_A}}\sum_{N=0}^{k-1}\frac{(2\overline{N_A})^N}{N!} \tag{A7}$$

which is the probability that the total number of counts remains smaller than k for an arbitrarily long time. This quantity becomes exponentially small when $\overline{N_A}\gg k$.

For a statistical mixture of coherent states with random phases [see Eq. (8), with $\overline{N_A}=\overline{N_B}$], $Q(k_+,k_-)$ becomes

$$Q(k_+,k_-)=[1-\Pi(k,\overline{N_A})]\ \frac{k!}{k_+!\,k_-!}\int_{-\pi/2}^{\pi/2}\frac{d\phi}{\pi}\times(\cos\phi)^{2k_+}\ (\sin\phi)^{2k_-}\ . \tag{A8}$$

The conditional probability $\mathcal{P}(k_+,k_-)$ defined in the text is equal to $Q(k_+,k_-)/[1-\Pi]$, since $1-\Pi$ is the probability of getting at least k counts.

[1] M.H. Anderson, J.R. Ensher, M.R. Matthews, C.E. Wieman and E.A. Cornell, Science **269**, 198 (1995).

[2] C.C. Bradley, C.A. Sackett, J.J. Tollett, and R.G. Hulet, Phys. Rev. Lett. **75**, 1687 (1995).

[3] K. Davis, M.O. Mewes, M.R. Andrews, N.J. van Druten, D.S. Durfee, D.M. Kurn, and W. Ketterle, Phys. Rev. Lett. **75**, 3969 (1995).

[4] A. J. Leggett and F. Sols, Found. Phys. **21**, 353 (1991). It is also shown in this reference that, for some class of interactions between A and B, the ground state of the total system has a definite relative phase between the two subsystems.

[5] A. Griffin, Phys. Rev. B **53**, 9341 (1996), and references therein.

[6] C.S. Adams, M. Sigel, and J. Mlynek, Phys. Rep. **240**, 143 (1994).

[7] The optical equivalent of this property has been recently discussed by K. Mølmer, Phys. Rev. A **55**, 3195 (1997).

[8] P.W. Anderson, in *The Lesson of Quantum Theory*, edited by J. de Boer, E. Dal, and O. Ulfbeck (Elsevier, Amsterdam, 1986).

[9] J. Javanainen and S.M. Yoo, Phys. Rev. Lett. **76**, 161 (1996).

[10] M. Naraschewski, H. Wallis, A. Schenzle, J.I. Cirac, and P. Zoller, Phys. Rev. A **54**, 2185 (1996).

[11] R.P. Feynman, R.B. Leighton, and M. Sands, *The Feynman Lectures on Physics, Quantum Mechanics* (Addison-Wesley, Reading, MA, 1989) Chap. 4, Sec. III.

[12] J.I. Cirac, C.W. Gardiner, M. Naraschewski, and P. Zoller, Phys. Rev. A **56**, R3714 (1996).

[13] C.W. Gardiner, *Quantum Noise* (Springer-Verlag, New York, 1991), Eq. (2.3.10), p. 34.

[14] For the states of interest $|\Psi(k_+,k_-)\rangle$ the distributions have a width $\leqslant\sqrt{N}\ll N$ and meet this condition.

[15] In the case $L>1$ for a general set of θ_j's, ϕ_0 is unique in $[-\pi/2,\pi/2[$. The symmetry $\phi\leftrightarrow-\phi$ for S is specific to the case $L=1$.

[16] We have used the inequality $\alpha\ln(\beta/\alpha)+(1-\alpha)\ln[(1-\beta)/(1-\alpha)]\leqslant 0$ for $0<\alpha,\beta<1$, issuing from the concavity of ln. This inequality is an equality only if $\beta/\alpha=(1-\beta)/(1-\alpha)=1$.

[17] M. Lewenstein and L. You, Phys. Rev. Lett. **77**, 3489 (1996).

[18] A similar result holds for superfluid helium and superconductors [F. Sols, Physica B **194-196**, 1389 (1994)], and for the order parameter $\langle\psi(\vec{r})\rangle$ of a single trapped condensate [E.M. Wright, D.F. Walls, and J.C. Garrison, Phys. Rev. Lett. **77**, 2158 (1996)].

[19] G. Baym and C. Pethick, Phys. Rev. Lett. **76**, 6 (1996).

[20] I.Sh. Averbukh and N.F. Perel'man, Phys. Lett. A **139**, 449 (1989); Zh. Éksp. Teor. Fiz. **96**, 818 (1989) [Sov. Phys. JETP **69**, 464 (1989)].

[21] E.D. Siggia and A.E. Ruckenstein, J. Phys. (Paris) **41**, C7-15 (1980).

[22] A.J. Leggett, Found. Phys. **25**, 113 (1995).

[23] C.W. Gardiner, *Quantum Noise* (Springer Verlag, New York, 1991), p. 245.

[24] H. Carmichael, *An Open System Approach to Quantum Optics*, Lecture Notes in Physics Vol. 18 (Springer, Berlin, 1993); K. Mølmer, Y. Castin, and J. Dalibard, J. Opt. Soc. Am. B **10**, 524 (1993); R. Dum, P. Zoller, and H. Ritsch, Phys. Rev. A **45**, 4879 (1992).

5.4 Sur les méthodes de changement d'échelle

Nous reproduisons ici deux articles sur des solutions de type changement d'échelle aux équations du mouvement d'un gaz en interaction dans un potentiel harmonique dépendant du temps. Le premier [17] est une solution de l'équation de Gross-Pitaevskii dans la limite de Thomas-Fermi, l'autre [58] est exact au niveau de l'équation de Schrödinger à N corps dans la limite unitaire.

Le travail [17] reproduit ci-après était guidé par des considérations d'ordre essentiellement pratique : les condensats piégés sont de petite taille (quelques dizaines de micromètres) donc difficiles à imager optiquement, d'où la procédure d'expansion par temps de vol (consécutive à la coupure du piège) utilisée par tous les groupes expérimentaux. De cette façon, le nuage d'atomes grossit d'un ordre de grandeur au moins, ce qui s'est révélé en particulier crucial pour l'observation des tourbillons quantiques.

Il était à craindre cependant, à cause des interactions entre particules, que l'image obtenue après temps de vol n'ait plus grand chose à voir ni avec le profil de densité initial ni avec la distribution en impulsion des atomes. Ce qui aurait constitué un obstacle fâcheux à l'interprétation des résultats expérimentaux.

Dans l'article ci-après, nous avons pu montrer analytiquement, à partir de l'équation de Gross-Pitaevskii, que ces craintes étaient infondées, et que le profil de densité lors du temps de vol subit un simple changement d'échelle (anisotrope si le potentiel de piégeage l'était), pourvu que le piège soit harmonique et les interactions assez fortes.

Ce type de solution à changement d'échelle fait partie maintenant d'une série assez longue de solutions, développée par différents auteurs, dans le cadre des approximations de champ moyen à la Gross-Pitaevskii, ou au-delà du champ moyen dans des théories hydrodynamiques, ou même pour l'équation de Schrödinger sur la fonction d'onde à N particules [58], article que nous reproduisons également ci-après. Leur grande importance pratique explique leur succès dans la communauté.

PHYSICAL REVIEW
LETTERS

VOLUME 77 30 DECEMBER 1996 NUMBER 27

Bose-Einstein Condensates in Time Dependent Traps

Y. Castin and R. Dum
Ecole Normale Supérieure, Laboratoire Kastler Brossel,. 24 Rue Lhomond, F-75231 Paris Cedex 05, France*
(Received 16 July 1996)

We present analytical results for the macroscopic wave function of a Bose-Einstein condensate in a time dependent harmonic potential. The evolution of the spatial density is a dilatation, characterized by three scaling factors which allow a classical interpretation of the dynamics. This approach is an efficient tool for the analysis of recent experimental results on the expansion and collective excitation of a condensate. [S0031-9007(96)01919-9]

PACS numbers: 03.75.Fi, 05.30.Jp

Recently the combination of laser cooling and evaporative cooling led to the observation of Bose-Einstein condensation in dilute atomic vapors [1–3]. The favored observation technique has been a time of flight measurement: the trapping potential is rapidly switched off and the spatial distribution of the expanding cloud is monitored. In more recent experiments the condensates were collectively excited by a time modulation of the trapping potential [4,5]. In these experiments the state of the condensate is strongly influenced by atomic interactions, which must therefore be included in a theoretical treatment. Work up to now consisted in the numerical solution of the time dependent nonlinear Schrödinger equation for the macroscopic wave function of the condensate [6]. We present here analytical results which allow a more lucid description of the condensate dynamics and an immediate comparison with experiment. To this end we introduce a quantum scaling transform [7] which is inspired by a model of a classical gas. Applying our results to time of flight measurements of expanding condensates [3] we obtain the scattering length of sodium. For condensates collectively excited by a time modulation of the trapping potential we present an *ab initio* calculation of the observed signal.

For dilute gases at low temperatures the atomic interactions can be modeled by a pseudopotential $g\delta(\vec{r})$, where $g > 0$ is related to the s-wave scattering length a by $g = 4\pi\hbar^2 a/m$ [8]. We describe the trap by an anisotropic time dependent harmonic potential

$$U(\vec{r},t) = \frac{1}{2}\sum_{j=1,2,3} m\omega_j^2(t) r_j^2 . \tag{1}$$

We restrict the discussion to the case of zero temperature, which is a realistic assumption for the experiments in [1,2]. The state of the condensate for a static trap can thus be described using a Hartree-Fock ansatz:

$$|\Psi\rangle = |\Phi\rangle \otimes \cdots \otimes |\Phi\rangle . \tag{2}$$

The minimization of mean energy gives the time independent Gross-Pitaevskii equation for $|\Phi\rangle$:

$$\mu\Phi(\vec{r}) = \left[-\frac{\hbar^2}{2m}\Delta + U(\vec{r},0) + Ng|\Phi(\vec{r})|^2\right]\Phi(\vec{r}) , \tag{3}$$

with $N - 1 \simeq N$.

In the regime where the atomic interactions are dominant $[Ng|\Phi(\vec{0})|^2 \simeq \mu \gg \hbar\omega_j$ for $j = 1,2,3]$ we can use the Thomas-Fermi approximation to solve (3) [9]; that is, we can neglect the kinetic energy term as compared to the interaction energy term. The result is

$$\Phi(\vec{r}) \simeq \Phi_{TF}(\vec{r}) = \left(\frac{\mu - U(\vec{r},0)}{Ng}\right)^{1/2} , \tag{4}$$

when $\mu \geq U(\vec{r},0)$, and $\Phi(\vec{r}) = 0$ otherwise. The chemical potential μ is determined by the normalization of $|\Phi\rangle$:

$$\mu = \frac{1}{2}\hbar\bar{\omega}\left(15Na\sqrt{\frac{m\bar{\omega}}{\hbar}}\right)^{2/5} , \tag{5}$$

where $\bar{\omega} = [\omega_1(0)\omega_2(0)\omega_3(0)]^{1/3}$.

0031-9007/96/77(27)/5315(5)$10.00

One can generalize the Hartree-Fock ansatz (2) to the time dependent case, in which Φ is a function of t. A time dependent variational calculus leads to an (explicitly) time dependent Gross-Pitaevskii equation [10,11]:

$$i\hbar\partial_t\Phi(\vec{r},t) = \Big[-\frac{\hbar^2}{2m}\Delta + U(\vec{r},t) + Ng|\Phi(\vec{r},t)|^2\Big]\Phi(\vec{r},t). \quad (6)$$

In the solution of (6) a Thomas-Fermi type approximation is not directly applicable, because the time variation of the trapping potential would convert potential energy into kinetic energy, which therefore could no longer be neglected. In this paper we identify a unitary transform which eliminates the extra kinetic energy.

We first introduce a model of a classical gas in which each particle experiences a force

$$\vec{F}(\vec{r},t) = -\nabla\big(U(\vec{r},t) + g\rho_{cl}(\vec{r},t)\big), \quad (7)$$

where $\rho_{cl}(\vec{r},t)$ is the spatial density in the gas normalized to N. At $t = 0$ the equilibrium condition $\vec{F} = 0$ gives $\rho_{cl}(\vec{r},0) = N|\Phi_{TF}(\vec{r},0)|^2$, that is, the classical solution for the steady state density coincides with the quantum solution in the Thomas-Fermi limit. For $t > 0$ the exact solution for the classical model can be obtained for the class of potentials (1); in this case, the gas merely experiences a dilatation, any infinitesimally small fraction of the expanding cloud moving along a trajectory

$$R_j(t) = \lambda_j(t)R_j(0) \qquad (j = 1,2,3). \quad (8)$$

From this ansatz we obtain for the evolution of the spatial density

$$\rho_{cl}(\vec{r},t) = \frac{1}{\lambda_1(t)\lambda_2(t)\lambda_3(t)} \times \rho_{cl}[\{r_j/\lambda_j(t)\}_{j=1,2,3},0]. \quad (9)$$

Newton's law $m\ddot{R}_j(t) = F_j[\vec{R}(t),t]$ applied for the trajectory (8) implies

$$m\ddot{\lambda}_j(t)R_j(0) = -(\partial_{r_j}U)[\vec{R}(t),t] + \frac{1}{\lambda_j\lambda_1\lambda_2\lambda_3}(\partial_{r_j}U)[\vec{R}(0),0] \qquad (j = 1,2,3). \quad (10)$$

From Eq. (9) we have expressed the gradient of $g\rho_{cl}(t)$ in terms of $\nabla g\rho_{cl}(t=0) = -\nabla U(t=0)$. For the harmonic potentials U of Eq. (1) both sides of Eq. (10) are proportional to $R_j(0)$. Equation (10) therefore holds for any $\vec{R}(0)$ and the ansatz (8) is self-consistent provided that the scaling factors $\lambda_j(t)$ satisfy

$$\ddot{\lambda}_j = \frac{\omega_j^2(0)}{\lambda_j\lambda_1\lambda_2\lambda_3} - \omega_j^2(t)\lambda_j \qquad (j = 1,2,3). \quad (11)$$

The initial conditions are $\lambda_j(0) = 1$ and since the gas is initially at rest, $\dot{\lambda}_j(0) = 0$. Taking the time derivative of Eq. (8) and eliminating the initial position by Eq. (8) we obtain for the local velocity of the expanding cloud

$$v_j(\vec{r},t) = r_j\frac{\dot{\lambda}_j(t)}{\lambda_j(t)}. \quad (12)$$

Equations (11) and (12) do not depend on the interaction strength g. The g dependence is entirely contained in the initial spatial density of the gas [12].

This classical solution motivates the ansatz for the solution of the quantum equation (6):

$$\Phi(\vec{r},t) = e^{-i\beta(t)}e^{im\sum_j r_j^2\dot{\lambda}_j(t)/2\hbar\lambda_j(t)} \times \frac{\tilde{\Phi}[\{r_k/\lambda_k(t)\}_{k=1,2,3},t]}{\sqrt{\lambda_1\lambda_2\lambda_3}}. \quad (13)$$

Equation (13) is a unitary transform combining a scaling in $\vec{r}$ and a gauge transform. The gauge transform subtracts from the momentum operator $\hat{\vec{p}}$ the local momentum of the expanding classical gas (12):

$$\hat{p}_j \to \hat{p}_j + m\frac{\dot{\lambda}_j(t)}{\lambda_j(t)}\hat{r}_j. \quad (14)$$

The scaling transform mimics the dilatation (9) obtained in the classical case. We insert the ansatz (13) in Eq. (6). For the convenient choice of the global phase factor $e^{-i\beta(t)}$, $\hbar\dot{\beta} = \mu/\lambda_1(t)\lambda_2(t)\lambda_3(t)$, we obtain after some algebra the following time evolution for $\tilde{\Phi}(\vec{r},t)$:

$$\Big[i\hbar\partial_t + \frac{\hbar^2}{2m}\sum_j\frac{1}{\lambda_j^2(t)}\partial_{r_j}^2\Big]\tilde{\Phi}(\vec{r},t) = \frac{1}{\lambda_1(t)\lambda_2(t)\lambda_3(t)}[-\mu + U(\vec{r},0) + Ng|\tilde{\Phi}(\vec{r},t)|^2]\tilde{\Phi}(\vec{r},t), \quad (15)$$

with the initial condition $\tilde{\Phi}(\vec{r},0) = \Phi(\vec{r},0)$. In the Thomas-Fermi regime the right hand side of Eq. (15) is initially very small; the kinetic energy terms on the left hand side are also small initially, and are expected to remain small in time, since the extra kinetic energy due to a change in the trapping potential has been absorbed in the unitary transform (13). We therefore expect that $\tilde{\Phi}(\vec{r},t)$ evolves weakly in time.

To show this point more rigorously we split $\tilde{\Phi}(\vec{r},t)$ into $\Phi(\vec{r},0) + \delta\tilde{\Phi}(\vec{r},t)$. From Eqs. (15) and (3) we find that $\delta\tilde{\Phi}(\vec{r},t)$ obeys a nonlinear inhomogeneous equation with a source term given by

$$S(\vec{r},t) = -\frac{\hbar^2}{2m}\sum_{j=1}^{3}\Big(\frac{1}{\lambda_j^2(t)} - \frac{1}{\lambda_1(t)\lambda_2(t)\lambda_3(t)}\Big)\partial_{r_j}^2\Phi(\vec{r},0). \quad (16)$$

In the Thomas-Fermi approximation the spatial derivatives of $\Phi(\vec{r},0)$ are neglected and the source term vanishes; in this case, $\delta\tilde{\Phi}(\vec{r},t)$ being initially zero remains zero, and $\Phi(\vec{r},t)$ remains constant [13]:

$$\tilde{\Phi}(\vec{r},t) \simeq \Phi(\vec{r},0)\,. \tag{17}$$

This result provides a generalization of the Thomas-Fermi approximation to time dependent problems. All the dynamics of the macroscopic wave function are contained in the evolution of three scaling parameters. In particular the condensate density is a time dependent inverted paraboloid:

$$N|\Phi(\vec{r},t)|^2_{TF} = \frac{\mu - \sum_{j=1}^{3} \frac{1}{2} m\omega_j^2(0) r_j^2/\lambda_j^2(t)}{g\lambda_1(t)\lambda_2(t)\lambda_3(t)}\,, \tag{18}$$

when the right hand side is positive and $|\Phi|^2_{TF} = 0$ otherwise.

We now apply the above results to experimental data obtained in the Ioffe-Pritchard trap of [3]. The trap is axially symmetric with respect to z and cigar shaped ($\omega_1 = \omega_2 \equiv \omega_\perp \gg \omega_3 \equiv \omega_z$).

We consider first the simplest case of a sudden and total opening of the trap at $t = 0$. The equations for the evolution of the scaling parameters (11) simplify to

$$\frac{d^2}{d\tau^2}\lambda_\perp = \frac{1}{\lambda_\perp^3\lambda_z}\,,$$
$$\frac{d^2}{d\tau^2}\lambda_z = \frac{\epsilon^2}{\lambda_\perp^2\lambda_z^2}\,, \tag{19}$$

where $\lambda_\perp$ stands for $\lambda_1 = \lambda_2$ and λ_z stands for λ_3. We have introduced a dimensionless time variable $\tau = \omega_\perp(0)t$ and a parameter $\epsilon = \omega_z(0)/\omega_\perp(0) \ll 1$. We solve (19) by an expansion in powers of ϵ. To zeroth order in ϵ, $\lambda_z = 1$ and the radial expansion scales as

$$\lambda_\perp(\tau) = \sqrt{1 + \tau^2}\,. \tag{20}$$

To second order in ϵ the axial expansion of the cloud is given by

$$\lambda_z(\tau) = 1 + \epsilon^2[\tau \arctan\tau - \ln\sqrt{1+\tau^2}] + O(\epsilon^4)\,. \tag{21}$$

For the experiments considered the term in ϵ^2 is not negligible.

We have performed a fit of the images obtained for two different times of flight in [3]. We used an inverted paraboloid for the density of the cloud, having as free parameters the radial width $W_\perp$, the axial width W_z, and the number of condensed atoms N. Figure 1 shows a cut along the x axis (that is, at $z = 0$) of the spatial density of the cloud integrated along y. According to Eq. (18) the aspect ratio of the cloud is given by

$$\frac{W_z(t)}{W_\perp(t)} = \frac{\lambda_z(t)\sqrt{2\mu/m\omega_z^2(0)}}{\lambda_\perp(t)\sqrt{2\mu/m\omega_\perp^2(0)}} = \frac{\lambda_z(t)}{\lambda_\perp(t)}\,\frac{1}{\epsilon}\,. \tag{22}$$

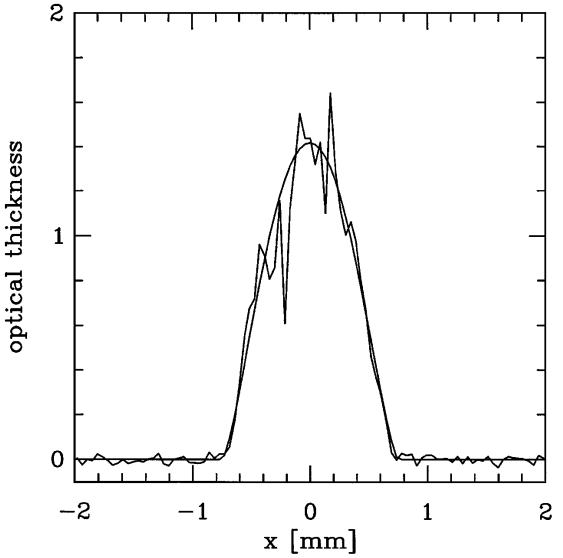

FIG. 1. Spatial density of an expanding condensate integrated along the y axis, cut along the x axis (that is, at $z = 0$). Experimental data obtained at MIT (expansion time of 40 ms) and fit from theory.

The fit gives the values of this ratio for two different expansion times, from which we calculate the two unknown frequencies $\omega_\perp(0)$ and $\omega_z(0)$, using Eqs. (20) and (21). From $W_\perp$ we calculate μ; the relation (5) then leads to a scattering length of $a = 42 \pm 15$ Bohr for sodium, in agreement with earlier measurements [14].

In a second generation of experiments a collective excitation of the condensate has been induced by a time modulation of the eigenfrequencies of the trapping potential [4,5]. In [5] the axial frequency is modulated as $\omega_z^2(\tau) = \omega_z^2(0)[1 - \eta(1 - \cos\Omega\tau)]$ [Ω in units of $\omega_\perp(0)$]. After the excitation the cloud freely oscillates in the unperturbed potential for an adjustable time. Finally, the trapping potential is switched off and the expanding cloud is monitored.

By including this experimental sequence in the evolution of the scaling paameters (11), we give an *ab initio* calculation of the time of flight signals. For a weak modulation ($\eta \ll 1$) the time evolution in the trap is obtained from a linearization of Eq. (11) around the steady state value 1. During the excitation process we obtain for the deviations $\delta\lambda_\perp$ and $\delta\lambda_z$:

$$\frac{d^2}{d\tau^2}\delta\lambda_\perp(\tau) = -4\delta\lambda_\perp(\tau) - \delta\lambda_z(\tau)\,, \tag{23}$$

$$\frac{d^2}{d\tau^2}\delta\lambda_z(\tau) = -2\epsilon^2\delta\lambda_\perp(\tau) - 3\epsilon^2\delta\lambda_z(\tau) + \epsilon^2\eta[1 - \cos(\Omega\tau)]\,. \tag{24}$$

To leading order in ϵ the eigenmodes of this linear system have frequencies [in units of $\omega_\perp(0)$] $\Omega_{\text{fast}} = 2$ and $\Omega_{\text{slow}} = \sqrt{\frac{5}{2}}\epsilon$ and are polarized along $(1, 1, 0)$ and $(1, 1, -4)$, respectively [15,16]. In the experiments the driving frequency Ω was set to Ω_{slow} to achieve a resonant excitation of the slow mode. To lowest order in ϵ, this allows us to keep only the slow mode component of the solution, for which $\delta\lambda_\perp = -\delta\lambda_z/4$. Equation (24) integrated for the time duration τ_e of the excitation then leads to

$$\delta\lambda_z(\tau_e) = \frac{2\eta}{5}[1 - \cos(\Omega_{\text{slow}}\tau_e)] - \frac{\eta}{5}\Omega_{\text{slow}}\tau_e \sin(\Omega_{\text{slow}}\tau_e). \quad (25)$$

In [5] the potential was modulated for five cycles so that $\tau_e = 5(2\pi/\Omega_{\text{slow}})$ and $\delta\lambda_z(\tau_e) = 0$, $\frac{d}{d\tau}\delta\lambda_z(\tau_e) = -2\pi\eta\Omega_{\text{slow}}$. The subsequent evolution in the unperturbed trapping potential is sinusoidal with the eigenfrequency Ω_{slow}; after the free oscillation time τ_o it leads to $\delta\lambda_z(\tau_e + \tau_o) = -4\delta\lambda_\perp(\tau_e + \tau_o) = -2\pi\eta \sin\Omega_{\text{slow}}\tau_o$.

Finally the trapping potential is switched off to monitor the excited condensate. The time evolution of the scaling parameters is obtained by linearizing Eq. (19) around the solutions Eqs. (20) and (21) with initial conditions given by the values of $\delta\lambda_{z,\perp}$ and their derivatives at $\tau = \tau_e + \tau_o$. After a time of flight τ_f we obtain, neglecting terms of order 2 in ϵ and terms vanishing in the limit $\tau_f \to \infty$,

$$\delta\lambda_\perp(\tau_e + \tau_o + \tau_f) = -\frac{1}{4}\tau_f\delta\lambda_z(\tau_e + \tau_o) - \frac{1}{4}[\pi\tau_f - 4\ln\tau_f + 1]\frac{d}{d\tau}\delta\lambda_z(\tau_e + \tau_o), \quad (26)$$

$$\delta\lambda_z(\tau_e + \tau_o + \tau_f) = \delta\lambda_z(\tau_e + \tau_o) + \tau_f\frac{d}{d\tau}\delta\lambda_z(\tau_e + \tau_o). \quad (27)$$

From this we determine the aspect ratio (22) of the expanding cloud. Figure 2 shows that our predictions are in good agreement with the experimental results of [5] for short free oscillation times τ_o. For longer times τ_o a damping of the oscillations is observed experimentally, which cannot be explained with our mean field treatment.

In conclusion, we have been able to extend the Thomas-Fermi approximation to the motion of a condensate in a time dependent harmonic potential: the time dependence is entirely contained in three scaling factors which can be obtained from the evolution of a classical gas. This provides an easy quantitative tool for the analysis of current experiments on trapped condensed gases. We have applied it to two recent experiments. From time of flight images of the condensate at two different expansion times we could calculate the scattering length a without relying on measurements of the trapping frequencies. For collective excitations of a condensate in the linear response regime we could predict not only the frequency but also the phase and amplitude of the measured signal (see Fig. 2). Our treatment can be applied in the nonlinear response regime as well, for example, for oscillations of the condensate induced by a strong modulation or by a partial opening of the trap.

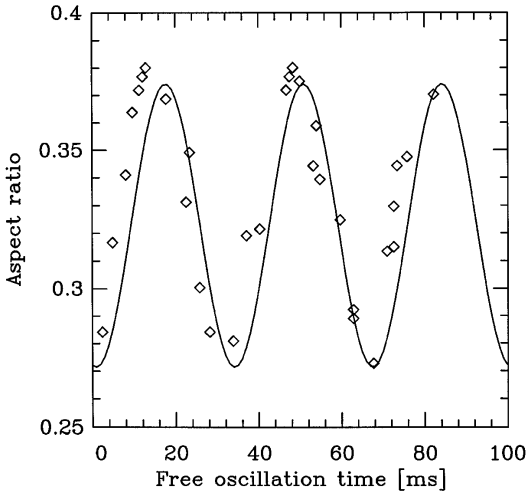

FIG. 2. Aspect ratio of the excited and expanded condensate as a function of free oscillation time τ_o. Expansion time $\tau_f = 40$ ms, $\omega_\perp(0) = 2\pi \times 250$ Hz, $\omega_z(0) = 2\pi \times 19$ Hz, $\eta = 0.005$. Solid line: theory. Diamonds: experimental data obtained at MIT.

We are grateful to the group at MIT for providing us with the experimental data. R. D. was supported by the European Community. We thank M.-O. Mewes, J. Dalibard, and C. Cohen-Tannoudji for helpful discussions.

*Laboratoire Kastler Brossel is a unité de recherche de l'Ecole Normale Supérieure et de l'Université Pierre et Marie Curie, associée au CNRS

[1] M. H. Anderson, J. R. Ensher, M. R. Matthews, C. E. Wieman, and E. A. Cornell, Science **269**, 198 (1995).
[2] K. Davis, M.-O. Mewes, M. R. Andrews, N. J. van Druten, D. S. Durfee, D. M. Kurn, and W. Ketterle, Phys. Rev. Lett. **75**, 3969 (1995).
[3] M.-O. Mewes, M. R. Andrews, N. J. van Druten, D. M. Kurn, D. S. Durfee, and W. Ketterle, Phys. Rev. Lett. **77**, 416 (1996).
[4] D. S. Jin, J. R. Ensher, M. R. Matthews, C. E. Wieman, and E. A. Cornell, Phys. Rev. Lett. **77**, 420 (1996).
[5] M.-O. Mewes, M. R. Andrews, N. J. van Druten, D. M. Kurn, D. S. Durfee, C. G. Townsend, and W. Ketterle, Phys. Rev. Lett. **77**, 988 (1996).
[6] P. A. Rupprecht, M. J. Holland, K. Burnett, and M. Edwards, Phys. Rev. A **51**, 4704 (1995).

[7] A similar treatment valid for isotropic traps has been developed independently by Y. Kagan, E. L. Surkov, and G. Shlyapnikov, Phys. Rev. A **54**, R1753 (1996).
[8] K. Huang, *Statistical Mechanics* (Wiley, New York, 1987).
[9] G. Baym and C. Pethick, Phys. Rev. Lett. **76**, 6 (1996).
[10] Ph. Nozières and D. Pines, *The Theory of Quantum Liquids* (Addison-Wesley, Reading, MA, 1990), Vol. II.
[11] This variational calculus can be justified by extending the Bogoliubov–de Gennes treatment of superfluidity to time dependent problems [R. Dum and Y. Castin (unpublished)].
[12] Those results can also be obtained using the hydrodynamic approach presented in [15] [C. Myatt (unpublished)].
[13] Linearizing the equation for $\delta\tilde{\Phi}(\vec{r},t)$ and assuming linear stability we obtain an upper bound for $||\delta\tilde{\Phi}(t)||$ scaling in the isotropic case as $\int_0^t dt'||S(t')|| \sim \int_0^t \omega(0)\,dt'|\lambda^{-2}(t') - \lambda^{-3}(t')|[\hbar\omega(0)/\mu]^{1/3} \to 0$ for $\mu/\hbar\omega(0) \to \infty$.
[14] E. Tiesinga, C. Williams, P. Julienne, K. Jones, P. Lett, and W. Phillips [NIST J. Res. **101**, 505 (1996)], special issue on BEC, edited by K. Burnett, M. Edwards, and C. Clark.
[15] Those modes can be obtained from a classical hydrodynamic treatment: S. Stringari, Phys. Rev. Lett. **77**, 2360 (1996).
[16] A third, axially antisymmetric mode along $(1,-1,0)$ with a frequency $\sqrt{2}\,\omega_\perp$ is obtained from linearization of Eq. (11) without assuming $\lambda_1 = \lambda_2$.

ELSEVIER

Available online at www.sciencedirect.com
SCIENCE DIRECT®

C. R. Physique 5 (2004) 407–410

COMPTES RENDUS PHYSIQUE

Physics/Statistical physics, thermodynamics

Exact scaling transform for a unitary quantum gas in a time dependent harmonic potential

Yvan Castin

Laboratoire Kastler Brossel, École normale supérieure, 24, rue Lhomond, 75231 Paris, France

Received 23 March 2004; accepted 30 March 2004

Presented by Jean Dalibard

Abstract

A unitary quantum gas is a gas of quantum particles with a binary interaction of infinite scattering length and negligible range. It has been produced in recent experiments with gases of fermionic atoms by means of a Feshbach resonance. Using the Fermi pseudo-potential model for the atomic interaction, we show that the time evolution of such a gas in an isotropic three-dimensional time dependent harmonic trap is exactly given by a gauge and scaling transform. ***To cite this article: Y. Castin, C. R. Physique 5 (2004).***

Résumé

Évolution d'un gaz quantique unitaire dans un potentiel harmonique variable : solution par changement d'échelle. Nous entendons par « gaz quantique unitaire » une assemblée de particules dont le mouvement est décrit quantiquement et qui interagissent par un potentiel de longueur de diffusion infinie et de portée négligeable devant leur distance moyenne et leur longueur d'onde thermique. Un tel gaz a été produit récemment à l'aide d'une résonance de Feshbach dans un gaz d'atomes fermioniques. En modélisant les interactions entre particules par le pseudo-potentiel de Fermi, nous montrons que l'évolution d'un gaz unitaire dans un potentiel de piégeage harmonique isotrope tridimensionnel de dépendence temporelle quelconque est décrite exactement par la composition d'un changement d'échelle et d'une transformation de jauge. ***Pour citer cet article : Y. Castin, C. R. Physique 5 (2004).***

Keywords: Unitary quantum gas; Scaling transform; Harmonic trap

Mots-clés : Gaz quantique unitaire ; Changement d'échelle ; Potentiel harmonique

1. Introduction

Experiments with quantum gases of spin 1/2 fermionic atoms are currently making rapid progresses. One of the most fascinating properties of these fermionic gases is the possibility to freely tune the sign and the strength of the atomic interactions without reducing the lifetime of the sample: the value of the s-wave scattering length a of two particles with opposite spin components can virtually be adjusted from $-\infty$ to $+\infty$ with a Feshbach resonance technique [1], without inducing any instability of the gas even in the unitary limit $a = \pm\infty$ [2]. These systems are still gases, in the sense that the effective range of the interaction potential is negligible as compared to the mean interparticle separation and to the thermal de Broglie

E-mail address: yvan.castin@lkb.ens.fr (Y. Castin).

1631-0705/$ – see front matter
doi:10.1016/j.crhy.2004.03.017

wavelength. We shall take advantage of this crucial property and model the true interaction potential by the so-called Fermi pseudo-potential [3].

Such stability of the strongly interacting Fermi gases opens up fascinating possibilities, e.g. the study of the crossover between a Bose–Einstein condensate of dimers (already observed, see [4–7]) and a BCS condensate of pairs, by passing through the strongly interacting regime $k_F|a| \gg 1$, where k_F is the Fermi momentum [8,9]. In the unitary limit $k_F|a| \to +\infty$, the thermodynamic properties of the spatially homogeneous gas are universal: they depend only on the Fermi energy and on the temperature. At zero temperature, the chemical potential of the homogeneous gas is then $\mu = \eta\mu_0$ where η is a pure number and μ_0 is the chemical potential of the ideal Fermi gas [2,10]. An accurate measurement of η would provide a crucial test of many-body theories [2,5,7].

The standard imaging technique used with quantum gases is to switch off the trapping potential, to let the gas expand and to perform a light absorption imaging of the atomic cloud. Such a ballistic expansion acts as a magnifying lens: it was used to reveal the vortex lattice in a rotating Bose–Einstein condensate [11], and very recently to obtain the value of the universal number η for the unitary Fermi gas [7]. Clearly the interpretation of the time of flight images strongly relies on a theoretical understanding of the time evolution of the gas in a time dependent harmonic potential. In the case of a pure Bose–Einstein condensate in the regime $k_F|a| \ll 1$, this was achieved starting from the Gross–Pitaevskii equation by a gauge plus scaling transform [12,13]. When the Bose or Fermi gas enters the strongly interacting regime $k_F|a| > 1$, no solution starting from first principles is available[1] and one relies on the hydrodynamic approximation [14].

Here we consider the idealized case of an isotropic and harmonic three-dimensional trapping potential. In the limit of an infinite scattering length, we show that the Fermi pseudo-potential has a scaling invariance that rigorously allows the use of a gauge plus scaling transform similar to the one of [15] to describe the time evolution of the gas due to an arbitrary variation of the trapping frequency.

2. The model based on the Fermi pseudo-potential

Consider an assembly of N non-relativistic particles, with an arbitrary spin. These particles may be indistinguishable bosons or fermions, or even be distinguishable. All the particles have the same mass m and interact *via* the same binary interaction potential independent of the spin degrees of freedom. The interaction potential is the Fermi pseudo-potential with coupling constant g related to the s-wave scattering length a by $g = 4\pi\hbar^2 a/m$. At this stage, $0 < |a| < +\infty$, we shall take the unitary limit $|a| \to +\infty$ later.

Let $\psi(\mathbf{r_1}, \ldots, \mathbf{r_N})$ be the wavefunction of the gas corresponding to a given (but arbitrary) spin configuration. The wavefunction ψ then evolves according to the Schrödinger equation:

$$i\hbar\partial_t\psi = \sum_{i=1}^{N}\left[-\frac{\hbar^2}{2m}\Delta_{\mathbf{r}_i} + U(\mathbf{r}_i)\right]\psi + \sum_{1\leqslant i<j\leqslant N} g\delta(\mathbf{r}_i - \mathbf{r}_j)\psi_{ij}^{\mathrm{reg}}. \tag{1}$$

Here $\Delta_{\mathbf{r}_i}$ is the three-dimensional Laplacian with respect to the spatial coordinates $\mathbf{r}_i$ of particle number i, U is the trapping potential seen by each particle and each ψ_{ij}^{reg}, the so-called regular part of ψ in $\mathbf{r}_i = \mathbf{r}_j$, is the following function of $N-1$ vectors of coordinates:

$$\psi_{ij}^{\mathrm{reg}}\big(\{\mathbf{r}_k, k \neq i, j\}, \mathbf{R_{ij}}\big) = \lim_{r_{ij}\to 0} \frac{\partial}{\partial r_{ij}}(r_{ij}\psi), \tag{2}$$

where r_{ij} is the norm of $\mathbf{r_{ij}} \equiv \mathbf{r}_i - \mathbf{r}_j$ and where the limit and the partial derivative are taken for fixed positions $\mathbf{r}_k$ of the $N-2$ particles other than particles i and j, and for a fixed position of the center of mass of the particles i and j, $\mathbf{R_{ij}} \equiv (\mathbf{r}_i + \mathbf{r}_j)/2$.

The domain of the Hamiltonian corresponding to the Fermi pseudo-potential is therefore not the Hilbert space of the non-interacting gas, but a functional space with specific boundary conditions for the wavefunction ψ. More precisely, as we now see, the model amounts to replacing the true interaction potential by *contact* conditions, i.e. by boundary conditions on ψ when the distance r_{ij} between two particles tends to zero, the wavefunction ψ otherwise evolving with the interaction free Schrödinger equation [16]. As the wavefunction ψ does not contain any delta singularity, each delta singularity in the interaction term of Eq. (1) has indeed to be compensated by a delta singularity in the kinetic energy term. In 3D this implies that ψ can diverge as $1/r_{ij}$ when $r_{ij} \to 0$, a divergence which is still square integrable. Two cases can occur:

[1] It was expected that a gauge plus scaling transform would provide an exact solution to the N-body problem in a strictly two-dimensional Bose gas in an isotropic harmonic trap [15], for an interaction potential modeled by a delta distribution. Actually a delta interaction potential in 2D does not lead to a mathematically well defined problem and the required regularisation [17] breaks the scaling invariance.

- case (i): $\lim_{r_{ij}\to 0}\psi = 0$: no delta singularity occurs from the kinetic energy operator, and there is no delta singularity from the interaction term as $\psi_{ij}^{\rm reg}$ vanishes. For instance, this is the case when particles i and j are indistinguishable fermions in the same spin state.
- case (ii): ψ has a $1/r_{ij}$ singularity:

$$\psi = \frac{A}{r_{ij}} + B + \mathrm{O}(r_{ij}), \tag{3}$$

where A and B are still functions of the $\mathbf{r}_k$'s with $k \neq i, j$, and of $\mathbf{R_{ij}}$. The regular part of ψ is then $\psi_{ij}^{\rm reg} = B$. Writing the kinetic energy operator for the pair of particles i, j as $\Delta_{\mathbf{r}_i} + \Delta_{\mathbf{r}_j} = \frac{1}{2}\Delta_{\mathbf{R_{ij}}} + 2\Delta_{\mathbf{r_{ij}}}$ and using $\Delta(1/r) = -4\pi\delta(\mathbf{r})$, we find that the total coefficient of $\delta(\mathbf{r}_i - \mathbf{r}_j)$ in the right-hand side of Eq. (1) vanishes provided that $A + aB = 0$.

A way of summarizing the two cases is then simply to impose the boundary conditions:

$$\psi(\mathbf{r_1}, \ldots, \mathbf{r_N}) = A\big(\{\mathbf{r}_k, k \neq i, j\}, \mathbf{R_{ij}}\big)\big[r_{ij}^{-1} - a^{-1}\big] + \mathrm{O}(r_{ij}) \tag{4}$$

the first case corresponding to $A = 0$ and the second one to $A \neq 0$. Having ensured that all the delta singularities cancel in the Schrödinger equation, we can now restrict it to the manifold where the positions of the particles are two by two distinct:

$$\mathrm{i}\hbar\partial_t\psi = \sum_{i=1}^{N}\left[-\frac{\hbar^2}{2m}\Delta_{\mathbf{r}_i} + U(\mathbf{r}_i)\right]\psi \quad \text{for } r_{ij} \neq 0,\ \forall i \neq j. \tag{5}$$

Eqs. (4) and (5) constitute the basis of our model.

3. Scaling transform in the unitary limit

We specialize the previous section to the case of the unitary quantum gases: the scattering length is now infinite, so that we set to zero the $1/a$ term in the boundary conditions (4), to obtain

$$\psi(\mathbf{r_1}, \ldots, \mathbf{r_N}) = \frac{A(\{\mathbf{r}_k, k \neq i, j\}, \mathbf{R_{ij}})}{r_{ij}} + \mathrm{O}(r_{ij}). \tag{6}$$

Note that the unitary limit does not look in any way singular in our formulation of the model, as the scattering length only appears through its inverse in Eq. (4). Also we restrict to the case of an isotropic harmonic potential:

$$U(\mathbf{r}) = \frac{1}{2}m\omega^2(t)r^2, \tag{7}$$

where the oscillation frequency $\omega(t)$ of a particle in a trap is constant and equal to ω_0 for $t < 0$ and has an arbitrary time dependence for $t \geqslant 0$. The ballistic expansion of the gas mentioned in the introduction corresponds to setting ω to zero for $t \geqslant 0$.

We assume that the state vector of the gas for $t < 0$ is a steady state of Schrödinger's equation with the energy E. The corresponding wavefunction for the considered spin configuration is ψ_0, which in particular obeys the boundary condition equation (6). Our ansatz for the time-dependent wavefunction, inspired from [12,13,15], is then

$$\psi(\mathbf{r_1}, \ldots, \mathbf{r_N}, t) = \mathcal{N}(t)\,\mathrm{e}^{\mathrm{i}\sum_{j=1}^{N} m r_j^2\dot{\lambda}(t)/2\hbar\lambda(t)}\psi_0\big(\mathbf{r_1}/\lambda(t), \ldots, \mathbf{r_N}/\lambda(t)\big), \tag{8}$$

where the time dependent normalisation factor $\mathcal{N}(t)$ and the time dependent scaling factor $\lambda(t)$ need to be determined. This ansatz is the combination of a gauge transformation (see the Gaussian phase factor) and a time dependent scaling transform (see the rescaling of the coordinates by $\lambda(t)$ in ψ_0).

The first step is to check that the ansatz equation (8) is in the right Hilbert space, i.e. that it satisfies the boundary conditions equation (6). The scaling transform indeed preserves the boundary conditions: it rescales and multiplies the function A by λ but does not lead to the appearance of a O(1) term in Eq. (6). Note that for a non-zero value of $1/a$ the conclusion would be different if $A \neq 0$. The gauge transform also preserves the boundary conditions: for fixed $\mathbf{r}_k$'s we write $r_i^2 + r_j^2 = 2R_{ij}^2 + r_{ij}^2/2$ so that for a fixed $\mathbf{R_{ij}}$, the gauge transform involves only as a non-constant factor

$$\mathrm{e}^{\mathrm{i}mr_{ij}^2\dot{\lambda}/4\hbar\lambda} = 1 + \mathrm{i}mr_{ij}^2\dot{\lambda}/4\hbar\lambda + \mathrm{O}\big(r_{ij}^4\big). \tag{9}$$

As $r_{ij}^2 \times A/r_{ij} = \mathrm{O}(r_{ij})$, the boundary conditions are preserved by the gauge transform, a conclusion that extends to the non-zero $1/a$ case.

What is left is to check that the free particle Schrödinger equation (5) is satisfied by the ansatz for an appropriate choice of $\lambda(t)$ and $\mathcal{N}(t)$. One calculates the time derivative and the Laplacian of the ansatz. One uses the fact that ψ_0 is an eigenstate of energy E to express the action of the kinetic energy operator on ψ_0 in terms of $r_j^2\psi_0$ terms and $E\psi_0$. Equating the terms $r_j^2\psi_0$ on both sides of Eq. (5) leads to

$$\ddot{\lambda}(t) = \frac{\omega_0^2}{\lambda^3(t)} - \omega^2(t)\lambda(t) \tag{10}$$

to be solved with the initial conditions $\lambda(t<0)=1$, $\dot{\lambda}(t<0)=0$. For a ballistic expansion, one finds $\lambda(t) = (1+\omega_0^2 t^2)^{1/2}$. Equating the terms proportional to ψ_0 gives $\dot{\mathcal{N}}/\mathcal{N} = -3N\dot{\lambda}/(2\lambda) - iE/(\hbar\lambda^2)$ which is readily integrated in $\mathcal{N}(t) = \lambda^{-3N/2}(t)\exp[-iE\int_0^t d\tau/\lambda^2(\tau)\hbar]$. The first factor in the right-hand side of this equation ensures the conservation of the norm of the wavefunction.

The ansatz equation (8) therefore gives, in the unitary limit, the exact time evolution of the initial state vector for an arbitrary time dependence of the isotropic harmonic potential. It rigorously confirms the scaling law that one would obtain from the zero temperature hydrodynamic approximation. It also allows to use the symmetry considerations developed in [15]: e.g. the limit of linear response to a sudden change in the frequency ω away from ω_0 gives rise to an undamped oscillation at frequency $2\omega_0$ which reveals the existence of N-body stationary states of energy $E \pm 2\hbar\omega_0$ coupled to ψ_0 by the excitation operator $\sum_{i=1}^N r_i^2$.

Acknowledgements

We thank L. Pricoupenko for discussions, A. Sinatra, I. Carusotto, J. Dalibard and C. Cohen-Tannoudji for comments. LKB is a research unit of École normale supérieure and Université Pierre et Marie, associated to CNRS.

References

[1] J.M. Vogels, C.C. Tsai, R.S. Freeland, S. Kokkelmans, B.J. Verhaar, D.J. Heinzen, Phys. Rev. A 56 (1997) R1067.
[2] K.M. O'Hara, S.L. Hemmer, M.E. Gehm, S.R. Granade, J.E. Thomas, Science 298 (2002) 2179.
[3] Y. Castin, in: R. Kaiser, C. Westbrook, F. David (Eds.), Coherent Atomic Matter Waves, Lecture Notes of Les Houches Summer School, EDP Sciences and Springer-Verlag, 2001, pp. 1–136.
[4] M. Greiner, C.A. Regal, D.S. Jin, Nature 426 (2003) 537.
[5] S. Jochim, M. Bartenstein, A. Altmeyer, S. Riedl, C. Chin, J.H. Denschlag, R. Grimm, Science 302 (2003) 2101.
[6] M.W. Zwierlein, C.A. Stan, C.H. Schunck, S.M.F. Raupach, S. Gupta, Z. Hadzibabic, W. Ketterle, Phys. Rev. Lett. 91 (2003) 250401.
[7] T. Bourdel, L. Khaykovich, J. Cubizolles, J. Zhang, F. Chevy, M. Teichmann, L. Tarruell, S. Kokkelmans, C. Salomon, cond-mat/0403091.
[8] P. Nozières, S. Schmitt-Rink, J. Low Temp. Phys. 59 (1985) 195.
[9] M. Randeria, in: A. Griffin, D. Snoke, S. Stringari (Eds.), Bose–Einstein Condensation, Cambridge University Press, Cambridge, 1995.
[10] J. Carlson, S.-Y. Chang, V.R. Pandharipande, K.E. Schmidt, Phys. Rev. Lett. 91 (2003) 050401.
[11] K.W. Madison, F. Chevy, W. Wohlleben, J. Dalibard, Phys. Rev. Lett. 84 (2000) 806.
[12] Y. Castin, R. Dum, Phys. Rev. Lett. 77 (1996) 5315.
[13] Y. Kagan, E.L. Surkov, G. Shlyapnikov, Phys. Rev. A 54 (1996) R1753.
[14] C. Menotti, P. Pedri, S. Stringari, Phys. Rev. Lett. 89 (2002) 250402.
[15] L.P. Pitaevskii, A. Rosch, Phys. Rev. A 55 (1997) R853.
[16] D.S. Petrov, C. Salomon, G.V. Shlyapnikov, cond-mat/0309010.
[17] M. Olshanii, L. Pricoupenko, Phys. Rev. Lett. 88 (2002) 010402.

5.5 Sur les méthodes de Monte-Carlo quantique

L'article présenté [47] est une illustration du type de calculs numériques exacts que l'on peut effectuer très simplement avec la nouvelle méthode de Monte-Carlo quantique que nous avons développée avec Jean Dalibard et Iacopo Carusotto [36]. Il s'agit du calcul de la distribution de probabilité du nombre de particules dans un condensat en interaction, pour des températures allant de presque zéro à des valeurs supérieures à la température critique.

En principe, les méthodes Monte-Carlo existantes (par intégrale de chemin, Path Integral Monte Carlo) doivent pouvoir être utilisées. Cependant, l'observable considérée est très complexe à calculer avec ces méthodes, qui privilégient l'espace des positions. Aussi les experts du domaine, qui maîtrisent la technique depuis des décennies, n'avaient-ils en fait jamais calculé cette observable, qui est pourtant l'une des plus importantes physiquement !

Par ailleurs, une comparaison est effectuée avec la théorie de Bogoliubov, le calcul de Bogoliubov de l'observable en question étant lui-même non trivial. Il y a excellent accord à basse température. C'est probablement le test le plus sévère jamais effectué de la théorie de Bogoliubov, car l'observable mise en jeu n'est pas seulement à un corps ou à deux corps, mais à N corps. Ceci a mis fin à une polémique sur la validité de la théorie de Bogoliubov dans un système unidimensionnel, qui était née du fait que la théorie de Bogoliubov ne prédit qu'une seule branche d'excitation, alors que le calcul exact de Lieb et Lieniger en trouve deux.

Enfin, comme le montrent les simulations, une mesure de la distribution de probabilité du nombre de particules condensées permettrait de révéler très directement la nature de type "état comprimé du champ" de l'état fondamental du gaz, ce qui n'a pas encore été fait.

Notons que nous avons continué à développer ces méthodes Monte-Carlo, en particulier pour voir la transition BCS d'un gaz unidimensionnel de fermions en interaction forte [57].

VOLUME 90, NUMBER 3 PHYSICAL REVIEW LETTERS week ending 24 JANUARY 2003

Condensate Statistics in One-Dimensional Interacting Bose Gases: Exact Results

Iacopo Carusotto and Yvan Castin

Laboratoire Kastler Brossel, Ecole Normale Supérieure, 24 rue Lhomond, 75231 Paris Cedex 05, France

(Received 12 June 2002; published 22 January 2003)

Recently, a quantum Monte Carlo method alternative to the path integral Monte Carlo method was developed for solving the N-boson problem; it is based on the stochastic evolution of classical fields. Here we apply it to obtain exact results for the occupation statistics of the condensate mode in a weakly interacting trapped one-dimensional Bose gas. The temperature is varied across the critical region down to temperatures lower than the trap level spacing. We also derive the condensate statistics in the Bogoliubov theory: this reproduces the exact results at low temperature and explains the suppression of odd numbers of noncondensed particles at $T \simeq 0$.

DOI: 10.1103/PhysRevLett.90.030401 PACS numbers: 05.30.Jp, 02.70.Ss, 03.75.Hh

The first achievement of Bose-Einstein condensation in weakly interacting atomic gases in 1995 has renewed the interest on basic aspects of the Bose-Einstein condensation phase transition [1]. In particular, an intense theoretical activity has been recently devoted to the study of the occupation statistics of the condensate mode: although no experimental result is available yet, we expect that it would provide a crucial test for many-body theories since, contrarily to more common one-body observables such as the density, it involves arbitrarily high order correlation function of the quantum Bose field. While there are now well-established results for the ideal Bose gas [2], calculations for the weakly interacting Bose gas have been performed within the framework of mean-field approximation only [3–5]. The intermediate regime around the critical temperature where the mean-field theory fails has therefore been left unexplored. Some controversy is still open about the validity of the Bogoliubov approach even at temperatures much lower than the critical temperature [6]. In the absence of experimental results, it is then very interesting to have exact theoretical results on the statistics of condensate occupation.

There exists an exact analytical solution to the bosonic N body problem [7], but restricted to the spatially homogeneous one-dimensional case. From the side of numerics, the path integral quantum Monte Carlo technique is able to give exact predictions for any observable of the gas [8] and was successfully used to calculate the mean condensate occupation [9] and the critical temperature [10]. In the path integral formulation, however, the position representation is priviledged which makes the calculation of highly nonlocal observables such as the condensate occupation probabilities rather involved.

In this Letter, we use instead a recently developed quantum Monte Carlo method based on the stochastic evolution of classical fields [11,12]. This new method has a much broader range of applicability than the standard path integral Monte Carlo technique: it can be applied to bosonic systems with complex wave functions, and even to interacting Fermi systems [13]. As compared to the positive-P method of quantum optics [14], it has the decisive advantage of having been proven to be convergent. In this Letter, we perform the first nontrivial application of this new method, calculating for the first time the exact distribution function of the number of condensate particles in the presence of interactions, for temperatures across the Bose-Einstein condensation temperature [15].

An ultracold trapped interacting Bose gas in D dimensions can be modeled by the Hamiltonian

$$\mathcal{H} = \sum_{\mathbf{k}} \frac{\hbar^2 \mathbf{k}^2}{2m} \hat{a}_{\mathbf{k}}^\dagger \hat{a}_{\mathbf{k}} + \frac{g_0}{2} \sum_{\mathbf{r}} dV \hat{\Psi}^\dagger(\mathbf{r}) \hat{\Psi}^\dagger(\mathbf{r}) \hat{\Psi}(\mathbf{r}) \hat{\Psi}(\mathbf{r}) + \sum_{\mathbf{r}} dV U_{\mathrm{ext}}(\mathbf{r}) \hat{\Psi}^\dagger(\mathbf{r}) \hat{\Psi}(\mathbf{r}); \quad (1)$$

the spatial coordinate $\mathbf{r}$ runs on a discrete orthogonal lattice of $\mathcal{N}$ points with periodic boundary conditions; V is the total volume of the quantization box and $dV = V/\mathcal{N}$ is the volume of the unit cell of the lattice. $U_{\mathrm{ext}}(\mathbf{r})$ is the external trapping potential, m is the atomic mass, and interactions are modeled by a two-body discrete delta potential with a coupling constant g_0. The field operators $\hat{\Psi}(\mathbf{r})$ satisfy the usual Bose commutation relations $[\hat{\Psi}(\mathbf{r}), \hat{\Psi}^\dagger(\mathbf{r}')] = \delta_{\mathbf{r},\mathbf{r}'}/dV$ and can be expanded on plane waves according to $\hat{\Psi}(\mathbf{r}) = \sum_{\mathbf{k}} \hat{a}_{\mathbf{k}} e^{i\mathbf{k}\mathbf{r}}/\sqrt{V}$ with $\mathbf{k}$ restricted to the first Brillouin zone of the reciprocal lattice. In order for the discrete model to correctly reproduce the underlying continuous field theory, the grid spacing must be smaller than the macroscopic length scales of the system like the thermal wavelength and the healing length.

In this Letter, we assume that the gas is at thermal equilibrium at temperature T in the canonical ensemble so that the unnormalized density operator is $\rho_{\mathrm{eq}}(\beta) = e^{-\beta\mathcal{H}}$ with $\beta = 1/k_B T$. It is a well-known fact of quantum statistical mechanics that this density operator can be obtained as the result of an imaginary-time evolution:

 0031-9007/03/90(3)/030401(4)$20.00

$$\frac{d\rho_{\rm eq}(\tau)}{d\tau} = -\frac{1}{2}[\mathcal{H}\,\rho_{\rm eq}(\tau) + \rho_{\rm eq}(\tau)\,\mathcal{H}] \qquad (2)$$

during a "time" interval $\tau = 0 \rightarrow \beta$ starting from the infinite temperature value $\rho_{\rm eq}(\tau = 0) = \mathbf{1}_{\rm N}$. We have recently shown [12] that the solution of the imaginary-time evolution (2) can be written exactly as a statistical average of Hartree operators of the form

$$\sigma = |N{:}\phi_1\rangle\langle N{:}\phi_2|, \qquad (3)$$

where, in both the bra and the ket, all N atoms share the same (not necessarily normalized) wave functions ϕ_α ($\alpha = 1, 2$). For the model Hamiltonian (1) here considered, this holds if each ϕ_α evolves according to the Ito stochastic differential equations:

$$d\phi_\alpha(\mathbf{r}) = -\frac{d\tau}{2}\Big[\frac{p^2}{2m} + U_{\rm ext}(\mathbf{r}) + g_0(N-1)\frac{|\phi_\alpha(\mathbf{r})|^2}{||\phi_\alpha||^2} - \frac{g_0(N-1)}{2}\frac{\sum_{\mathbf{r}'} dV|\phi_\alpha(\mathbf{r}')|^4}{||\phi_\alpha||^4}\Big]\phi_\alpha(\mathbf{r}) + dB_\alpha(\mathbf{r}), \qquad (4)$$

with a noise term given by

$$dB_\alpha(\mathbf{r}) = i\sqrt{\frac{d\tau\, g_0}{2V}}\mathcal{Q}_\alpha\Big\{\phi_\alpha(\mathbf{r})\sum_{\mathbf{k}>0}[e^{i[\mathbf{k}\cdot\mathbf{r}+\theta_\alpha(\mathbf{k})]} + \text{c.c.}]\Big\}, \qquad (5)$$

where the projector $\mathcal{Q}_\alpha$ projects orthogonally to ϕ_α, the index $\mathbf{k}$ is restricted to a half space and the $\theta_\alpha(\mathbf{k})$ are independent random angles uniformly distributed in $[0, 2\pi]$.

Starting from this very simple but exact stochastic formulation, a Monte Carlo code was written in order to numerically solve the stochastic differential equation (4). As a first step, a sampling of the infinite temperature density operator has to be performed in terms of a finite number of random wave functions $\phi^{(i)}$. Since the effective contributions of the different realizations to the final averages can be enormously different, the statistics of the Monte Carlo results can be improved by using an *importance sampling* technique [8] in order to avoid wasting computational time. This is done using the identities

$$\mathbf{1}_{\rm N} = \int_1 \mathcal{D}\phi\, |N{:}\phi\rangle\langle N{:}\phi| = \int_1 P_0[\phi]\mathcal{D}\phi\, \frac{|N{:}\phi\rangle\langle N{:}\phi|}{P_0[\phi]}, \qquad (6)$$

where the integration is performed over the unit sphere $||\phi^2|| = \langle\phi|\phi\rangle = \sum_{\mathbf{r}} dV\,|\phi|^2 = 1$ and where the *a priori* distribution function $P_0[\phi]$ can be freely chosen in order to maximize the efficiency of the calculation. For the numerical calculations here reported, the following $P_0[\phi]$ has been used

$$P_0[\phi] = ||e^{-h_{GP}\beta/2}|\phi\rangle||^{2N}, \qquad (7)$$

since it joined the possibility of a simple sampling with a fast convergence. In this expression, h_{GP} is the Gross-Pitaevskii Hamiltonian $h_{GP} = \frac{p^2}{2m} + U_{\rm ext}(\mathbf{r}) + N g_0|\phi_0(\mathbf{r})|^2 - \mu$, ϕ_0 is the wave function which minimizes the Gross-Pitaevskii energy functional, and μ is the corresponding chemical potential. With respect to the ideal Bose gas distribution function previously used [12], the present form (7) for $P_0[\phi]$ has the advantage of taking into account the fact that the condensate mode can be strongly modified by interactions. More details on the actual sampling of $P_0[\phi]$ can be found in [12].

Each realization $\phi^{(i)}_{1,2}$ is then let to evolve according to the stochastic evolution in imaginary time (4) from its $\tau = 0$ value $\phi^{(i)}_{1,2} = \phi^{(i)}$ to the inverse temperature of interest $\tau = \beta$. The expectation values of any observable at temperature T can then be calculated as averages over the Monte Carlo realizations; e.g., the partition function $\text{Tr}[\rho]$ is given by $\text{Tr}[\rho] = \overline{\langle\phi_2|\phi_1\rangle^N}$. In particular, the condensate wave function $\phi_{\rm BEC}(\mathbf{r})$ is the eigenvector of the one-body density matrix

$$\langle\hat{\Psi}^\dagger(\mathbf{r}')\hat{\Psi}(\mathbf{r})\rangle = \frac{1}{\text{Tr}[\rho]}\,\overline{\phi_1(\mathbf{r})\phi_2^*(\mathbf{r}')\langle\phi_2|\phi_1\rangle^{N-1}}, \qquad (8)$$

corresponding to the largest eigenvalue, that is to the largest mean occupation number [16]. The complete probability distribution $P(N_0)$ for the occupation statistics of the condensate mode is obtained via the expression $P(N_0) = \text{Tr}[\hat{\mathcal{P}}_{N_0}\rho]\,\text{Tr}[\rho]^{-1}$, where $\hat{\mathcal{P}}_{N_0}$ projects onto the subspace in which the condensate mode contains exactly N_0 atoms; in terms of the ansatz (3), the expectation value of the projector can be written as

$$\text{Tr}[\hat{\mathcal{P}}_{N_0}\rho] = \frac{N!}{N_0!\,(N-N_0)!}\,\overline{(c_2^* c_1)^{N_0}\,\langle\phi_2^\perp|\phi_1^\perp\rangle^{N-N_0}}, \qquad (9)$$

where we have split $\phi_\alpha(\mathbf{r})$ as $c_\alpha\phi_{\rm BEC}(\mathbf{r}) + \phi_\alpha^\perp(\mathbf{r})$ with $\phi_\alpha^\perp(\mathbf{r})$ orthogonal to the condensate wave function.

In Figs. 1–3 we have summarized the results of the Monte Carlo calculations for a one-dimensional, harmonically trapped gas with repulsive interactions. In Fig. 1, we have plotted the condensate wave function density profile $|\phi_{\rm BEC}(x)|^2$ for different values of the temperature, see solid lines. As the temperature decreases, the enhanced atomic density at the center of the cloud gives a stronger repulsion among the condensate atoms and therefore a wider condensate wave function. In this low temperature regime, we have found a good agreement between the Monte Carlo results and the Bogoliubov prediction for the condensate wave function including the first correction to the Gross-Pitaevskii equation due to the presence of noncondensed atoms [17]; see dashed lines in Fig. 1. This was expected, since the numerical examples in this paper are in the weakly interacting regime $n\xi \approx 15 \gg 1$, where n is the density at the trap center and $\xi = (\hbar^2/2mg_0n)^{1/2}$ is the corresponding healing length. For high temperatures, the wave function $\phi_{\rm BEC}(x)$ tends to the harmonic oscillator ground state.

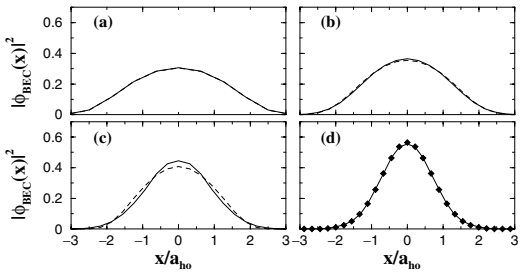

FIG. 1. Solid lines: exact results for the condensate wave function density profile $|\phi_{\mathrm{BEC}}(x)|^2$ for $N = 125$ atoms in a one-dimensional harmonic trap at different temperatures $k_BT/\hbar\omega = 1$ (*a*), 10 (*b*), 20 (*c*), 50 (*d*). ω is the trap frequency, $|\phi_{\mathrm{BEC}}|^2$ is in units of the inverse of $a_{\mathrm{ho}} = \sqrt{\hbar/m\omega}$. The coupling constant is $g_0 = 0.08\,\hbar\omega\, a_{\mathrm{ho}}$. Comparison with Bogoliubov predictions (dashed lines) in (*a*)–(*c*) and with harmonic oscillator ground state (diamonds) in (*d*). In (*a*) the two lines are indistinguishable on the scale of the figure. Monte Carlo calculations were performed using 3×10^4 realizations on a $\mathcal{N} = 16$ (*a*), 64 (*b*), (*c*) or 128 point (*d*) grid.

The wave function $\phi_{\mathrm{BEC}}(x)$ can then be used to determine the occupation statistics of the condensate mode via (9). The signature of Bose condensation is apparent in Fig. 2: the occupation statistics of the condensate mode at high temperatures has the same shape as a noninteracting, thermally occupied mode, its maximum value being at $N_0 = 0$. For decreasing T, $P(N_0)$ radically changes its shape; at low T, its maximum is at a nonvanishing value of N_0 and its shape is strongly asymmetric with a longer tail going towards the lower N_0 values, as already noticed in the mean-field approach of [5]. This transition ressembles the one occurring in a laser cavity for a pumping rate which goes from below to above threshold [18].

For even lower values of the temperature, see Fig. 3, most of the atoms are in the condensate and the probability distribution $P(N_0)$ tends to concentrate around values of N_0 close to N. However, interactions prevent the atomic sample from being totally Bose condensed even at extremely low temperatures. Moreover, the probability of having an odd number of noncondensed atoms is strongly reduced with respect to the probability of having an even number (see the strong oscillations in the $k_BT = 0.4\,\hbar\omega$ curve of Fig. 3). A quantitative interpretation of this effect in terms of the Bogoliubov approximation will be given in the following part of the paper.

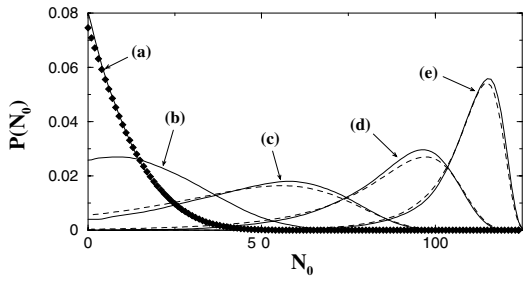

FIG. 2. Solid lines: exact results for the distribution function $P(N_0)$ of the number of condensate atoms for decreasing temperatures from left to right: $k_BT/\hbar\omega = 50$ (*a*), 33 (*b*), 20 (*c*), 10 (*d*), 5 (*e*). Same parameters as in Fig. 1. For curves (*c*)–(*e*), comparison with Bogoliubov predictions (dashed lines); for curve (*a*), comparison with the ideal gas (diamonds). The Monte Carlo calculations were performed using 3×10^4 realizations on a grid of $\mathcal{N} = 128$ (*a*), (*b*) or $\mathcal{N} = 64$ points (*c*)–(*e*).

We now compare the exact results with the prediction of the number-conserving Bogoliubov approximation [17,19]. The Bogoliubov Hamiltonian has the form

$$\mathcal{H}_{\mathrm{Bog}} = \frac{1}{2} dV\, (\vec{\Lambda}^\dagger, \vec{\Lambda}) \cdot \eta \mathcal{L} \begin{pmatrix} \vec{\Lambda} \\ \vec{\Lambda}^\dagger \end{pmatrix}, \tag{10}$$

with

$$\mathcal{L} = \begin{pmatrix} h_{\mathrm{GP}} + \mathcal{Q}_0 N g_0 |\phi_0|^2 \mathcal{Q}_0 & \mathcal{Q}_0 N g_0 \phi_0^2 \mathcal{Q}_0^* \\ -\mathcal{Q}_0^* N g_0 \phi_0^{*2} \mathcal{Q}_0 & -h_{\mathrm{GP}} - \mathcal{Q}_0^* N g_0 |\phi_0|^2 \mathcal{Q}_0^* \end{pmatrix}. \tag{11}$$

The matrix η is defined according to

$$\eta = \begin{pmatrix} \mathbf{1} & 0 \\ 0 & -\mathbf{1} \end{pmatrix}, \tag{12}$$

and the projector $\mathcal{Q}_0$ projects orthogonally to the Gross-Pitaevskii ground state ϕ_0. The operators $\vec{\Lambda}$ are defined according to $(\vec{\Lambda})_{\mathbf{r}} = \hat{A}_0^\dagger \hat{\Psi}_\perp(\mathbf{r})$, where $\hat{\Psi}_\perp(\mathbf{r})$ is the projection of the field operator orthogonally to ϕ_0 and where $\hat{A}_0 |N_0{:}\phi_0\rangle = |N_0 - 1{:}\phi_0\rangle$ if $N_0 > 0$ and 0 otherwise. Neglecting the possibility of completely emptying the condensate mode, $\hat{A}_0$ and $\hat{A}_0^\dagger$ can be shown to commute. Under this approximation, the $\vec{\Lambda}$ are bosonic operators. The probability $\Pi(\delta N)$ of having δN noncondensed atoms can be calculated within the Bogoliubov approximation by means of the characteristic function [4]

$$f(\theta) = \sum_{\delta N} \Pi(\delta N)\, e^{i\,\delta N\,\theta} \simeq \mathrm{Tr}\left[e^{i\theta\,\delta\hat{N}} \frac{1}{\mathcal{Z}} e^{-\beta \mathcal{H}_{\mathrm{Bog}}} \right], \tag{13}$$

with $\delta\hat{N} = dV \vec{\Lambda}^\dagger \cdot \vec{\Lambda}$ and $\mathcal{Z} = \mathrm{Tr}[e^{-\beta\mathcal{H}_{\mathrm{Bog}}}]$; when the probability of emptying the condensate mode is not

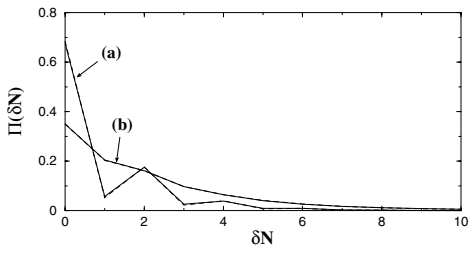

FIG. 3. Solid lines: exact results (10^5 realizations on a $\mathcal{N} = 16$ point grid) for the distribution function $\Pi(\delta N) = P(N_0 = N - \delta N)$ of the number of noncondensed atoms at low temperatures $k_BT/\hbar\omega = 0.4$ (*a*) and 1 (*b*). Same parameters as in Figs. 1 and 2. Dashed lines: Bogoliubov predictions.

totally negligible, the Bogoliubov prediction for $\Pi(\delta N)$ has to be truncated to the physically relevant $\delta N \leq N$ values and then renormalized to 1. The details of the calculation will be given elsewhere, we go here to the result

$$f(\theta) \simeq \prod_{j=1}^{2(\mathcal{N}-1)} \left[\frac{2\lambda_j}{1+\lambda_j - e^{i\theta}(1-\lambda_j)} \right]^{1/2}, \qquad (14)$$

in which the λ_j are the eigenvalues of $\mathcal{M} = \eta \tanh(\beta \mathcal{L}/2)$; from such an expression, the occupation probabilities $\Pi(\delta N)$ are immediately determined by means of an inverse Fourier transform. The results are shown as dashed lines in Figs. 2 and 3 where they are compared to the exact results from Monte Carlo simulations; the agreement is excellent provided the noncondensed fraction is small, i.e., at sufficiently low temperatures.

In order to understand the oscillating behavior shown by the lowest temperature curve of Fig. 3, we calculate the ratio of the probability Π_{odd} of having an odd value of δN to the probability Π_{even} of having an even value:

$$\frac{\Pi_{\text{odd}}}{\Pi_{\text{even}}} = \frac{f(0) - f(\pi)}{f(0) + f(\pi)} \simeq \frac{1-R}{1+R}, \qquad (15)$$

where $R = \prod_j \lambda_j^{1/2} = \det[\mathcal{M}]^{1/2} = \prod_m \tanh(\beta \epsilon_m/2)$ and m runs over the $\mathcal{N}-1$ eigenenergies ϵ_m of the Bogoliubov spectrum. In order to have oscillations in $\Pi(\delta N)$, the ratio (15) must be small as compared to 1 which requires a temperature smaller than the energy of the lowest Bogoliubov mode. These oscillations are therefore a property of the ground state of the system. In the Bogoliubov approximation, the Hamiltonian is quadratic in the field operators so that its ground state is a squeezed vacuum, which indeed contains only even values of δN, a well-known fact of quantum optics [20]. From a condensed matter point of view, several existing variational ansatz for the ground state corresponding to a condensation of pairs also exhibit this property [21,22]. Physically, this is ultimately related to the fact that the leading interaction process changing the condensate occupation at zero temperature, that is the scattering of two condensate particles into two noncondensed modes and vice versa, does not change the parity of δN, as it is apparent in the Bogoliubov Hamiltonian (10).

In conclusion, we have determined with a newly developed stochastic field quantum Monte Carlo method the exact distribution function of the number N_0 of condensate particles in a one-dimensional weakly interacting trapped gas. The signature of Bose condensation is the appearance of a finite value for the most probable value of N_0. At temperatures below the trap oscillation frequency, configurations with an odd number of noncondensed particles are strongly suppressed, which we interpret successfully within the Bogoliubov approximation. Possible extensions of this work are (i) the determination of critical temperature shift for an interacting Bose gas in the limit of a vanishing scattering length, still subject of some controversy [23], (ii) exact calculations for finite temperature Bose gases with vortices in rotating traps, and (iii) the determination of the BCS critical temperature in two-component Fermi gases.

This work was stimulated by interactions with I. Cirac. We acknowledge useful discussions with A. Leggett and J. Dalibard. I. C. acknowledges a Marie Curie grant from the EU under Contract No. HPMF-CT-2000-00901. Laboratoire Kastler Brossel is a Unité de Recherche de l'ENS et de l'Université Paris 6, associée au CNRS.

[1] For a review, see F. Dalfovo, S. Giorgini, L. P. Pitaevskii, and S. Stringari, Rev. Mod. Phys. **71**, 463 (1999).
[2] M. Holthaus and E. Kalinowski, Ann. Phys. (N.Y.) **276**, 321 (1999), and references therein.
[3] S. Giorgini, L. P. Pitaevskii, and S. Stringari, Phys. Rev. Lett. **80**, 5040 (1998).
[4] V. Kocharovsky, Vl. Kocharovsky, and M. O. Scully, Phys. Rev. Lett. **84**, 2306 (2000).
[5] A. Sinatra, C. Lobo, and Y. Castin, J. Phys. B **35**, 3599 (2002).
[6] Z. Idziaszek, M. Gajda, P. Navez, M. Wilkens, and K. Rzążewski, Phys. Rev. Lett. **82**, 4376 (1999).
[7] E. H. Lieb and W. Liniger, Phys. Rev. **130**, 1605 (1963).
[8] D. M. Ceperley, Rev. Mod. Phys. **71**, S438 (1999).
[9] W. Krauth, Phys. Rev. Lett. **77**, 3695 (1996).
[10] P. Grüter, D. Ceperley, and F. Laloë, Phys. Rev. Lett. **79**, 3549 (1997).
[11] I. Carusotto, Y. Castin, and J. Dalibard, Phys. Rev. A **63**, 023606 (2001).
[12] I. Carusotto and Y. Castin, J. Phys. B **34**, 4589 (2001).
[13] O. Juillet, Ph. Chomaz, D. Lacroix, and F. Gulminelli, Phys. Rev. Lett. **88**, 142503 (2002).
[14] A. Gilchrist, C. W. Gardiner, and P. D. Drummond, Phys. Rev. A **55**, 3014 (1997).
[15] In [12] the condensate statistics is calculated for the ideal Bose gas only: the absence of noise terms makes the Monte Carlo method converge trivially. This is no longer the case in the presence of interactions.
[16] O. Penrose and L. Onsager, Phys. Rev. **104**, 576 (1956).
[17] Y. Castin and R. Dum, Phys. Rev. A **57**, 3008 (1998).
[18] M. O. Scully, Phys. Rev. Lett. **82**, 3927 (1999).
[19] C. W. Gardiner, Phys. Rev. A **56**, 1414 (1997).
[20] D. F. Walls and G. J. Milburn, *Quantum Optics* (Springer-Verlag, Berlin, 1994).
[21] M. Girardeau and R. Arnowitt, Phys. Rev. **113**, 755 (1959).
[22] A. J. Leggett, Rev. Mod. Phys. **73**, 307 (2001).
[23] M. Wilkens, F. Illuminati, and M. Kraemer, J. Phys. B **33**, L779 (2000); M. Holzmann, G. Baym, J.-P. Blaizot, and F. Laloë, Phys. Rev. Lett. **87**, 120403 (2001); P. Arnold and G. Moore, *ibid.* **87**, 120401 (2001); V. A. Kashurnikov, N. V. Prokof'ev, and B. V. Svistunov, Phys. Rev. Lett. **87**, 120402 (2001).

5.6 Sur la formation de tourbillons quantiques

Les deux articles reproduits, [40] et [51], donnent une description d'ensemble de la formation des réseaux de tourbillons dans les expériences du groupe de Jean Dalibard sur les condensats de Bose-Einstein en rotation : le premier article [40] identifie le mécanisme de nucléation à l'œuvre dans les expériences, qui est une instabilité de type hydrodynamique, et le deuxième montre que le régime turbulent induit par cette instabilité peut par lui-même conduire à la cristallisation du réseau, sans que l'on ait à invoquer d'autre mécanisme de type dissipatif. Ces résultats sont allés à l'encontre de beaucoup d'idées reçues et ont dû affronter un certain scepticisme.

Une première idée reçue, solidement ancrée dans la communauté de la physique de la matière condensée et à laquelle nous avons cru au début, était que la nucléation des tourbillons quantiques devrait être due à une instabilité énergétique du condensat sans tourbillon dans le référentiel du piège tournant ; ceci inclut le mécanisme de type Landau, dans lequel l'un des modes de surface du condensat acquiert une énergie négative. Cependant, cette attente a été infirmée par les résultats expérimentaux de Jean Dalibard, non seulement quantitativement (la fréquence de rotation minimale pour l'apparition des tourbillons est supérieure à celle prédite) mais aussi qualitativement : il existe dans l'expérience une fréquence de rotation maximale, au-delà de laquelle les tourbillons ne se forment plus, ce qui est incompréhensible dans le cadre d'une instabilité énergétique puisqu'une augmentation de la fréquence de rotation ne peut que l'accentuer. L'article [40] apporte la clé du problème : les tourbillons se forment dans l'expérience par instabilité hydrodynamique du condensat tournant, instabilité qui se manifeste seulement si le potentiel tournant excite de façon résonnante un mode bien identifié du condensat, et qui disparaît donc à trop vitesse de rotation trop élevée.

Peut-on montrer théoriquement que cette instabilité hydrodynamique conduit à la formation d'un réseau de tourbillons, par simple évolution non linéaire du condensat gouvernée par l'équation de Gross-Pitaevskii, ou faut-il cette fois inclure un mécanisme d'origine thermique ? C'est à ce stade qu'apparut une deuxième idée reçue, suivant laquelle la nature purement hamiltonienne (donc conservative et réversible) de l'équation de Gross-Pitaevskii ne pouvait pas conduire à la cristallisation des tourbillons. Idée en apparence confirmée par des simulations numériques ! Et cependant allant à l'encontre des idées de la physique statistique classique sur les systèmes non intégrables. L'article [51], par une étude numérique poussée à 3D, infirme la seconde idée reçue et montre que la non intégrabilité de l'équation de Gross-Pitaevskii permet une 'thermalisation' de l'état turbulent du champ atomique consécutif à l'instabilité hydrodynamique. Ce qui a été confirmé depuis par d'autres groupes que le nôtre, aussi bien à 2D qu'à 3D. Les études numériques antérieures n'avaient pas vu la cristallisation car elles n'avaient pas fait évoluer le champ assez longtemps.

Ceci a montré que la transposition directe d'attentes et de résultats de physique de la matière condensée ne permet pas toujours de résoudre les problèmes fondamentaux soulevés par les expériences sur les atomes ultrafroids.

VOLUME 87, NUMBER 19 PHYSICAL REVIEW LETTERS 5 NOVEMBER 2001

Dynamic Instability of a Rotating Bose-Einstein Condensate

Subhasis Sinha and Yvan Castin

Laboratoire Kastler Brossel, Ecole normale supérieure, 24 rue Lhomond, 75 231 Paris Cedex 5, France

(Received 18 January 2001; revised manuscript received 21 May 2001; published 17 October 2001)

We consider a Bose-Einstein condensate subject to a rotating harmonic potential, in connection with recent experiments leading to the formation of vortices. We use the classical hydrodynamic approximation to the nonlinear Schrödinger equation to determine almost analytically the evolution of the condensate. We predict that this evolution can exhibit dynamical instabilities, for the stirring procedure previously demonstrated at ENS and for a new stirring procedure that we put forward. These instabilities take place within the range of stirring frequency and amplitude for which vortices are produced experimentally. They provide therefore an initiating mechanism for vortex nucleation.

DOI: 10.1103/PhysRevLett.87.190402 PACS numbers: 03.75.Fi, 05.30.Jp

Quantized vortices in superfluid helium II, in particular the issue of vortex nucleation in a rotating container, have long been the subject of intense work [1]. With the recent production of gaseous Bose-Einstein condensates [2], the subject has gained a renewed interest. On the experimental side, three groups have succeeded in obtaining vortices in atomic condensates, with two different techniques: a phase imprinting technique at JILA [3] and the equivalent of the helium rotating bucket experiment at ENS [4] and at MIT [5]. At ENS, a rotating laser beam superposed onto the magnetic trap holding the atoms creates a harmonic rotating potential with adjustable anisotropy ϵ and rotation frequency Ω. For a well chosen range of variation for Ω one or several vortices are nucleated, and then detected as holes in the density profile of the gas after ballistic expansion [4] or by a measurement of the angular momentum of the condensate [6]. A striking feature of the ENS experimental results is that, for a very weak anisotropy ϵ, nucleation of vortices takes place in a narrow interval of rotation frequencies $[\Omega_{\min}, \Omega_{\max}]$ around $0.7\omega_\perp$, where $\omega_\perp$ is the mean oscillation frequency of the atoms in the x-y plane, whatever the number of atoms or the oscillation frequency ω_z along z in the experiment [7].

While the JILA experiment is well understood theoretically [8], the situation is more involved for the ENS experiment. Several theoretical articles, inspired by the case of superfluid helium, have tried to predict the value of the lower vortex nucleation frequency $\Omega_{\min}$ from purely thermodynamic arguments [9–15]. The proposed values for $\Omega_{\min}$ are significantly different from the observed value of $0.7\omega_\perp$, or depend on the trap aspect ratio $\omega_z/\omega_\perp$ or on the atom number, in contradiction with the observations at ENS. Also, thermodynamical reasonings are not able to predict the upper vortex nucleation frequency $\Omega_{\max}$, which is also close to $0.7\omega_\perp$ for low anisotropy ϵ.

In this Letter, we consider the time dependent problem of a condensate subject to a harmonic stirring potential. We use the classical hydrodynamic approximation to the time dependent Gross-Pitaevskii equation (GPE), an approximation well justified for the ENS parameters [16]. We are then able to reformulate the partial differential hydrodynamic equations in terms of ordinary differential equations, which allows an almost analytical solution [17]. Our main result is the discovery of dynamical instabilities in the evolution of the condensate for a certain range of the rotation frequency and of the trap anisotropy. These instabilities will invalidate the classical hydrodynamic approximation after some evolution time. We have checked with a numerical solution of the Gross-Pitaevskii equation that vortices then enter the condensate.

The existence of such a dynamical instability explains why in earlier numerical work the time dependent Gross-Pitaevskii equation was found to nucleate vortices [13,18,19]. Furthermore, the instability range that we predict is very close to the experimentally observed range of vortex nucleation, for various stirring procedures. For the stirring procedure of [4,6], we recover the "universal" numerical value 0.7 for $\Omega/\omega_\perp$ leading to vortex nucleation for low anisotropies ϵ. We provide a simple physical interpretation of this value: For $\Omega/\omega_\perp = 1/\sqrt{2} \simeq 0.7$ the harmonic stirring potential resonantly excites a quadrupole mode of the condensate [20], which induces large oscillations of the condensate and eventually a dynamical instability sets in. We also investigate a new excitation procedure to nucleate vortices, which has recently been implemented at ENS [21]: The rotation of the stirring potential is set up very slowly. The gas then follows adiabatically a branch of steady state until the branch becomes dynamically unstable. The corresponding lower rotation frequency Ω that we predict for vortex nucleation is also very close to the experimental value.

In our model, atoms are trapped in a harmonic potential rotating at the instantaneous frequency $\Omega(t)$ around the z axis. For convenience, all the calculations of this paper are done in a rotating frame where the trap axes are fixed. The trapping potential then reads

$$U(\vec{r},t) = \frac{1}{2} m\omega_\perp^2 \Big\{ [1 - \epsilon(t)]x^2 + [1 + \epsilon(t)]y^2 + \left(\frac{\omega_z}{\omega_\perp}\right)^2 z^2 \Big\}, \quad (1)$$

 0031-9007/01/87(19)/190402(4)$15.00

where m is the mass of an atom, and $\epsilon(t)$ is the trap anisotropy at time t. The parameters $\omega_\perp$ and ω_z are the oscillation frequencies of the atoms in transverse and axial directions for vanishing anisotropy of the stirring potential. Within the mean-field approximation, the time evolution of the condensate field or macroscopic wave function $\psi(\vec{r},t)$ can be described by the time dependent Gross-Pitaevskii equation [22]:

$$i\hbar\,\frac{\partial\psi}{\partial t} = \left[-\frac{\hbar^2}{2m}\,\vec{\nabla}^2 + U(\vec{r},t) + g|\psi|^2 - \Omega(t)\hat{L}_z\right]\psi\,, \tag{2}$$

where $g = 4\pi\hbar^2 a/m$ is the coupling constant, proportional to the s-wave scattering length a of the atoms, here taken to be positive, and where the inertial term proportional to the angular momentum operator $\hat{L}_z$ along the z axis accounts for the frame rotation. The condensate field ψ can be written in terms of density ρ and phase S:

$$\psi(\vec{r},t) = \sqrt{\rho(\vec{r},t)}\,e^{iS(\vec{r},t)/\hbar}. \tag{3}$$

The equation obtained from the GPE for ρ is just the continuity equation. The equation for S contains the so-called quantum pressure term $\hbar^2\vec{\nabla}^2\sqrt{\rho}/2m\sqrt{\rho}$ that we neglect here as compared to the mean-field term ρg in the Thomas-Fermi approximation. We obtain

$$\frac{\partial\rho}{\partial t} = -\mathrm{div}\left[\rho\left(\frac{\vec{\nabla}S}{m} - \vec{\Omega}(t)\times\vec{r}\right)\right], \tag{4}$$

$$-\frac{\partial S}{\partial t} = \frac{(\vec{\nabla}S)^2}{2m} + U(\vec{r},t) + g\rho - [\vec{\Omega}(t)\times\vec{r}]\cdot\vec{\nabla}S\,. \tag{5}$$

A very fortunate feature of the harmonic trap is that these superfluid hydrodynamic equations can be solved exactly for a condensate initially at equilibrium in the nonrotating trap with the following quadratic ansatz for the condensate density and phase [23]:

$$\rho_c(\vec{r},t) = \rho_0(t) + \frac{m\omega_\perp^2}{g}\sum_{i,j=1}^{3} x_i A_{ij}(t) x_j\,, \tag{6}$$

$$S_c(\vec{r},t) = s_0(t) + m\omega_\perp\sum_{i,j=1}^{3} x_i B_{ij}(t) x_j\,, \tag{7}$$

where x_1, x_2, and x_3 are the coordinates along the x, y, and z axes, respectively. The time dependent dimensionless coefficients A_{ij} and B_{ij} form 3×3 symmetric matrices A and B which from Eqs. (4) and (5) obey the evolution equations:

$$\omega_\perp^{-1}\,\frac{dA}{dt} = -2A\,\mathrm{Tr}B - 2\{A,B\} + \frac{\Omega}{\omega_\perp}[R,A], \tag{8}$$

$$\omega_\perp^{-1}\,\frac{dB}{dt} = -2B^2 - W - A + \frac{\Omega}{\omega_\perp}[R,B], \tag{9}$$

where $\{,\}$ stands for the anticommutator, $[,]$ stands for the commutator of two matrices, the matrix W is diagonal, with components $W_{11} = [1-\epsilon(t)]/2$, $W_{22} = [1+\epsilon(t)]/2$, and $W_{33} = (\omega_z/\omega_\perp)^2/2$, and the matrix R, originating from the vectorial product in $\hat{L}_z$, has vanishing elements except for $R_{12} = -R_{21} = 1$ [24]. Note that these equations do not depend on the number of atoms nor on the coupling constant g.

In a first stage, it is very important to study steady state solutions of the above equations. We restrict ourselves to solutions that have the same symmetry as the initial state: even parity along z, this parity being preserved by time evolution. We then find a unique class of solutions, reproducing the results of [25]: The condensate phase varies as $S(\vec{r}) = m\omega_\perp\beta xy$, where β is a real root of

$$\beta^3 + \left(1 - 2\frac{\Omega^2}{\omega_\perp^2}\right)\beta - \frac{\Omega}{\omega_\perp}\,\epsilon = 0\,. \tag{10}$$

The steady state matrix A is diagonal with elements given in [25]. We have plotted in Fig. 1 the values of β as functions of the rotation frequency Ω for a fixed anisotropy ϵ. For Ω between zero and a bifurcation value $\Omega_{\mathrm{bif}}(\epsilon)$ depending on ϵ, there is a single branch of solution for β. This branch is supplemented by two extra branches when $\Omega > \Omega_{\mathrm{bif}}(\epsilon)$.

We now turn back to the time dependent problem. Clearly, a condensate with a vortex cannot be described within the quadratic ansatz [(6) and (7)] as the phase S_c corresponds to an irrotational velocity flow. The actual scenario for the vortex nucleation that we put forward is the following: Initially very small deviations $\delta\rho(\vec{r},t)$ of the condensate density and $\delta S(\vec{r},t)$ of the condensate phase from the quadratic shapes ρ_c and S_c may grow exponentially fast in the course of time evolution, eventually leading the condensate to a structure very different from Eqs. (6) and (7). This may happen when a dynamical instability is present.

To reveal such an instability, we obtain, from the evolution Eqs. (4) and (5), linearized equations of motion for

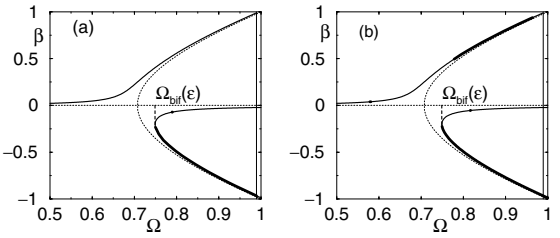

FIG. 1. Phase parameter β for a steady state condensate as a function of the rotation frequency Ω in units of $\omega_\perp$. Dotted lines: $\epsilon = 0$. Solid lines: $\epsilon = 0.022$. For $\epsilon = 0.022$ and $\omega_z/\omega_\perp = 0.1$, the thick lines on the curves indicate where the solution has a dynamical instability (a) of degree $n = 2$ and (b) of degree $n = 3$. The vertical line is the border of the center of mass instability domain for $\epsilon = 0.022$.

initially small deviations $\delta\rho$ and δS from ρ_c and S_c:

$$\frac{D\delta\rho}{Dt} = -\mathrm{div}\left(\rho_c \frac{\vec{\nabla}\delta S}{m}\right) - \delta\rho \frac{\vec{\nabla}^2 S_c}{m}, \qquad (11)$$

$$\frac{D\delta S}{Dt} = -g\delta\rho\,. \qquad (12)$$

In these equations, we have introduced the convective derivative $\frac{D}{Dt} \equiv \frac{\partial}{\partial t} + \vec{v}_c(\vec{r},t)\cdot\vec{\nabla}$, where $\vec{v}_c = \vec{\nabla}S_c/m - \vec{\Omega}\times\vec{r}$ is the velocity field of the condensate in the rotating frame. A polynomial ansatz for δS and $\delta\rho$ of an arbitrary total degree n in the coordinates x, y, and z solves these linear equations exactly [26]. This is another nice consequence of the harmonicity of the trap. In practice, we calculate the evolution operator $\mathcal{U}_n(t)$ mapping the coefficients of the polynomials at time zero onto their values after a time evolution t. Dynamical instability takes place when one or several eigenvalues of $\mathcal{U}_n$ grow exponentially fast with time t. Note that, after rescaling of the variables, Eqs. (11) and (12) become independent of the number of atoms and of the coupling constant g, in a way similar to Eqs. (8) and (9).

Now we perform a linear stability analysis for two different stirring procedures of the condensate.

Procedure I.—The ellipticity of the stirring potential ϵ is kept fixed and the rotation frequency $\Omega(t)$ of the stirrer is very slowly ramped up from zero to its final value. The condensate, initially in steady state with a vanishing parameter β, adiabatically follows the upper branch of steady states with $\beta \geq 0$ (see Fig. 1). It is then sufficient to determine the dynamic stability of the upper branch of steady states. This greatly simplifies the calculation as one just has to identify eigenmodes of Eqs. (11) and (12) evolving in time as $\exp(\lambda t)$, where the eigenvalue λ is a complex number. Dynamical instability takes place when λ can have a strictly positive real part. As shown in Fig. 1 for $\epsilon = 0.022$, we find that the upper branch for β is stable for modes of degree $n = 2$ but presents two instability intervals for the modes of degree $n = 3$, a very narrow interval around $\Omega = 0.58\omega_\perp$ and a broader interval starting at $\Omega = 0.778\omega_\perp$.

We have investigated in a systematic way the instability range of the upper branch of steady states, by varying the anisotropy ϵ, the rotation frequency Ω, and the degree n. The instability domain in the $\Omega - \epsilon$ plane for modes of degree 3 is mainly made of a crescent, and the inclusion of higher degree modes ($n = 4, 5$) add extra crescents from above (see Fig. 2a). Each crescent has on the $\epsilon = 0$ axis (i) a broad basis at $\Omega > \omega_\perp/\sqrt{2}$, with a nonzero instability exponent, and (ii) a very narrow edge at $\Omega = \omega_\perp/\sqrt{n} < \omega_\perp/\sqrt{2}$, with a vanishing instability exponent. We show in Fig. 2b that the maximal instability exponent for $n = 3$ has a remarkably weak dependence on $\omega_z/\omega_\perp$.

Procedure II.—This is the original experimental scenario of [4,6], where the stirring potential is rotated at a fixed frequency and the ellipticity of the stirrer is turned on from zero to its final value ϵ_f abruptly. In this case, we cannot rely on adiabatic following for the condensate density and phase, so we solve the time dependent Eqs. (8) and (9) for $\rho_c(t)$ and $S_c(t)$. Then we perform a linear stability analysis as discussed above: We evolve a generic polynomial ansatz of degree n for the fluctuations $\delta\rho$ and δS according to Eqs. (11) and (12), which allows one to construct the evolution operator $\mathcal{U}_n(t)$ and to calculate $Z_{\max}(t)$, the eigenvalue of $\mathcal{U}_n(t)$ with the largest modulus. Then we define the mean instability exponent $\mathrm{Re}\langle\lambda\rangle$ as the mean slope of $\ln|Z_{\max}(t)|$ as a function of time.

This reveals that within a certain range of rotation frequency the system becomes dynamically unstable (see the solid line in Fig. 3). In the limit of a low anisotropy ϵ, the

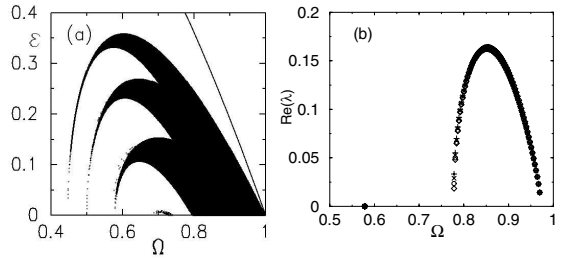

FIG. 2. For the upper branch of steady state condensates: (a) Dark areas: instability domain in the $\Omega - \epsilon$ plane for $\omega_z/\omega_\perp = 0.1$ for degrees n equal to 3, 4, and 5 (crescents from bottom to top). There is no dynamical instability for $n \leq 2$. Solid line: border $\Omega^2 = (1-\epsilon)\omega_\perp^2$ of the branch existence domain. (b) Maximal instability exponent $\mathrm{Re}(\lambda)$ for $n = 3$ as a function of Ω, for $\epsilon = 0.022$, and $\omega_z/\omega_\perp = 0.1$ ($\diamond$), 0.5 ($\bigcirc$), 1.0 ($\times$), and $\sqrt{8}$ ($+$). Ω and $\mathrm{Re}(\lambda)$ are in units of $\omega_\perp$.

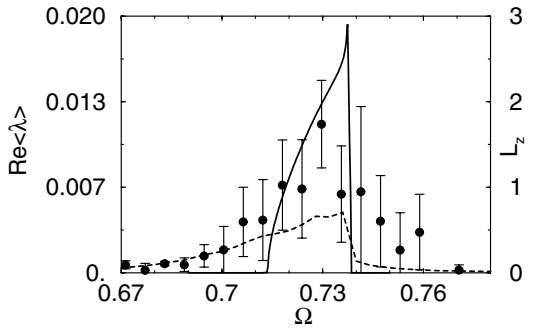

FIG. 3. For the stirring procedure II, with $\epsilon_f = 0.01$ and $\omega_z/\omega_\perp = 0.1$: Solid line: mean instability exponent $\mathrm{Re}\langle\lambda\rangle$ (see text) of the vortex-free classical hydrodynamic solution ρ_c, S_c as a function of Ω, for $n = 3$. Dashed line: mean angular momentum per particle $\bar{L}_z$ (see text) obtained from ρ_c, S_c. Filled disks: experimentally measured angular momentum L_z per particle in the condensate after vortices have possibly entered the condensate [7]. The initial steady state condensate in the calculation of $\bar{L}_z$ has a chemical potential $\mu = 10\hbar\omega_\perp$, close to the experimental value. $\mathrm{Re}\langle\lambda\rangle$ and Ω are in units of $\omega_\perp$, and L_z, $\bar{L}_z$ are in units of $\hbar$.

instability sets in when the rotation frequency Ω is close to the value $\simeq 0.7\omega_\perp$: In the lab frame, the stirring potential of frequency 2Ω is then resonant with a quadrupole mode [16,27] of the condensate of frequency $\sqrt{2}\,\omega_\perp$, and induces large amplitude oscillations of the condensate, resulting in a dynamical instability. More precisely, the condensate described by the quadratic ansatz ρ_c, S_c has an angular momentum oscillating in time around a nonzero value $\bar{L}_z$. This value $\bar{L}_z$ is a peaked function of the rotation frequency Ω, shown in the dashed line in Fig. 3. The peak of $\bar{L}_z$ is not exactly located at $\Omega = 0.7\omega_\perp$ because of nonlinear effects in Eqs. (8) and (9). The peak structure of the instability exponent in Fig. 3 is similar to the peak structure of $\bar{L}_z$, with a narrower width as dynamical instability of the vortex free solution ρ_c, S_c sets in for the higher values of $\bar{L}_z$ only. For values of Ω significantly above or below $0.7\omega_\perp$, the stirrer is out of resonance with the quadrupole mode and induces only small and stable oscillations of the condensate. For larger values of ϵ, the instability interval in Ω broadens. We have also checked that the instability interval depends weakly on $\omega_z/\omega_\perp$.

What is the connection between the dynamical instabilities found here and the nucleation of vortices? To obtain a theoretical answer to this question, one has to go beyond a linear stability analysis to determine the evolution of the condensate in the long run: For a few values of the rotation frequency Ω and for procedures I and II, we have checked by a numerical integration of the time dependent GPE in three dimensions, that vortices are indeed nucleated in the predicted instability domains: after some evolution time, the angular momentum in the numerical solution suddenly becomes larger than the classical hydrodynamic prediction, as vortices enter the condensate. An experimental answer to this question for the stirring procedure I has been provided recently at ENS [21]: The first clear evidence of a vortex appears for a rotation frequency $\Omega = 0.77\omega_\perp$, very close to our prediction $\Omega = 0.778\omega_\perp$. The agreement is also very good for procedure II as shown in Fig. 3: Our instability domain in Ω coincides with the experimental vortex nucleation interval within a few percent.

In summary, the dynamical instabilities that we have identified provide an initiating mechanism for the production of vortices in a condensate stirred by a harmonic potential, in excellent agreement with the experimental results at ENS.

We thank S. Rica, V. Hakim, G. Shlyapnikov, F. Chevy, K. Madison, and J. Dalibard for helpful discussions. We acknowledge financial support from Ministère de la Recherche et de la Technologie. LKB is a research unit of Ecole normale supérieure and of Université Pierre et Marie Curie, associated to CNRS.

[1] R. J. Donnelly, *Quantized Vortices in Helium II* (Cambridge University, Cambridge, England, 1991).
[2] For a review, see, e.g., *Bose-Einstein Condensation in Atomic Gases,* edited by M. Inguscio, S. Stringari, and C. E. Wieman (IOS Press, Amsterdam, 1999).
[3] M. R. Matthews, B. P. Anderson, P. C. Haljan, D. S. Hall, C. E. Wieman, and E. A. Cornell, Phys. Rev. Lett. **83**, 2498 (1999).
[4] K. W. Madison, F. Chevy, W. Wohlleben, and J. Dalibard, Phys. Rev. Lett. **84**, 806 (2000).
[5] J. R. Abo-Shaeer, C. Raman, J. M. Vogels, and W. Ketterle, Science **292**, 476 (2001).
[6] F. Chevy, K. W. Madison, and J. Dalibard, Phys. Rev. Lett. **85**, 2223 (2000).
[7] F. Chevy, K. Madison, V. Bretin, and J. Dalibard (to be published).
[8] J. Williams and M. Holland, Nature (London) **401**, 568 (1999).
[9] G. Baym and C. J. Pethick, Phys. Rev. Lett. **76**, 6 (1996).
[10] F. Dalfovo and S. Stringari, Phys. Rev. A **53**, 2477 (1996).
[11] S. Sinha, Phys. Rev. A **55**, 4325 (1997).
[12] E. Lundh, C. J. Pethick, and H. Smith, Phys. Rev. A **55**, 2126 (1997).
[13] D. L. Feder, A. A. Svidzinsky, A. L. Fetter, and C. W. Clark, Phys. Rev. Lett. **86**, 564 (2001).
[14] Y. Castin and R. Dum, Eur. Phys. J. D **7**, 399 (1999).
[15] T. Isoshima and K. Machida, Phys. Rev. A **60**, 3313 (1999).
[16] S. Stringari, Phys. Rev. Lett. **77**, 2360 (1996).
[17] This reformulation is possible here because the stirring potential is harmonic. In the presence of an obstacle, the situation is much more involved. See, e.g., C. Josserand, Y. Pomeau, and S. Rica, Physica (Amsterdam) **134D**, 111 (1999); C. Huepe and M.-É. Brachet, Physica (Amsterdam) **140D**, 126 (2000).
[18] B. M. Caradoc-Davies, R. J. Ballagh, and K. Burnett, Phys. Rev. Lett. **83**, 895 (1999).
[19] David L. Feder, Charles W. Clark, and Barry I. Schneider, Phys. Rev. A **61**, 011601 (2000).
[20] At MIT the gas was stirred with a strongly anharmonic potential [5] which excites modes other than quadrupole and broadens the nucleation frequency interval.
[21] K. Madison, F. Chevy, V. Bretin, and J. Dalibard, Phys. Rev. Lett. **86**, 4443 (2001).
[22] F. Dalfovo, S. Giorgini, L. P. Pitaevskii, and S. Stringari, Rev. Mod. Phys. **71**, 463 (1999).
[23] ρ_c is set to zero where the ansatz is negative.
[24] A scaling formulation of the ansatz is given by P. Storey and M. Olshanii, Phys. Rev. A **62**, 033604 (2000).
[25] A. Recati, F. Zambelli, and S. Stringari, Phys. Rev. Lett. **86**, 377 (2001).
[26] We take "degree" of the modes in the strict sense: the degree of the highest degree monomial with nonvanishing coefficient.
[27] F. Dalfovo and S. Stringari, Phys. Rev. A **63**, 011601(R) (2001).

VOLUME 92, NUMBER 2 PHYSICAL REVIEW LETTERS week ending 16 JANUARY 2004

Vortex Lattice Formation in Bose-Einstein Condensates

Carlos Lobo, Alice Sinatra, and Yvan Castin
Laboratoire Kastler Brossel, Ecole Normale Supérieure, 24 rue Lhomond, 75231 Paris CEDEX 05, France
(Received 30 January 2003; published 15 January 2004)

We show that the formation of a vortex lattice in a weakly interacting Bose condensed gas can be modeled with the nonlinear Schrödinger equation for both $T = 0$ and finite temperatures without the need for an explicit damping term. Applying a weak rotating anisotropic harmonic potential, we find numerically that the turbulent dynamics of the field produces an effective dissipation of the vortex motion and leads to the formation of a lattice. For $T = 0$, this turbulent dynamics is triggered by a rotational dynamic instability of the condensate. For finite temperatures, noise is present at the start of the simulation and allows the formation of a vortex lattice at a lower rotation frequency, the Landau frequency. These two regimes have different vortex dynamics. We show that the multimode interpretation of the classical field is essential.

DOI: 10.1103/PhysRevLett.92.020403 PACS numbers: 03.75.Lm

Vortex lattices exist in many domains of physics, from neutron stars to superconductors or liquid helium. In none of these systems has the formation of the lattice been understood at the level of a microscopic theory. Several groups have recently observed the formation of a vortex lattice in weakly interacting Bose gases [1–4] and are able to monitor this formation in real time. This gives us the chance to understand the problem of lattice formation in a relatively simple system. Indeed there have been theoretical attempts to understand the formation process [5–8] with simulations of the Gross-Pitaevskii equation for the condensate wave function. All of them stress the need for explicitly including a damping term representing the noncondensed modes to which the vortices have to give away energy to relax to a lattice configuration. In this Letter, we consider this problem in the framework of the classical theory of a complex field [9] whose exact equation of motion is the nonlinear Schrödinger equation (NLSE). First, we show that lattice formation is predicted within this framework without the addition of damping terms. Second, we provide two distinct scenarios of vortex lattice formation (dynamics, temperature dependence of the formation time, and critical rotation frequency) that can be directly compared with the experiments. We study the formation of the lattice in 3D from an initially nonrotating Bose condensed gas both at $T = 0$ and at finite temperature. Contrary to the common belief, we find that the dynamic instability, which was predicted in [10] to occur above a certain threshold value of the trap rotation frequency, leads to the formation of a vortex lattice. The formation time is in this case only weakly dependent of the temperature and the observed scenario and time scales are comparable to those seen in present experiments. For a lower trap rotation frequency corresponding to the Landau frequency, but only at finite temperature, we identify a new scenario not yet observed experimentally in which the vortices enter a few at a time and gradually spiral towards the center.

We start our simulations with the nonrotating classical field in thermal equilibrium. For $T = 0$, the system initially is a pure condensate and the field is proportional to the condensate wave function ϕ given by the Gross-Pitaevskii equation in the absence of rotation, $\psi = \sqrt{N_0}\phi$, where N_0 is the condensate atom number. For finite temperatures, we sample the initial thermal equilibrium in the Bogoliubov approximation at a given temperature T for a fixed number N_0 of condensate particles. In this approximation, the classical field is given by $\psi(\mathbf{r}, 0) = \sqrt{N_0}\phi(\mathbf{r}) + \psi_\perp(\mathbf{r})$. The random field $\psi_\perp(\mathbf{r})$ orthogonal to ϕ [11] representing the thermal noise is given by

$$\psi_\perp(\mathbf{r}) = \sum_n b_n u_n(\mathbf{r}) + b_n^* v_n^*(\mathbf{r}), \tag{1}$$

where u_n and v_n are the Bogoliubov mode functions associated with ϕ and b_n are independent random c numbers taken from a Gaussian distribution that obeys the classical equipartition formula, $\langle b_n^* b_n \rangle = k_B T/\epsilon_n$, ϵ_n being the Bogoliubov energy of mode n. In practice, to sample this distribution we use the Brownian motion method described in [11]. In our work, the field ψ is to be interpreted not as the condensate wave function but as the whole matter field. We present here results from single realizations of the field ψ which experimentally correspond to single runs. We have checked that different realizations lead to similar results.

In our simulations, we consider a Bose condensed gas initially trapped in a cigar-shaped harmonic potential with oscillation frequencies whose ratio is 1:1:0.25, with 10^5 atoms of mass m and a coupling constant $g = 0.0343$ in units of $\hbar\omega a_0^3$, where ω is the radial frequency and $a_0 = \sqrt{\hbar/m\omega}$ is the oscillator length. The corresponding chemical potential is $\mu = 8\hbar\omega$. We start each simulation with the gas in thermal equilibrium. We abruptly turn on the trap anisotropy which leads to a change in the radial frequencies: $\omega_{x,y}^2 = \omega^2(1 \mp \epsilon)$, where $\epsilon = 0.025$. Then

 0031-9007/04/92(2)/020403(4)$22.50

the rotation frequency $\Omega(t)$ of this anisotropy is slowly increased from zero to a final value Ω_f over $500\omega^{-1}$, to follow Procedure I in [10]. After that, we let the gas evolve in the presence of the rotating anisotropy until the angular momentum of the gas reached a steady state.

The calculation is performed in the rotating frame so that the NLSE takes the form

$$i\hbar\partial_t\psi = \left[-\frac{\hbar^2}{2m}\Delta + U(\mathbf{r}) + g|\psi|^2 - \Omega(t)L_z\right]\psi, \quad (2)$$

where L_z is the angular momentum operator along z, and U is the anisotropic harmonic potential. The field ψ is subject to periodic boundary conditions in the rotating frame [12]. Our grid size is $32 \times 32 \times 128$ corresponding to an energy cutoff of $32\hbar\omega$ per spatial direction, although we have also run simulations on a $64 \times 64 \times 256$ grid (see below).

Zero initial temperature.—This set of simulations can be divided into two groups: those for which the final rotation frequency is $\Omega_f/\omega \leq 0.7$ and those with $\Omega_f/\omega \geq 0.75$. Between these two values lies the threshold for the dynamic instability of the condensate which changes the subsequent dynamics dramatically [10,13]. In the first group, as the rotation frequency gradually increases with time, the condensate adiabatically follows a steady state, apart from excitations of the surface modes leading to a very small oscillation of the angular momentum [see curve for $\Omega_f = 0.7\omega$ in Fig. 2(a) (below)]. With increasing Ω_f, the condensate's final state becomes more and more elliptically deformed, surrounded by a ring of vortices which, however, never enter it. The second group shows a completely different behavior when $\Omega(t)/\omega \simeq 0.75$ (see left column of Fig. 1): The instability sets in; the condensate becomes slightly S-shaped at $t \simeq 450\omega^{-1}$ before being highly deformed and undergoing very turbulent motion [5]. This is accompanied by a large increase in angular momentum of the gas from almost zero when $\Omega(t) < 0.75\omega$ to between $5\hbar$–$7\hbar$ per particle [see Fig. 2(a)]. At this point ($t \simeq 670\omega^{-1}$) several vortices enter the high density region and, in less than $200\omega^{-1}$, settle down to form a well-defined lattice. After this, a period of relaxation of around $800\omega^{-1}$ begins with the initially rotating lattice finally stopping in the rotating frame. There remains a small random motion of the vortices around their equilibrium positions in the lattice together with density fluctuations in and around the condensate.

At the end of the simulation, damping of the vortex motion has occurred and the initial energy of the vortex motion has been transferred in an effectively irreversible way to other degrees of freedom of the field. A similar phenomenon has been observed for the relative motion of two condensates [15]. *If we assume that the field has reached a thermal distribution*, we can calculate the temperature of the system by taking the final state of the simulation and evolving it with the conjugate gradient method in a trap rotating at Ω_f. This reduces its energy

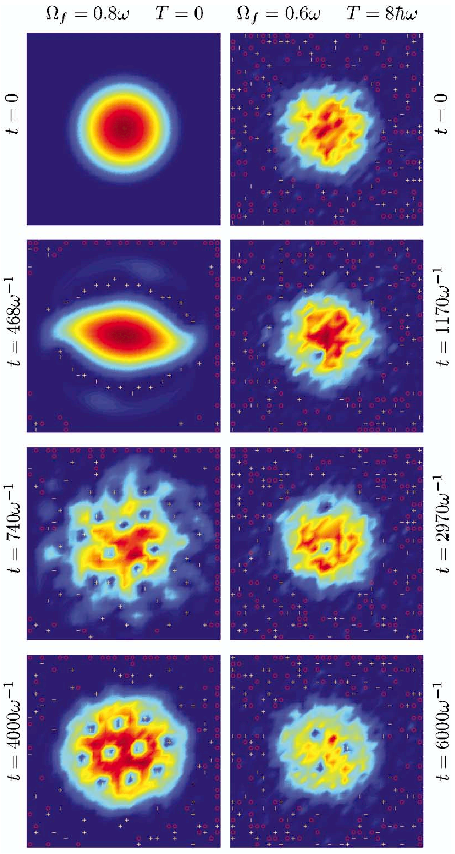

FIG. 1 (color online). Cut along the radial plane ($z = 0$) of the system spatial density at different times. Crosses (circles) indicate the position of vortices of positive (negative) charge [14]. Left column: $T = 0$, $\Omega_f = 0.8\omega$. Top to bottom: initial state; near instability; turbulent behavior; end of simulation. Right column: $k_BT = 8\hbar\omega$, $\Omega_f = 0.6\omega$. Top to bottom: initial state; entry of first vortex; entry of second vortex; end of simulation with a three-vortex lattice.

and takes it to the local minimum associated with the vortex lattice. We then calculate the energy difference ΔE between the final state of the simulation and the one at the minimum. Assuming that Bogoliubov theory is valid, ΔE must correspond to the energy of a classical thermal distribution of weakly coupled harmonic oscillators of amplitude b_n which obeys the equipartition formula $\langle b_n^* b_n\rangle\epsilon_n = k_BT$, with n being the Bogoliubov mode number. So, if $\mathcal{N}$ is the number of modes in the system (and keeping in mind that we have to subtract the one corresponding to the condensate), then we have

$$\Delta E = \sum_n \langle b_n^* b_n\rangle\epsilon_n = (\mathcal{N} - 1)k_BT. \quad (3)$$

The final temperature is $0.616\hbar\omega$ for $\Omega_f = 0.75\omega$ and $0.754\hbar\omega$ for $\Omega_f = 0.8\omega$, in other words it is extremely small, less than a tenth of the chemical potential.

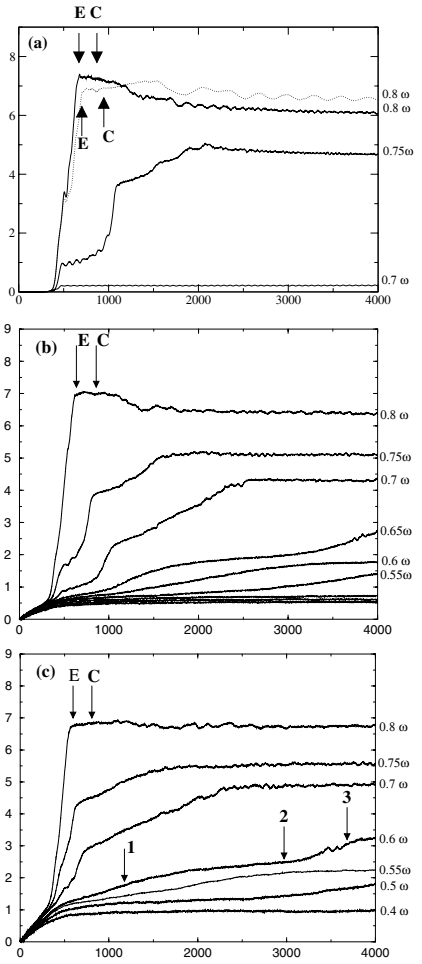

FIG. 2. Total angular momentum of the system in units of $\hbar$ per atom as a function of ωt. The arrows marked E and C indicate the entry of the vortices into the condensate and the crystallization of the lattice for $\Omega_f = 0.8\omega$. (a) $T = 0$, solid lines from bottom to top: $\Omega_f/\omega = 0.7(0), 0.75(7), 0.8(10)$; dashed line: $\Omega_f/\omega = 0.8(10)$ with a grid size of $64 \times 64 \times 256$. All other curves were done on a $32 \times 32 \times 128$ grid. In parenthesis is the number of vortices in the lattice at the end of the simulation. (b) $k_BT = 4\hbar\omega$, $\Omega_f/\omega = 0.4(0), 0.45(0), 0.5(0), 0.55(1), 0.6(1), 0.65(2), 0.7(6), 0.75(7), 0.8(10)$. (c) $k_BT = 8\hbar\omega$, $\Omega_f/\omega = 0.4(0), 0.5(1), 0.55(1), 0.6(3), 0.7(7), 0.75(7), 0.8(10)$. The arrows correspond to the approximate entry time of the vortices for $\Omega_f = 0.6\omega$ as shown in Fig. 1. Note that the total angular momentum shows no signature of the entries.

We have also carried out a simulation on a larger grid ($64 \times 64 \times 256$) to check the dependence on size. We chose $\Omega_f = 0.8\omega$ and compared it with the one on the $32 \times 32 \times 128$ grid. The vortex nucleation and crystallization phases are very similar and occur at roughly the same times. At longer times, two differences arise: First, there are large underdamped oscillations of the angular momentum [see Fig. 2(a)]. An analysis of the simulation suggests that these oscillations are those of the scissors mode. Second, the final temperature ($0.094\hbar\omega$) differs by the ratio of the number of modes as expected: At time $t = 500\omega^{-1}$ when $\Omega(t) = \Omega_f$, ψ had not yet reached the boundary in the smaller grid case and so the evolution of ψ on both grids was identical up to this time with the same total energy which was conserved at later times resulting in the same value of ΔE. This exemplifies the fact that, in classical field theories, the relationship between energy and temperature depends on the energy cutoff.

Since the thermal occupation of the modes is directly proportional to the temperature, we expect that all relaxation processes which involve scattering from or into those modes (such as Landau-Beliaev damping) will be reduced. We are thus led to the conclusion that, for our simulations starting at $T = 0$, relaxation rates in the period after the formation of the lattice could depend on the size of the grid. However, with the present numerical results, we were not able to demonstrate this.

Finite initial temperature.—We performed simulations starting with $k_BT = 4\hbar\omega$ and $k_BT = 8\hbar\omega$. Now not only the condensate but also other modes are occupied in the initial state, with a thermal distribution. For a final rotation frequency below that of the dynamic instability, the situation is quite different from that of the zero temperature case: The condensate is never deformed and the vortices do enter the condensate if $\Omega_f \geq 0.55\omega$ for $k_BT = 4\hbar\omega$ and if $\Omega_f \geq 0.5\omega$ for $k_BT = 8\hbar\omega$. In contrast to the $T = 0$ case at a frequency below that of the dynamic instability, all the noncondensed modes are now thermally occupied allowing the condensate to exchange particles, energy, and angular momentum with the noncondensed cloud. Therefore, as soon as Ω_f is greater than the Landau frequency (at which the vortex-free condensate is no longer a minimum of the energy [6]), the condensate moves gradually toward an energy minimum with one or more vortices. We have found numerically by imaginary time evolution that the Landau frequency is 0.51ω. During the real time evolution corresponding to $\Omega_f = 0.6\omega$ (right column of Fig. 1), we find that the vortices enter only one at a time. That is, as the angular momentum of the cloud increases, one vortex out of the group of vortices that surrounds the condensate will enter it and spiral slowly clockwise towards the center on a time scale of hundreds of ω^{-1}. After that vortex has reached the center, a second one enters slowly, repeating the trajectory of the first until it starts to interact with it, and the two orbit around each other for a while after which a third will enter. At the end of the simulation, coinciding with the achievement of the plateau in angular momentum, the lattice becomes stationary in the rotating frame and no further vortex enters the condensate. For $\Omega_f = 0.7\omega$, we find that the condensate deforms itself elliptically after which three vortices enter at the same time and form a rotating lattice. After that, and spaced by

several hundred ω^{-1}, a fourth and then a fifth vortex enter. Finally, two further vortices enter simultaneously to form the final seven vortex lattice. At each intermediate stage there is always a well-defined lattice present although it is not stationary in the rotating frame. We should contrast this with the scenario of [6,7], where a large number of vortices enter all at once into the condensate in a ring configuration and then some of them form a lattice while others are shed and leave the condensate.

For Ω_f above the dynamic instability frequency, the situation is quite similar to the corresponding one at $T = 0$. Once the instability has set in the lattice is formed for both temperatures in about $200\omega^{-1}$ as in the $T = 0$ case [see Figs. 2(b) and 2(c)]. This weak temperature dependence was also found experimentally [16]. We find a time for the lattice to stop rotating on the order of $100\omega^{-1}$, much shorter than at $T = 0$.

It is important to emphasize the multimode interpretation of the field. Transposing Penrose and Onsager's definition to the classical field theory, the condensate wave function is defined as the eigenvector corresponding to the largest eigenvalue of the one-body density matrix $\langle \psi^*(\mathbf{r}')\psi(\mathbf{r})\rangle$ where the average is over an ensemble of initial states. If the system becomes turbulent because it encounters an instability, the trajectories of the neighboring realizations will diverge exponentially. However, after averaging, we believe that the condensate wave function will not be a turbulent function. For $T = 0$, there is only one initial state and so we replace ensemble averaging by one over time in the steady state regime [17]. In our simulations with $\Omega_f = 0.8\omega$, the system must therefore be understood as becoming intrinsically multimode even though we started at $T = 0$ with a pure condensate. This shows that any theoretical model which singles out the condensate mode for separate treatment with a Gross-Pitaevskii–type equation could run into trouble in turbulent situations since the separation between condensed and noncondensed modes would be hard to keep.

Conclusions.—We have identified two very different scenarios for the crystallization of the vortex lattice in the classical field model. In the first one, the vortex and the subsequent lattice formation are triggered by a dynamic instability which sets in for a threshold value of the rotation frequency of the trap. Many vortices enter the condensate at the same time and settle into a lattice in about $200\omega^{-1}$. In this scenario, the lattice formation time is essentially the same for both $T = 0$ and finite temperatures in agreement with experimental observation [16]. In the second scenario, observed only at finite temperatures, vortices appear for a lower value of the rotation frequency corresponding to the Landau frequency, and so no dynamic instability occurs. The vortices enter one by one into the condensate and settle into a lattice before the entry of the following one. Thus far, there has been no experimental check of this second scenario.

We thank B. Durin, L. Carr, I. Carusotto, G. Shlyapnikov, and J. Dalibard for useful contributions. C. L. acknowledges support from the Fundação para a Ciência e Tecnologia of Portugal. We acknowledge financial support from Région Ile de France. L. K. B. is a unit of ENS and of Université Paris 6 associated to CNRS.

Note added.—We have been informed that crystallization of the vortex lattice has also been observed in a simulation without a damping term by the group of Bigelow [18].

[1] K.W. Madison, F. Chevy, W. Wohlleben, and J. Dalibard, Phys. Rev. Lett. **84**, 806 (2000).
[2] J. R. Abo-Shaeer, C. Raman, J. M. Vogels, and W. Ketterle, Science **292**, 476 (2001).
[3] P. C. Haljan, I. Coddington, P. Engels, and E. A. Cornell, Phys. Rev. Lett. **87**, 210403 (2001).
[4] E. Hodby, G. Hechenblaikner, S. A. Hopkins, O. M. Maragó, and C. J. Foot, Phys. Rev. Lett. **88**, 010405 (2002).
[5] D. L. Feder, A. A. Svidzinsky, A. L. Fetter, and C.W. Clark, Phys. Rev. Lett. **86**, 564 (2001).
[6] M. Tsubota, K. Kasamatsu, and M. Ueda, Phys. Rev. A **65**, 023603 (2002); K. Kasamatsu, M. Tsubota, and M. Ueda, Phys. Rev. A **67**, 033610 (2003).
[7] A. A. Penckwitt, R. J. Ballagh, and C.W. Gardiner, Phys. Rev. Lett. **89**, 260402 (2002).
[8] E. Lundh, J.-P. Martikainen, and K.-A. Suominen, Phys. Rev. A 67, 063604 (2003).
[9] K. Damle, S. N. Majumdar, and S. Sachdev, Phys. Rev. A **54**, 5037 (1996); Yu. Kagan and B. Svistunov, Phys. Rev. Lett. **79**, 3331 (1997); M. J. Davis, S. A. Morgan, and K. Burnett, Phys. Rev. Lett. **87**, 160402 (2001).
[10] S. Sinha and Y. Castin, Phys. Rev. Lett. **87**, 190402 (2001).
[11] A. Sinatra, C. Lobo, and Y. Castin, J. Phys. B **35**, 3599 (2002).
[12] Periodic boundary conditions (PBC) in the lab frame would stop the rotation of the noncondensed gas. We checked that PBC in the rotating frame do not set a pure condensate into rotation as the condensate density is negligible at the grid borders. The harmonic trap anisotropy is then crucial for the vortex formation at $T = 0$ by triggering the dynamic instability of [10].
[13] K. Madison, F. Chevy, V. Bretin, and J. Dalibard, Phys. Rev. Lett. **86**, 4443 (2001).
[14] Vortex positions are found by integrating the gradient of the phase around each grid square in the plane.
[15] A. Sinatra, P. Fedichev, Y. Castin, J. Dalibard, and G.V. Shlyapnikov, Phys. Rev. Lett. **82**, 251 (1998).
[16] J. R. Abo-Shaeer, C. Raman, and W. Ketterle, Phys. Rev. Lett. **88**, 070409 (2002).
[17] L. D. Landau and E. M. Lifshitz, *Statistical Physics* (Pergamon, Oxford, 1980), 3rd ed., Pt. 1, Sect. 1; K. Góral, M. Gajda, and K. Rzążewski, Phys. Rev. A **66**, 051602(R) (2002).
[18] N. Bigelow, 2002 Summer Session on Atomic Gases in Benasque, Spain.

5.7 Publications avec des expérimentateurs

Les textes [14] et [42] ci-dessous reproduits sont deux articles expérimentaux dont nous sommes coauteur. Nous les avons choisis non seulement pour leur retentissement (ils ont constitué des 'premières') mais aussi pour opposer leurs genèses.

Pour le premier [14], sur les oscillations de Bloch d'un gaz d'atomes ultrafroids, nous avons effectué les calculs de faisabilité expérimentale dès que l'idée fut lancée ; ces calculs étant encourageants, l'expérience fut décidée et réalisée assez rapidement.

Le cas du second article [42], sur la première observation d'un soliton à ondes de matière, est très différent. L'idée de produire des solitons à partir d'un condensat piégé nous est venue lors de discussions avec Maxim Olshanii en 1996. Nous avons mentionné cette possibilité (sans rien publier) à plusieurs groupes expérimentaux (dont celui de Randy Hulet à Rice University), mais il existait une barrière de faisabilité liée au fait que la taille d'un soliton correspondait à un pixel seulement du système d'imagerie, si bien que l'expérience proposée était considérée comme très difficile. Fin 2001, lors d'un séminaire interne de l'équipe 'atomes froids' donné par Julien Cubizolles, fut mentionné le fait que le dispositif expérimental de l'époque conduisait naturellement à la formation d'un potentiel harmonique antipiégeant ; cet élément en apparence anodin, combiné au projet latent de production de soliton que nous avions en tête depuis 5 ans, nous donna soudainement une idée permettant de lever l'objection sur l'observabilité du soliton.

VOLUME 76, NUMBER 24 PHYSICAL REVIEW LETTERS 10 JUNE 1996

Bloch Oscillations of Atoms in an Optical Potential

Maxime Ben Dahan, Ekkehard Peik, Jakob Reichel, Yvan Castin, and Christophe Salomon
Laboratoire Kastler Brossel, Departement de Physique, Ecole Normale Supérieure, 24 rue Lhomond, 75231 Paris Cedex 05, France
(Received 19 January 1996)

Ultracold cesium atoms are prepared in the ground energy band of the potential induced by an optical standing wave. We observe Bloch oscillations of the atoms driven by a constant inertial force. We measure the momentum distribution of Bloch states and effective masses different from the mass of the free atom. [S0031-9007(96)00366-3]

PACS numbers: 32.80.Pj, 03.75.–b

The early quantum theory of electrical conductivity in crystal lattices by Bloch and Zener [1,2] led to the striking prediction that a homogeneous static electric field induces an oscillatory rather than uniform motion of the electrons. These so-called Bloch oscillations have never been observed in natural crystals because the scattering time of the electrons by the lattice defects is much shorter than the Bloch period. In semiconductor superlattices the larger spatial period leads to a much shorter Bloch period (~600 fs) and Bloch oscillations have recently been observed through the emission of THz radiation by the electrons [3]. Here we present Bloch oscillations of atoms in the fundamental energy band of a periodic optical potential. We directly measure the atomic momentum distribution evolving in time under the influence of a constant inertial force for various potential depths. We experimentally observe oscillation periods in the millisecond range as well as positive and negative effective masses.

Bloch oscillations are a pure quantum effect which can be explained in a simple one-dimensional model. The periodicity of the lattice (period d) leads to a band structure (Fig. 1) of the energy spectrum of the particle and the corresponding eigenenergies $E_n(q)$ and eigenstates $|n, q\rangle$ (Bloch states) are labeled by the discrete band index n and the continuous quasimomentum q; $E_n(q)$ and $|n, q\rangle$ are periodic functions of q with period $2\pi/d$ and q is conventionally restricted to the first Brillouin zone $]-\pi/d, \pi/d]$ [4]. Under the influence of a constant external force F, weak enough not to induce interband transitions, a given Bloch state $|n, q(0)\rangle$ evolves (up to a phase factor) into the state $|n, q(t)\rangle$ according to

$$q(t) = q(0) + Ft/\hbar\,. \tag{1}$$

This evolution is periodic with a period $\tau_B = h/|F|d$ corresponding to the time required for the quasimomentum to scan a full Brillouin zone. The mean velocity in $|n, q(t)\rangle$

$$\langle v\rangle_n(q(t)) = \frac{1}{\hbar}\,\frac{dE_n(R(q(t))}{dq} \tag{2}$$

is an oscillatory function of time with zero mean. As a consequence, a wave packet prepared with a well-defined quasimomentum in the nth band will also oscillate in position with an amplitude $\Delta_n/2|F|$ where Δ_n is the energy width of the nth band.

In our experiments the periodic potential results from the light shift of the ground state of atoms illuminated by a laser standing wave. The laser is detuned far from any atomic resonance so that spontaneous emission can be neglected. This configuration was first used in the context of atom diffraction [5] leading to the development of atom optics elements, interferometry [6,7], or studies of quantum chaos [8]. In periodic potentials using lasers closer to resonance, spatial ordering has been observed [9]. In this case the concept of a band structure is useful [10], but experimental evidence for it has only been indirect because spontaneous emission spreads the atom distribution over the whole Brillouin zone [11]. Using one-dimensional Raman laser cooling [12,13] we first prepare a gas of free atoms with a momentum spread $\delta p = \hbar k/4$ in the direction of the standing wave, where $\hbar k$ is the photon momentum. The corresponding atomic coherence length $h/\delta p$ extends over several periods $d = \lambda/2 = \pi/k$ of the optical lattice. By adiabatically switching on the light potential this initial momentum distribution is turned into a statistical mixture of Bloch states in the ground energy band with a quasimomentum width $\delta q = \delta p/\hbar$ much smaller than the

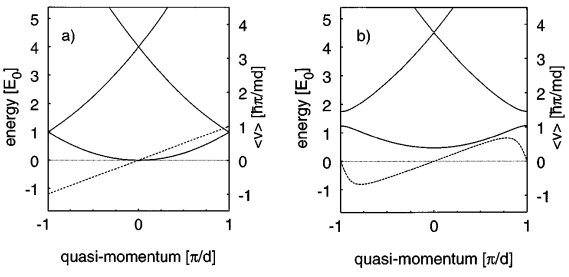

FIG. 1. Band structure $E_n(q)$ (solid line) for a particle in a periodic potential $U(z) = U_0 \sin^2 \pi z/d$ and mean velocity $\langle v\rangle_0(q)$ in the fundamental band (dashed line): (a) free particle case, (b) $U_0 = E_0 = \hbar^2\pi^2/2md^2$. A gap opens at $q = \pm\pi/d$. Under the influence of a weak uniform force, a particle prepared in the fundamental band remains in this band and performs a motion periodic in time called a Bloch oscillation.

 0031-9007/96/76(24)/4508(4)$10.00

width $2k$ of the Brillouin zone. We mimic a constant external force by introducing a tunable frequency difference $\delta\nu(t)$ between the two counterpropagating laser waves creating the optical potential. The reference frame in which the optical potential is stationary is now moving with velocity $\delta\nu(t)\lambda/2$. For a linear variation in time of $\delta\nu(t)$ a constant inertial force $F = -ma = -m\lambda\frac{d}{dt}\delta\nu(t)/2$ is exerted on the atoms in this frame. After a given evolution time t_a, we abruptly switch off the light potential and measure the momentum distribution of the Bloch state at time t_a with a resolution of $\hbar k/18$.

This model system presents several advantages: (i) The initial momentum distribution is well defined and can be tailored at will. (ii) By contrast to solid state systems, the periodic potential, being created by light, can be easily turned on and off. This gives direct access to the momentum distribution of Bloch states. (iii) There is virtually no dissipation or scattering from defects of the potential or from interaction between particles. We observe Bloch periods in the millisecond range, i.e., 10 orders of magnitude longer than in semiconductors.

Our experimental setup for subrecoil laser cooling of cesium atoms has been described previously [13,14]. We use a magneto-optical trap in a low pressure vapor cell to capture atoms and precool them to about 6 μK. After turning off the magnetic field we perform 1D Raman cooling with horizontal beams from two diode lasers that are phase locked to a tunable frequency difference around the cesium hyperfine splitting of 9.12 GHz. We use a sequence of Raman square pulses [13], resonant with velocity classes centered at $\pm v_R$, $\pm 2v_R$, and $\pm 4v_R$ where v_R is the recoil velocity $\hbar k/m = 3.5$ mm/s. In a cooling time of 12 ms this produces a narrow velocity distribution of atoms in the $F = 3$ ground state, with a nearly Lorentzian line shape of half width at half maximum of $0.24v_R$.

After the cooling phase all lasers are switched off except one of the Raman lasers which generates the optical potential. We split it into two beams and pass each of them through an acousto-optic modulator to control its power and frequency. These beams are superimposed onto the horizontal optical axis of the Raman beams in counterpropagating directions. They have the same linear polarization, equal intensities, and are detuned by $\delta/2\pi = 30\,\text{GHz} = 5700\Gamma/2\pi$ from the $6S_{1/2} \rightarrow 6P_{3/2}$ atomic resonance line (wavelength $\lambda = 852$ nm), where $\Gamma/2\pi = 5.3$ MHz is the natural width of the $6P_{3/2}$ state.

Initially the two beams have the same frequency and their dipole coupling to the atom leads to a light shift which is nearly identical for all Zeeman sublevels of $F = 3$ and varies with the atomic position as $U(z) = U_0 \sin^2 kz$. The potential depth is given by $U_0 = (2/3)\hbar\Gamma(I/I_0)(\Gamma/\delta)$, where I is the laser intensity in one beam, $I_0 = 2.2$ mW/cm^2. With a peak intensity of up to 40 mW/cm^2 ($1/\sqrt{e}$ diameter $\approx$4.5 mm) the depth of the potential can be varied between 0 and about $6E_R$ where $E_R = \hbar^2k^2/2m = h \cdot 2.068$ kHz is the recoil energy. Since the spontaneous emission rate is at most 4 s^{-1}, it can be totally neglected during our $\sim$10 ms interaction time.

Initially ($U_0 = 0$) only the Bloch states at the bottom of the ground state energy band are significantly populated. In order to prevent a transfer of population into the higher energy bands the standing wave has to be turned on slowly enough. We have used as adiabaticity criterion the usual condition

$$|\langle n, q|d/dt|0, q\rangle| \ll |E_n(q) - E_0(q)|/\hbar\,. \qquad (3)$$

In the case $U_0 \leq E_R$ the energy difference in (3) for $n = 1$ remains finite [$E_1(0) - E_0(0) \sim 4E_R$] and condition (3) reads $|\frac{d}{dt}U_0/E_R| \ll 32\sqrt{2}E_R/\hbar$ [15]. For larger values of U_0/E_R the energy gap increases and adiabaticity is more easily fulfilled. We use a rise time of 200 μs, largely in the adiabatic regime.

Next a linear frequency ramp of duration t_a up to 8 ms is applied to one of the beams. The resulting inertial force $F = -ma$ has to be small enough to prevent interband transitions which are the most probable when the quasimomentum $q(t)$ given by (1) reaches the edge of the Brillouin zone: For $q = k$ condition (3) imposes $|ma\lambda/2| \ll (\pi/8)U_0^2/E_R$ for $U_0 \leq 10E_R$. We have used accelerations ranging from 0.43 m/s^2 ($d\delta\nu/dt = 10^6$ Hz/s) for a potential depth $U_0 = 0.5E_R$ to 13.2 m/s^2 for $U_0 = 6E_R$. We have checked by a measurement of the final momentum distribution (explained below) that these values do not lead to a significant transfer of atoms to higher bands for several periods of Bloch oscillations. The corresponding frequencies $1/\tau_B$ of the Bloch oscillations are in the range 60 to 1900 Hz.

After a given acceleration time t_a, the standing wave is turned off fast (fall time $\approx 1\,\mu$s) so that the free atoms keep the momentum distribution corresponding to the Bloch states. This distribution is probed by a 3 ms long velocity-selective Raman pulse of variable detuning. This pulse transfers atoms in a narrow momentum class (resolution $\hbar k/18$) from the $F = 3$ to the $F = 4$ ground state hyperfine level and the fluorescence signal from these atoms is used to measure their number. Scanning of the Raman detuning gives the atomic momentum distribution in the laboratory frame, from which the distribution in the accelerated frame is obtained by a translation of $-mat_a$.

Figure 2 shows the momentum distribution in the accelerated frame at various times t_a, for $U_0 = 2.3E_R$ and $a = -0.85$ m/s^2. The initial peak shifts linearly with time while its weight decreases. Simultaneously a second peak emerges at a distance $2\hbar k$; its increasing weight becomes equal to the one of the first peak when $t_a = \tau_B/2$ where $\tau_B = 2\hbar k/|F|$. It keeps growing until $t_a = \tau_B$ where the initial momentum distribution is recovered: The atoms have performed a full Bloch oscillation. Further evolution reproduces this pattern periodically.

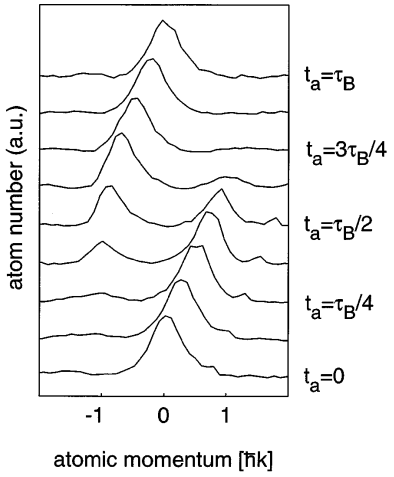

FIG. 2. Bloch oscillations of atoms: momentum distributions in the accelerated frame for equidistant values of the acceleration time t_a between $t_a = 0$ and $t_a = \tau_B = 8.2$ ms. The light potential depth is $U_0 = 2.3E_R$ and the acceleration is $a = -0.85$ m/s^2. The small peak in the right wing of the first five spectra is an artifact.

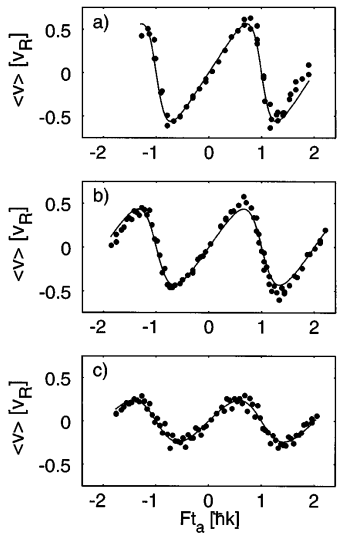

FIG. 3. Mean atomic velocity $\langle v \rangle$ as a function of the acceleration time t_a for three values of the potential depth: (a) $U_0 = 1.4E_R$, (b) $U_0 = 2.3E_R$, (c) $U_0 = 4.4E_R$. The negative values of Ft_a were measured by changing the sign of F. Solid lines: theoretical prediction.

These results can be explained as follows. Bloch states of quasimomentum q are coherent superpositions of plane waves, i.e., momentum states $|p = \hbar(q + 2jk)\rangle$ (j integer). Because of the applied force, q evolves in time according to (1) with the initial condition $q(0) = 0$. In the perturbative case considered here ($U_0 \ll 16E_R$), for $q(t_a) \sim 0$ the Bloch state $|n = 0, q(t_a)\rangle$ is very close to the momentum state $|p = \hbar q(t_a)\rangle$: It has very small populations $[\sim (U_0/16E_R)^2 \simeq 1\%]$ on the $|p = \hbar q(t_a) \pm 2\hbar k\rangle$ momentum states. For $q(t_a)$ close to k, the Bloch state is mainly a linear superposition of the $|p = \hbar q(t_a)\rangle$ and $|p = \hbar[q(t_a) - 2k]\rangle$ momentum states, with equal amplitudes for $q(t_a) = k$, i.e., for $t_a = \tau_B/2$. For $\tau_B/2 < t_a < \tau_B$, $q(t_a)$ scans the $]-k, 0[$ interval of the Brillouin zone and the momentum distribution is turned back into the single initial peak.

In order to further illustrate the oscillatory motion of the atoms, we have deduced from our data the mean atomic velocity as a function of t_a for different values of the potential depth U_0 and for an acceleration $a = \pm 0.85$ m/s^2. We reduce the smoothing effect due to the width of the quasimomentum distribution as follows: We slice the initial momentum peak into narrow channels labeled i, centered at $q_i(0)$ and of width $k/18$. Following the time evolution of each of these slices, we calculate the mean velocity for the atoms in momentum channels $\hbar q_i(t_a), \hbar q_i(t_a) \pm 2\hbar k$ where $q_i(t)$ evolves according to (1). The contributions of the different channels are combined in one curve after a time translation of $\hbar q_i(0)/F$. We have plotted in Fig. 3 the results for three values of U_0/E_R. The measured Bloch periods agree with the expected value (8.2 ms) to within an uncertainty of 4% and do not depend on U_0. For $U_0 = 0.54E_R$ the amplitude of the Bloch oscillations is $0.68\hbar k$ and corresponds to an oscillation in position of 3.1 μm. These amplitudes decrease with growing U_0 [cf. Fig. 4(a)]: The band flattens out as a consequence of the smaller tunnel coupling between neighboring sites of the lattice.

A striking feature of the oscillations presented in Fig. 3 is their asymmetry, which is particularly pronounced for low values of the optical potential: The slope of the mean velocity near the edge of the Brillouin zone ($Ft_a = \pm\hbar k$) is steeper than that near the zone center ($Ft_a = 0, \pm 2\hbar k$). This effect can be described in terms of effective masses: The dynamics of the particle is equivalent to that of a particle in free space: $m^* d\langle v \rangle/dt = F$ with an effective mass $m^*(q)$ given by $\hbar^2/m^* = d^2E_0(q)/dq^2$, which is in general different from the real mass because of the interaction with the potential. In the center and at the edge of the Brillouin zone, the energy band is approximately parabolic, the effective mass is constant, and $\langle v \rangle$ evolves linearly in time. By measuring the slope of $\langle v \rangle(t_a)$ around $t_a = 0$ ($q = 0$) and $t_a = \pm\tau_B/2$ ($q = \pm k$) in Fig. 3, we deduce these two effective masses. In Fig. 4(b), we present their variation with the potential depth U_0. For weak potentials ($U_0 \to 0$), $m^*(q = 0)$ tends to the free atom mass m and $m^*(q = k)$ tends to 0. With increasing potential depth the atoms are more tightly bound and the effective masses increase in absolute value. For

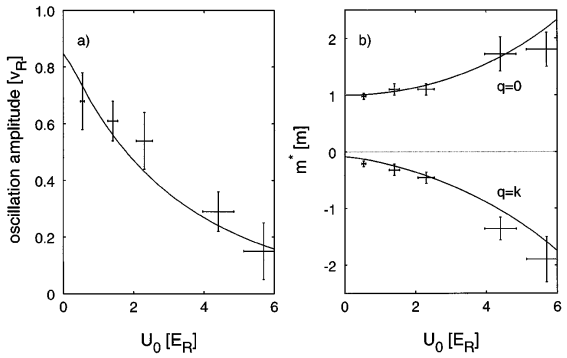

FIG. 4. Amplitude of the Bloch oscillations (a) and effective masses m^* for $q = 0$ and $q = k$ in units of the cesium atomic mass (b) vs potential depth U_0. Solid lines: theory.

$U_0 = 5.7E_R$, $m^*(0)$ is about twice as large as the free mass. In the limit $U_0 \to \infty$ the absolute values of $m^*(0)$ and $m^*(k)$ become equal and diverge as $1/\Delta_0$.

We have calculated numerically the band structure for our experimental values of U_0. The mean velocity of the Bloch states obtained from Eq. (2) is averaged over a statistical mixture of Bloch states corresponding to the experimental resolution, i.e., having a Gaussian distribution of quasimomentum q with standard deviation $k/18$ [16]. The solid lines in Figs. 3 and 4 show the results of these calculations with no adjustable parameter. The agreement with the experimental data is quite good. By integrating over time the data $\langle v(t_a)\rangle$ of Fig. 3 [see Eq. (2)], we have also reconstructed experimentally the fundamental energy band.

Finally we have made preliminary investigations of atom acceleration in the case $U_0 = 5.7E_R$. We could still observe Bloch states after $15\tau_B$. In the laboratory frame, this corresponds to a coherent momentum transfer of $30\hbar k$, producing an atomic beam with subrecoil momentum spread ($\hbar k/4$) in the beam direction. After optimization, this technique should be useful to produce atomic beams with long coherence length from cold atoms prepared in a trap.

We are grateful to C. Cohen-Tannoudji, G. Grynberg, G. Bastard, J. Dalibard, and M. Raizen for stimulating discussions. E. P. and J. R. acknowledge support from the European Union through the HCM program. This work was supported in part by NEDO, CNES, and Collège de France. Laboratoire Kastler Brossel is Unité de Recherche de l'Ecole Normale Supérieure et de l'Université Pierre et Marie Curie, associée au CNRS.

[1] F. Bloch, Z. Phys. **52**, 555 (1929).
[2] C. Zener, Proc. R. Soc. London A **145**, 523 (1934).
[3] C. Waschke, H. Roskos, R. Schwedler, K. Leo, H. Kurz, and K. Köhler, Phys. Rev. Lett. **70**, 3319 (1993).
[4] See, e.g., N. W. Ashcroft and N. D. Mermin, *Solid State Physics* (Saunders, Philadelphia, 1976).
[5] P. L. Gould, G. A. Ruff, and D. E. Pritchard, Phys. Rev. Lett. **56**, 827 (1986); P. J. Martin, B. G. Oldaker, A. H. Miklich, and D. E. Pritchard, Phys. Rev. Lett. **60**, 515 (1988).
[6] For a recent review, see C. S. Adams, M. Sigel, and J. Mlynek, Phys. Rep. **240**, 143 (1994).
[7] E. Rasel, M. Oberthaler, H. Batelaan, J. Schmiedmayer, and A. Zeilinger, Phys. Rev. Lett. **75**, 2633 (1995); D. M. Giltner, R. W. McGowan, and S. A. Lee, Phys. Rev. Lett. **75**, 2638 (1995).
[8] F. L. Moore, J. C. Robinson, C. Bharucha, P. E. Williams, and M. G. Raizen, Phys. Rev. Lett. **73**, 2974 (1994).
[9] For a recent review, see M. G. Prentiss, Science **260**, 1078 (1993).
[10] Y. Castin and J. Dalibard, Europhys. Lett. **14**, 761 (1991).
[11] M. Doery, M. Widmer, J. Bellanca, E. Vredenbregt, T. Bergeman, and H. Metcalf, Phys. Rev. Lett. **72**, 2546 (1994).
[12] M. Kasevich and S. Chu, Phys. Rev. Lett. **69**, 1741 (1992).
[13] J. Reichel, F. Bardou, M. Ben Dahan, E. Peik, S. Rand, C. Salomon, and C. Cohen-Tannoudji, Phys. Rev. Lett. **75**, 4575 (1995).
[14] J. Reichel, O. Morice, G. M. Tino, and C. Salomon, Europhys. Lett. **28**, 477 (1994).
[15] The adiabaticity criterion would have been more stringent for a value of q closer to the boundary k of the Brillouin zone, where the band gap vanishes with U_0.
[16] The averaging has a significant influence only for the smallest values of U_0 and around $q = \pm k$ where $\langle v\rangle$ changes very quickly. It explains why the oscillation amplitude does not converge to v_R in Fig. 4(a) and why the effective mass $m^*(k)$ does not tend to 0 in Fig. 4(b), for $U_0 \to 0$.

tunnel framed by universally conserved basic amino acids (Fig. 6B). Because open complex formation occurs without breaking covalent bonds in the DNA, the RNAP claws must open at some point during the process of open complex formation to allow the template strand to slip into its channel. Subsequent closure of the claws would then establish the tunnel. This requirement for prior states (intermediates) during the steps of open complex formation with different conformations of the enzyme, combined with the good match between footprinting data and the complete open complex model, leads us to suggest that the complex represented in this holoenzyme/fork-junction structure closely resembles the final RP_o.

The RF structure, and the models derived from it, raise key questions that are central to understanding transcription initiation. How is RP_o generated from RP_c (Fig. 5A)? How do transcription activators interact with the complex to enhance the rate of transcription initiation? The structures and models presented here provide a basis for designing more decisive experiments probing these questions and more.

References and Notes

1. K. S. Murakami, S. Masuda, S. A. Darst, *Science* **296**, 1280 (2002).
2. P. L. deHaseth, M. L. Zupancic, M. T. J. Record, *J. Bacteriol.* **180**, 3019 (1998).
3. Y. Guo, J. D. Gralla, *Proc. Natl. Acad. Sci. U.S.A.* **95**, 11655 (1998).
4. T. Gaal *et al.*, *Mol. Microbiol.* **42**, 939 (2001).
5. S. Keilty, M. Rosenberg, *J. Biol. Chem.* **262**, 6389 (1987).
6. L. Tsujikawa, O. Tsodikov, P. de Haseth, *Proc. Natl. Acad. Sci. U.S.A.* **99**, 3493 (2002).
7. E. A. Campbell *et al.*, *Cell* **104**, 901 (2001).
8. G. Zhang *et al.*, *Cell* **98**, 811 (1999).
9. E. A. Campbell *et al.*, *Mol. Cell* **9**, 527 (2002).
10. In the crystal, two DNA fork junctions pack against each other at their blunt, upstream ends (Fig. 1A), forming a pseudo-continuous double-helix related by a crystallographic twofold symmetry axis perpendicular to the DNA helical axis. Thus, the double-stranded upstream ends of the symmetry-related fork junctions were placed with an end-to-end spacing of 3.4 Å (corresponding to base-pair stacking in double-stranded B-form DNA), with the symmetry axis in the middle.
11. M. L. Craig, W.-C. Suh, M. T. J. Record, *Biochemistry* **34**, 15624 (1995).
12. J. Mecsas, D. W. Cowing, C. A. Gross, *J. Mol. Biol.* **220**, 585 (1991).
13. W. Metzger, P. Schickor, H. Heumann, *EMBO J.* **8**, 2745 (1989).
14. P. Schickor, W. Metzger, W. Wladyslaw, H. Lederer, H. Heumann, *EMBO J.* **9**, 2215 (1990).
15. K. A. Barne, J. A. Bown, S. J. W. Busby, S. D. Minchin, *EMBO J.* **16**, 4034 (1997).
16. C. A. Gross *et al.*, *Cold Spring Harbor Symp. Quant. Biol.* **63**, 141 (1998).
17. S. A. Darst *et al.*, in *Nucleic Acids & Molecular Biology*, F. Ekstein, D. M. J. Lilley, Eds. (Springer, London, 1997), vol. 11, pp. 27–40.
18. B. A. Young *et al.*, *Cell* **105**, 935 (2001).
19. X. Huang, F. J. Lopez de Saro, J. D. Helmann, *Nucleic Acids Res.* **25**, 2603 (1997).
20. M. Tomsic *et al.*, *J. Biol. Chem.* **276**, 31891 (2001).
21. O. N. Ozoline, M. A. Tsyganov, *Nucleic Acids Res.* **23**, 4533 (1995).
22. M. Buckle, I. K. Pemberton, M.-A. Jacquet, H. Buc, *J. Mol. Biol.* **285**, 955 (1999).
23. D. W. Cowing, J. Mecsas, M. T. J. Record, C. A. Gross, *J. Mol. Biol.* **210**, 521 (1989).
24. R. T. Kovacic, *J. Biol. Chem.* **262**, 13654 (1987).
25. R. L Gourse, W. Ross, T. Gaal, *Mol. Microbiol.* **37**, 687 (2000).
26. Y. H. Jeon *et al.*, *Science* **270**, 1495 (1995).
27. Y. H. Jeon, T. Yamazaki, T. Otomo, A. Ishihama, Y. Kyogoku, *J. Mol. Biol.* **267**, 953 (1997).
28. R. H. Ebright, S. Busby, *Curr. Opin. Genet. Devel.* **5**, 197 (1995).
29. W. Ross, A. Ernst, R. L. Gourse, *Genes Dev.* **15**, 491 (2001).
30. E. Nudler, E. Avetissova, V. Markovtsov, A. Goldfarb, *Science* **273**, 211 (1996).
31. S. A. Weston, A. Lahm, D. Suck, *J. Mol. Biol.* **226**, 1237 (1992).
32. T. M. Gruber, D. A. Bryant, *J. Bacteriol.* **179**, 1734 (1997).
33. M. Lonetto, M. Gribskov, C. A. Gross, *J. Bacteriol.* **174**, 3843 (1992).
34. Y. Harada *et al.*, *Nature* **409**, 113- (2001).
35. T. A. Jones, J.-Y. Zou, S. Cowan, M. Kjeldgaard, *Acta Crystallogr. A* **47**, 110 (1991).
36. A. Nicholls, K. A. Sharp, B. Honig, *Proteins Struct. Funct. Genet.* **11**, 281 (1991).
37. M. Carson, *J. Appl. Crystallogr.* **24**, 958 (1991).
38. R. Lavery, H. Sklenar, *J. Biomol. Struct. Dyn.* **6**, 63 (1988).
39. Z. Otwinowski, in *Proceedings of the CCP4 Study Weekend*, W. Wolf, P. R. Evans, A. G. W. Leslie, Eds. (SERC Daresbury Laboratory, Warrington, UK, 1991) pp. 80–86.
40. N. Casan-Pastor, P. Gomez-Romero, G. B. Jameson, L. C. W. Baker, *J. Am. Chem. Soc.* **113**, 5685 (1991).

41. We thank M. Pope for the gift of the W_{12} cluster, G. Schneider for the gift of Ta_6Br_{14}, and T. Gaal and R. Gourse for providing the full con promoter sequence before publication; D. Thiel and the staff at the Cornell High Energy Synchrotron Source and M. Becker and L. Berman at NSLS X25 for support during data collection; K. Kinosita and R. Landick for important discussion; and D. Jeruzalmi, S. Nair, and H. Yamaguchi for invaluable advice. Figure 1B was made using the program O (*35*). Figures 2, 4, 5, and 6 were made using the program GRASP (*36*). Figure 3 was made using the program RIBBONS (*37*). Supported by a Norman and Rosita Winston Postdoctoral Fellowship and a Human Frontiers Sciences Program Postdoctoral Fellowship (K.S.M.); National Research Service Award number NIH GM20470 (E.A.C.); and, in part, by NIH grants GM53759 and GM61898 (S.A.D.)

Supporting Online Material

(www.sciencemag.org/cgi/content/full/296/5571/1285/DC1)
Material and Methods
References and notes
fig. S1
table S1

7 January 2002; accepted 21 March 2002

Formation of a Matter-Wave Bright Soliton

L. Khaykovich,[1] F. Schreck,[1] G. Ferrari,[1,2] T. Bourdel,[1] J. Cubizolles,[1] L. D. Carr,[1] Y. Castin,[1] C. Salomon[1]*

We report the production of matter-wave solitons in an ultracold lithium-7 gas. The effective interaction between atoms in a Bose-Einstein condensate is tuned with a Feshbach resonance from repulsive to attractive before release in a one-dimensional optical waveguide. Propagation of the soliton without dispersion over a macroscopic distance of 1.1 millimeter is observed. A simple theoretical model explains the stability region of the soliton. These matter-wave solitons open possibilities for future applications in coherent atom optics, atom interferometry, and atom transport.

Solitons are localized waves that travel over long distances with neither attenuation nor change of shape, as their dispersion is compensated by nonlinear effects. Soliton research has been conducted in fields as diverse as particle physics, molecular biology, geology, oceanography, astrophysics, and nonlinear optics. Perhaps the most prominent application of solitons is in high-rate telecommunications with optical fibers (*1*).

We use a Bose-Einstein condensate (BEC) of a dilute atomic gas of lithium atoms as a macroscopic matter-wave to form a soliton. Nonlinearity is provided by binary atomic interactions leading to the mean-field potential $U(\vec{r}) = gn(\vec{r}) = 4\pi\hbar^2 an(\vec{r})/m$, where a is the scattering length, $n(\vec{r})$ the spatial density, and m the atomic mass. For $a < 0$ the effective interaction is attractive, and a trapped BEC is only stable for a number of atoms less than a critical number above which collapse occurs (*2–4*). When the BEC is confined in only two directions, matter-waves have dispersion in the free direction owing to their kinetic energy, $E_{kin} \propto k^2$, where k is the atomic wave vector. The balance between this dispersion and the attractive mean-field energy can lead to the formation of bright solitons as shown theoretically (*5–7*). Until now, only dark solitons have been observed in BECs with repulsive interactions ($a > 0$)

[1]Laboratoire Kastler Brossel, Ecole Normale Supérieure, 24 rue Lhomond, 75231 Paris Cedex 05, France. [2]European Laboratory for Non-Linear Spectroscopy–Istituto Nazionale per la Fisica della Materia, Largo E. Fermi 2, Firenze 50125, Italy.

*To whom correspondence should be addressed. E-mail: salomon@lkb.ens.fr

(*8*, *9*). These solitons are characterized by a notch in the BEC density profile with a phase step across the soliton center. They propagate within the BEC with a velocity less than the speed of sound, but so far are found to decay before reaching the edge of the condensate.

We report the formation of a matter-wave bright soliton, a freely propagating self-bound atomic gas. The soliton is produced from a ^{7}Li BEC in the internal atomic state $|F = 1, m_F = 1\rangle$. In this state a Feshbach resonance allows us to continuously tune the scattering length from a positive to negative value by means of an applied magnetic field (*10*, *11*), a requirement for the production of a bright soliton.

In our experimental setup (*12*–*14*), 4×10^8 ^{7}Li atoms are loaded from a magneto-optical trap into a strongly confining Ioffe-Pritchard (IP) magnetic trap. Atoms are in the $|F = 2, m_F = 2\rangle$ state for which the scattering length is $a = -1.4$ nm. Evaporative cooling lowers the temperature from 2 mK to 10 μK, after which $\sim 6 \times 10^5$ atoms remain. Atoms are then transferred into a far detuned optical dipole trap at the intersection of two Nd:YAG (yttrium-aluminum-garnet) Gaussian laser beams (Fig. 1) with common waists of 38(3) μm (*15*). The 9.5, W laser power is split between the two beams by means of two acousto-optic modulators.

The transfer from the magnetic trap to the optical trap is done in two steps. First, the power of the YAG beams is ramped over 200 ms to a value such that the radial oscillation frequency of the atoms is 1.8 kHz in the vertical beam and 3.3 kHz in the horizontal beam, which matches that of the IP trap. Second, the magnetic trap is slowly turned off over 200 ms,

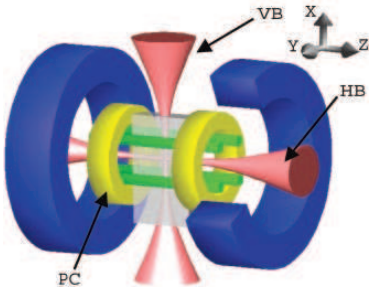

Fig. 1. Experimental setup for soliton production. ^{7}Li atoms are evaporatively cooled in a Ioffe-Pritchard magnetic trap and transferred into a crossed optical dipole trap in state $|F = 1, m_F = 1\rangle$ where they Bose condense. Magnetic tuning of the scattering length to positive, zero, and negative values is performed with the two pinch coils (PC). Switching-off the vertical trapping beam (VB) allows propagation of a soliton in the horizontal 1D waveguide (HB). Absorption images of solitons and BECs are recorded on a charge-coupled device camera in the *x*, *z* plane.

keeping only a 5-G bias field. The transfer efficiency is nearly 100%. Then, transfer from the state $|F = 2, m_F = 2\rangle$ to the state $|F = 1, m_F = 1\rangle$ is performed by rapid adiabatic passage with a microwave-frequency sweep scanning 1 MHz in 10 ms at ~820 MHz. The transfer efficiency is better than 95%. Among all ^{7}Li hyperfine states that can be trapped in the dipole trap, $|F = 1, m_F = 1\rangle$ is particularly useful as it is the lowest energy state in which two-body losses, which are relatively strong in the state $|F = 2, m_F = 2\rangle$ (*13*), are completely suppressed. Furthermore, this state is predicted to have a Feshbach resonance near 725 G (*11*), allowing magnetic tuning of the scattering length (Fig. 2). An adjustable magnetic field is produced by the pinch coils of our IP trap. Their inductance is small so that their current can be changed on a time scale shorter than ~200 μs. As in previous work on ^{23}Na and ^{85}Rb (*16*, *17*), we locate the ^{7}Li Feshbach resonance through observation of a dramatic loss of trapped atoms that we experimentally identify as being due to three-body recombination. The resonance position is found at 720(15) G, in good agreement with theory (725 G) (*11*).

We then produce a ^{7}Li BEC in the crossed dipole trap by forced evaporation achieved by lowering the depth of the optical trapping potential (*18*). Between $B = 0$ and $B = 590$ G, the scattering length is small ($|a| \leq 0.4$ nm), hindering efficient evaporative cooling (Fig. 2). Therefore, we operate at a magnetic field of 665 G in the wing of the Feshbach resonance where $a \cong +2.1$ nm and where three-body losses remain moderate. The horizontal (vertical) optical power is lowered from 5.5 W (1.5 W) to 1.15 W (0.9 W) in 100 ms, and then to 0.27 W (0.19 W) in 150 ms. A condensate with $N \sim 2 \times 10^4$ atoms, about half of the total number of atoms, is obtained in a nearly isotropic trap where atoms have oscillation frequencies of 710, 1000, and 710 Hz along *x*, *y*, and *z* axes. We then tune the scattering length to zero to reduce three-body losses.

To transform the BEC into a bright soliton, the trapping geometry is adiabatically deformed to a cylindrical geometry obtained by keeping only the horizontal trapping beam. To ensure adiabatic deformation of the condensate, the vertical beam power is ramped down to 3 mW in 200 ms, which reduces the axial oscillation frequency of the atoms to $\omega_z \cong 2\pi \times 50$ Hz while the radial oscillation frequency remains $\omega_\perp = 2\pi \times 710$ Hz. The effective interaction is then tuned through changes in the magnetic field in 50 ms. Finally, switching off the vertical beam with a mechanical shutter releases the BEC into the horizontal one-dimensional (1D) waveguide. In the axial direction, the coils that are used to provide the offset field produce a slightly expulsive harmonic potential for the state $|F = 1, m_F = 1\rangle$, which overcomes the dipole trap. The resulting axial force on the atoms is conveniently written as $-m\omega_z^2 z$, where the frequency ω_z is now imaginary. Typically, $\omega_z = 2i\pi \times 78$ Hz for $B = 520$ G. After an adjustable evolution time in the horizontal guide, the bias magnetic field is turned off, and 400 μs later an absorption image is recorded (Fig. 3; see supplemental movie on *Science* Online at www.sciencemag.org/cgi/content/full/296/5571/1290/DC1) where the formation of the soliton is seen.

We compare the evolution of an ideal gas (Fig. 3A), $a \cong 0$ for $B = 520$ G, with a gas with attractive interactions (Fig. 3B), $a = -0.21$ nm for $B = 425$ G. In both cases the cloud drifts toward the left because of a small offset, ≅50 μm, between the maximum of the expulsive potential and the initial position of the atoms. The width of the expanding cloud in the horizontal waveguide is considerably broader in the noninteracting case, while for all times of observation the soliton width remains equal to the resolution limit of our imaging system, 9(1) μm axially (*19*). The cloud contains $6(2) \times 10^3$ atoms and propagates over a distance of 1.1 mm without any detectable dispersion, a clear signature of a bright soliton (*20*). No decay of the soliton is observed in the 10 ms it remains in the detection region. A substantial fraction of

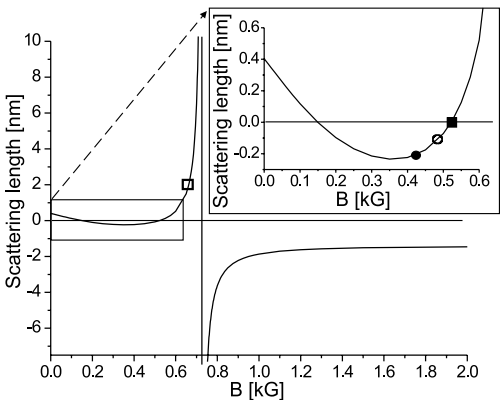

Fig. 2. Predicted magnetic field dependence of the scattering length *a* for ^{7}Li in state $|F = 1, m_F = 1\rangle$ (*11*). (**Inset**) Expanded view of the 0 to 0.6 kG interval with the various values of *a* used to study soliton formation. (□) Initial BEC; (■) ideal BEC gas; (○) attractive gas; (●) soliton.

atoms, ≅2/3, remains in a noncondensed pedestal around the soliton, clearly visible for intermediate propagation times in the guide.

We then made measurements of the wave-packet size versus propagation time for three values of the scattering length: $a \cong 0$, $a \cong -0.11$ nm, and $a \cong -0.21$ nm (Fig. 4). For $a \cong 0$ (Fig. 4A), the interaction between atoms is negligible, and the size of the cloud is governed by the expansion of the initial condensate distribution under the influence of the negative curvature of the axial potential. The measured size is in excellent agreement with the predicted size of a noninteracting gas subjected to an expulsive harmonic potential: Taking the curvature as a fit parameter (solid line in Fig. 4A), we find $\omega_z = 2i\pi \times 78(3)$ Hz, which agrees with the expected value of the curvature produced by the pinch coils (*14*). For $a = -0.11$ nm and $B = 487$ G, the size of the wave packet is consistently below that of a noninteracting gas (Fig. 4B, solid line). Attractive interactions reduce the size of the atomic cloud but are not strong enough to stabilize the soliton against the expulsive potential. When a is further decreased to -0.21 nm, the measured size of the wave packet no longer changes as a function of guiding time, indicating propagation without dispersion even in the presence of the expulsive potential (Fig. 4C).

To theoretically analyze the stability of the soliton, we introduce the 3D Gross-Pitaevskii energy functional

$$E_{GP} = \int d^3r \left[\frac{\hbar^2}{2m} |\nabla\Psi(\vec{r})|^2 + \frac{Ng}{2}|\Psi(\vec{r})|^4 + \frac{1}{2} m \left[\omega_\perp^2 (x^2+y^2) + \omega_z^2 z^2\right] |\Psi(\vec{r})|^2 \right] \quad (1)$$

where the condensate wave function Ψ is normalized to 1. In Eq. 1 the first term is the kinetic energy responsible for dispersion; the second term is the interaction energy, which in the present case of attractive effective interactions ($g < 0$) causes the wave function to sharpen; and the third term is the external potential energy. We introduce the following two-parameter variational ansatz to estimate minimal-energy states of E_{GP}:

$$\Psi(\vec{r}) = \frac{1}{\sqrt{2\pi\sigma_\perp^2 l_z}} \frac{1}{\cosh(z/l_z)} \exp\left(-\frac{x^2+y^2}{2\sigma_\perp^2}\right) \quad (2)$$

where $\sigma_\perp$ and l_z are the radial and axial widths of the wave function. The functional form of the well-known 1D soliton has been chosen for the longitudinal direction (*5*), while in the transverse direction a Gaussian ansatz is the optimal one for harmonic confinement. For each l_z we minimize the mean energy over $\sigma_\perp$; the resulting function of l_z is plotted (Fig. 5) for various values of the parameter $Na/a_\perp^{ho}$ where $a_\perp^{ho} = (\hbar/m\omega_\perp)^{1/2}$. For very small axial sizes, the interaction energy becomes on the order of $-\hbar\,\omega_\perp$ and the gas loses its quasi-1D nature and collapses (*3*, *4*). For very large axial sizes, the expulsive potential energy dominates and pulls the wave function apart. For intermediate sizes, attractive interactions balance both the dispersion and the effect of the expulsive potential; the energy presents a local minimum (solid line in Fig. 5). This minimum supports a macroscopic quantum bound state. However, it exists only within a narrow window of the parameter $Na/a_\perp^{ho}$. In our experiments $\omega_\perp = 2\pi \times 710$ Hz and $\omega_z = 2i\pi \times 70$ Hz for $B = 420$ G, so that $a_\perp^{ho} = 1.4$ μm; for $N|a|$ larger than $(N|a|)_c = 1.105$ μm, a collapse occurs (dashed curve in Fig. 5), while for $N|a|$ smaller than $(N|a|)_e = 0.88$ μm the expulsive potential causes the gas to explode axially (dotted curve in Fig. 5).

For our experimental conditions and $a = -0.21$ nm, the number of atoms that allows the soliton to be formed is $4.2 \times 10^3 \leq N \leq 5.2 \times 10^3$, in good agreement with our measured number $6(2) \times 10^3$. The expected axial size of the soliton is $l_z \cong 1.7$ μm, which is below the current resolution limit of our imaging system. To verify the presence of a critical value of $N|a|_e$ needed to stabilize the soliton, we have performed the measurements with the same a but with a reduced number of atoms, $N = 2 \times 10^3$. At 8 ms guiding time the axial size of the wave packet increased to 30 μm, indicating that no soliton was formed.

One may speculate as to the formation dynamics of the soliton in the elongated trap before its release in the optical waveguide. Because the atom number in the initial BEC, $2 \times$

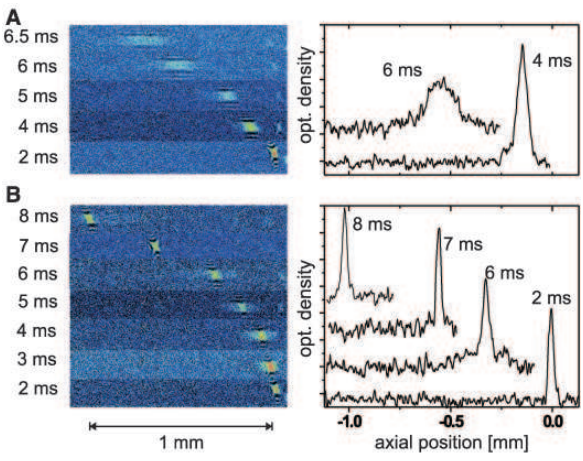

Fig. 3. Absorption images at variable delays after switching off the vertical trapping beam. Propagation of an ideal BEC gas (**A**) and of a soliton (**B**) in the horizontal 1D waveguide in the presence of an expulsive potential. Propagation without dispersion over 1.1 mm is a clear signature of a soliton. Corresponding axial profiles are integrated over the vertical direction.

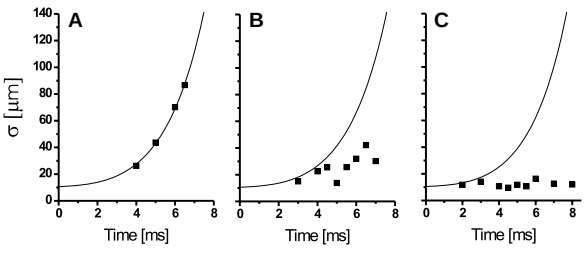

Fig. 4. Measured root mean square size of the atomic wave packet Gaussian fit as a function of propagation time in the waveguide. (**A**) $a = 0$, ideal gas case; (**B**) $a = -0.11$ nm; (**C**) $a = -0.21$ nm; solid lines: calculated expansion of a noninteracting gas in the expulsive potential.

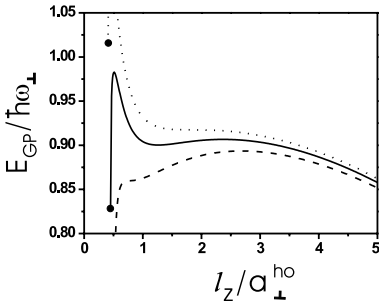

Fig. 5. Theoretical energy diagram of an attractive Bose gas subjected to an expulsive potential for $\omega_z/\omega_\perp = i \times 70/710$. The energy as a function of the axial size after minimization over the tranverse size is shown for three values of $N|a|$: within the stability window (solid curve), at the critical point for explosion $(N|a|)_e$ (dotted curve), and at the critical point for collapse $(N|a|)_c$ (dashed curve). End points of the curves indicate collapse, i.e., $\sigma_\perp = 0$.

10^4, is about three times as large as the measured atom number in the soliton, it is likely that during the 50 ms phase where a is changed from 0 to negative values, one or several collapses occur until the critical number for a stable BEC is reached. Indeed, the collapse time constant is predicted to be much less than 50 ms for our experimental conditions (*21*). During the transfer into the 1D waveguide, the BEC is transformed into a soliton and the noncondensed cloud is clearly observed at guiding times up to 6 ms as a broader background distribution. Nonadiabatic projection of the BEC from the confining onto the expulsive potential is expected to play a negligible role here, according to numerical simulations (*22*). At longer times, the noncondensed atoms spread apart and become undetectable. Thus, during the propagation phase the soliton decouples itself from the noncondensed fraction, resulting in a nearly pure soliton.

Finally, removal of the expulsive axial potential will allow us to extend the stability domain toward lower values of $N|a|$ and longer observation times. The soliton size could then be measured in situ, as well as its lifetime. The study of coherence properties of solitons and of binary collisions between solitons is an immediate extension of the present work.

References and Notes

1. See, for example, the recent special issue: *Chaos* **10**, 471 (2000).
2. P. A. Ruprecht, M. J. Holland, K. Burnett, M. Edwards, *Phys. Rev. A* **51**, 4704 (1995).
3. C. C. Bradley, C. A. Sackett, R. G. Hulet, *Phys. Rev. Lett.* **78**, 985 (1997).
4. J. L. Roberts *et al.*, *Phys. Rev. Lett.* **86**, 4211 (2001).
5. V. E. Zakharov, A. B. Shabat, *Sov. Phys. JETP* **34**, 62 (1972).
6. V. M. Pèrez-Garcìa, H. Michinel, H. Herrero, *Phys. Rev. A* **57**, 3837 (1998).
7. L. D. Carr, M. A. Leung, W. P. Reinhardt, *J. Phys. B* **33**, 3983 (2000).
8. S. Burger *et al.*, *Phys. Rev. Lett.* **83**, 5198 (1999).
9. J. Denschlag *et al.*, *Science* **287**, 97 (2000).
10. E. Tiesinga, B. J. Verhaar, H. T. S. Stoof, *Phys. Rev. A* **47**, 4114 (1993).
11. V. Venturi, C. Williams, personal communication.
12. M.-O. Mewes, G. Ferrari, F. Schreck, A. Sinatra, C. Salomon, *Phys. Rev. A* **61**, 011403R (2000).
13. F. Schreck *et al.*, *Phys. Rev. A* **64**, 011402R (2001).
14. F. Schreck *et al.*, *Phys. Rev. Lett.* **87**, 080403 (2001).
15. See, for instance, R. Grimm, M. Weidemüller, Y. B. Ovchinnikov, *Adv. At. Mol. Opt. Phys.* **42**, 95 (2000).
16. S. Inouye *et al.*, *Nature* **392**, 151 (1998).
17. J. L. Roberts, N. R. Claussen, S. L. Cornish, C. E. Wieman, *Phys. Rev. Lett.* **85**, 728 (2000).
18. M. D. Barrett, J. A. Sauer, M. S. Chapman, *Phys. Rev. Lett.* **87**, 010404 (2001).
19. In the vertical direction, a residual astigmatism of the imaging system gives a resolution limit of 16 μm.
20. Over this distance, the change in magnetic field due to the curvature is 0.1 G, and therefore the change in the scattering length is negligible (Fig. 2).
21. Y. Kagan, A. E. Muryshev, G. V. Shlyapnikov, *Phys. Rev. Lett.* **81**, 933 (1998).
22. L. D. Carr, Y. Castin, in preparation.

23. We are grateful to K. Corwin, M. Olshanii, G. Shlyapnikov, C. Williams, V. Venturi, and B. Esry for important contributions to this work and to J. Dalibard and C. Cohen-Tannoudji for useful discussions. Supported by the DAAD (F.S.), the European Union network CT 2000-00165 CAUAC (G.F.), and the NSF MPS-DRF 0104447 (L.D.C.). This work was supported by CNRS, Collège de France and Région Ile de France. Laboratoire Kastler Brossel is Unité de recherche de l'Ecole Normale Supérieure et de l'Université Pierre et Marie Curie, associated with CNRS.

19 February 2002; accepted 5 April 2002

Electrochemistry and Electrogenerated Chemiluminescence from Silicon Nanocrystal Quantum Dots

Zhifeng Ding,[1] Bernadette M. Quinn,[1] Santosh K. Haram,[1] Lindsay E. Pell,[2] Brian A. Korgel,[2]* Allen J. Bard[1]*

Reversible electrochemical injection of discrete numbers of electrons into sterically stabilized silicon nanocrystals (NCs) (~2 to 4 nanometers in diameter) was observed by differential pulse voltammetry (DPV) in *N*,*N*′-dimethylformamide and acetonitrile. The electrochemical gap between the onset of electron injection and hole injection—related to the highest occupied and lowest unoccupied molecular orbitals—grew with decreasing nanocrystal size, and the DPV peak potentials above the onset for electron injection roughly correspond to expected Coulomb blockade or quantized double-layer charging energies. Electron transfer reactions between positively and negatively charged nanocrystals (or between charged nanocrystals and molecular redox-active coreactants) occurred that led to electron and hole annihilation, producing visible light. The electrogenerated chemiluminescence spectra exhibited a peak maximum at 640 nanometers, a significant red shift from the photoluminescence maximum (420 nanometers) of the same silicon NC solution. These results demonstrate that the chemical stability of silicon NCs could enable their use as redox-active macromolecular species with the combined optical and charging properties of semiconductor quantum dots.

In a bulk semiconductor, electrons and holes move freely throughout the crystal. However, in a nanocrystal, confinement of the electrons and holes leads to a variety of optical and electronic consequences, including size-dependent molecular-like optical properties, greater electron/hole overlap for enhanced photoluminescence (PL) efficiencies, and discrete single-electron/hole charging. Because of their enormous surface area–to–volume ratios, nanocrystals (NCs) are highly susceptible to heterogeneous redox chemistry with the surrounding environment. Depending on the semiconductor and the surface chemistry, this chemical reactivity can lead to either fatal chemical degradation or new useful properties, such as reversible photocatalytic and electrochromic properties and redox reactivity.

Semiconductor NCs have been prepared with narrow size distributions, controlled surface chemistry, and internal bulk crystal structure (*1*, *2*), and adsorbed capping ligands are often used to control size and prevent irreversible aggregation. Although the electrochemical properties of monolayer-protected metallic NCs have been well documented (*3*, *4*), reports concerning the electrochemical properties of semiconductor NCs remain scarce (*5*–*9*). Difficulties include the limited potential window available in aqueous solutions, the limited solubility of many NCs in nonaqueous solvents, and the need for highly pure, isolated, monodisperse dots. Compound semiconductor NCs, such as CdS, are also chemically unstable upon electron transfer. For example, CdS NCs are irreversibly oxidized and reduced when electron transfer occurs at an electrode (*9*). Elemental semiconductor NCs, such as Si and Ge, should be more stable. Here we show that monolayer-protected Si NCs are chemically stable upon electron and hole injection; furthermore, electron/hole annihilation through electron transfer reactions between NCs, or NCs with redox-active coreactants, leads to visible light production [electrogenerated chemiluminescence (ECL)].

We recently developed a new synthetic strategy to produce Si NCs terminated with a

[1]Department of Chemistry and Biochemistry, [2]Department of Chemical Engineering, Center for Nano- and Molecular Science and Technology, Texas Materials Institute, The University of Texas at Austin, Austin, TX 78712, USA.

*To whom correspondence should be addressed. E-mail: ajbard@mail.utexas.edu (A.J.B.); korgel@mail.che.utexas.edu (B.A.K.).

Chapitre 6

Orientations futures de nos travaux

Nous avons vu que la dernière percée effectuée dans le domaine des atomes ultrafroids consiste en la possibilité de préparer des gaz d'atomes fermioniques fortement dégénérés dans le régime d'interaction forte, c'est-à-dire dans le régime où le produit $k_F a$ (du module du vecteur d'onde de Fermi k_F et de la longueur de diffusion a associée au potentiel d'interaction entre atomes) est beaucoup plus grand que un en valeur absolue. Ceci est rendu possible par la technique dite des résonances de Feshbach qui permet, par l'application d'un champ magnétique, d'ajuster la valeur de la longueur de diffusion virtuellement entre $+\infty$ et $-\infty$! Les gaz de Fermi ainsi produits sont en interaction plus forte que les étoiles à neutrons, pour lesquelles $k_F|a| < 1$, et sont par ailleurs stables, c'est-à-dire qu'ils ne présentent pas de pertes appréciables par collisions inélastiques. Ils permettent d'étudier le passage continu d'un condensat de Bose-Einstein de molécules dimères à un condensat de paires de Cooper (état BCS), par variation continue de $1/a$ de $+\infty$ à $-\infty$. En particulier, ils donnent naissance, dans la limite $k_F|a| \to +\infty$, à un nouveau système quantique à N corps, le gaz quantique unitaire, peut-être le problème quantique à N corps le plus pur car il est à zéro paramètre, la valeur de la longueur de diffusion disparaissant du Hamiltonien.

Ces gaz de Fermi en interaction forte constituent donc, comme on le verra plus bas, une partie importante de nos projets de recherche. Mais l'on voit émerger dans le domaine une autre thématique, l'utilisation des gaz quantiques pour simuler des Hamiltoniens modèles dont la résolution, difficile par ailleurs, permettrait de résoudre certains problèmes ouverts de la physique de la matière condensée, comme la supraconductivité à haute température critique, les états fortement corrélés de type Hall quantique, ou les effets respectifs du désordre et des interactions dans les systèmes d'électrons présentant des transitions de type conducteur-isolant. Comme indiqué plus bas, l'introduction d'un désordre contrôlé dans les systèmes d'atomes froids est un élément important de nos projets.

À long terme, et ceci conclura la liste de nos projets, la possibilité de manipuler de l'information quantique à l'aide de systèmes atomiques ultrafroids est aussi à envisager sérieusement, depuis qu'existe la possibilité expérimentale de préparer des condensats gazeux sur des micro-puces, la première étape étant peut-être l'étude de la possibilité de produire des états fortement intriqués de type "chats de Schrödinger" avec des atomes.

6.1 Étude de gaz de fermions superfluides en rotation

Un enjeu actuellement très important est d'obtenir expérimentalement une preuve de la superfluidité de ces gaz fermioniques. Cette superfluidité semble acquise du côté de la résonance de Feshbach où les longueurs de diffusion sont positives, les fermions

s'assemblant alors en molécules bosoniques dont on a observé la condensation de Bose-Einstein. La superfluidité n'a cependant pas été démontrée expérimentalement du côté où les longueurs de diffusion sont négatives, qui inclut le domaine des condensats de paires de Cooper à la BCS.

Les théoriciens pensaient initialement qu'il suffirait de mettre en évidence un comportement de nature hydrodynamique de ces gaz (par exemple, en regardant leur expansion après coupure du piège les contenant) pour démontrer leur superfluidité. Cependant, dans le régime d'interaction forte, même la phase non superfluide du gaz peut adopter un comportement hydrodynamique. Il est bien compris maintenant qu'il s'agit de mettre un évidence un comportement caractéristique de l'hydrodynamique superfluide, absent de l'hydrodynamique d'un gaz normal. L'un des meilleurs candidats semble être la production et l'observation de tourbillons quantiques dans un gaz de Fermi en rotation.

Nous avons donc le projet d'étudier le diagramme de phase du système dans le plan (longueur de diffusion, fréquence de rotation), dans un premier temps à température nulle avec la fonction d'essai variationnelle de BCS. Ce diagramme contiendra beaucoup d'informations : par exemple, la fréquence minimale de rotation à partir de laquelle les tourbillons quantiques peuvent être stabilisés, ainsi que l'évolution d'un réseau de tourbillons stationnaire lorsqu'on change la longueur de diffusion de part et d'autre de la résonance de Feshbach. Ce passage d'un côté à l'autre de la résonance semble être très pertinent du point de vue expérimental car la détection des tourbillons est facile du côté des condensats de dimères bosoniques, chaque tourbillon se manifestant par un trou de bon contraste dans le profil de densité du nuage, alors qu'aucun trou de bon contraste n'est attendu du côté BCS.

Par ailleurs, au moins du côté bosonique, on s'attend à avoir une transition de phase quantique d'un condensat à une phase fortement corrélée de type effet Hall quantique fractionnaire, lorsque la fréquence de rotation du gaz est égale à la fréquence d'oscillation des atomes dans le potentiel de piégeage harmonique. Dans ce cas, en effet, le Hamiltonien d'un atome est formellement identique à celui d'une particule chargée dans un champ magnétique uniforme, si bien que ceci ouvre la possibilité d'étudier l'effet Hall quantique fractionnaire avec des atomes ! Les techniques théoriques à utiliser sont des diagonalisations exactes à petit nombre de particules, et nous envisageons à ce propos une collaboration avec Thierry Jolicœur du Laboratoire Pierre Aigrain de l'Ecole normale supérieure. Un problème ouvert sera alors de déterminer si cette transition de phase quantique peut perdurer au-delà de la résonance de Feshbach, c'est-à-dire du côté des longueurs de diffusion négatives.

6.2 Les gaz quantiques dans le régime d'interaction forte

6.2.1 Problèmes à petit nombre de corps pour une interaction modèle : étude analytique

Le problème des gaz quantiques en interaction forte réclame une modélisation du potentiel d'interaction beaucoup plus prudente que dans le régime d'interaction faible. Il convient en particulier de vérifier que le Hamiltonien modèle choisi, en général à base d'interactions de contact régularisées, est bien hermitien et conduit à une équation de Schrödinger admettant effectivement des solutions. Il faut voir aussi si le contenu physique est assez riche pour bien modéliser les expériences.

Un bon exemple de cette problématique est l'utilisation du modèle dit du pseudo-potentiel de Fermi. Ce modèle ne comporte pas toujours des solutions acceptables mathématiquement, et peut conduire à des spectres continus non bornés inférieurement (ce qui est un signe de non hermiticité). C'est le cas du problème à trois corps bosoniques avec le pseudo-potentiel de Fermi, qui est un problème mal posé.

Le projet consiste à tester différents modèles par la résolution exacte de problèmes à 3 ou 4 corps, ce qui donnera confiance ensuite pour leur utilisation dans d'éventuelles études analytiques du problème à N corps. Une application remarquable des interactions de contact est le calcul de la longueur de diffusion de deux dimères formés de fermions liés, par G. Shlyapnikov et D. Petrov, à l'aide du pseudo-potentiel de Fermi. Mais qu'en est-il dans le cas de dimères formés de bosons ? Que substituer au pseudo-potentiel de Fermi ?

Une autre série d'applications de ces calculs sera d'étudier la diffusion mutuelle d'atomes ou de molécules en présence d'un fort confinement, pour ouvrir la voie à des expériences en dimensionalité effective réduite (2D ou 1D), avec à la clé l'observation à 2D de la transition de Kosterlitz-Thouless dans le régime d'interaction forte. Tout ceci fera l'objet de la thèse de Félix Werner.

6.2.2 Le gaz quantique unitaire : étude numérique par Monte-Carlo quantique

La difficulté de l'étude du gaz quantique unitaire (au moins à basse température) est qu'il ne semble y avoir aucun petit paramètre (même si une piste à creuser consiste à prendre $1/D$ comme petit paramètre, où D est la dimension de l'espace-temps ; une collaboration est prévue avec Antoine Georges, du centre de physique théorique de l'École polytechnique, sur la méthode "dynamical mean field theory", exacte en dimension infinie). Pour obtenir des prédictions précises, en particulier à température non nulle, une étude numérique par Monte-Carlo quantique semble nécessaire.

Dans le cas des bosons, les méthodes Monte-Carlo quantiques sont très efficaces pour échantillonner de manière exacte l'état d'équilibre thermodynamique. Cependant, il semble que le gaz quantique unitaire ne puisse pas être, pour des bosons, l'état fondamental d'un quelconque Hamiltonien modèle avec des interactions à très courte portée. Ce qui interdit d'utiliser l'hypothèse d'équilibre thermodynamique...

Que se passe-t-il dans le cas des fermions ? La sagesse populaire sait bien que les méthodes Monte-Carlo quantiques peuvent être sujettes, dans ce cas, au problème de signe : la fonction de partition s'obtient comme la moyenne Monte-Carlo d'une quantité de signe variable ; une presque parfaite compensation des contributions > 0 et < 0 peut se produire alors, conduisant à une complexité algorithmique exponentielle (et donc rédhibitoire) en le nombre de particules. Cependant, il existe des exceptions à cette règle : le "determinantal Monte Carlo" pour des fermions sur réseau avec interactions attractives ne présente aucun problème de signe. Or, nous avons récemment construit un modèle sur réseau qui semble bien décrire le gaz quantique unitaire dans l'espace continu (à la limite où le pas du réseau tend vers zéro) et qui correspond à des interactions attractives entre les fermions. Ceci ouvre la voie aux simulations Monte-Carlo quantiques pour ces gaz, voie dans laquelle nous nous engagerons.

6.3 Localisation d'Anderson d'ondes matérielles

Il a été prévu qu'une onde soumise à un potentiel aléatoire s'étendant dans tout l'espace possède des états stationnaire de carré sommable : l'onde, au lieu de se propager, est localisée spatialement par le désordre. L'observation de ce phénomène de localisation d'Anderson avec des ondes lumineuses avait été annoncée il y a quelques années dans un échantillon de poudres de semi-conducteurs, mais est maintenant controversée, l'amortissement de l'intensité lumineuse incohérente transmise, exponentiel en la taille de l'échantillon, pouvant être interprété non seulement comme un effet de localisation d'Anderson mais aussi comme un simple effet d'absorption. Par ailleurs, l'observation avec des électrons dans les systèmes de physique de la matière condensée est indirecte et d'interprétation rendue difficile par l'existence d'interactions entre électrons et d'un couplage à un bain thermique.

Il est donc intéressant d'étudier ce problème fondamental avec d'autres systèmes présentant une absorption, des interactions et une décohérence négligeables ou contrôlables.

Nous avons déjà étudié théoriquement la possibilité de localiser la lumière dans un nuage dense d'atomes ultrafroids, dans un modèle simple négligeant le mouvement des atomes (une partie du travail doctoral d'Emmanuel Mandonnet, effectuée sous notre direction). Les effets prédits sont alors spectaculaires : pour une variation modeste de la densité atomique autour de la valeur critique conduisant à la localisation, les temps maximaux de piégeage de la lumière dans le gaz varient de plusieurs ordres de grandeur. La prise en compte du mouvement des atomes est cependant nécessaire pour rendre ces prédictions réalistes. C'est un problème difficile, et l'on peut craindre que l'interaction dipolaire résonnante entre un atome excité et un atome fondamental conduise à l'accélération des deux atomes, ce qui pourrait casser l'effet d'interférence à la base de la localisation d'Anderson.

Nous proposons donc d'ouvrir une nouvelle ligne d'attaque, celle de la localisation des ondes de matière cohérentes (issues d'un condensat de Bose-Einstein) dans un potentiel désordonné, par exemple dans le potentiel lumineux aléatoire d'une figure de tavelure. Une étude théorique doit être faite pour distinguer les effets de localisation d'un simple piégeage des atomes dans des minima locaux de potentiel lumineux. Elle semble cependant difficile à mener à 3D dans le potentiel d'une figure de tavelure.

Mais nous avons très récemment identifié une façon plus contrôlable de créer un potentiel désordonné, éliminant l'objection du risque de piégeage des atomes dans des minima locaux de potentiel, et conduisant aussi à un modèle plus facilement analysable. L'idée est d'utiliser deux espèces atomiques :

- L'espèce numéro 1 est piégée aux nœuds d'un réseau optique, chaque nœud comportant de façon aléatoire soit un seul atome dans l'état vibrationnel fondamental, soit aucun atome ; une telle configuration peut être produite expérimentalement en partant d'une phase fortement corrélé dite "de Mott", dans laquelle il y a un atome par site, et en induisant ensuite des pertes. Il faut se placer bien sûr dans un régime où l'effet tunnel est négligeable, pour assurer que le désordre soit stationnaire.
- L'espèce numéro 2 ne 'voit' pas le potentiel optique piégeant l'espèce 1, par exemple parce que sa fréquence de résonance est différente. Elle se propage donc en subissant des diffusions sur les atomes de l'espèce 1, diffusions qui sont élastiques lorsque l'énergie cinétique de l'espèce 2 est inférieure au quantum de vibration de l'espèce 1 dans les micro-puits du réseau.

Ainsi, l'espèce 2 est susceptible de subir la localisation d'Anderson dans le potentiel désordonné créé par l'espèce 1. Ce potentiel est représentable par une somme de potentiels

de contact, ce qui rend le modèle calculable, au contraire d'un potentiel de type 'figure de tavelure'! On pourra ensuite introduire des ingrédients contrôlés dont les physiciens de la matière condensée se demandent comment ils affectent la localisation d'Anderson : un bain thermique artificiel couplé à l'espèce 2 (construit à partir de certaines techniques proposées par Peter Zoller), ainsi que des canaux multiples de diffusion pour l'espèce 1 (par exemple, en la piégeant dans différents guides à ondes de matière couplés par effet tunnel), ou même des interactions entre atomes de l'espèce 1.

6.4 États intriqués de type "chats de Schrödinger" et traitement quantique de l'information avec des gaz atomiques

Dans un régime de très basse température, avec des systèmes à très petit nombre de particules (de l'ordre d'une dizaine ou d'une centaine d'atomes), les mécanismes de décohérence intrinsèques à un gaz atomique condensé (pertes de particules par collisions inélastiques, interaction du condensat avec les particules non condensées) sont fortement réduits, et l'on peut espérer mettre alors en évidence expérimentalement des effets purement quantiques de dynamique du champ dans un condensat, en particulier dans des expériences sur micro-puces. Ceci ouvrirait la voie à un traitement quantique de l'information avec des condensats.

Nous avons donc pour objectif d'explorer théoriquement les potentialités qu'ont ces systèmes de produire des états quantiques intriqués, par exemple de type 'chats de Schrödinger', en incluant les différents mécanismes de décohérence mentionnés plus haut. Deux lignes d'attaque principales nous paraissent se présenter.

La première possibilité est d'utiliser l'évolution temporelle du système, rendue non triviale par les interactions, à partir d'un état simple à préparer. L'exemple type est celui du champ bosonique à deux modes spatialement séparés : un condensat (correspondant à une phase relative du champ bien définie entre les deux modes) évolue, par le seul effet des interactions entre particules de chaque mode, en un chat de Schrödinger, c'est-à-dire ici en la superposition cohérente de deux condensats dans des états orthogonaux.

La seconde possibilité est d'identifier des systèmes dont l'état fondamental est lui-même un chat de Schrödinger. Un exemple simple est celui de modes bosoniques couplés (par effet tunnel pour des modes spatiaux séparés) et avec interaction attractive entre les particules. La difficulté est alors de pouvoir préparer le système à une température plus basse que l'écart d'énergie entre l'état fondamental et le premier état excité, ce qui peut exiger l'élaboration de techniques de refroidissement encore plus performantes que celles existantes, par exemple par suivi adiabatique.

À plus long terme, cette ligne de recherche se généralisera en l'étude d'un possible traitement quantique de l'information avec des atomes froids. La configuration la plus prometteuse pour l'instant paraît être celle d'atomes piégés aux nœuds d'un réseau optique, comment le montrent les travaux pionniers de Peter Zoller et Ignacio Cirac pour la théorie, et d'Immanuel Bloch pour les expériences.

Chapitre 7

Curriculum vitæ

Yvan CASTIN
Né le 11/05/1966 à Metz, marié, un enfant.
Chargé de Recherche CNRS, CR1
Laboratoire Kastler Brossel, Ecole normale supérieure
24, rue Lhomond, 75 231 Paris Cedex 5.
Tél : 01 44 32 34 25 Fax : 01 44 32 34 34
Courriel : yvan.castin@lkb.ens.fr

Formation

- 1984-1986 : Classe préparatoire au lycée Louis le Grand, Paris.
- 1986 : Entrée à l'Ecole normale supérieure (Ulm sciences, groupe maths).
- 1987 : Licence de physique (mention TB).
- 1988 : Maîtrise de physique (mention TB), et DEA de physique quantique (Paris VI, mention TB, rang : 1).
- 1989 : Magistère de physique (mention TB).
- 1990 : Agrégation de physique (rang : 3).
- 1988-1992 : Thèse de physique quantique au Laboratoire Kastler Brossel de l'Ecole normale supérieure, sous la direction de Jean Dalibard : "Les limites du refroidissement laser dans les mélasses optiques à une dimension".
- 1990-1991 : Agrégé préparateur au Département de physique de l'Ecole normale supérieure.
- 1991-1992 : Scientifique du contingent au CEA-DAM.
- 1992-1993 : Agrégé préparateur au Département de physique de l'Ecole normale supérieure.
- Depuis septembre 1993 : chargé de recherche au CNRS, dans le groupe du Professeur Cohen-Tannoudji au Laboratoire Kastler Brossel.

Distinctions

- 1984 : $3^{\text{ème}}$ prix au Concours général de mathématiques.
- 2001 : lauréat du grand prix Jacques Herbrand de l'Académie des Sciences.

Organisation de manifestations scientifiques

- Atelier international sur les condensats de Bose-Einstein au centre de physique des Houches, du 1^{er} au 5 avril 1996
- Atelier sur les gaz quantiques piégés, au château du CNRS de Gif-sur-Yvette, du 6 au 9 février 2000

– Euroconférence sur les gaz quantiques, San Feliu de Guixols (Espagne), en septembre 2003.

Enseignement

– travaux dirigés de mécanique quantique au Magistère interuniversitaire de physique de Paris en 1990-91 et 1992-93
– travaux dirigés de mécanique quantique au DEA de physique quantique de l'ENS-Paris de 1995 à 2000, et d'optique non linéaire de 1995 à 1997.
– cours de mécanique quantique au DEA de physique quantique (devenu M2 de physique quantique) depuis 2001.
– cours sur les condensats dans des écoles doctorales parisiennes : à l'ENS en 1997 et 1998, puis à Orsay de 1999 à 2004.
– cours dans des écoles de physique, notamment aux Houches (été 1999, printemps 2003, automne 2004) et à Cargèse en 1994, 1996 et 2000.

Encadrement de travaux de recherche

– (co)encadrement de 6 thèses : celles de Pippa Storey (décembre 1996), d'Emmanuel Mandonnet (mars 2000), de Christophe Mora (mars 2004), de Giulia Tonini (18 mars 2005), de Félix Werner (en cours), de Pietro Massignan (en cours).
– encadrement de 9 chercheurs post-doctoraux de longue durée depuis 1995 : Ralph Dum, Alice Sinatra, Subhasis Sinha, Iacopo Carusotto, Michele Modugno, Anna Minguzzi, Carlos Lobo, Lincoln Carr, Uri Gavish.

Chapitre 8

Liste des publications

8.1 Articles dans des revues à comité de lecture

1. Castin Y., Wallis H. et Dalibard J., JOSA B **6** 2046 (1989),"Limit of Doppler Cooling."
2. Castin Y. et Mølmer K., J. Phys. B **23** 4101 (1990), "Atomic momentum diffusion in a $\sigma_+ - \sigma_-$ laser configuration : influence of an internal sublevel structure."
3. Castin Y. et Dalibard J., Europhys. Lett. **14** 761 (1991), "Quantization of Atomic Motion in Optical Molasses."
4. Dalibard J., Castin Y. et Mølmer K., Phys. Rev. Lett. **68** 580 (1992), "Wave-Function Approach to Dissipative Processes in Quantum Optics."
5. Berg-Sørensen K., Castin Y., Bonderup E. et Mølmer K., J. Phys. B **25** 4195 (1992), "Momentum diffusion of atoms moving in laser fields."
6. Mølmer K., Castin Y. et Dalibard J., JOSA B **10** 524 (1993), "A Monte-Carlo Wave Function Method in Quantum Optics."
7. Berg-Sørensen K., Castin Y., Mølmer K. et Dalibard J., Europhys. Lett. **22** 663 (1993), "Cooling and Tunneling of Atoms in a 2D laser field."
8. Drewsen M., Laurent Ph., Nadir A., Santarelli G., Clairon A., Castin Y., Grison D. et Salomon C., Appl. Phys. B **59** 283 (1994), "Investigation of sub-Doppler cooling effects in a cesium magneto-optical trap."
9. Castin Y., Berg-Sørensen K., Dalibard J. et Mølmer K., Phys. Rev. A **50** 5092 (1994), "Two-dimensional Sisyphus cooling."
10. Morice O., Castin Y. et Dalibard J., Phys. Rev. A **51** 3896-3901 (1995), "Refractive index of a dilute Bose gas."
11. Castin Y. et Mølmer K., Phys. Rev. Lett. **74** 3772-3775 (1995), "Monte Carlo wavefunction analysis of 3D optical molasses."
12. Castin Y. et Mølmer K., Phys. Rev. A **51** R3426-3428 (1995) "Maxwell-Bloch equations : a unified view of non-linear optics and non-linear atom optics."
13. Mølmer K. et Castin Y., Quantum Semiclass. Opt. **8** 49-72 (1996), "Monte Carlo wavefunctions in quantum optics".
14. Ben Dahan M., Peik E., Reichel J., Castin Y. et Salomon C., Phys. Rev. Lett. **76** 4508-4511 (1996), "Bloch Oscillations of Atoms in an Optical Potential".
15. D. Boiron, A. Michaud, P. Lemonde, Y. Castin, C. Salomon, S. Weyers, K. Szymaniec, L. Cognet et A. Clairon, Phys. Rev. A **53** R3734-3737 (1996), "Laser Cooling of Cesium Atoms in Gray Optical Molasses down to 1.1μKelvin".

16. Castin Y. et Mølmer Klaus, Phys. Rev. A **54** 5275 (1996), "Monte Carlo wave functions and non-linear master equations".
17. Castin Y. et Dum R., "Bose-Einstein condensates in time dependent traps", Phys. Rev. Lett. **77** 5315-5319 (1996).
18. Peik E., Ben Dahan M., Bouchoule I., Castin Y. et Salomon C., "Bloch Oscillations of Atoms, Adiabatic Rapid Passage and Monokinetic Atomic Beams", Phys. Rev. A **55** 2989 (1997).
19. Peik E., Ben Dahan M., Bouchoule I., Castin Y., Salomon C., "Bloch oscillations and an accelerator for cold atoms", Applied Physics B **65**, 685-692 (1997).
20. Castin Y. et Dalibard J., "Relative phase of two Bose-Einstein condensates", Phys. Rev. A **55** 4330 (1997)
21. Castin Y. et Dum R., "Instability and depletion of an excited condensate in a trap", Phys. Rev. Lett. **79** 3553 (1997).
22. Villain P., Lewenstein M., Dum R., Castin Y., You L., Imamoglu A., Kennedy T.A.B., "Quantum dynamics of the phase of a Bose-Einstein condensate", Journal of Modern Optics, **44** 1775-1799 (1997).
23. Castin Y. et Dum R., "Low temperature Bose-Einstein condensates in time dependent traps : beyond the $U(1)$-symmetry breaking approach", Phys. Rev. A **57** 3008-3021 (1998).
24. Castin Y., Cirac J.I. et Lewenstein M., "Reabsorption of Light by Trapped Atoms", Phys. Rev. Lett. **80** 5305 (1998).
25. Sinatra A. et Castin Y., "Phase Dynamics of Bose-Einstein Condensates : Losses versus Revivals", Eur. Phys. J. D **4**, 247-260 (1998).
26. A. Sinatra, P. Fedichev, Y. Castin, J. Dalibard, G. Shlyapnikov, "Dynamics of two interacting Bose-Einstein condensates", Phys. Rev. Lett. **82** 251-254 (1998).
27. M. Holzmann, Y. Castin, "Pair correlation function of an inhomogeneous interacting Bose-Einstein condensate", Eur. Phys. J. D **7**, 425-432 (1999).
28. S. Kulin, Y. Castin, M. Ol'shanii, E. Peik, B. Saubaméa, M. Leduc, C. Cohen-Tannoudji, "Exotic Quantum Dark States", Eur. Phys. J. D **7**, 279-284 (1999).
29. Y. Castin, R. Dum, "Bose-Einstein condensates with vortices in rotating traps", Eur. Phys. J. D **7**, 399-412 (1999).
30. G. Bruun, Y. Castin, R. Dum, K. Burnett, "BCS Theory for Trapped Ultracold Fermions", Eur. Phys. J. D **7**, 433-439 (1999).
31. A. Sinatra, Y. Castin, "Binary Mixtures of Bose-Einstein Condensates : Phase dynamics and Spatial Dynamics", Eur. Phys. J. D **8**, 319 (2000).
32. E. Mandonnet, A. Minguzzi, R. Dum, I. Carusotto, Y. Castin, and J. Dalibard, "Evaporative cooling of an atomic beam", Eur. Phys. J. D **10**, 9-18 (2000).
33. Y. Castin, R. Dum, E. Mandonnet, A. Minguzzi, I. Carusotto, "Coherence properties of a continuous atom laser", Journal of Modern Optics **47**, 2671-2695 (2000).
34. A. Sinatra, Y. Castin, C. Lobo, "A Monte Carlo formulation of the Bogolubov theory", Journal of Modern Optics **47**, 2629-2644 (2000).
35. P. Milman, Y. Castin, L. Davidovich, "Decoherence as phase diffusion", Phys. Rev. A **61**, 063803 (2000).
36. I. Carusotto, Y. Castin, J. Dalibard, "N boson time dependent problem : a reformulation with stochastic wave functions", Phys. Rev. A **63**, 023606 (2001).

37. Y. Castin, C. Herzog, "Bose-Einstein condensates in symmetry breaking states", Comptes Rendus de l'Académie des Sciences de Paris, tome 2, série IV, 419-443 (2001).
38. A. Minguzzi, G. Ferrari, Y. Castin, "Dynamic structure factor of a superfluid Fermi gas", Eur. Phys. J. D **17**, 49 (2001).
39. Alice Sinatra, Carlos Lobo, Yvan Castin, "Classical-Field Method for Time Dependent Bose-Einstein Condensed Gases", Phys. Rev. Lett. **87**, 210404 (2001).
40. Subhasis Sinha, Yvan Castin, "Dynamic instability of a rotating Bose-Einstein condensate", Phys. Rev. Lett. **87**, 190402 (2001).
41. I. Carusotto, Y. Castin, "An exact stochastic field method for the interacting Bose gas at thermal equilibrium", J. Phys. B **34**, 4589-4608 (2001).
42. L. Khaykovich, F. Schreck, G. Ferrari, T. Bourdel, J. Cubizolles, L.D. Carr, Y. Castin, C. Salomon, "Formation of a matter-wave bright soliton", Science **296**, 1290 (2002).
43. P. Rosenbusch, D. S. Petrov, S. Sinha, F. Chevy, V. Bretin, Y. Castin, G. Shlyapnikov, and J. Dalibard "Critical Rotation of a Harmonically Trapped Bose Gas", Phys. Rev. Lett. **88**, 250403 (2002).
44. Alice Sinatra, Carlos Lobo, Yvan Castin, "The truncated Wigner method for Bose condensed gases : limits of validity and applications", J. Phys. B **35**, 3599-3631 (2002).
45. L. Carr, Y. Castin, "Dynamics of a matter-wave bright soliton in an expulsive potential", Phys. Rev. A **66**, 063602 (2002).
46. Michele Modugno, Ludovic Pricoupenko, Yvan Castin, "Bose-Einstein condensates with a bent vortex in rotating traps", Eur. Phys. J. D **22**, 235-257 (2003).
47. I. Carusotto, Y. Castin, "Condensate statistics in one-dimensional interacting Bose gases : exact results", Phys. Rev. Lett. **90**, 030401 (2003).
48. I. Carusotto, Y. Castin, "Exact reformulation of the bosonic many-body problem in terms of stochastic wavefunctions : convergence issues", Laser Physics **13**, 509-516 (2003).
49. C. Mora, Y. Castin, "Extension of Bogoliubov theory to quasicondensates", Phys. Rev. A **67**, 053615 (2003).
50. I. Carusotto, Y. Castin, "An exact reformulation of the Bose-Hubbard model in terms of a stochastic Gutzwiller ansatz", New J. Phys. **5**, 91 (2003).
51. Carlos Lobo, Alice Sinatra, Yvan Castin, "Vortex Lattice Formation in Bose-Einstein Condensates", Phys. Rev. Lett. **92**, 020403 (2004).
52. I. Carusotto, Y. Castin, "Superfluidity of the 1D Bose gas", C. R. Physique **5**, 107-127 (2004).
53. L. Pricoupenko, Y. Castin, "One particle in a box : The simplest model for a Fermi gas in the unitary limit", Phys. Rev. A **69**, 051601(R) (2004).
54. L. Carr, T. Bourdel, Y. Castin, "Limits of sympathetic cooling of fermions by zero temperature bosons due to particle losses", Phys. Rev. A **69**, 033603 (2004).
55. L. Carr, Y. Castin, G. Shlyapnikov, "Achieving a BCS transition in an atomic Fermi gas", Phys. Rev. Lett. **92**, 150404 (2004).
56. L. Carr, Y. Castin, "Limits of sympathetic cooling of fermions : The role of the heat capacity of the coolant", Phys. Rev. A **69**, 043611 (2004).

57. Y. Castin, I. Carusotto, "Coherence and correlation properties of a one-dimensional attractive Fermi gas", Optics Communications **243**, 81-106 (2004).
58. Y. Castin, "Exact scaling transform for a unitary quantum gas in a time dependent harmonic potential", Comptes Rendus Physique **5**, 407 (2004).

8.2 Actes de congrès ou d'écoles d'été

59. Castin Y., Mølmer K., Dalibard J. et Cohen-Tannoudji C., in Laser Spectroscopy IX, Feld M., Mooradian A. et Thomas J. édit., "New Physical Mechanisms in Laser Cooling."
60. Dalibard J., Arimondo E., Aspect A., Castin Y., Cohen-Tannoudji C., Kaiser R., Mølmer K., Salomon C., Vansteenkiste N., "Deceleration and cooling of neutral atoms using lasers", Annales de physique **15**, 25-30 (1990).
61. Castin Y., Dalibard J. et Cohen-Tannoudji C., in Proceedings of the LIKE workshop, mai 1990, Moi L. édit., "The Limits of Sisyphus Cooling."
62. Dalibard J. et Castin Y., dans les comptes-rendus de l'École Internationale de Physique "Enrico Fermi", CXX Course "Frontiers in laser spectroscopy", juin-juillet 1992, Hänsch T.W. et Inguscio M. édit., "Laser Cooling from the Semi-Classical to the Quantum Regime."
63. Castin Y., Dalibard J. et Mølmer K., in *Proceedings of the thirteenth international conference on atomic physics* (ICAP XIII) ; Walther H., Hänsch T.W. et Neizert B. édit., A.I.P. 1993, "A Wave Function approach to dissipative processes."
64. Castin Y., Berg-Sørensen K., Mølmer K. et Dalibard J., in *Fundamental of Quantum Optics*, LNIP 420, Ehlothzky F. édit., Springer-Verlag 1993, "Multidimensional Laser Cooling : quantum approaches."
65. Castin Y., Dalibard J. et Cohen-Tannoudji C., *Bose-Einstein Condensation* (BEC 93), Griffin A., Snoke D. W. et Stringari S. édit., Cambridge University Press (1995), p. 173-201, "Laser cooling and trapping of neutral atoms."
66. Castin Y., Dalibard J. et Cohen-Tannoudji C., *Advances in Quantum Phenomena*, NATO ASI Series, Beltrametti E.G. et Lévy-Leblond J.-M. édit., Plenum Press, New York (1995), p.47-63 "Quantum effects with ultra-cold atoms."
67. Castin Y., actes de l'École d'été sur les lasers et leurs applications scientifiques et médicales (Cargèse 1994), Pocholle J.-P., Fabre C., Chavel P. et Saget J.-C. édit., Les Éditions de Physique 1996, p.427-463, "Refroidissement d'atomes par laser et optique atomique."
68. Olshanii M., Castin Y. et Dalibard J., "A model for an atom laser",p. 7, Proceedings of the 12$^{\text{th}}$ International Conference on Laser Spectroscopy, M. Inguscio, M. Allegrini and A. Sasso editors, World Scientific, Singapore (1996).
69. M. Olshanii, Y. Castin et J. Dalibard, p.575-582, "Almost Bose-Einstein Phase Transition in VSCPT Cooling", Proceedings of the International School of Physics "Enrico Fermi", Course CXXXIV, A. Aspect, W. Barletta and R. Bonifacio Eds.), IOS Press, Amsterdam, 1996.
70. J. Dalibard and Y. Castin, "Towards coherent atomic samples using laser cooling", Proceedings of the 15th International conference on Atomic Physics, Amsterdam 1996, H.B. van Linden van den Heuvell, J.T.M. Walraven and M.W. Reynolds editors, p. 180-191 (World Scientific, Singapore, 1997).

71. Boiron D. Michaud A., Lemonde P. Castin Y., Salomon S., Weyers S., Szymaniec K., Cognet L. et Clairon A., Proc. of the fifth Symposium on Frequency Standards and Metrology, Woodshole, USA, éd. J. Bergquist, P. 499, 1996.
72. Peik E., Ben Dahan M., Bouchoule I., Castin Y. et Salomon C., "Bloch Oscillations of Atoms in an Optical Potential", Proceedings of the 15th International conference on Atomic Physics, Amsterdam 1996, J. Walraven and M. Reynolds editors (World Scientific, 1996)
73. Castin Y., Proceedings of the DFG meeting "Time dependent phenomenons and methods in quantum systems of physics and chemistry", "Quantum motional effects with laser cooled atoms", Würzburg (2-4/3/1998).
74. Y. Castin, Proceedings of the workshop "Nuclear Matter in different phases and transitions", Les Houches (31/3-10/4/1998), p.173-192 : *Bose-Einstein condensation of trapped atomic gases*, Kluwer Academic Publishers (Dordrecht, 1999).
75. M. Ben Dahan, E. Peik, I. Bouchoule, Y. Castin, C. Salomon, "Quantum transport with cold atoms : Bloch oscillations in an optical potential", Ann. Phys. Fr. **23**, C1-111 (1998).
76. Y. Castin, p.1-136, in *Coherent atomic matter waves*, Lecture notes of Les Houches summer school, edited by R. Kaiser, C. Westbrook, and F. David, EDP Sciences and Springer-Verlag (2001).
77. Y. Castin, S. Sinha, "Nucleation of Vortices in a Rotating Bose-Einstein Condensate", p.61-69, Proceedings of the XV International Conference on Laser Spectroscopy, Snowbird (10-15 June 2001), ed. S. Chu, V. Vuletic, A. J. Kerman, C. Chin, World Scientific (Singapore, 2002).
78. I. Carusotto, Y. Castin, "Exact reformulation of the bosonic many-body problem in terms of stochastic wave functions : an elementary derivation", Annales Henri Poincaré **4**, S783-S792 Suppl. 2 (2003).
79. Y. Castin, "Simple theoretical tools for low dimension Bose gases", Lecture notes of the 2003 Les Houches Spring School, *Quantum Gases in Low Dimensions*, M. Olshanii, H. Perrin, L. Pricoupenko, Eds., J. Phys. IV France **116**, p.89-132 (2004).

8.3 Articles de vulgarisation

80. F. Bardou et Y. Castin, "Le refroidissement laser subrecul : fonctions d'onde stochastiques et vols de Lévy", p.7-14, Images de la Physique 1998.
81. Y. Castin, R. Dum et A. Sinatra, "Bose condensates make quantum leaps and bounds", p.27-42, Physics World **12** numéro 8, août 1999.
82. Y. Castin, "Un prix Nobel pour les condensats de Bose-Einstein atomiques gazeux", Lettre du SPM (CNRS), mars 2002.
83. Y. Castin, "Les atomes ultrafroids", *Pour la Science*, numéro 300, p.134-138, octobre 2002.
84. Y. Castin, "La saga des condensats quantiques", *Pour la Science*, numéro 326, p.114-119, décembre 2004.